THE EFFECT OF STEEL BAR CORROSION ON THE BOND STRENGTH OF CONCRETE MANUFACTURED WITH CEMENT REPLACEMENT MATERIALS

by

Adel A. Elbusaefi

Thesis Submitted in Fulfilment of the Requirement for the Degree of Doctor of Philosophy of Cardiff University

School of Engineering

Cardiff University

June 2014

PAPERS PRODUCED FROM THIS THESIS

1. Elbusaefi, A., Lark, R and Gardner, D "The effect of rebar corrosion on the bond strength of reinforced concrete structures manufactured using cement replacement materials" Fourth International Symposium Bond In Concrete (BIC) June 17-20, 2012, Brescia, Italy.

2. Elbusaefi, A., Lark, R and Gardner, D "Corrosion of reinforcement steel embedded in concretes manufactured with various cement replacement materials and their gas permeability". 9th *fib* International PhD Symposium in Civil Engineering July 22-25, 2012, Karlsruhe Institute of Technology (KIT), Germany.

DECLARATION

This work has not been previously been accepted in substance for any degree and is not concurrently submitted candidature for any degree.

Signed ……. (candidate) Date ……

Statement 1

This thesis is being submitted in partial fulfilment of the requirements for the degree of PhD.

Signed ……. (candidate) Date ……

Statement 2

This thesis is the result of my own independent work/investigation, except where otherwise stated. Other sources are acknowledged by explicit reference.

Signed ……. (candidate) Date ……

Statement 3

I hereby give consent for my thesis, if accepted, to be available for photocopying and for inter-library loan, and for the title and summary to be made available to outside organisations.

Signed ……. (candidate) Date ……

ABSTRACT

This thesis presents a study of the bond strength between corroded and uncorroded steel reinforcement and the surrounding concrete within steel reinforced structures. The work is based on concretes manufactured with different types of cement replacement materials, and investigates the influence of the corrosion rate of steel as predicted by concrete permeability. The cement replacement binders included CEM II, blended cements of fly ash (PFA), ground granulated blast-furnace slag (GGBS), metakaolin (MK) and silica fume (SF).

The experimental work was conducted by placing 200mm cube test specimens in a saline solution (3.5% NaCl) for different exposure times (3, 7, 10, 14 and 20 days) with an applied external current of 10 mA between the reinforcing steel and a stainless steel counter electrode. Pull-out tests were conducted to evaluate the bond strength between the concrete and the steel reinforcement. The permeability coefficients of concretes were investigated using a relative gas permeability test. The specimens used for determining permeability were cylindrical 100mm diameter and 100mm length, which were oven dried at 105 ºC.

The experimental results indicated that the bond strength was governed by concrete properties. Furthermore, the bond strength of the corroded specimens was found to depend on the corrosion levels and varied across all concrete types, depending on the concrete microstructure. Moreover, when the corrosion level exceeded 1.74%, the bond strength began to decline. Thereafter, the bond strength continued to reduce as the corrosion time of the reinforced concrete increased.

The relationship between the compressive strength and gas permeability of concretes was inconclusive but the latter does depends on the cement replacement levels. The PFA concretes had the lowest permeability compared to the other two types of concrete (CEM II and GGBS). The permeability of concretes and corrosion rates with different types and levels of cement replacement materials significantly decreased as the age of concretes increased. The improvements in gas permeability and corrosion rate were observed when 40% of cement weight was replaced with PFA.

The ABAQUS program was used to model the bond-slip behaviour of different concrete mixes, in addition to a plastic damage model. A cohesive zone element was employed for the steel-concrete interface. During analysis, the numerical model was validated

against the results obtained from the experimental tests. The numerical results showed good agreement with the experimental results for CEM II, GGBS and SF concrete specimens, but in the case of PFA concrete where the numerical result of bond strength was overestimated by to the experimental ones.

Keywords: Concrete, Reinforcement, Bond strength, Cement replacement materials, Gas permeability,

To my father (in memory) who left

me during my study

ACKNOWLEDGEMENTS

I would like to express my sincere appreciation to my supervisors **Prof. Bob Lark and Dr. Diane Gardner** for their invaluable guidance encouragement; great patience and guidance are all highly appreciated. This thesis would not have been possible without their direction, support and enthusiasm. In addition, I would also like to thank **Prof. Tony Jefferson** for helpful dissection and his advice in LUSAS programme during this research.

I wish to express my sincere thanks to **my late father**, who died on 29 September 2012. He and **my mother** have given unwavering encouragement and support towards all my academic endeavours which have also contributed to the successful completion of this thesis.

I would like to extend my deepest gratitude to **laboratory staff** in Cardiff University particularly, Carl Wadsworth, Ian King, Harry Lane and Des Sanford who assisted me during the laboratory experiments. My science appreciation also extends to all my colleagues and others who have provided assistance at various occasions.

My great gratitude and my sincere thanks are to be dedicated towards **my wife Fadia** and **my kids Fadie and Ali** for their invaluable encouragement and support during my study. Without them, none of this would have been possible.

Finally, I am deeply grateful to all family members as well as all my friends, for their support and encouragement, they owe everything and without them it would not have come here.

TABLE OF CONTENTS

LIST OF FIGURES

LIST OF TABLES

NOTATIONS

The following symbols are used in this thesis

Cl	=	Corrosion level	%
C_R	=	Corrosion rate	mpy
d_a	=	Diameter of coarse aggregate	mm
d_b	=	Diameter of reinforcement bar	(mm)
E_c	=	Elasticity Modulus of concrete	(kN/mm^2)
E_s	=	Young's modulus of reinforcement bar	(kN/mm^2)
f_c	=	Concrete compressive strength	(N/mm^2)
f_{ct}	=	Splitting tensile strength of concrete	(N/mm^2)
f_{cu}	=	Cube compressive strength	(N/mm^2)
f_t	=	Splitting tensile strength	(N/mm^2)
G_f	=	Fracture energy per unit area	(N/mm)
k_{ef}	=	Intrinsic permeability	m^2
k_{nn}	=	Normal stiffness	(N/mm^3)
k_{ss}	=	Shear stiffness	(N/mm^3)
k_{tt}	=	Shear stress	(N/mm^3)
l	=	Length of specimen	mm
$P_{1/2}$	=	Half original cell pressure	N/m^2
P_{atm}	=	Atmospheric pressure	N/m^2
Pc_0	=	Initial pressure a the outer face of cylinder at beginning of test	N/m^2
r_c	=	Inner radius of concrete cylinder	mm
R_r	=	Relative rib area	(-)
t	=	Time	s
V_0	=	Volume of gas reservoir and gas around specimen	m^3

εt	=	Strain at maximum tensile strength	(-)
μ	=	Dynamic viscosity	Ns/m^2
v	=	Poisson's ratio	(-)
ρ	=	Density	kg/m^3
σ	=	Stress	(N/mm^2)
τ_u	=	Ultimate bond strength	(N/mm^2)

ABBREVIATIONS

2D	=	Two-dimensional finite element model
ACI	=	American Concrete Institute
ASTM	=	American Society for Testing and Materials
CO_2	=	Carbon dioxide
CZM	=	Cohesive zone element
DOF	=	Degree of freedoms
EC2	=	Eurocode 2
FE	=	Finite element
FEA	=	Finite element analysis
GGBS	=	Ground granulated blast furnace slag
ITZ	=	Interface transition zone
JEM	=	Joint element method
LVDT	=	Linear Variable Differential Transformer
MC90	=	Model code 1990
MC94	=	LUSAS Multi-crack model (model 94)
MK	=	Metakaolin
NaCl	=	Sodium chloride
NEFM	=	Non-linear elastic fracture mechanics
OPC	=	Ordinary Portland cement
PFA	=	Pulverised fuel ash
POT	=	Pull-out test
RC	=	Reinforced concrete
RCPT	=	Rapid Chloride permeability Test
RCPT	=	Rapid Chloride permeability Test

RILEM	=	Reunion Internationale des Laboratories d'Essais et de Recherches surles Materiaux et les Constructions
SCMs	=	Supplementary cementitious materials
SF	=	Silica fume
W/c	=	Water to cement ratio

CHAPTER 1

INTRODUCTION

1.1 Background

Reinforced concrete is the most important aspect in the construction industry. Besides the cheap constructive aspects of the combination of both materials, the alkalinity of the concrete causes a natural protective effect on the steel surface which prevents corrosion of the steel as much as possible. The environmental conditions include the penetration of chlorides (e.g. de-icing salts or from seawater) and the carbonation of the concrete. This protective effect may fail, however, the temporal quantification of these processes to estimate the life of reinforced concrete structures is an important task both in the planning phases of new building and as part of the repair of existing ones. The corrosion of steel reinforcement in reinforced concrete is one of the most significant problems which affects structures and infrastructure around the world and particularly structures in coastal areas. It causes cracking/spalling of concrete reduces the effective cross-sectional area of the steel reinforcement and weakens the bond between steel and concrete. This can seriously affect the durability and service life of RC structures and, as a consequence, infrastructure such as bridge decks can be a major concern to many transportation agencies. Considerable resources are spent on repairing and rehabilitating deteriorating concrete structures. It is reported that steel reinforcement corrosion in concrete has cost approximately $100 billion annually world-wide for maintenance and repairs for concrete infrastructure (Chen, 2004). It is estimated that more than $13.6 billion is required each year for the repair and rehabilitation of highway bridge

structures in the USA (Nace, 2013), Additionally, the Department of Transport (DoT) estimated that more than £616.5 million is required for repairing motorway road bridges in the UK (Broomfield, 2007). In the Middle East where the hot climate and saline ground water increases the problem of corrosion, a situation which is made more difficult by problems associated with concrete curing, has led to very short lifetimes for reinforced concrete structures (Rasheeduzzafar et al., 1992).

The most significant causes of reinforced steel corrosion are carbon dioxide and chloride ions ingress into concrete (Figure 1.1) and their migration to the steel surface. For instance, de-icing salts destroy the passive layer of iron oxide around the reinforcement, which in turn leads to rapid corrosion. The corrosion of reinforced steel results in the reduction of the cross-sectional area of the steel bar and a build up of corrosion products, which in turn reduces the steel's ductility and strength. The products of corrosion occupy a volume 2 to 6 times larger than that of the original reinforced steel (Liu and Weyers, 1998). The initial corrosion products around the steel bar surface create longitudinal cracking, spalling and delamination of the concrete cover. Losses of concrete cover will in turn result in loss of confinement with a reduction in bond strength at the interfacial zone between the steel bar and the concrete. The soft layer produced through collected corrosion products on the bar surface might successfully decrease the friction component of the bond strength. Thus, the deterioration of the ribs of deformed bars decreases the interlocking forces between the ribs of bars and surrounding concrete structure. This deteriorates the main mechanism of the bond strength between deformed bars and concrete, considerably reducing the bond in the process.

Figure 1.1: Photograph of bridge on the M4 in London, the reinforcement corrosion due to the de-icing salt (Fesi, 2012)

Moreover, concrete permeability is an important factor in the control of the movement of chloride ions through concrete towards the reinforcing bar. It is well known that the volume and size of the interconnected capillary pores in the cement paste affect concrete permeability. Consequently, achieving low permeability of concrete can improve its resistance to the penetration of fluids, chloride ions, alkali ions, carbonation and other causes of chemical attack (Gunevisi et al., 2009 and Elahi et al., 2010).

The use of supplementary cementitious materials (SCMs), such as ground granulated blast-furnace slag (GGBS), pulverised fuel ash or fly ash (PFA), silica fume (SF) and metakaolin (MK) has become very common in concrete manufacture because of the ability of these materials to significantly improve the durability of concrete by decreasing the permeability. An additional advantage is the reduction in the carbon dioxide emissions associated with the manufacture of cement; thus the SCMs are considered more environmentally sustainable materials (Oner and Akyuz 2007 and Owaid et al., 2012).

1.2 Significance of the research

Bond between the steel reinforcement and concrete is essential to ensure the composite interaction of the two materials. At very low stress, bond strength is mainly due to the chemical bond between the concrete and the steel bar but it becomes dependent on the mechanical interlock between the steel ribs and the concrete once slippage happens. There are many factors influencing the bond between the concrete and reinforcement steel, such as concrete strength, concrete composition and environments. The corrosion steel reinforcement in concrete is governed by availability of oxygen, moisture and carbonation (CO_2). Although mineral admixtures have been widely used in concrete, they have a lesser effect on the diffusivity of both chlorides and carbonation than the incorporation of cementitious material in blended cements. The latter are used to protect steel reinforcement in concrete against corrosion by reducing the structure's permeability resistance against chloride ions. Based on the results of previous research detailed in this review, it can indeed be said that there is very little published data on the bond strength of concrete containing cementitious materials since the majority of the research that has been conducted in this area has focused on the bond strength of concrete containing 100% Portland cement. Furthermore, there is also a growing interest in the use of alternative cementitious material (SCMs), including fly ash, ground granulated blast-furnace slag, silica fume and metakaolin. It is these SCMs and their effects on the bond strength of steel bars in reinforced concrete, which are investigated in this thesis. Subsequent changes in durability as a result of differing SCMs at a range of replacement levels are considered through the measurement of the permeability of concrete.

1.3 The objectives and scope of this research

The main aim of this research is to investigate the bond strength of reinforced concrete structures under a range of corrosion levels of steel bars embedded in concrete made with cementitious materials. Moreover, bond deterioration due to steel reinforcement corrosion is the most important parameter in the loss of bond strength between the steel and the surrounding concrete. The use of cement replacement materials, which reduce the concrete permeability, is proven to improve the corrosion resistance of steel in concrete is therefore also of interest. The objectives of this project are summarised below:

- To undertake bond tests in order to investigate the influence of a range of corrosion levels on the bond strength of reinforced concrete manufactured with different cement replacement material.
- To investigate the effect of the concrete's composition and micro-structure, as characterised by the gas relative permeability test on the corrosion resistance and bond strength of RC structures.
- To investigate the relationship between the rate of corrosion of reinforcement steel and the intrinsic permeability of the concrete.
- To model the experimental arrangement and validate the model with experimental data using a two-dimensional non-linear finite element model developed in LUSAS and ABAQUS programmes.

1.4 Organisation of the thesis

This thesis is divided into seven chapters; the first of which is the introduction, background and aims and objectives of this research. Chapter 2 encompasses a review of the current literature, which is divided into three main sections. The first section

describes the bond strength between steel and concrete including bond mechanisms and the effect of corrosion on bond strength. The second section summarises the corrosion of steel bars in concrete and the corrosion mechanism. Lastly, section three describes the concrete permeability and the use of supplementary cementitious materials including fly ash, silica fume, metakaolin and ground granulated blast-furnace slag to reduce the corrosion of steel reinforcement in concrete.

In Chapter 3, experimental methodology for this study is described, including the materials; the details of specimens used and the permeability test as well as the setup for the accelerated corrosion test, the bond tests and the gas permeability tests.

Chapter 4 presents the results and discussion of the concrete properties, the corrosion level and the bond strength of uncorroded and corroded steel bars embedded in concretes made with a range of cement replacement materials. It also presents a comparison of exposure time and the results of the pullout tests with and without corrosion with a comparison to CEB-FIP Model Code 1990.

Chapter 5 deals with the results and discussions of the gas permeability tests for concretes made with a range of cement replacement materials at varying replacement levels, including the relationship between the corrosion rate of steel bars, the gas permeability coefficient and curing time.

In Chapter 6 the finite element modelling results and comparison with experimental data based on the experimental results in Chapter 4 are described to validate the relationship between the numerical and experimental data.

Finally, Chapter 7 presents the conclusions of the experimental and numerical studies and proposes areas of future investigation for this research.

CHAPTER 2
LITERATURE REVIEW

2.1 Introduction

The importance of the integrity of engineering structures cannot be over-emphasised. Corrosion of reinforcing steel is therefore of great concern for the construction industry as well as many other industries worldwide. When steel corrodes in concrete, there is the possibility of spalling, cracking of the concrete section, reduction in the cross sectional area of the reinforcing steel, and reduction in the bond strength between the steel and the surrounding concrete. These problems will eventually affect the integrity and service life of the structure, so should be avoided. Low concrete permeability helps in restricting the corrosion rate by improving the electrical resistivity of concrete, thereby decreasing the flow of hydroxyl ions from anode to cathode. The use of cement replacement materials is becoming more common in concrete structures. This is due to the favourable permeability and good corrosion resistance of the resulting concrete. While many studies have investigated the effect of corrosion on the bond strength behaviour and flexure of reinforced concrete, they have primarily used concrete made with normal Portland cement, and cement replacement materials have received comparably less experimental attention. The literature survey presented in this chapter therefore describes the previous studies carried out regarding the bond strength of corroded reinforcement bars and the permeability of concrete composition with different cement replacement materials. Also given in this chapter is a brief summary of

important points for understanding the phenomenon of bond strength in reinforced concrete.

2.2 Bond between steel bar and concrete

Bond stress is defined as the transfer of stress loads across the interface between the concrete and reinforcement bars. It represents the interaction between the steel reinforcement and the surrounding concrete (Amleh and Gosh, 2006). The primary mechanism of bond is the mechanical interlocking between the concrete and any deformations (i.e. ribs) of the steel bar.

2.2.1 Bond-slip Mechanisms

The bond between reinforcing bar and concrete comprises three distinct mechanisms: chemical adhesion, friction and mechanical interlock (ACI 408, 2003).

(i) Chemical adhesion: adhesion is the chemical bond created on the contact surface between the steel reinforcement and the surrounding concrete. This can be broken down at very low load, allowing slip between the reinforcing steel and the concrete.

(ii) Friction: friction especially between the steel bar surface and concrete. The friction force plays a significant role between the concrete and the deformed bar (ribs).

(iii) Mechanical interlock: This shear bond becomes more significant with increasing relative displacement under composite mechanisms. The force transfer mechanism is primarily due to the mechanical interlocking between the ribs of steel and concrete. The mechanisms of chemical adhesion and friction are the most significant in the case of smooth bars (Figure 2.1). For deformed bars, the mechanical interlock of the steel bar ribs within the concrete is the principal

mechanism which governs the bond strength-slip behaviour (Wang and Liu, 2003; Bamonte and Gambarova, 2007; Gambarova, 2012).

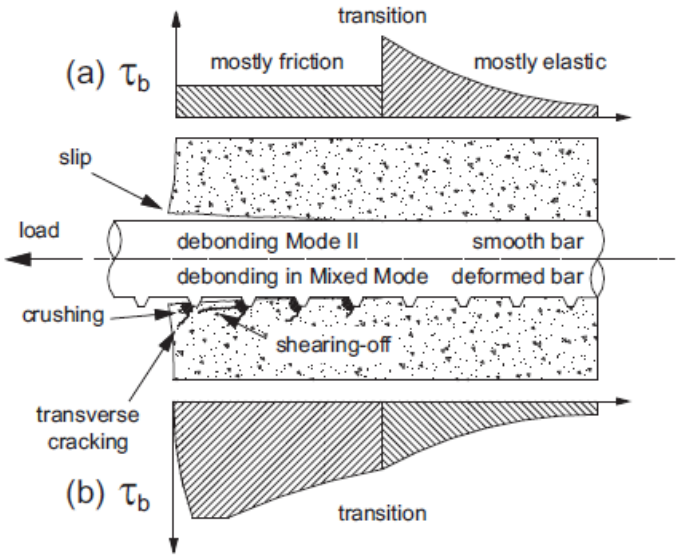

Figure 2.1 : (a) Bond mechanisms in smooth bar; (b) Deformed bars (Bamonte and Gambarova, 2007)

According to FIB (2000), the bond stress behaviour can be characterized by four stages, as shown in Figure 2.2 and described in the following paragraphs.

Stage I (uncracked), for low levels of bond stress, the main resistance mechanism is often chemical adhesion between the mortar matrix and the surface of the steel bar. At this stage, with low bond stresses, the resistance of the pulling forces for plain (smooth) steel bars relies only on chemical and physical adhesion. These bars have low bond performances suggesting that chemical and physical adhesion only play a minor role in the case of deformed bars and offer minimal resistance. As seen in Figure 2.2, the stress-slip relationship of this mechanism accounts for the low bond stress, $\boldsymbol{\tau} < \boldsymbol{\tau}_1$ where $\boldsymbol{\tau}_1$ = (0.2 to 0.8) f_{ct} (FIB, 2000). Note that the relative displacement of the bar is always measured with reference to the undisturbed concrete and consists of two parts, the relative slip at the interface and shear deformations in the concrete

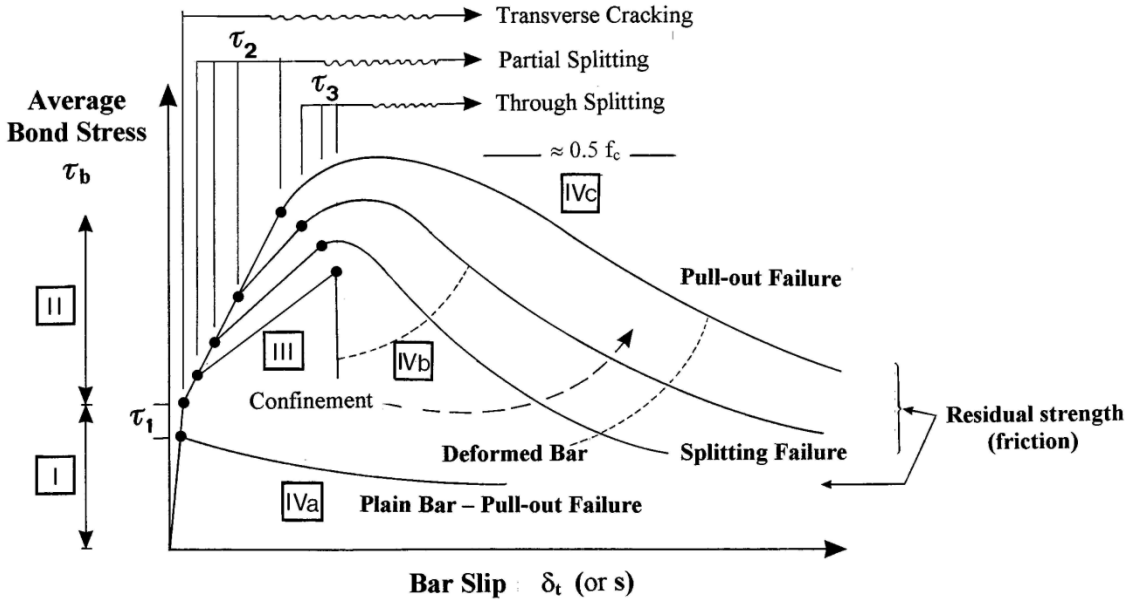

Figure 2.2: Bond stress-slip (FIB, 2000)

Stage II (first cracking) is when an increase in the bond stress results in the loss of the chemical and physical adhesion. Large bearing stresses under the lugs of deformed bar are induced by the interaction between the ribs and concrete. Transverse micro cracks result at the tips of the ribs and allow the bar to slip, however, the wedging of the lugs remains small enough not to induce concrete splitting (FIB, 2000).

Stage III occurs when the concrete material directly in front of the ribs crushes as the bond stress values develop to around (1-3) f_{ct} (FIB, 2000), forming a crushed concrete wedge in front of the lugs of the bar. The slip of the bar is mainly attributed to the crushing of the concrete material. It should be noted that the wedge has a smaller angle than that of the face of the ribs, enhancing the wedge action of the deformed bar on the concrete which is enhanced by the crushed concrete stuck to the front of the lugs (Paulay and Park, 1975). As a consequence, the layer of concrete surrounding the bar exerts a confinement condition on the bar owing to the reaction of hoop stresses, which is upheld until the wedging forces reach the level of hoop stress and develop

longitudinal cracks, initialising splitting failure. The bond stress increases until a split reaches the outer surface which is known as through splitting (τ_3) as shown in Figure 2.2. The magnitude of τ_3 is dependent on the degree of confinement.

Stage IV initialisation depends on the level of transverse reinforcement. Following the attainment of the τ_3 bond stress value, the longitudinal splitting cracks break through the whole concrete cover and result in failure. Shear links and stirrups surrounding the bar may still contribute to the bond efficiency after this point and maintain the strength despite large slip values. As shown in Figure 2.2, the curve is representative of a bar with light to medium transverse reinforcement.

2.2.2 Bond strength measurement

In order to investigate the bond- slip behaviour, there are many different types of tests to measure the bond between reinforcement and concrete. The most common of these tests are the pull-out tests and the beam tests, (see Figure 2.3). These tests have advantages and disadvantages some of which have been described and discussed by several researchers (Oliver et al., 2002; RILEM 1983 and Ferguson et al., 1955). The bond beam test closely reflects the influence of flexure. As such, it has the potential to capture the real bonding mechanism and de-bonding behaviour of the RC specimens under loading due to its similarity to an RC beam subject to bending. The pull-out test is relatively simple to use for short bond lengths. The steel bar is cast into a concrete specimen and is then pulled out directly from the concrete block which may lead to three general types of failure; (i) pull-out failure, where the concrete surrounding the steel bar fails in shear generated by the rebar ribs, (ii) splitting failure, where radial cracks are formed around the steel reinforcement such that the specimen splits when these cracks reach the outer of the concrete surface and (iii) yielding of the steel bar. It has the advantages of simplicity and enables bond strength to be calculated from the

measurement of slip between the steel reinforcement and concrete. Thus, this test would be adequate for studying the influence of various parameters of bond strength such as the slip resistance of different concrete mixes, some with cement replacement materials, and different levels of steel reinforcement corrosion. According to BS EN 10080:2005, unlike deformed bars should be bonded only over a limited length whereas plastic sleeves are commonly used to prevent the adhesion layer between the steel reinforcement and the concrete at the de-bond regions.. These methods are intended to determine the bond strength and provide a basis for the determination of bond performance characteristics of steel reinforcement based on the surface configuration of the ribbed bar.

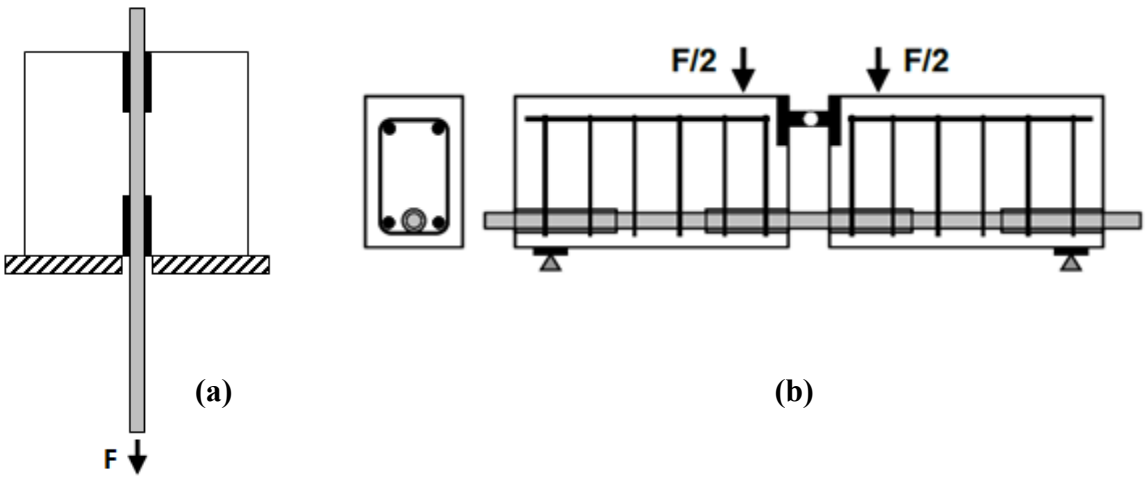

Figure 2.3: (a) Pull-out Test; (b) Beam Test (RILEM/CEB/FIB 1983)

2.3 Factors affecting on the bond strength of concrete

Bond strength between the steel reinforcement and concrete is affected by many factors. Important amongst these factors are the steel reinforcement properties, concrete properties and other environment factors (i.e. corrosion and temperature). These factors

which influence the bond strength steel/concrete interface are discussed in detail in the following sections.

2.3.1 Effect of bar profile

Steel reinforcement geometry largely contributes to bond strength. It has been recognised that deformed bars have better bond properties than smooth bars. The reason is that deformed bars benefit from the mechanical anchorage supplied by the concrete keys between the ribs. A number of investigations were carried out to determine the influence of the rib height on bond behaviour. The results showed that for unconfined bars, the relative rib area (R_r) (defined as the projected rib area normal to the bar axis divided by the nominal bar perimeter multiplied by the centre to centre rib spacing) has no influence on bond strength. For confined bars, however, the bond strength increases by increasing the relative rib area (ACI 408 2003). In this way, the bond strength of reinforcing bar is a function of relative rib area. In general, increasing the relative rib area of steel bar, increases the bond strength (Cairns and Abdullah, 1995; Darwin and Graham, 1993; El-Hacha et al., 2006). Recently, Chan (2012) investigated the effect of different grades of deformed bar types with different rib patterns and relative rib area (R_r) on bond strength. It was observed that the specimens with steel bars which had the higher R_r exhibited higher bond stress.

2.3.2 Effect of bar diameter

The steel bar size is one of the most important factors affecting the bond stress between steel reinforcement and the surrounding concrete. The ribbed bar influences the bond strength, while larger bar diameters develop lower bond strength compared to smaller bar diameters. This effect is acknowledged in ACI 408 (2003) by suggesting a steel bar size factor in its development length formula. Moreover, the influence of reinforcing bar diameter on the bond strength has been investigated by several researchers. Ichinose et

al. (2004) have provided experimental evidence that the influence of the bar size on the bond strength depends on the level of confinement. In their tests, the bond strength was found to decrease with increasing bar size for specimens with low levels of confinement and splitting failures, but this effect was negligible for specimens with high levels of confinement and pull-out failures. This was somewhat supported by Turk and Yildirim (2003) who reported that the diameter of the steel bar had a very important effect on the bond strength. Other researchers, such as De Larrard et al. (1993) reported that the bond strength of a 10mm diameter reinforcing bar was higher than that of large diameter steel reinforcement suggesting that the bond strength decreased with increasing diameter of steel reinforcement.

2.3.3 Effect of compressive and tensile strength of concrete

The bond strength mechanism is actually dependent on the stress transfer from the steel reinforcement to the concrete with compression and shear interaction forces. Therefore, the bond behaviour is dependent on both the compressive and the tensile strength of concrete. When considering splitting and pull-out modes of bond failure, the tensile strength f_{ct} of concrete is a more important parameter than the compressive strength because splitting is approximately proportional to $(f_{c'})^{1/2}$, where fc' is the compressive strength of concrete and the bond strength traditionally has been indicated as $(f_{c'})^{1/2}$. However, regression analysis on different experimental results showed that a superior correlation exists between bond strength and $(f_{c'})^{1/4}$ for bond failure (ACI 408 2003). Arel and Yazici (2012) investigated the effect of different compressive strength and tensile strength of concrete on the bond strength between steel and concrete. The concrete strength ranged between 13.46 to 75.40 N/mm^2. They found that the bond strength increased with an increase in both the compressive strength and tensile strength of concrete. Kankam (2003) studied the influence of concrete grade on the bond

strength by using two different concrete grades (53 N/mm^2 and 31 N/mm^2). It was found that the higher concrete strength specimen had greater bond stress than the specimen with lower concrete strength. In another study, Valcuende and Parra (2009) studied the bond strength of steel reinforcement embedded in self-compacting concrete (SCC) and vibrated concrete (VC). This can be explained by the differences between the two types of concretes which vary with the compressive strength. In addition, this may possible be explained by SCC having greater fill capacity, which enables them to cover the reinforcements completely without the need for vibrators and its smaller amount of bleeding also reduce the occurrence of voids between the steel and concrete but in VC the process depends on the vibration treatment being correct.

2.3.4 Effect of concrete cover

The concrete cover is the distance between the reinforcing bar surface and the exterior face of the concrete element. It is another important parameter which governs bond stress failure. The increase of cover thickness can increase the bond stress at failure as a result of increasing the confinement on the steel bar prior to failure. Some authors have studied the effect of concrete cover on bond strength; they reported that the bond strength was increased with increasing the depths of concrete cover (Tepfers 1979 and Chana, 1990). Recently, Yalcier et al. (2012) studied the influence of concrete cover thickness of three different depths (i.e. 15mm, 30mm and 45mm) on bond strength. They reported that the bond strength was significantly increased when the concrete cover depth increased and the bond specimens were failed by pull-out failure.

2.3.5 Other factors

There are other factors that influence the bond strength between reinforcing bar and concrete, including environmental effects such as steel bar rusting. The effect of the corrosion of steel reinforcement on structural behaviour is considered a major issue

today, as demonstrated by many experimental studies (Almusallam et al., 1996; Lee et al., 2002; Lundgren, 2002; Fang et al., 2004 and Dahou et al., 2009). This factor will be explained in further detail in the following section. In addition, high/low temperatures affect bond strength as reported by Royles and Morley (1983) Van der Veen (1992). Bingöl and Gül (2009) reported that the residual bond strength increased when temperature ranged from 50˚C to 150˚C due to the increase in the residual compressive strength. After that, the residual bond strength was decreased as temperature reached 150˚C. Moreover, Haddad et al. (2008) studied the influence of elevated temperature on bond strength of steel bar embedded in concrete. They found that the residual bond strength decreased slightly as the exposure temperature was raised to 350 ˚C due to the increase intensity and cracks with temperature leading to a reduction in concrete confinement of the steel reinforcement.

2.4 Corrosion of steel reinforcement in reinforced concrete

In reinforced concrete (RC) structures, concrete provides protection to the reinforcement bar. The dense and impermeable concrete provides the physical protection, whereas the alkalinity of the pore solution provides the chemical protection. The alkaline environment of concrete (pH 12-13) implies the formation of a passive film on the surface of the reinforcement bar that provides steel with corrosion protection (Glass and Buenfeld, 2000). However, the two main phenomena such as carbonation and chloride attack may lead to a breakdown in the surface layer of ferrous hydroxide that covers the steel in the alkaline concrete environment Ann and Song (2007). Carbonation characterised by the reaction between atmospheric carbon dioxide (CO_2) and water in concrete pores to form insoluble carbonate which, with the reduction of the pH value of the pore solution of concrete, leads to the corrosion of reinforcing steel. In

contrast, the chloride ions, for instance, sodium chloride found in sea water and salts used in the de-icing practices on the transportation network and calcium chloride ($CaCl_2$) still found in concrete admixtures, can result in the free passage of chloride ions through the concrete cover and depassivation of the reinforcing bar.

In reinforced concrete, corrosion affects the bond behaviour of the reinforcement due to the loss of steel bar cross-section. The concrete bond strength does not solely depend on the properties of the concrete but also on other factors such as; spalling and cracking of the concrete cover (see Figure 2.4).

1. Spalling is largely caused by the separation and disintegration of concrete. The main cause of spalling is growth of the corrosion products of the reinforcing bar leading to cracking and bulging of the concrete cover.
2. The corrosion of reinforcing steel or freezing and thawing can cause the separation of a coating from a substrate or the layers of coating from each other along a plane nearly parallel to the surface of concrete in a process known as delamination.

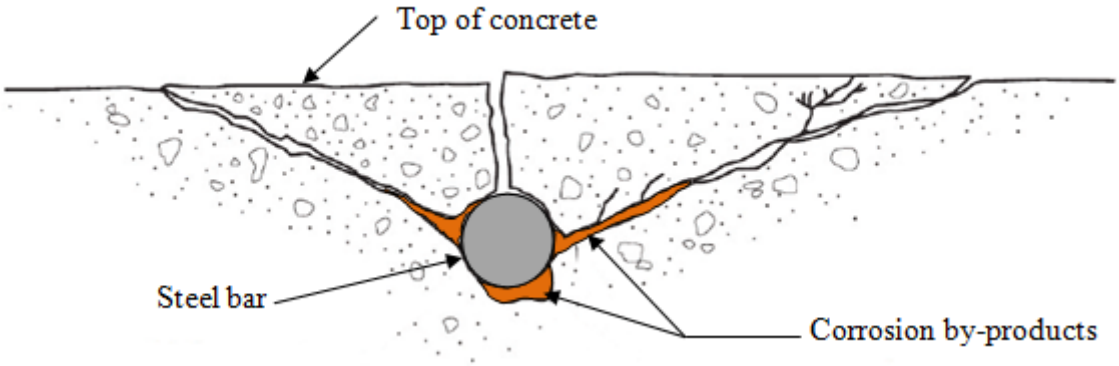

Figure 2.4: Diagrammatic representation of damage induced by corrosion cracking and spalling of concrete cover (modified from Baingo, 2012)

2.4.1 Mechanism of corrosion in concrete

As far as reinforced concrete is concerned, in the absence of chlorine ions and carbonate, the anodic reaction, which is the dissolution of iron, brings about the oxidation of the iron to ferrous iron (Fe^{2+}). On the other hand, the cathodic reaction uses the oxygen that diffuses to the steel in concrete through porous concrete and cracks to produce OH^- ions. The products of anodic and cathodic reactions then react to form a stable film. As well as being stable, this film is passive and helps to prevent further corrosion (Broomfield, 2007).

The anodic reaction:

$$Fe \rightarrow Fe^{2+} + 2e^- \quad (2.1)$$

The cathodic reaction:

$$2e^- + H_2O + \tfrac{1}{2}O_2 \rightarrow 2OH^- \quad (2.2)$$

In the presence of chloride ions, the corrosion of steel in concrete begins when the passive layer of the steel is broken. When chloride ions and carbonate are introduced into the reinforced concrete, the ions tend to attack the existing passive nature, thereby promoting the corrosion process. If the corrosion is caused by a chloride attack or carbonation, the chemical reaction remains the same but the chlorine ions which have the same charge as the OH^- competes with it to form films with Fe^{2+}. The films formed by the chlorine are mostly non-passive/soluble and cause a further corrosion process to continue (Broomfield, 2007 and Neville, 1995).

The anodic and cathodic reactions are the first steps in the process of rust formation. In the next stage, hydroxyl ions travel through the electrolyte and react with ferrous ions to form ferrous hydroxide which is, in turn further oxidised to rust (see Figure 2.5).

$Fe^{2+} + 2OH^- \rightarrow Fe(OH)_2$ (ferrous hydroxide) (2.3)

$4Fe(OH)_2 + 2H_2O + O_2 \rightarrow 4Fe(OH)_3$ (Ferric hydroxide) (2.4)

$2Fe(OH)_2 \rightarrow Fe_2O_3 . H_2O + 2H_2O$ (Hydrated ferric oxide) (2.5)

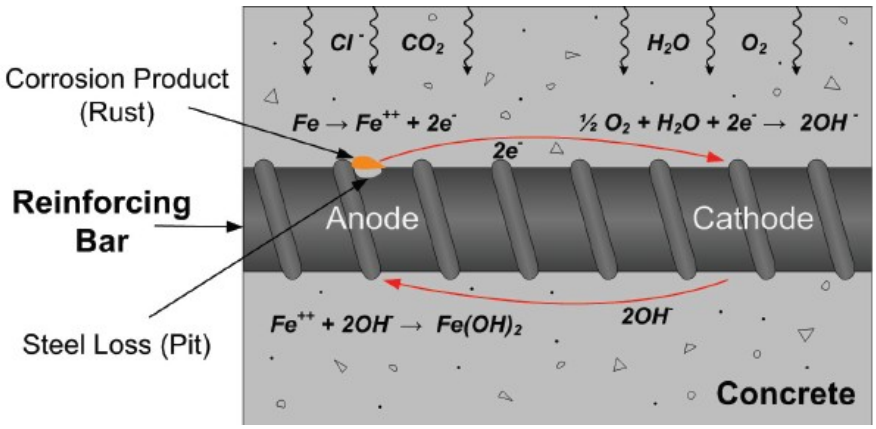

Figure 2.5: Schematic illustration of the corrosion of reinforcement in concrete (Ahmad, 2003)

When fully dense, the Fe_2O_3 volume is two times greater than the steel it substitutes, and upon hydration, the ferric oxide becomes porous due to the expansion it undergoes, then increasing the steel/concrete interface from two to ten, leading to fracturing and spalling. This gives the flaky rust layer on the surface of the reinforcing bar and can cause cracking and spalling of the cover concrete (Broomfield, 2007).

The corrosion process for steel reinforcement in concrete can be simplified as was first introduced by Tuutti (1982), wherein the service life of the RC structures with respect to the corrosion of steel reinforcement is usually divided into two distinct phases, the corrosion initiation phase and the corrosion propagation phase as shown in Figure 2.6:

- Initiation period, during which the steel remains in a passive state. The onset of corrosion corresponds to reinforcement de-passivation due to either carbonation of the concrete cover or accumulation of chloride ions at the rebar layer.
- Propagation period, during which the structure deteriorates as a result of loss of reinforcing bar cross-sectional area and accumulation of corrosion products around the steel surface. This phase lasts until an unacceptable degree of corrosion damage has occurred.

For chloride-induced corrosion, the initiation stage corresponds to the period of time during which chlorides penetrate the concrete without observed damage, until the chloride concentration required to start the corrosion process, also known as the threshold value (Martín-Pérez, 1999), is reached. Once the steel bar has been de-passivated, the corrosion rate is the rate-determining parameter of the progress of corrosion –induced damage.

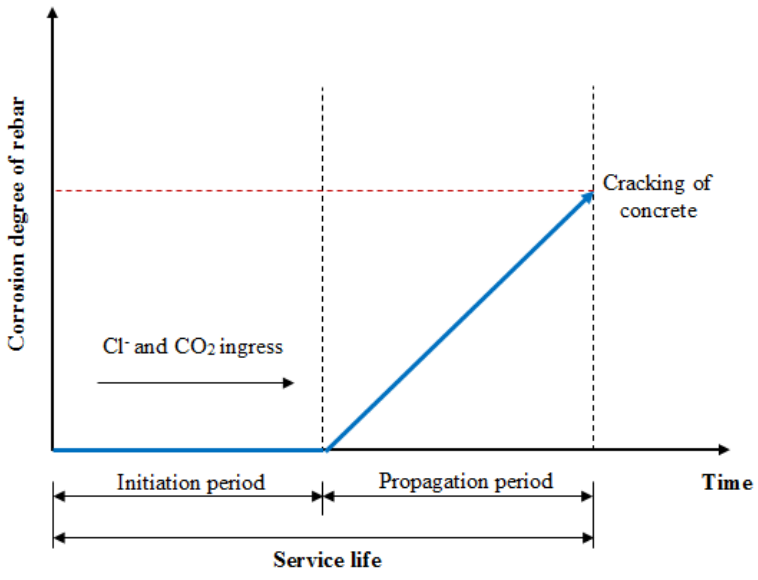

Figure 2.6: The corrosion process of reinforcing steel (Tuutti, 1982)

2.4.2 Pitting localised corrosion

The presence of pitting is regarded as localised corrosion. Localised corrosion is always associated with chloride ions and not with carbon dioxide ingress. The compounds formed during pitting corrosion are different from those formed in general corrosion as they have less volumetric expansion (FIB, 2000). Localised corrosion occurs at discrete sites along the reinforcing bar, often causing deep pits. As consequence this leads to very rapid and significant loss of the cross-sectional area of the steel bar (Batis and Rakanta, 2005). Pitting corrosion can completely penetrate the cross section of steel reinforcement in a relatively short period of time.

2.5 Chloride-induced corrosion in concrete

Chloride attack is a major concern in reinforced concrete. The chloride may originate from the constituents of the concrete mix itself or from the diffusion of chloride ions from the surrounding environment (Roberge, 2000). It may also be introduced as an impurity within the aggregates. In developing countries where there is no easy access to clean water, sea water is used in the concrete mix which introduces chloride into the system. Chlorides always act as catalysts to the corrosion process when they are found in sufficient concentration. Another way by which chloride is introduced is through the de-icing process. In temperate regions such as the UK, Canada and Norway where seasonal snow fall occurs, the salts of chloride are used in the de-icing process. This salt can penetrate the reinforced concrete and cause corrosion to occur. Even structures built by the sea or used by the sea can have chlorine introduced to them through seawater. The chlorine in pore solution causes the adjacent metal to go into dissolution at a local site (Broomfield, 2007). There are three main theories that have been given for the interaction of chloride ions with a steel bar. According to the adsorption theory chloride

ions are adsorbed onto the surface of the reinforcement in preference to dissolved oxygen and hydroxyl ions and the reaction rate of iron with the chlorides is higher and soluble complexes are formed. In the oxide film theory, it is postulated that the chlorides attack the passive layer surrounding the steel bar through pores and attack the iron underneath (ACI 222, 2001). This interaction and adsorption of chloride ions onto the steel (re-bar) increases the elimination rate of the iron ions out of the reinforcing steel bar into solution. Lastly, the transitory complex theory states that a soluble iron chloride is formed rather than the insoluble film formed with hydroxyl ions when chlorides replace the hydroxyl ions and the passive layer is then disrupted. Iron chloride breaks into the chloride ion then migrates away from the anode. This is assumed also to free the chloride ions and allows them to continuously react with the reinforcing steel bars (ACI 222, 2001).

2.5.1 Effect of corrosion of reinforcement on bond strength

Corrosion of steel reinforcement in concrete reduces bond strength between steel and concrete and thus affects the durability and serviceability of concrete structures. In last few decades, the influence of corroded steel reinforcement on the bond strength of reinforced concrete members has been investigated by numerous researchers. Al-sulaimani et al. (1990) found from studies of the effect of steel reinforcement corrosion and bond strength up to approximately 1% of corrosion level due to the increased roughness of the reinforcing bar surface at early stages with a firmly adherent layer of rust. This is in agreement with experimental results obtained from RC beam tests, which increased in bond strength when the degree of corrosion increased up to 4% due to the increase of radial pressure caused by the expansion of the corrosion products (Mangat and Elgarf, 1999b). Almusallam et al. (1996) also demonstrated that in the pre-cracking stage the bond strength is increased, but with an increase in the corrosion level the slip

at the ultimate bond strength reduces. Experimental studies showed an increase in bond strength during the initial corrosion level to about 2%. In agreement with the above results, significant literature has been published in this area by Cabrera (1996), Amleh and Mirza. (1999), Auyeung et al. (2000), Fang et al. (2004) and Ouglova et al. (2008). Initially, the increase in bond strength was attributed to the production of a firm layer of rust around the reinforcing steel bar which, results in increased bond strength. After the development of longitudinal corrosion cracks the bond strength reduced dramatically and the reduction in bond strength was attributed to the loss of the bearing component as a result of the ribs of the steel bars being decreased by corrosion. In addition, with a high corrosion level the tensile hoop stress in surrounding concrete exceeded the tensile strength, leading to splitting of concrete cover which decreased the bond strength and increased the slip. Figure 2.7 shows the relationship between bond strength and corrosion level based on published data from pull-out tests for different steel bar diameters.

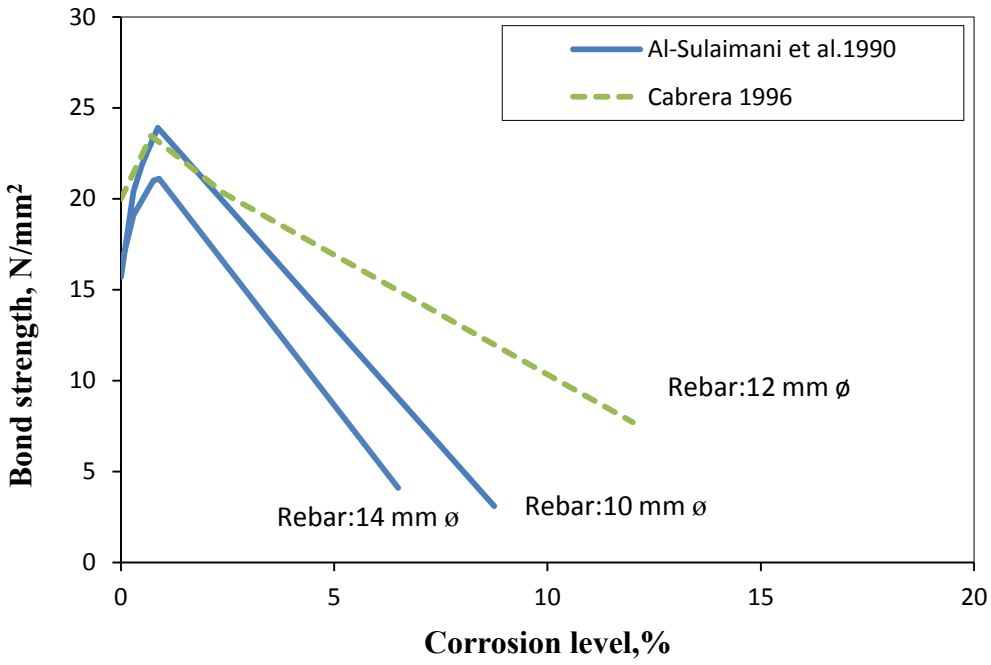

Figure 2.7: Bond strength versus corrosion level (data from Al-Sulaimani et al. 1990; Cabrera, 1996)

Moreover, many researchers have continued to investigate the effect of corrosion on bond strength by using various analytical and numerical models (Berra et al., 2003 and Lundgren 2005a, 2005b). Fang et al. (2006) investigated the influence of reinforcement corrosion on bond between steel and surrounding concrete by using a pull-out test and finite element analysis (FEA). In their study, steel corrosion was examined by an electrolyte corrosion technique. Deformed bars 20mm in diameter were used, and all the results concluded that the bond strength of the unconfined steel bar (no corrosion) was not significantly lower than the confined strength, but for corroded bars (around 4-6% in terms of corrosion level), the bond strength of unconfined steel bars was lower than confined steel bar by 30% to 45%. However, both the analysis and results of the experiments exhibited to that of the bond strength of unconfined steel bars corresponded to the confined steel bars with similar corrosion. The results of the FE analysis displayed a reasonably good agreement with the experiments regarding bond strength and bond stiffness.

More recently, an experimental study was conducted by Abosrra et al. (2011) to evaluate the effect of corrosion of embedded steel in concrete of different compressive strengths (20, 30 and 46 N/mm^2). They observed that the bond strength was affected by the corrosion levels. They also found that when the exposure time increased up to 7 days the bond strength was reduced due to the formation of longitudinal cracks because of corrosion. Moreover, another experimental investigation was carried out by Yalciner et al. (2012) to study the effect of corroded steel reinforcement on the bond strength. Their study was designed to use different compressive strength of concrete (23 and 51 N/mm^2) with three different concrete cover depths (15mm, 30mm and 45mm). It was observed that the bond strength of control specimens (un-corroded) were increased with

an increase in compressive strength and concrete cover depth. Moreover, they concluded that the results for specimens with higher concrete strength and corroded steel reinforcement for specimen with low concrete cover concrete showed a higher percentage of bond strength degradation because of concrete cracking during the pull-out tests.

Mansoor and Zahang (2013) studied the influence of corrosion of reinforcing bar on bond through the use of two different concrete strengths. Their study found that the deformed bar was affected by corrosion level, the bond strength was decreased by approximately 16% when the corrosion level increased up to 2%. Moreover, the corrosion rate of steel with high concrete strength was lower than that of the low concrete strength which may be attributed to lower porosity and impermeability of concrete.

To date, the results obtained from studies carried out to investigate the influence of corrosion indicated a considerable decrease in the bond strength with an increase in corrosion level. However, limited studies were reported on the effect of corroded steel reinforcement on bond strength with cement replacement materials.

2.5.2 Effect of corrosion on the flexural strength of RC members

The effect of corrosion on flexural strength has been investigated by a large number of researchers and is well understood. Several studies conducted in this area are explained briefly in the following section with a critical evaluation of their applicability to corrosion influences on the flexural strength of reinforced concrete beams.

The early work of Almusallam et al. (1996) concerned tests on 63mm × 305mm × 711mm simply supported one-way slabs (centre to centre 610mm span) reinforced with five 6 mm diameter bars placed at 57mm centres. The slab specimens were partially

immersed in 5% NaCl solution, and a constant current of 2A was applied to the reinforcing bars. It was observed that the corroded bar changed the failure mode in the control samples to bond shear failure in the corroded slabs, and a reduction in the ultimate flexural strength of the slabs was also observed; 25% and 60% reduction in ultimate strength for 5% and 25% reinforcing steel corrosion respectively.

Mangat and Elgarf (1999) investigated the effect of corrosion on the flexural strength of RC beams by examining a total of 111 simply supported beams. The beam specimens were tested using four-point loading and all beams were subjected to an accelerated corrosion technique in the laboratory. The flexural capacity compared to control samples (0% corrosion) was reduced to about 25% in residual strength and the ultimate flexural strength was significantly reduced to about 75% at 10% of corrosion. Yoon et al. (2000) reported on the mutual influence of mechanical loading and the corrosion of steel reinforcement on the serviceability of RC beams. It was found that both the loading level and loading history could significantly affect the rate propagation of corrosion. Furthermore, when increasing the degree of corrosion, the failure mode transferred from a shear failure to bond splitting.

Other authors, Ballim and Reid (2003) investigated the effect of reinforcing bar corrosion on the performance of the reinforced concrete beam in terms of simultaneous load and varying conditions of corrosion. At an early stage, 6% of the mass of steel bar was corroded, the deflection of the beams (at SLS) was increased by 40-70% when compared to the deflection of the control specimens.

Chung et al. (2004) carried out a series of slab tests with 10mm diameter steel bars during which the slabs were tested with a four point load. The specimens were subjected to 3% salt solution and an accelerated corrosion method was used. The corrosion level

varied from 0% for the control samples to 15% for other samples. They observed that up to a 2% level of corrosion rapidly reduces the resisting force. The results of the analysis showed that there was an apparent influence of the corrosion level on bond strength and development length. Also, when the corrosion level reached more than 2%, the resisting force rapidly decreased.

Many researchers have developed models to predict the flexural strength of corroded RC beams. Wang and Liu (2006), Azad et al. (2007), and Lundgren (2007) reported that the analytical results of predictions for the flexural strength of RC beams agreed well with the experimental results.

A recent study by Chung et al. (2008) tested 70 simply supported slabs with 10 mm diameter bar using a four- point load. It was observed that the behaviour of the slabs with the corrosion of the reinforcing bar can be predicted with good accuracy. They found that a small quantity of corrosion increased the flexural capacity of the slabs, however, when the significant loss of the reinforcement area exceeds 2%, the capacity of slabs decreases at higher corrosion levels.

2.6 Factors affecting the corrosion of reinforcement

The corrosion of steel bars in concrete is affected by a wide range of parameters such as water-to-cement ratio, permeability, concrete cover, crack width and the use of supplementary cementitious materials (SCMs), but the two discussed here (crack width and SCMs) are considered to be the most important because of the critical need to ensure the durability of concrete construction in severe exposure conditions.

2.6.1 Effect of crack width

In the past, several researchers have studied the impact of cracks on the generation and development of reinforced concrete corrosion. Mehta and Gerwick (1982) discussed the

problem of identifying whether corrosion causes cracking or cracks cause the corrosion of concrete. They suggested that the total area covered by cracks next to the surface of the steel plays an important role for significant corrosion to occur and corrosion protection must be assured by use of good quality concrete and suitable cover.

Alonso et al. (1998) reported that an increase in porosity (w/c ratio) produces a delay in the generation of cracks from corrosion and this was attributed to the higher quantity of void space available to accommodate corrosive products without stress generation. Indeed, many recent theoretical models for predicting the time to initial cover cracking have incorporated a 'free-expansion' step to account for the time required for corrosion products to fill the porous cement paste surrounding the reinforcing steel.

Francois and Arliguie (1998) observed that the width of cracks less than 0.5mm influences the initiation of the corrosion, but at later stages the crack width has an insignificant influence on the process of corrosion. However, the same investigators reported that, the corrosion development was not affected by the crack widths or by a crack itself but rather it was affected by the penetration of chloride due to paste-aggregate interface damage caused by the blending load to reinforced concrete beam and then in the corrosion of the steel bar.

In another study Mohammed et al. (2001) the effect of crack width on corroded reinforcing bar was investigated, with single crack specimens, 100 × 100 × 400mm and crack widths of 0.1, 0.3, and 0.7mm. It was concluded that at the early age of exposure to chloride ions a relationship between the rate of corrosion and crack width was observed at 0.3mm. The crack width and corrosion rate relationship is unclear compared with the water-to-cement ratio and the corrosion rate relationship.

2.6.2 Effect of SCMs on corrosion of steel bar

The corrosion of reinforcing steel is considered the major durability problem of reinforced concrete. The use of Portland cement and supplementary cementitious materials, SCMs (such as fly ash, ground granulated blast-furnace slag, metakaolin and silica) can significantly improve the corrosion resistance in reinforced concrete and reduce the permeability of concrete. A number of researchers have studied the effect of SCMs on the corrosion rate, and these will be studied in further detail below.

Several researchers have studied steel bars embedded in concrete. For instance, Cabrera (1996) examined the effect of fly ash on the rate of reinforcing bar corrosion by using, up to 30% low calcium fly ash (PFA), typical of the UK. The results concluded that the fly ash concrete samples showed superior corrosion resistance than the ordinary Portland cement (OPC) because the PFA reduced the permeability of concrete, but Al-Amoudi et al. (1993) investigated the long-term corrosion of reinforcing bars embedded in ordinary Portland cement (OPC) and fly ash (PFA) concrete. The steel bar was immersed into 5% NaCl solution. They found that the corrosion resistance of concrete made with blended cements was better than that of the OPC concrete which was about one-half to one-twelfth of the control concrete specimens. This is due to the combined influence of permeability and reduction in the penetration of chloride ions in these concretes. Choi et al. (2006) tested the reinforcing steel embedded in fly ash concrete by immersing the specimen in 3.5% NaCl solution. In this study it was concluded that the partial replacement of fly ash has led to an improvement in corrosion resistance and a reduction of corrosion rate because of the reduction of permeability to chloride ions.

Ha et al. (2007) also investigated the effect of fly ash replacement levels (10-40%) on the corrosion performance of reinforcement in concrete and mortar. These were

evaluated by accelerated short-term techniques and subjected to 3% NaCl solutions. It is clear that up to 30% of fly ash replacement enhanced the resistance of the corrosion properties of steel in concrete and improved the permeability characteristics of concrete. This resulted in delaying the initial corrosion time and the corrosion rate was 0.098 mpy. Similarly, Saraswathy et al. (2003) also studied the use of up to a critical level of 20-30% fly ash replacement cement and showed that it improved both the corrosion resistance and concrete strength while, Scott and Alexander (2007) investigated that the fly ash with up to a 30% replacement with a crack of width 0.2mm or 0.7mm, resulted in at least a 40% reduction in the corrosion rate compared to ordinary Portland cement (OPC).

Huang et al. (1996) determined that the use of up to 10%, 15% and 30% replacement of cement with ground granulated blast furnace slag (GGBS) concrete offered significant corrosion resistance. Similar findings by Arya and Xu (1995) also reported that the corrosion of the mild steel bar in concrete reduced with increasing GGBS content, with the exception of the first 7 days after casting. Moreover, Torii et al. (1995) reported that the resistance to chloride penetration of 50% GGBS concrete was almost the same as that of 10% SF concrete. Furthermore, the results by Pal et al. (2002) showed that with increasing GGBS content, the corrosion rate and carbonation depth reduced. They studied the corrosion behaviour of an embedded steel bar with proportions of GGBS cement of 30%, 50%, and 70%. Also, there was an electrochemical examination and accelerated carbonation test for steel bar corrosion. The findings reveal that an increase in slag proportion is associated with a decrease in the rate of corrosion of steel reinforcement in slag concrete.

Moreover, another experimental investigation was carried out by Yeau and Kim (2005) to evaluate the corrosion resistance of two types of ordinary Portland cement mixed with varying percentages (0, 20, 40 and 55%) of GGBS cement replacement. They measured the surface area of corrosion on embedded steel and found the coefficient of permeability of ASTM Type I Portland cement concrete was lower than that of ASTM Type V Portland cement concrete. Their results indicated that the corroded surface area was dependent on the thickness of the concrete cover and the amount of GGBS cement replacement. In addition, the concrete (Type I) containing 40% GGBS can increase the corrosion resistance of reinforcing bar by more than two times, compared to the control concrete mix (without GGBS).

In another study by Cheng et al. (2005), it was reported that up to 40% GGBS cement replacement or more can be used with Type I Portland cement in order to increase the corrosion resistance of reinforcing steel in concrete and reduce the corrosion probability. Also, in their study the RCPT (Rapid Chloride permeability Test) results indicated that the lowest total charge-passed was 1864C in the 60% GGBS mix and the highest total charge-passed was 10271 C in the control mix (0% GGBS) sample. Recently, Topcu and Boga (2010) studied the influence of mineral admixtures on steel corrosion in cement reinforced concrete. GGBS cement replacement levels from 0% to 50% were and employed and it was found that by using GGBS mineral admixture up to a 25% replacement level corrosion resistant concrete.

2.7 Numerical modelling

Most of the existing numerical studies of the bond behaviour of RC elements are focused on solving models which independently account for the behaviour of the

concrete and the reinforcing material. Modelling their interaction is achieved via the application of a non-linear analysis using a specific bond-slip law.

In elastic models the strain-stress relationship for interface materials can be expressed in the following linear formulation:

For concrete $\sigma_C = E_C . \varepsilon_C$ (2.6)

For steel $\sigma_S = E_S . \varepsilon_S$ (2.7)

Considering the equilibrium and compatibility conditions for the pull-out test specimen shown in Figure 2.8 (a) and (b), the following equations can be presented (Jiang et al., 1984; FIB, 2000) (*assuming uniform stress σ_c on the relevant area A_c*):

$$d\sigma_c . A_C + d\sigma_s . A_S = 0 \quad or \quad d\sigma_s = \frac{-A_C . d\sigma_c}{A_S} \tag{2.8}$$

From (figure 2.7a), the bond stress (τ (s)) can be expressed as:

$$\tau(s) = \frac{A_S . d\sigma_s}{\pi . \emptyset . dx} \qquad or \quad \frac{d\sigma_s}{dx} = \frac{4.\tau(s)}{\emptyset} \tag{2.9}$$

From (Figure 2.8b), the stress-strain relation can be expressed as:

$$\varepsilon_s - \varepsilon_c = \frac{ds}{dx} = s' \quad or \quad s' = \frac{\sigma_s}{E_S} - \frac{\sigma_C}{E_C} \tag{2.10}$$

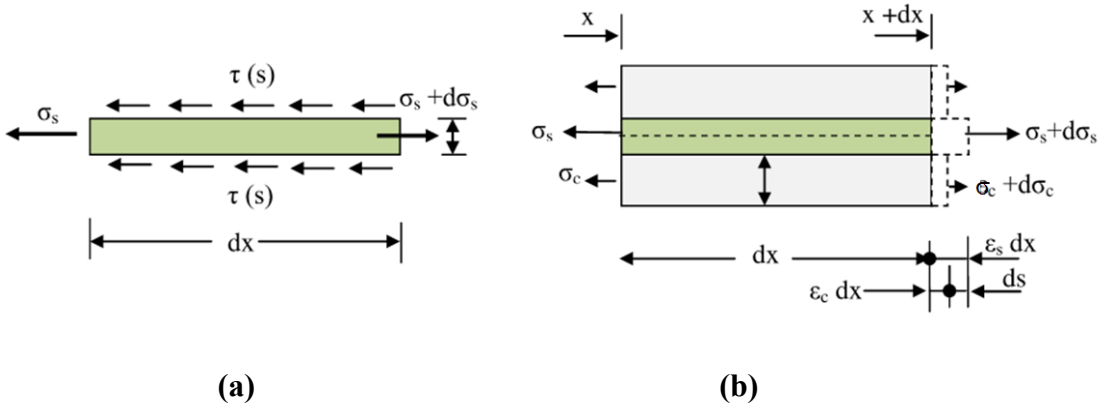

Figure 2.8: (a) Stress acting on reinforcing bar (length dx); (b) Stress and strains in the steel and in the concrete

2.7.1 Model Code 1990 for interface model

Many authors have already investigated the behaviour of steel bars and a number of analytical bond-slip models have been developed. One of the most widely used bond stress-slip relationships was proposed by Eligehausen et al. (1983) which has been the basis for the CEB-FIP Model Code (CEB-FIP 1990) as reported in Table 2.1 for confined concrete with good bond conditions.

Table 2.1: Parameters for bond-slip model (CEB-FIP Model Code 1990)

Parameters	**units**	**Model Code 90**
S_1	mm	1.0mm
S_2	mm	3.0mm
S_3	mm	Distance between ribs
α	-	0.4
τ_{max}	N/mm^2	$2.5.\sqrt{f_c}$
τ_f	N/mm^2	$0.40.\ \tau_{max}$

The bond-slip curve consists of three parts, namely the ascending part of curve, and followed by a plateau and then the descending part of the curve as shown in Figure 2.9. The ascending region of the model follows the formula given in Eq. 2.11(a-d) (CEB-FIP 1990).

$$\tau(s) = \tau_{max}\left(\frac{S}{S_1}\right)^{\alpha} \quad \text{for} \quad 0 \le S \le S_1 \qquad (2.11a)$$

$$\tau(s) = \tau_{max} \quad \text{for} \quad S_1 \le S \le S_2 \qquad (2.11b)$$

$$\tau(s) = (\tau_{max} - \tau_f\left(\frac{S-S_2}{S_3-S_2}\right) \quad \text{for} \quad S_2 \le S \le S_3 \qquad (2.11c)$$

$$\tau(s) = \tau_f \quad \text{for} \quad S > S_3 \qquad (2.11d)$$

Where τ is the bond strength; τ_{max} is maximum bond strength; τ_f is ultimate bond strength and s is ultimate displacement.

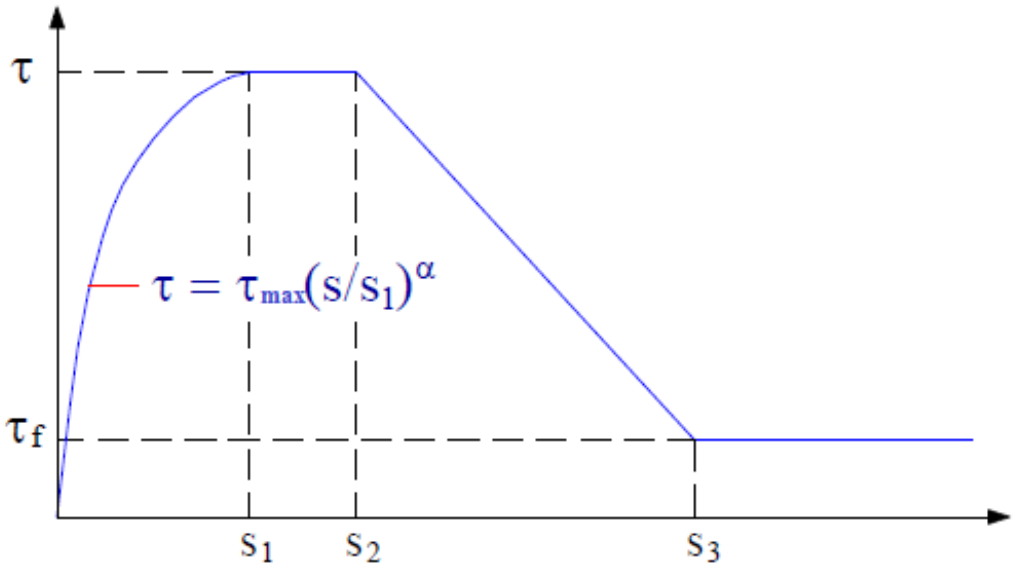

Figure 2.9: Analytical relationship of bond stress-slip (CEB-FIP MC 1990)

2.7.2 The bond - slip of steel reinforcement

There are two common approaches for incorporating the effect of reinforcement concrete interaction into the finite element analysis of reinforced concrete structures, namely the bond-link and the bond-zone element methods.

2.7.2.1 Bond-link element method

One of the earliest attempts to describe the bond in RC beams is that of Ngo and Scordelis (1967). A link element was defined, which can be conceptualised as two orthogonal springs which connect the steel bar node to the corresponding concrete node (see Figure 2.10(a)). Moreover, the bond link element has no physical dimensions, the two connected nodes have the same coordinates, and as a result they have the same degrees of freedom (DOF). This approach has been used in many finite element model packages e.g. ANSYS and ABAQUS.

2.7.2.2 Bond-zone element method

The bond zone element was developed by De Groot et al. (1981). The contact surface between the steel bar and concrete, along with the surrounding concrete in immediate proximity, was modelled by a material law that represents the special properties of the bond-zone (Khalfallah, 2008). This method can be implemented in ABAQUS and is consequently used in the present study reported in Chapter six of this thesis (see Figure 2.10 (b)).

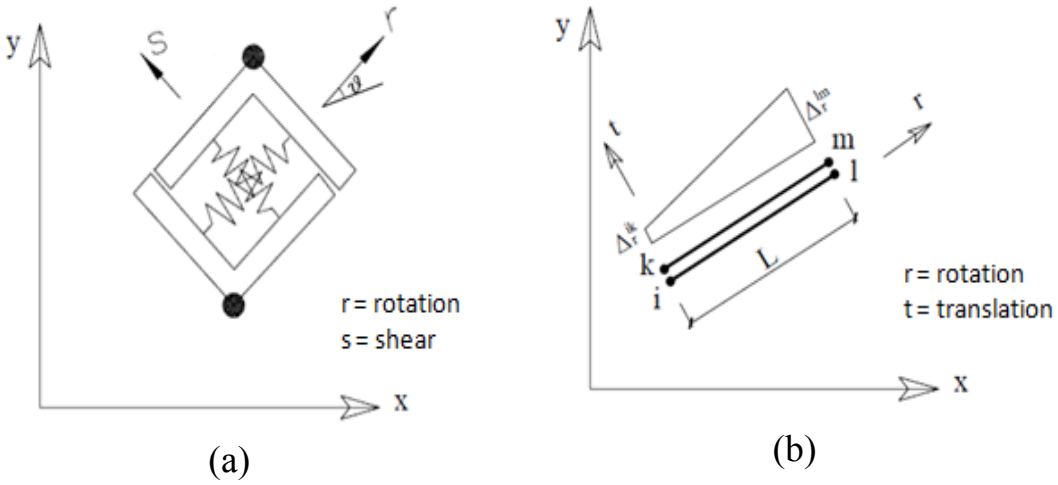

Figure 2.10: (a) Bond link element; (b) Bond zone element

2.8 Concrete Permeability

Permeability is an important characteristic essential for assessing the performance of concrete. Moisture can move into concrete by the processes of pressure driven flow and diffusion. Permeability is defined as the property that governs the rate of flow of a fluid into a porous solid (Neville, 1995). The permeability of concrete is dependent on the size, distribution and connectivity of capillary pores within the cement paste. The permeability is hence an important factor for controlling the movement of gases, liquids and chloride ions through the pore structure of concrete. It is therefore one of the most important properties affecting the durability of structure.

2.9 Factors affecting permeability of concrete

The permeability of concrete is affected by the component materials and the mix composition. The main factors influencing concrete permeability are the water to cement (w/c) ratio, damage of concrete (i.e. chemical and physical), aggregate size and the nature and quantity of cement replacement materials (mix composition) (Elshab, 1997 and Gardner, 2005).

2.9.1 Effect water-to-cement ratio on the permeability

The w/c ratio is the most important factor governing concrete permeability. The permeability increases with increasing w/c ratio due to an accompanying increase in porosity. Lydon (1995) investigated the effect of w/c ratio on the intrinsic permeability of two types of concrete. It was found that the permeability increased with w/c ratio, with specimens whose ratio was 0.5 exhibiting a higher intrinsic permeability than those with a w/c ratio of 0.4. Sanjuán and Muñoz-Martialay (1996) studied the effect of w/c ratios on the air permeability of concrete. In their study, the range of w/c ratio was

between 0.37 and 0.52, and the specimens were preconditioned at 20, 40 and 80 °C. They found that the air permeability coefficient increased with increasing w/c ratio especially in samples at higher temperature (80 °C). In another study by Ahmad et al. (2005) it was found that the w/c ratio has a significant influence on permeability of concrete. It was shown that the permeability increased considerably with an increase in w/c ratio. They also reported, in accordance that the permeability increased more rapidly when the w/c ratio approached 0.6.

2.9.2 Effect of damage of concrete (Physical, Chemical)

The damage of concrete is a key factor affecting the permeability of concrete, and can be considered in two groups: corrosion and physical damage. Chemical damage occurs as a result of a chemical reaction which produces a corrosion layer on the steel bar surface, which in turn leads to cracking and damage of concrete as explained earlier in the literature review (see section 2.4).

Wang et al. (1997) investigated the relationship between crack characteristics and concrete permeability. In their study, splitting strength concrete specimens were used to measure the effect of crack width on permeability. They found that the permeability of concrete increased with an increase in crack width. They also concluded that a crack width smaller than 50μm had little effect on concrete permeability, but as the crack was increased from 50 to 200μm, concrete permeability increased rapidly. Picandet et al. (2001) investigated the effect of axial compressive loading on the gas permeability of concrete. Mechanical damage was induced by applying compressive uniaxial loading onto concrete cylinders of length 220mm and diameter 110mm using a hydraulic press under load control specimens. The stress level was applied under cyclic loading which varied between 60% and 90% of the ultimate strength. A 50mm thick disc was then

extracted from the central part of the concrete cylinders to be used in the intrinsic gas permeability test. They concluded that a uniaxial compressive load at 90% of the ultimate strength increased the permeability by approximately one order of magnitude after unloading when compared to the undamaged sample. Kermani (1991) found that concrete permeability increased with an increase in applied stress level also depended on the type of mix and the magnitude of the applied pressure. Recently, Tegguer et al. (2013) concluded that the gas permeability of both ordinary Portland concrete (OPC) and high performance concrete (HPC) increased with an increase of the residual strain. This is attributed to the gas flow through the pores (and also through cracks in the case of cracked concrete). Therefore, the gas permeability was higher when higher residual strain was higher.

Yi et al. (2011) investigated the effect of hydraulic pressure and crack width on the water permeability. They reported that an increase in crack width and hydraulic pressure resulted in a considerable increase in water transport. They added that the crack had little effect on concrete permeability when it was smaller than 50μm but when the crack width was increased between 50 and 100μm the concrete permeability value increased rapidly by approximately 19 times.

2.9.3 Effect of cement replacement materials on permeability

Supplementary cementitious material is widely used in concrete, and has increasingly been accepted as a cement replacement material in construction for improving the properties of concrete or mortar. The use of pulverised fuel ash or fly ash, ground granulated blast-furnace slag, metakaolin and silica fume seems to improve the workability during the production of concrete and to enhance the durability of concrete (Siddique and Khan, 2011). Many researchers have investigated the effect of using

replacement materials on the permeability of concrete. It is the general consensus that the use of cementitious materials decreases the permeability of concrete.

An early study by Nagataki and Ujike (1986) showed that concrete containing fly ash cured in water after 91 days had a lower air permeability compared to a control specimen made without fly ash. This was due to the pozzolanic reaction of fly ash occurring in the later stages of curing. They found that the concrete with fly ash replacement materials at 28 days was equivalent to the control concrete specimen, since it exhibited the same level of compressive strength. In a related study, Thomas and Matthews (1992) found that three concretes made with fly ash levels of 15, 30 and 50% cement replacement exhibited a reduction in the oxygen permeability value of approximately 50, 60 and 86% respectively compared to the control concrete (without fly ash).

McCarthy and Dhir (2005) studied the effect of a high volume of fly ash (45%) on air permeability by using various inlet pressures to measure the flow resistivity. It was concluded that the intrinsic permeability was reduced by increasing the compressive strength. The values were lower than that of control concrete (OPC) by between 20% and 40%. Another investigation by Van den Heede et al. (2010) also studied the influence of high-volume 50% fly ash (HVFA) on the gas permeability of concrete. In their study, the specimens were complete dried at 105°C. They observed that the concrete containing fly ash had lower oxygen permeability values as compared to the control concrete; 78.9% and 68.0% lower at 28 and 91 days of curing, respectively. Kasai et al. (1983) studied the air/gas permeability of mortar containing fly ash and ground granulated blast-furnace slag. The study was concerned with the durability aspects of concrete with respect to carbonation. In the case of 7 days of curing, the

specimens having blended cement displayed a higher permeability than that of the specimen with Portland cement. However, the permeability of the mortar specimen made with blended cement decreased with increasing curing time. In general, the permeability was found to be directly related to the compressive strength development of the mortar.

Shi et al. (2009) investigated the effect of fly ash on the nitrogen gas permeability of high-performance concrete (HPC) up to 180 days of age. Fly ash replacement levels were 0, 15, 30, 45 and 60% by weight and the water/binder ratios were 0.25 and 0.3. They found that the coefficients of gas permeability of concrete with a PFA content of up to 45% were slightly higher than that of the control HPC but when the increase in PFA content was up to 60% with a higher w/b ratio of 0.3, the gas permeability coefficient significantly increases due to the fact that HPC is much denser and hydrates slower than normal concrete. According to Bamforth (1991) and McCarthy and Dhir (2005) fly ash can cause a significant decrease in the permeability of normal concrete. This is due to the increase of fly ash content and enhanced microstructure because of pozzolanic reaction.

Recently, Nath and Sarker (2013) studied the effect of high volumes of fly ash on the water permeability of concrete. In their study, the cement replacement used was 30% and 40% class F fly ash. They concluded that incorporation of fly ash reduced the water permeability at an early age and beyond a curing time of 180 days the water permeability was lower than that found in the Portland cement specimen. They further showed that the concrete made with 40% fly ash at 180 days of curing invoked a greater reduction in water permeability than that made with 30% fly ash.

Güneyisi et al. (2012) investigated the effect of both metakaolin (MK) and silica fume (SF) on the gas permeability of high performance concrete. In their study, concrete was manufactured with w/c ratios of 0.25 and 0.35, and the percentages of cement replacement were 5% and 15% for both MK and SF concretes. Oxygen was used to determine the coefficient of gas permeability. Moreover, to condition them the specimens were dried at 105°C in an oven and were tested at the age of 28 days to ensure that the change in weight of each specimen was less than 1%. The authors concluded that the MK and SF concretes had significantly lower permeability coefficient at both w/c ratios compared to that of the control concrete. This is due to the refinement in concrete pore structure caused by the addition of MK and SF cement replacement.

Song et al. (2010) studied the effect of silica fume on the permeability of concrete. In their study, the percentage of silica fume employed was 8% and 12%. They reported that the permeability of concrete was dramatically decreased when the silica fume replacement was at 8%. It was also concluded that the permeability was lowered further when silica fume content was increased up to 12%. This is attributed to the fineness of silica fume.

2.9.4 Effect of conditioning (moisture content)

The moisture content of concrete specimens has been found to be an important factor affecting the concrete permeability. Many researchers have studied the influence of conditioning or moisture content of the concrete by using high temperature to accelerate the drying process to remove moisture from concrete. Martin (1986) found that the moisture content of a concrete sample will considerably reduce its permeability. Prior to testing, samples should be stored in air for at last two months after being removed from the water tank. A study by Lydon (1993) examined the effect of moisture content on

permeability of concrete. It was found that moisture content plays a major role in determining the relative permeability of concrete. A change in the value of moisture content by 1% had a greater effect than changing the w/c ratio from 0.65 to 0.40. Elshab (1997) examined the influence of different methods of curing regime on the permeability of different concrete (NSC and HSC). This was done by examining the effect of (a) curing in air, (b) in water followed by air and (c) curing by wrapping the specimens with two layers of Clingfilm for 7 days. The effect of moisture levels in the concrete cubes could then be observed. It was found that the highest relative permeability values were achieved for air-dried cubes as a uniform moisture distribution had been achieved, while the water-cured specimens had the lowest relative permeability values.

A study by Sanjuán and Muñoz-Martialay (1996) investigated the influence of the preconditioning temperature on the air permeability of concrete as a consequence of the internal changes in moisture. The specimens were oven-dried at 40, 60 and 80°C to a constant weight before testing. It was observed that the coefficient of air permeability of concrete increases with preconditioning temperature due to the lower degree of concrete saturation. Other researchers, such as Sugiyama et al. (1996) have conducted gas permeability tests on concrete subjected to various drying procedures, such that the concretes were at different degrees of saturation at the time of test. The results showed that the influence of drying on gas permeability was significant, and that the drying method had to be known to order to correlate the permeability with the chloride diffusion coefficient.

In summary, it is well know that the concrete moisture content has a significant influence on the measured permeability. Gardner (2005) examined the effect of the moisture content of the specimen on the gas permeability for both normal (NSC) and

high strength concrete (HSC) at two conditioning temperatures, 85 °C and 105 °C. Initial findings identified that a conditioning of 105 °C may damage the concrete, although it provided a quicker means of testing the permeability of concrete. It was concluded that in the case of permeability, the effect of concrete grade is significantly greater than the influence of conditioning temperature. In view of this conclusion, regarding the importance of the nature of the concrete, there is no apparent advantage in conditioning at 85 °C rather than at 105 °C especially as conditioning at 85 °C takes longer. Furthermore, it was found that the gas permeability of concrete is influenced by the moisture content. This was achieved through drying the specimens to achieve varying levels of weight loss and determining what effect this would have on the permeability of concrete.

2.10 Measurement of concrete Permeability

Permeability of concrete is the most important factor in determining the flow rate of liquid, gases and chlorides. There are many techniques commonly used to measure the concrete permeability. In this section three methods will be described: water permeability test; rapid chloride permeability test; and gas permeability test. The first two tests will be described only briefly because they are not used in this study. The gas permeability test has been used in this study to measure gas permeability of concrete, and hence more details of this method are given in the section 2.10.3.

2.10.1 Water Permeability Test (WPT)

The concrete water permeability test is considered to be an indirect method of measuring permeability. One of the main assumptions in this test is the validity of Darcy's Law, which states that velocity is proportional to the first power of the hydraulic gradient. It is therefore valid only for laminar flow conditions. Laminar fluid

flows are characterised by layers moving smoothly relative to one another with momentum transfer occurring at the molecular level. As velocity increases, the flow becomes more turbulent. There is established evidence to validate the application of Darcy's Law for measuring the flow of water through concrete (Collins, 1987). The water permeability coefficient can be calculated according to Darcy's law according to Eq 2.12.

$$K = \frac{\rho L g Q}{P A} \tag{2.12}$$

Where:

K = the coefficient of water permeability (m/s)

ρ = the density of water (kg/m^3)

g = the acceleration due to gravity 9.81(m/s^2)

Q = the flow rate (m^3/s)

L= the length of the concrete sample (m),

P= the water pressure (Pa)

A= the cross-sectional area of the specimen (m^2)

2.10.2 Rapid Chloride Permeability Test (RCPT)

There are several methods for the measurement of chloride permeability, but the traditional method is the rapid chloride permeability test (RCPT), developed by Whiting (1981). The RCPT is widely used, and consists of monitoring the electric current passed in 6 hours through a concrete specimen with a potential difference of 60 volts across it. The total charge passed, in coulombs, is related to chloride permeability.

2.10.3 Gas permeability tests

Penetration of gases into concrete may adversely affect its durability, especially in the case of carbon dioxide, which causes carbonation of the concrete and eventual loss of corrosion protection of the steel reinforcement. The penetration of gases from the inside of concrete contaminant structures (whether for storage, industrial processes, or disposal of hazardous, sometimes radioactive, waste) may also need to be controlled by designers in order to avoid build-up of pressure (Martin, 1986). The gas permeability of concrete has primarily been measured by two different methods, the relative permeability test and the intrinsic permeability test.

Martin (1986) developed a method test to measure the relative permeability of concrete in which Nitrogen gas was used because it was inert and did not react with concrete. A 100mm cube was drilled on two opposite faces with a central 6mm hole allowing it to be fastened between two cork pads and two steel plates, with the whole assembly being bolted together, as seen in Figure 2.11. Nitrogen gas was stored in a reservoir such that it could pass into the central hole of the concrete sample and permeate through the specimen to exit into the atmosphere. The standard initial pressure of gas used in the experiment was 10 bar. The rate of pressure drop in the reservoir was measured and then translated into a corresponding permeability index for the concrete. It was found that the moisture content was the main factor affecting the permeability results. Martin found the test to be quick and simple to carry out, with good repeatability provided the specimens were allowed to dry sufficiently before testing.

Later, Lydon (1993) measured the relative permeability of concrete by using a modified version of Martin's (1986) test set-up. A 100mm cube with a 6mm hole drilled into the centre of the sample. The cube sample was sealed inside a pressure cell, with the hole in the top of the specimen being aligned with a hole in the lid of the cell (see Figure 2.11).

The cell was charged with nitrogen gas at a pressure of 10 bar. The nitrogen gas is allowed entry into the cell after which it exits to atmosphere through the drilled hole in the top of the sample. The cell was connected to a reservoir of gas and the decay of pressure in the reservoir was monitored, and hence the relative permeability value of the concrete obtained. In addition, this method has the advantage that any size of geometry of specimen can be tested (subject to the cell size). The test provides a simple method to measure the permeability of concrete as the preparation time is reasonably short and the specimen can be repeatedly tested.

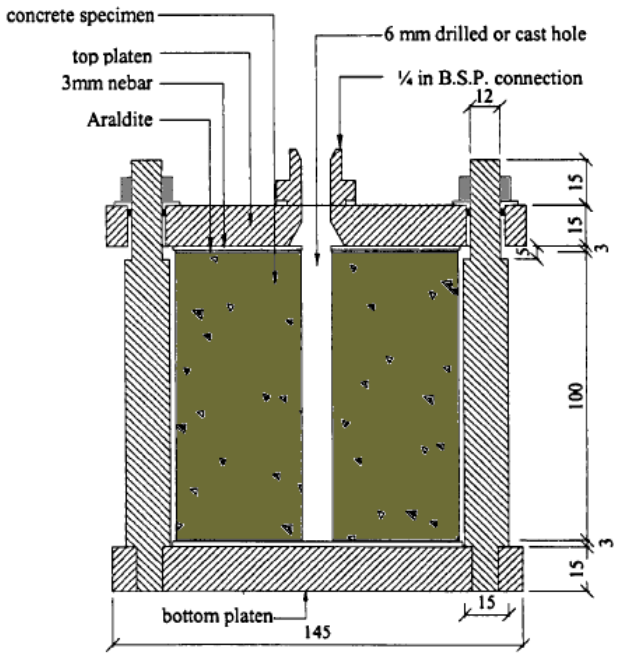

Figure 2.11: Section through the pressure cell (Martin, 1986)

Lydon and Mahawish (1991) developed a permeability test which measures the volume of gas which permeates a concrete specimen under a constant pressure. This test measures intrinsic permeability by causing unidirectional steady state flow through a defined path length of the concrete and the flow rate of the gas is recorded.

The intrinsic permeability coefficient (D_s) can be calculated as follows; (Lydon and Mahawish, 1991).

$$D_S = \frac{2VL\eta 10^{-5}}{A(P^2-1)} \quad (2.13)$$

Where:

V= volume flow rate of the permeating gas (m^3/s)

L= the path length (m)

η= the coefficient of viscosity of the gas (Ns/m^2)

A= the cross sectional area of concrete (m^2)

P= absolute pressure of the gas (bar)

Another method has been proposed by Gardner (2005) to calculate the intrinsic permeability of concrete with gas using the relative gas permeability results (see Eq.2.14). This equation was used to calculate the coefficient of gas permeability for cylindrical specimen concrete as follows:

$$k_{ef} = \frac{\ln\left|\frac{(P_{1/2}+P_{atm})(P_{c0}-P_{atm})}{(P_{1/2}-P_{atm})(P_{c0}+P_{atm})}\right|}{2t_{1/2}\pi h P_{atm}} V_0 \mu \ln(r_c/r_h) \quad (2.14)$$

Where:

k_{ef} = permeability coefficient (m^2)

$P_{1/2}$ = half pressure (578250 N/m^2)

P_{c0}= initial pressure (1053250 N/m^2)

h = height of sample (m)

P_{atm}= atmosphere pressure (N/m^2)

$t_{1/2}$ = time to reach $P_{1/2}$ (s)

r_c = outer radius of cylinder (m)

r_h= radius of hole (m)

V_0 = the combined volume of the reservoir and the gas surrounding the sample (m^3)

μ= dynamic viscosity (1.76×10^{-5} Ns/m^2)

2.11 Conclusions

Steel bar corrosion in aggressive environments is a primary cause of deterioration of concrete structures. Corroded steel embedded in the concrete leads to cracking, spalling of concrete cover, decreasing bond strength, reduction of steel cross-section and loss of serviceability of the reinforced concrete. This literature review has examined the influence of corrosion of reinforcing steel on bond behaviour of concrete structures. It is particularly evident that the main properties affecting the corrosion process are strength, cover thickness, permeability and cracking.

Based on the results of the previous researchers efforts detailed in this literature review.

- It can be said that despite the fact that several studies investigated the bond strength and flexure beam behaviour with ordinary Portland cement (OPC), very limited experimental investigations have been conducted regarding the bond strength behaviour with different cement replacement materials.
- The influence of the change in age of concrete with the use of additives and cement replacement materials on the corrosion rates of steel bar have not been included in the previous studies.
- The permeability of ordinary Portland cement can be distinctly higher than that of other cementitious materials. On the other hand, the concrete permeability depends on the type of cement replacement, curing time and percentage of cement replacement. Very limited information is available to investigate the influence of cement replacement and age on the gas permeability and corrosion rate when using the same mix proportions.

- No data has been reported on the relationship between permeability and corrosion rate of a steel bar in concrete.

Therefore, experimental studies will be performed to study the effect of cement replacement materials (cementitious materials) on the steel bar corrosion in concrete, and the effects of corrosion on the bond behaviour. Also, the influence of concrete permeability on the corrosion rate of steel bar will be investigated.

CHAPTER 3

EXPERIMENTAL PROCEDURES

3.1 Introduction

This chapter presents the main experimental test programme, which studies the effect of corrosion and use of cement replacement materials on the bond behaviour of steel reinforcement. The chapter also covers the specimen design, specimen preparation, mixing, details of casting and curing. To carry out the study, the following tests were used: accelerated corrosion, torsion test, pull-out tests and gas permeability test. The pull-out test (POT) was used to evaluate the bond strength between the steel reinforcement and the concrete, which was subject to five different levels of corrosion. To achieve a range of steel corrosion levels in concrete over a short period of time, the accelerated corrosion test using an electrochemical technique was employed. Additionally, the study included testing using the relative gas permeability test in order to evaluate the intrinsic permeability coefficient of the concrete. This particular parameter provides an indication of concrete durability and the rate at which corrosion may progress.

3.2 Materials

3.2.1 Cementitious materials

The cementitious materials which were used in this study will be explained in the following section.

3.2.1.1 Cement

The cement used in this study was a siliceous fly ash Portland cement (CEM II/B-V 32.5R) containing up to 7% fly ash, manufactured by Lafarge Cement UK Ltd, in accordance with BS EN 197-1:2000. The chemical composition and physical properties are presented in Table 3.1.

3.2.1.2 Pulverised fuel ash

Pulverised fuel ash (PFA) is also known as fly ash. PFA is a by-product of burning pulverised coal in furnaces of modern electrical power stations. The majority of PFA particles are spherical and amorphous ranging in size from 10 to100μm. The PFA is divided into two distinct categories, class F and class C, according to their chemical composition (Neville, 1995 and Haque and Kayali, 1998). In this research class F fly ash was used which was supplied by Ash Resources Ltd. The chemical composition and physical properties are presented in Table 3.1.

3.2.1.3 Ground granulated blast-furnace slag

The ground granulated blastfurnace slag (GGBS) is a by-product from the blast-furnaces used in the manufacture of iron. Blast-furnaces are fed with a controlled mixture of iron-ore, coke and limestone (Hadj-sadok et al., 2011). In Great Britain, GGBS is usually supplied as a separate component for concrete and can replace 70% or more of the Portland cement (Hanson, 2013). It was manufactured according to BS 6699 and supplied by Hanson UK. The chemical composition and physical properties are presented in Table 3.1.

3.2.1.4 Metakaolin

Metakaolin (MK) is an artificial pozzolana (ARGICAL-M1000). It is obtained by calcining of kaolinitic clay at temperature between 500 ºC and 800 ºC. In general, MK has particle size finer than cement but not as fine as silica fume. It was manufactured by

IMERYS performance & filtration minerals. The chemical composition and physical properties are presented in Table 3.1and Appendix A.

3.2.1.5 Silica fume

Silica fume (SF) is also referred to as micro-silica. SF is a by-product of the smelting process silicon and ferrosilicon alloys. It is extremely fine with particle sizes of 0.1 to 0.5μm, and such has a large surface area between 13,000 and 30,000 m^2/kg. It exists in a grey powder form SF and has a high silica content. Silica fume is used in concrete up to 10% (Shi et al., 2012). The SF used in this study was supplied by Elkem and its chemical composition and physical properties are presented in Table 3.1.

3.2.2 Fine aggregate and coarse aggregate

The fine aggregate used was a natural, marine-dredged sand (0-4mm) from the Bristol Channel, whereas the maximum size of coarse aggregate used was a 4-10mm crushed limestone aggregate, locally supplied from the Cornelly Quarry (South Wales) with an angular shape. Both the coarse and fine aggregate were dried, conforming to BS EN 12620.2002; prior to use. A particle size analysis of fine and coarse aggregate was conducted according to BS EN 933-1:1997 standards, details of which are provided in Appendix A.

Table 3.1: Chemical compositions and physical properties of cement and cement replacement materials used in concrete mixtures

Chemical Composition,%	**Cementitious materials**				
	CEM II**	GGBS*	PFA*	MK**	SF**
Silicon dioxide (SiO_2)	29.91	41.78	51.44	55.00	98.40
Aluminium oxide(Al_2O_3)	11.18	10.56	27.00	40	0.20
Iron oxide (Fe_2O_3)	4.13	0.27	6.13	1.40	0.01
Calcium oxide (CaO)	45.00	34.65	2.42	0.30	0.20
Magnesium oxide (MgO)	2.43	7.33	1.26		0.10
Sodium oxide (Na_2O)	0.38	0.50	0.66	0.80	0.15
Potassium oxide (K_2O)	1.45	0.64	2.72		0.20
Loss on ignition (LOI)	-	-	-	1%	0.50%
Physical property					
Specific gravity (g/cm^3)	3.15	2.9	2.6	2.5	2.4

* Chemical compositions of GGBS and PFA were obtained from XRD in Cardiff University Laboratories.
** Chemical and physical properties were provided by manufacture (CEM II, MK and SF).

3.2.3 Steel reinforcement

The steel reinforcement bar used in batch A was 12mm diameter high yield steel, the reinforcing bar (A) of Grade 500C supplied by the CELSA Group UK. The bars have two longitudinal ribs and rows of alternately inclined transverse ribs on both sides of the bars as shown in Figure 3.1. The bars conformed to BS4449:2005 and were used in the first group of experiments (set 1). Also, the reinforcing bar (batch B) was obtained commercially and used in the second group of experiments (set 2). Three 350-mm-long samples of ribbed bar were used to carry out tensile testing in the Cardiff University

Structural Performance (CUSP) Laboratories. The mechanical properties of the steel reinforcement bar are given in Table 3.2.

Table 3.2: Mechanical properties of steel reinforcement bars

Bar types	**Bar diameter**	**0.2% Proof**			**Ultimate**		**Modulus of elasticity**
	mm	Load (kN)	Stress (N/mm^2)	C.O.V (%)	Load (Kn)	Stress (N/mm^2)	(kN/mm^2)
A	12	62.2	550.5	0.90	74.0	654.4	194.9
B	12	58.8	519.9	0.34	72.3	640.0	200.8

A= CELSA steel bar; B = Steel bar provided from market.

Figure 3.1: Photograph of 12 mm (Grade 500C) CELSA reinforcing bar

3.3 Mix design, casting and curing methods

The cubes of the pull-out test specimens (detailed later) were cast from 11 separate batches of concrete which were divided into two groups: the first group consisted of one control batch (CEM II/B-V 32.5R), then four mixes containing different percentages of

GGBS, PFA, MK and SF and are presented in Table 3.3a. The second group consisted of one control batch and five mixes containing different percentage levels of PFA and GGBS with different exposure times, as presented in Table 3.3b. A w/c ratio of 0.45 was selected to obtain a target 28-day compressive strength of 45 N/mm^2. The mix proportions used were kept constant for all batches. The components were mixed together using a 300-kg-capacity concrete mixer (Belle 200 XT Premier Concrete Mixer) for three minutes. The water was then added in small amounts over a two-minute period, and the mixing was continued for a further three minutes. After the mixing process was complete, a slump test was carried out for each mix according to BS 12350-2:2009 the results of which are given in Table 3.3a and b. Prior to casting, all moulds used for the mix were oiled. Fresh concrete was then poured and compacted into the wooden moulds with the reinforcement bar in a horizontal orientation. The filling process was performed in three layers and the concrete was compacted using a vibrating table, both on completion and in-between each layer. In addition, the compressive strength and tensile strength of the concrete were measured by using 100mm cubes and 200mm × 100mm diameter cylinder specimens cast from the same concrete batches. The details and member of the specimens are shown in Table 3.4. After casting, all the samples were left in their moulds overnight at room temperature and then de-moulded approximately 24 hours later, at which point the exposed steel reinforcement bar was wrapped using waterproof tape to prevent water from reaching the surface of the exposed sections of the reinforcement bar during the curing time. Finally, all samples were covered with damp hessian which was sprayed with water twice a day for 28 days at laboratory temperature until the date of testing. Moreover, all cubes for compression tests and cylinders in each batch were also kept under the wet hessian until the date of testing.

Table 3.3a: Concrete mixture proportions (Set -1)

Concrete mix (batches)	**Cement content**	**GGBS**	**PFA**	**MK**	**SF**	**water**	**Fine aggregate**	**Coarse aggregate**	**W/C**	**Slump**
	(kg/m^3)	(kg/m^3)	kg/m^3	(kg/m^3)	(kg/m^3)	(kg/m^3)	(kg/m^3)	(kg/m^3)	(-)	mm
CEM II control	410	-	-	-	-	185	710	1070	0.45	125
CEM II + 50 % GGBS	205	205	-	-	-	185	710	1070	0.45	75
CEM II + 30 % PFA	287	-	123	-	-	185	710	1070	0.45	120
CEM II + 10 % MK	369	-	-	41	-	185	710	1070	0.45	80
CEM II + 10 % SF	369	-	-	-	41	185	710	1070	0.45	60

Table 3.3b: Concrete mixture proportions (Set -2)

CEM II control	410	-	-	-	-	185	710	1070	0.45	130
CEM II + 50 % GGBS	205	205	-	-	-	185	710	1070	0.45	90
CEM II + 60 % GGBS	246	164	-	-	-	185	710	1070	0.45	85
CEM II + 30 % PFA	287	-	123	-	-	185	710	1070	0.45	130
CEM II + 40 % PFA	246	-	164	-	-	185	710	1070	0.45	85
CEM II + 45 % PFA	222.5	-	184.5	-	-	185	710	1070	0.45	95

Table 3.4: Summary of concrete specimens

Concrete mix	**No. of Pull-out test specimens**	**No. of Compressive test specimens**	**No. of Tensile test specimens**	**No. of Torsion test Specimens**
CEM II	20 cubes	18 cubes	6 cylinders	3 cylinders
CEM II + 30 % PFA	20 cubes	18 cubes	6 cylinders	3 cylinders
CEM II + 40 % PFA	5 cubes	9 cubes	3 cylinders	-
CEM II + 45 % PFA	5 cubes	9 cubes	3 cylinders	-
CEM II + 50 % GGBS	20 cubes	18 cubes	6 cylinders	3 cylinders
CEM II + 60 % GGBS	5 cubes	9 cubes	3 cylinders	-
CEM II + 10 % MK	15 cubes	9 cubes	3 cylinders	3 cylinders
CEM II + 10 % SF	15 cubes	9 cubes	3 cylinders	3 cylinders

The code numbers of the specimens are described in the following figure (Figure 3.2). For example, 00-CEM II-0 means the specimen contains 0% of cement replacement materials, is normal CEM II concrete, and the un-corroded specimens.

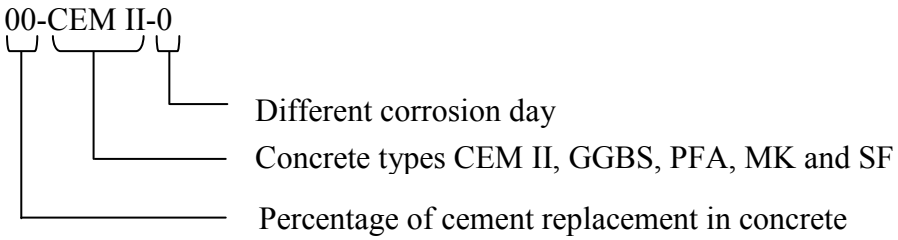

Figure 3.2: Specimen identification code

3.4 Specimen design

3.4.1 Pull-out test specimen design

The dimensions of the pull-out specimens were 200mm × 200mm × 200mm with a single ribbed bar of 12mm diameter embedded in the centre of the concrete cube. Prior to casting, all the reinforcement bars were cleaned using a wire brush to remove any rust on the steel surface. The bond length for the steel bar was selected to be four times that of the steel bar diameter, i.e. 50mm, this being the length of the bar bonded to the concrete to be corroded. The bond length of the bar was placed at the centre of the concrete cube with 40mm of length protruding from the top of the specimen and with the outer 75mm of the reinforcing bar enclosed in a PVC tube to ensure that these sections remained un-bonded. Additionally, the reinforcement bar was covered with tape for a distance of 75mm from both ends of the cube so that the corrosion could take place only within the 50mm bonded length. Figure 3.3 shows details of the sample used for the pull-out test.

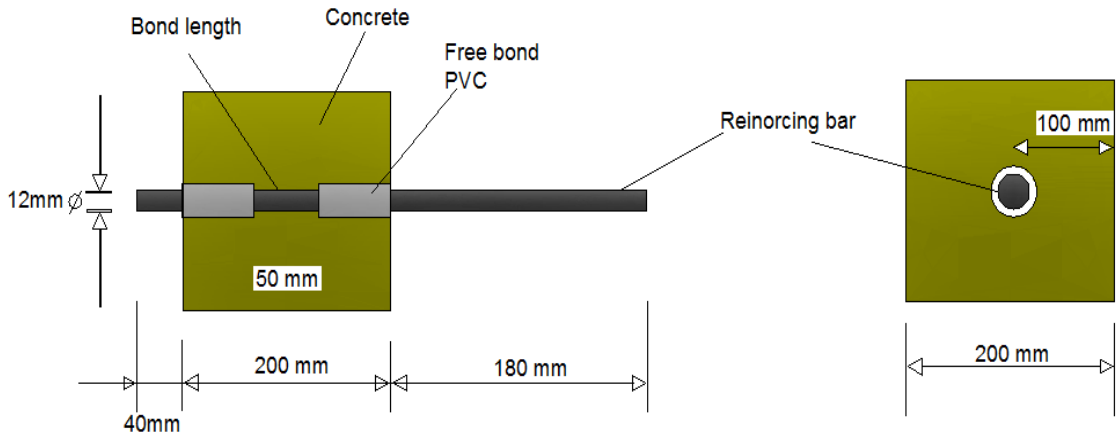

Figure 3.3: Geometry of pull-out test specimen

3.4.2 Specimen design for permeability tests

Samples of 100mm diameter by 100mm height were cored from two 350mm × 325mm × 100mm slabs for each mix using an Ajax Radial Arm Corer after 28 days of curing. The specimens were then prepared for gas permeability testing, having been kept under hessian until the date of testing. A summary of the testing ages is given in Table 3.5. The details of the samples are presented in Figure 3.4. After the coring operation, all the samples were drilled using a 6mm rotary drill to produce a 6mm diameter cylindrical hole in the centre of all samples at the age of 28 days. The specimens were kept under wet hessian until the date of testing.

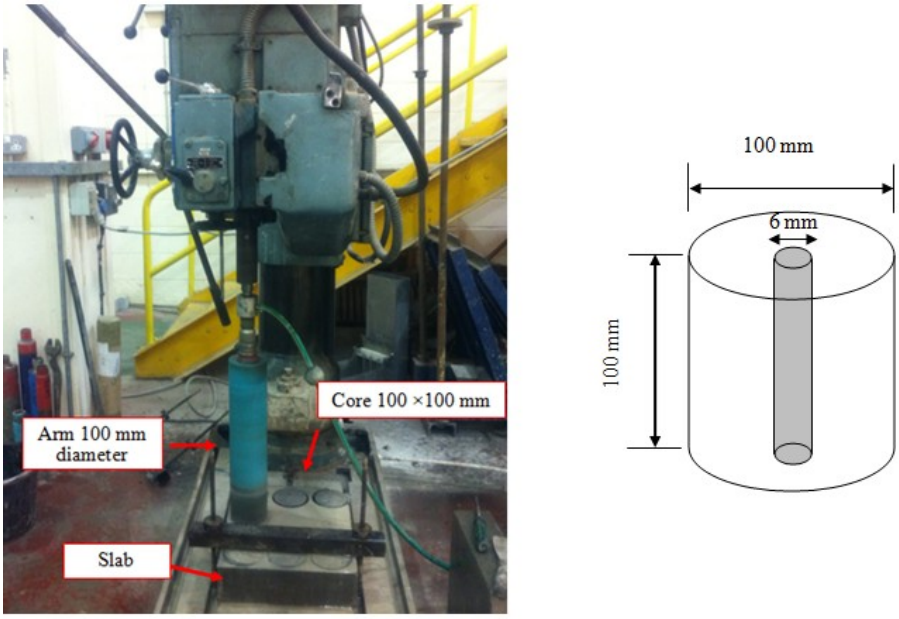

(a) **(b)**

Figure 3.4: Schematic diagram of (a) Photograph of Ajax Radial Arm machine; (b) Geometry of permeability test specimen

Table 3.5: Summary of permeability specimens

Concrete mix	**Gas permeability specimen age**							
	28 days	33 days	38 days	46 days	52 days	70 days	90 days	180 days
CEMII	12	3	3	3	6	3	3	3
CEMII +50% GGBS	12	3	3	3	6	3	3	3
CEMII +60% GGBS	6	3	3	3	6	3	3	3
CEMII +30% PFA	12	3	3	3	6	3	3	3
CEMII +40% PFA	6	3	3	3	6	3	3	3
CEMII +45% PFA	6	3	3	3	6	3	3	3
CEMII +10% MK	6							
CEMII +10% SF	6							

3.4.3 Curing method for permeability specimens

After the samples had been cured under damp hessian for 28 days, these samples for permeability testing up to 33, 38, 46, 52, 70, 90 and 180 days were kept under wet hessian in a laboratory until the testing age.

3.5 Test methods

3.5.1 Hardened concrete tests

The most important properties of hardened concrete are the compressive strength, tensile strength and Young's modulus, which are the most common performance parameters used by engineers in the design of concrete structures.

The compressive strength of concrete was determined by crushing a standard 100mm concrete cube and the tensile of the concrete was conducted on a cylinder of 100mm

diameter × 200mm length. The concrete cubes were tested at the ages of 28, 46, 52, 70, 90 and 180 days with three cubes from each mix at a particular age. The mean result obtained from three cubes was taken as the cube compressive strength. According to the specification of BS EN 12390-3:2009, they were subject to uniaxial force at a rate of 180 kN/min until failure. The mean values of the three cylinders were taken from each mix being tested at the age of 28 days according to BS EN 12390-6:2000. These cylinders were loaded on their sides with uniaxial force at a rate of 60 kN/min until failure.

3.5.2 Torsion test

One of the tests used to evaluate the concrete characteristics, especially to determine the tensile strength and Young's modulus for concrete mixes. This test was chosen in this study because: Young's modulus can be measured in addition to the tensile strength; a very precise graph of the tensile strength-deformation can be obtained the test is easy to prepare and carry out and finally, a number of researchers in the same laboratory have used this test. The procedure for the torsion test is that described by Sardis (2001). The general solution for the torque-twist relationship of a linear elastic material is:

$$\frac{T}{J} = \frac{\tau}{r} = \frac{G\gamma}{L} \tag{3.1}$$

Where:

T = torque

J = polar second moment of area

τ = shear stress of radius

r = radius of specimen

G = shear stress

γ = ration

L = length over which rotation is measured

For a brittle material, which is weak in tension, failure in a torsion test is expected to occur by tensile fracture at 45^o to the longitudinal axis of the core. Norris et al. (1990) and Sardis (2001) reported that the maximum elastic shear stress $f_{s\ max}$ at the sample surface approaches a limiting value equal to 0.85 times that of the uniaixal tensile strength of the material (f_t).

$$f_{s\ max} = 0.85 f_t \tag{3.2}$$

The system of load and reaction points has been designed such that the distance between the pairs of loads on the cylinder split collar is 250mm, hence the torque (T) can be expressed as:

$$T = 0.25P \tag{3.3}$$

Furthermore, Stergianos (2000) notes that the test also enables the indirect evaluation of Young's modulus of the concrete, where ν is Poisson's ratio which is assumed to be 0.2 (this value of 0.2 for ν is typical of that reported by the CEM-FIP Mode Code 1990)), the Young's modulus (E_c) is determined from the shear modulus of concrete (G):

$$E_c = 2G\ (1+ \nu) \tag{3.4}$$

For each mix, three cylinders 100mm diameter × 200mm long were prepared for the torsion test after 28 days of curing and they were left at room temperature for approximately four hours to make sure that the surface of samples were dried from water, which could have had a detrimental effect on the adhesion required to bind the samples to the metal collars. Two end collars were then fixed at the ends of the cylinder test samples and used to transmit the torsion, adhesive glue (polypaste) being used to fix the end collars to the samples. When the polypaste had completely dried, the samples

were then tested in the torsion test machine on the next day. The test arrangement is presented in Figure 3.5.

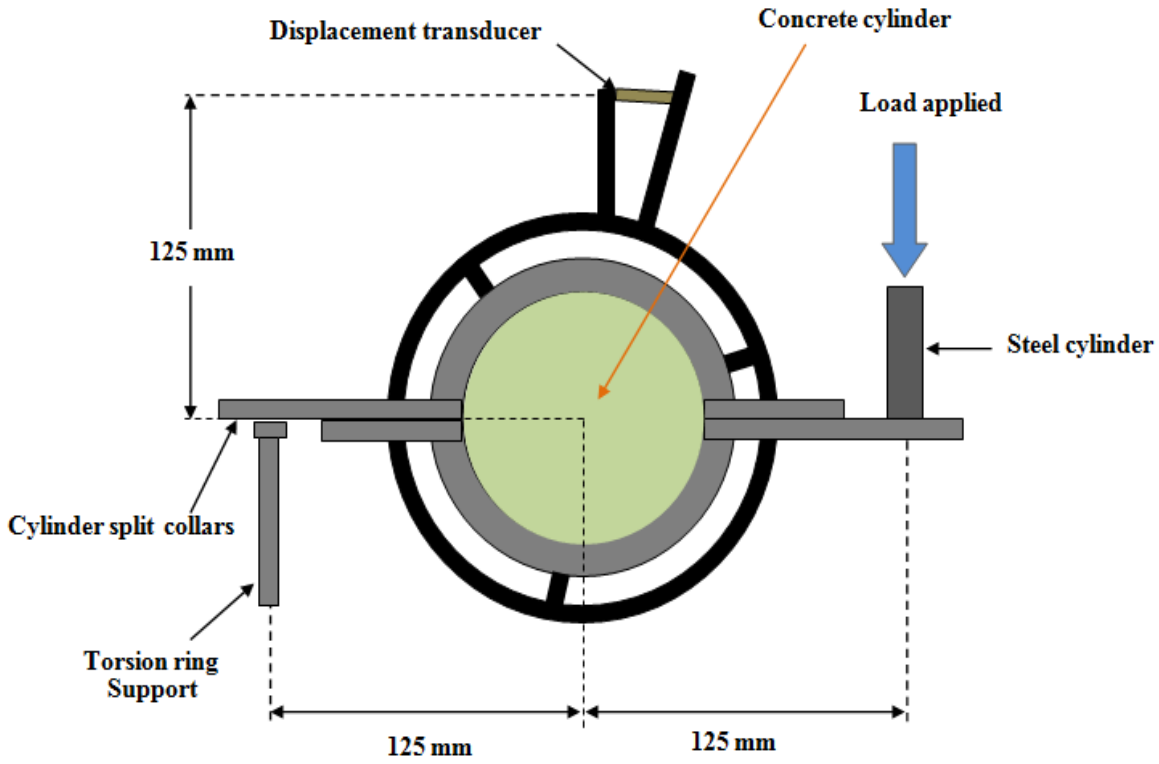

Figure 3.5: Test arrangement of torsion test

3.5.3 Gas permeability test

Testing of concrete permeability was discussed in some detail in section 2.10, where some common methods of testing were described. In this section, the focus is on the method that was used to evaluate the relative gas permeability in this particular study. The testing of the relative gas permeability of the different concrete mixes was conducted by the method that was originally developed by Martin (1986) and modified by Lydon (1993), and described in full by Gardner (2005). After the drilling process, the surfaces and central 6 mm hole of the cylinders were cleaned by using compressed air to remove any dust; these cylinders were then dried in an oven at a temperature of 105

(±5) ºC which was chosen to accelerate the drying process to eliminate moisture within the samples, as shown in Figure 3.6. Their weight was recorded on a daily basis until no more than 0.02% weight loss was observed between consecutive readings in a 24-hour period, this being the requirement suggested by Gardner (2005), after which they were taken from the oven and kept in the desiccator at 20 ºC until the start of the permeability test.

Figure 3.6: Conditioning regime (oven)

The schematic diagram of the permeability test and the permeability cell is presented in Figure 3.7. Three specimens were tested for each age (i.e. 28, 33, 38, 46, 52, 70, 90 and 180 days). At the beginning of each test, the two concrete cylindrical samples were taken from the desiccator to be cleaned using compressed air and they were then weighed. The gas test procedure in this study was described in full by Gardner et al.

(2007). The cylindrical samples were placed in the permeability cells and a thin layer of Vaseline was applied to the top face of the sample to ensure a good seal, making sure that no Vaseline entered the drilled hole. The nitrogen was stored in a cylinder bottle, and when the testing process started the nitrogen was allowed to flow into the reservoir until a pressure of 10 bar was achieved. The test was then commenced; a computer was used to record the data as a text file by logging the pressure loss via a pressure transducer in both reservoirs. The gas permeability coefficient k_{ef} (m^2) is calculated using Equation (2.14) in the section 2.10 3.

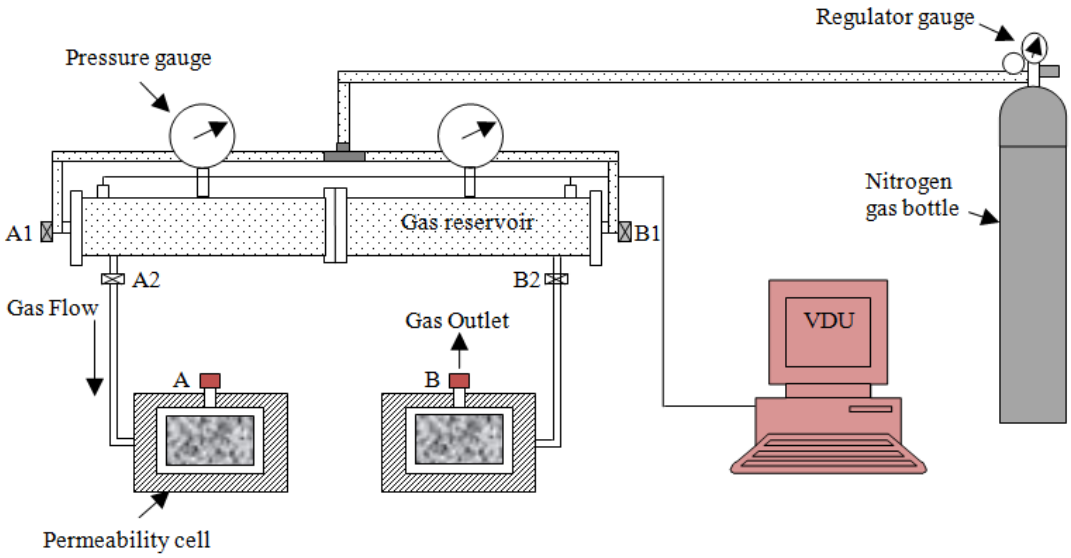

(a) Test arrangement for permeability

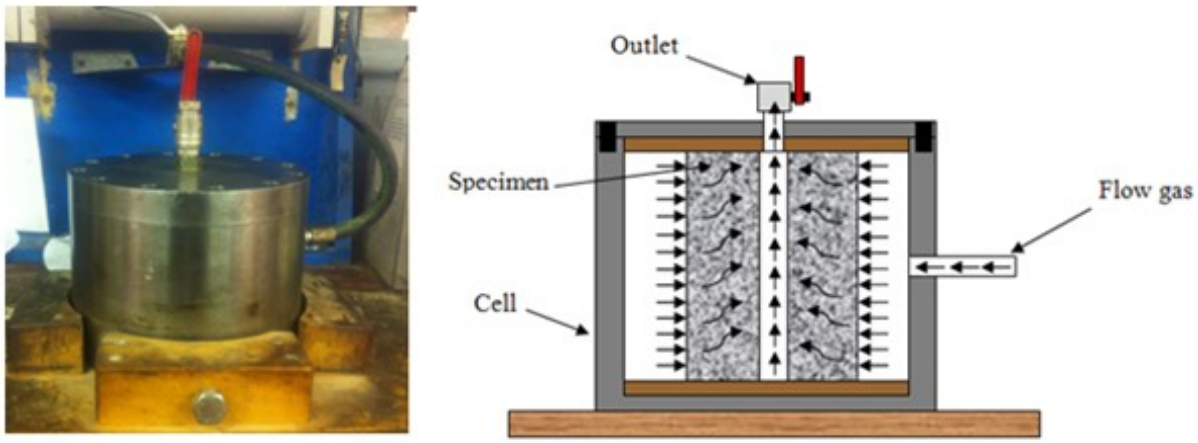

(b) Detail of permeability cell

Figure 3.7: Schematic diagram of (a) Test arrangement for permeability; (b) Detail of permeability cell

3.5.4 Accelerated corrosion testing of steel reinforcement

Corrosion is a slow degradation process for reinforcement bars in a corrosive environment where it normally takes many years for the reinforcing materials to corrode completely and cracks to appear on the surface of the concrete. However, the scientific justification for artificial corrosion using impressed current is strong, since it dramatically reduces the initiation period required for breakdown of the passive layer of film from years to days (Amleh, 2000). In order to achieve a significant corrosion level in a reasonable amount of time, an accelerated corrosion technique is used in laboratories worldwide which has many advantages, in addition to savings in time and money. One advantage over other accelerated techniques is the ability to control the rate of corrosion. In this study, corrosion was initiated by immersing the pull-out cubes in 3.5% sodium chloride solution (by weight of water) and the electrochemical corrosion technique was used to induce accelerated corrosion of the reinforcement bar embedded in the concrete. The samples were immersed in plastic tanks containing an aqueous solution of 3.5% NaCl by weight for two days until the level of the solution remained approximately 40mm below the surface of the concrete block. The direct-current supply was then applied to the steel bar using a series circuit to ensure a constant current of 10 mA through all the samples, which corresponded to a current density value of 0.53 mA/cm^2. This was somewhat lower than that used by several other experimental studies, which typically have been between a minimum of 2 mA/cm^2 and maximum of 10 mA/cm^2 (Al-Sulaimani et al., 1990; Almusallam et al., 1996; Fang et al., 2004; Fang et al., 2006; Kivell et al., 2011) but the aim was to generate only low levels of corrosion and localized cracking and may have some high levels of corrosion. A schematic representation of the corrosion test set-up is given in Figure 3.8 a and b where, the steel bar acted as the anode as it was connected to the positive terminal of the external power

supply, while a stainless steel plate also placed in the tank acted as the cathode. In order to investigate different corrosion levels, accelerated corrosion was carried out for 3, 7, 10, 14 and 20 days and the corrosion test started after 28 days of curing.

On completion of the accelerated corrosion, it was confirmed that there was no visual evidence of cracking or splitting of the concrete. However, it was noted that after 14 and 20 days of corrosion a very small quantity of ferrous oxide (rust) could be seen in the PVC tubes and there was some corrosion on the unbounded section of the bar.

After the accelerated corrosion was completed and the samples were tested by the pull-out method, the samples were wet-cut using a circular concrete-cutting saw and the corrosion was removed from the reinforcement bar by using an iron brush; the weight of the steel bar was then compared with that prior to corrosion. The corrosion level (C_L) was calculated using Equation (3.5) as follows:

$$\text{corrosion level, } C_L = \frac{(G_0 - G)}{(g_0 l)} \times 100\% \quad (3.5)$$

Where:

G_0 = the initial weight of the reinforcement bar before corrosion

G = the final weight of the steel bar after removal of the corrosion

g_0 = the weight per unit length of the reinforcement bar (G_0/L)

l = the bond length

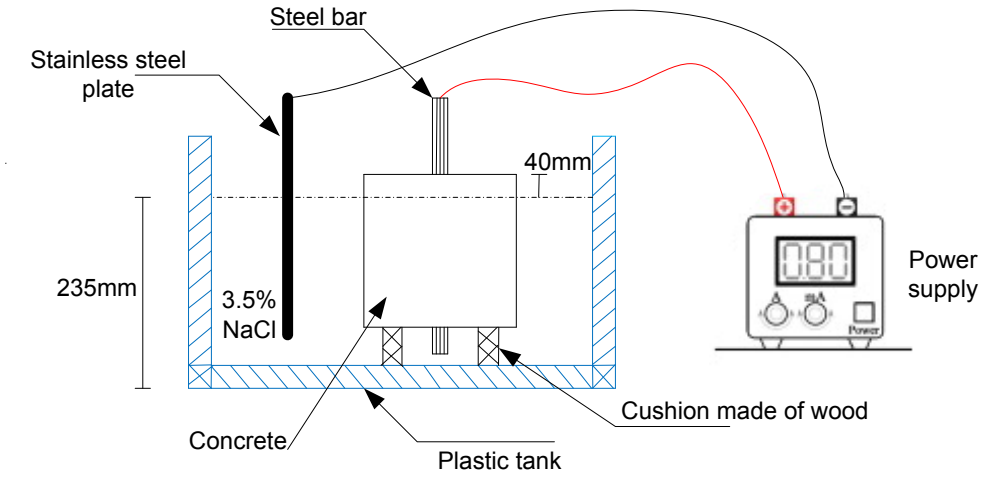

(a) Set-up for accelerated corrosion

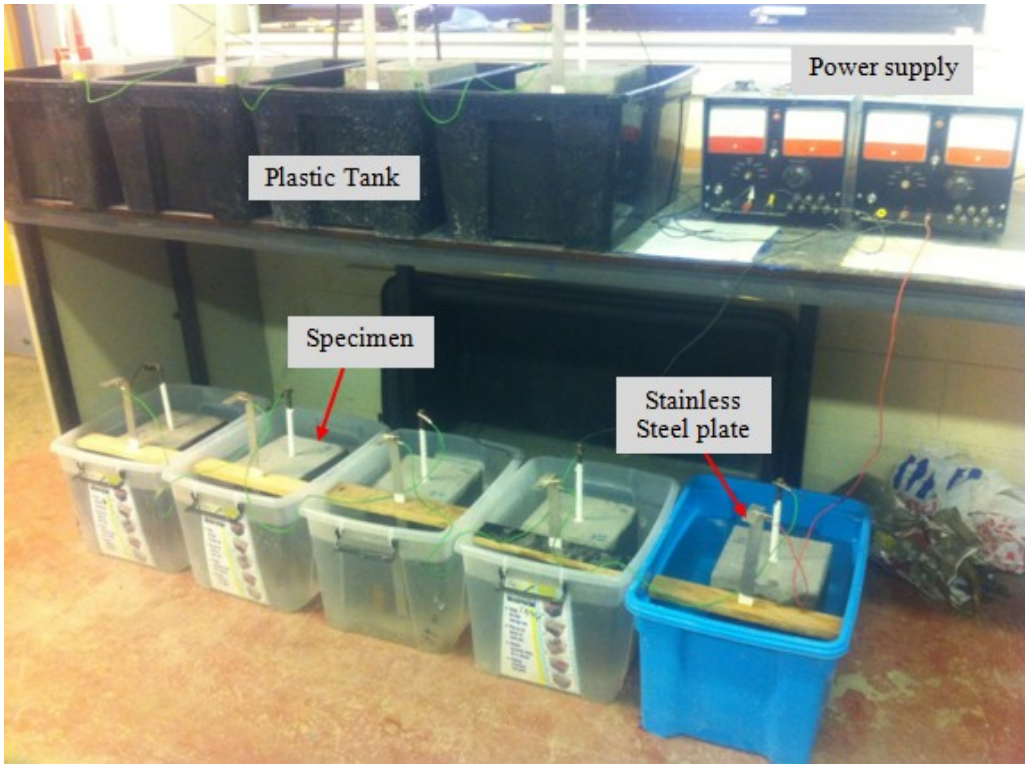

(b) Photograph of set-up for accelerated corrosion

Figure 3.8: Schematic diagram of (a) Set-up for accelerated corrosion; (b) Photograph of set-up for accelerated corrosion

In terms of the mass loss of steel reinforcement due to corrosion it can be estimated by following Faraday's law

$$mass\ loss = \frac{time \times current \times 55.847}{2 \times 96{,}487} \quad (3.6)$$

The quantity of charge applied for any given electrolysis is given by the product of time (s) and current (A) (Auyeung et al., 2000). For the corrosion process, for each mole of iron oxidised, 2 moles of electrons are given out, consuming a charge of 2 × 96,487 coulomb. The mass loss is then calculated by multiplying the applied charge (C) by the molar mass (55.847 g/mol for iron) and dividing by the charge needed per mole.

3.5.5 Pull-out tests

Two different types of test can be used to obtain the bond stress between the steel reinforcement bars and the pull-out test is a typical experimental test that is done to study the bond behaviour. The pull-out test is most commonly used for short embedment length, which evaluates the bond stress along a single reinforcing bar. In this test the reinforcement bar was embedded in a concrete cube while a force was applied to pull the steel bar out from the cube of concrete, which was continued until the slip of the steel bar reached 5mm. This test has the advantages of simplicity and the ease of determining the bond strength. The main aim of the pull-out test is to determine the bond behaviour between reinforcement bars and concrete. The test was condcuted according to RILEM CEB FIP (1983). The cube bond tests were performed using a specially designed loading test frame, as shown in Figure 3.9. The loading frame consisted of two square plates in which the top plate was clamped to the upper head of an Avery Dennison machine that had a maximum load capacity of 600 kN. The pull-out samples were placed into the frame with the reinforcement bar passing through the central hole of the reaction plate. A 5mm rubber pad was used to reduce friction

between the reaction plate and concrete cube specimen, making sure that distribution of stress was applied to the face of the cube, and tensile force was applied. The load was measured with the electronic load cell of the machine, and the displacement (slip) was measured using two Linear Variable Differential Transducer (LVDTs) fixed in a holder by a single fixing screw. The displacement transducers' holder was then clamped to the top end of the reinforcement bar to measure its movement relative to the top surface of the concrete cube. The application of the load was in displacement control and the pull-out load was applied to the sample at a rate of 0.01mm/s using an automatic data-acquisition system for recording the data. The slip of the steel reinforcement bars was recorded from the beginning until the slip reached 5mm; the average value of the two transducers was used. Three samples were tested for each corrosion level and control samples (uncorroded).

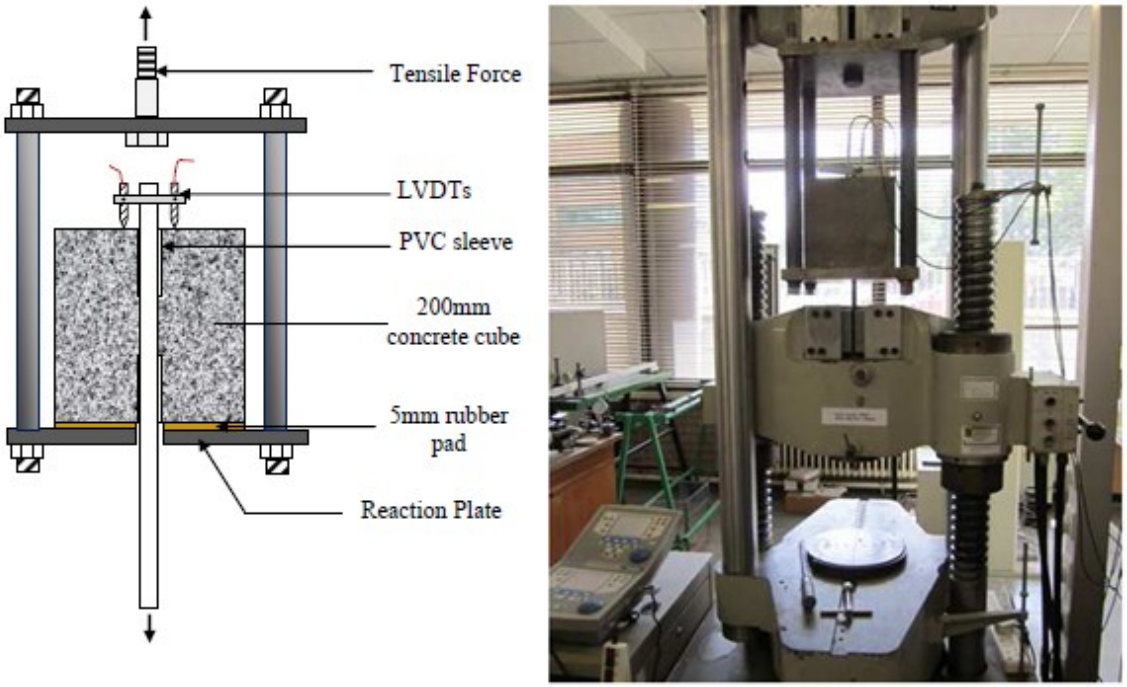

Figure 3.9: Pull-out test arrangement

The bond strength was calculated as being the steel force divided by the surface area of the embedment length, as presented in Equation (3.7).

$$\tau_u = \frac{\mathrm{P}}{\pi . d_b . l_b} \tag{3.7}$$

Where: τ_u is the bond strength in N/mm^2, P is the applied load (N); d_b is the bar diameter (mm) and l_b is the bond length (mm).

CHAPTER 4

THE EFFECT OF STEEL BAR CORROSION ON THE BOND STRENGTH OF REINFORCED CONCRETE

4.1 Introduction

This chapter describes a study of the ultimate bond strength of a series of corroded and un-corroded reinforced concrete specimens. The influence of concrete made with a range of CEM II cements containing various cement replacement materials on the corrosion level was investigated using the accelerated corrosion method. By performing a pull-out test, the bond strength was investigated for various corrosion levels and the results are described in this chapter. The bond strengths developed in the present study varied with the splitting tensile strength and concrete strength for the concrete mixes used. Moreover, the detailed results of these tests will be presented and discussed in the following two sections. The first section will discuss the results of artificial accelerated corrosion methods, with the effects of the cement replacement type on the corrosion level as the primary consideration. The second section will present the results of the pull-out tests previously described in chapter 3, along with the results of the investigation into the effects of concrete made with different cement replacement materials on the bond strength of un-corroded and corroded specimens.

4.2 Mechanical properties results

The variations of compressive strength and elastic modulus results for all the different concrete mixes with different cement replacement materials (CEM II, GGBS, PFA, MK

and SF) are presented in Table 4.1 and Table 4.2. It can be seen from Table 4.1 that the compressive strengths of 50% GGBS and 30% PFA mixes were slightly lower than that of the CEM II mix, while the compressive strengths of the 10% MK and 10% SF mixes were higher at 28 days. Moreover, the coefficient of variation for the MK concrete strength was found to be 9.3% at 28 days (Table 4.1). This high variation may be attributed to poor hydration (pozzolanic reaction), but also indicating a large spread of the results in the compressive strength. The compressive strength gains were found to be 14.60%, 2.78%, 7.77%, 1.80% and 9.35% for the CEM II, 50% GGBS, 30% PFA, 10% MK, and 10% SF mixes between 28 days and 46 days, respectively. According to these results, an increase in the compressive strength was observed for all concrete mixes because of the increased curing time and the increased rate of strength gain from further hydration and the production of calcium-silicate-hydrate (C-S-H) gel. Megat Johari et al. (2011) reported that the different cementitious materials significantly affected the compressive strength at all ages, particularly between 28 to 90 days.

Table 4.1: Mechanical properties of concrete (Set-1)

Concrete Mix	**Compressive strength (N/mm^2)**				**Splitting strength (N/mm^2)**	**Elastic modulus, (E_c,kN/mm^2)**	
	28-day	**COV %**	**46-day**	**COV %**	**28-day**	**28-day**	**COV %**
CEM II	54.0	1.98	61.9	3.76	4.5	35.8	4.06
CEM II+50%GGBS	49.2	2.12	51.6	1.10	4.4	36.0	5.80
CEM II+30%PFA	37.3	1.88	40.2	3.42	3.2	34.8	2.19
CEM II+10%MK	60.6	9.30	61.7	0.89	4.4	38.3	2.74
CEM II+10%SF	54.6	1.16	59.7	2.0	4.4	36.7	2.61

Note: [a] E_c =Elastic modulus of concrete (torsion test).

Table 4.2: Mechanical properties of concrete (Set-2)

Concrete mix	**Compressive strength (N/mm^2)**				**Splitting strength (N/mm^2)**
	28-day	**COV %**	**52-day**	**COV %**	
CEM II	43.1	0.98	50.0	2.40	3.7
CEM II+50%GGBS	43.0	0.64	51.4	2.42	3.9
CEM II+60%GGBS	38.1	7.35	43.6	1.81	3.4
CEM II+30%PFA	31.1	1.42	37.3	3.10	3.0
CEM II+40%PFA	28.4	4.62	35.0	2.83	2.9
CEM II+45%PFA	26.7	1.11	31.1	2.82	2.6

In Table 4.2, the compressive strengths of the concrete mixes at 28 and 52 days are reported. The compressive strength of the CEM II mix was higher than that of the other mixes at 28 days. However, at 52 days, it can also be observed that the compressive strength of the 50% GGBS mix was greater by 0.49% than that of the corresponding control mix, whereas the compressive strength of the 60% GGBS mix was 13% lower than the control mix. According to Table 4.2, with addition of the 30%, 40%, and 45% PFA mixes had consistently lower compressive strengths than that of the control mix, at 25.45%, 30% and 37.89%, respectively, the reduction in the compressive strength caused by the lower pozzolanic reaction of PFA. This is due to the slow reaction between $Ca(OH)_2$ and pozzolanic materials. Chindaprasirt et al. (2005) reported that the compressive strength of blended cement decreased as an increase in the replacement of fly ash. Furthermore, from the results reported in Table 4.1, it was also noticed that the mean elastic modulus values of concrete made with cement replacement of 50% GGBS, 10% MK, and 10% SF were higher by approximately 2.5% to 7% than the control mix, while conversely the 30% PFA concrete had the lowest value of elastic modulus compared with the control mix (CEM II), with a coefficient of variation of 2.19%. This may be because the pozzolanic reaction of PFA cement is slower at early ages. Persson (1998) also reported that the elasticity modulus of fly ash was lower at early ages but

increased at later ages (28 days). From these results, it can be observed that the strength of the concrete increased with increasing age due to the influence of further cement hydration. Whilst the concrete mixes with 30%, 40% and 45% of PFA exhibited the lowest compressive strengths of all the mixes at 28 days, they underwent the greatest increase in strength between 28 and 52 days about 20%, 23.2% and 16.5% respectively, which may be attributed to the additional pozzolanic reactions occurring at this time, particularly in the higher volume PFA mixes.

4.2.1 The relationship between concrete strength and splitting tensile strength

The relationship between splitting tensile and compressive strength depends on many factors, such as the concrete age, the curing condition, air content and aggregate type (Neville, 1995). The effect of cementitious materials, such as variations in the cement replacement of concrete, can also change this relationship. Figure 4.1 plots the splitting tensile strength against the compressive strength for all the different concrete mixes at 28 days. It can be seen that in the CEM II specimen and concrete containing the 50% GGBS, 10% MK, and 10% SF concrete, there is a significant increase in the splitting tensile strength, i.e., 27%, 30%, 50% and 29% respectively, compared with the 30% PFA concrete. This is due to the fact that the compressive strengths of these mixes were significantly higher than that of the PFA concrete. Moreover, the PFA cement content (30%, 40% and 45%) had a splitting tensile strength which was lower by 47.5%, 49.5% and 61.6% than the control concrete at 28 days, respectively. The splitting tensile values of these mixes were ranged from 8.6% to 10.5% of their compressive strengths. This is because of the delayed pozzolanic reaction of the PFA concrete at early ages compared to that of the control mix. This is probably attributable to the high volume of fly ash as a result of using CEM II/B-V 32R, which already contains siliceous fly ash of 7%. This higher content of fly ash led to a reduction in the gain of strength. Gencel et al. (2012) reported that

the tensile strength of concrete reduces with increased fly ash content. Similar findings were also reported by Kayail and Sharfuddin (2013).

As presented in this Figure 4.1, a good correlation exists between the compressive strength and splitting tensile strength, with a correlation coefficient of 0.93. Moreover, the tensile strength of concrete results obtained in this investigation is comparable with Eurocode 2 (2004) as shown in Figure 4.1. The solid line indicates the results obtained using Eurocode 2, which shows values approximately 10% to 20% lower than the experimental results. This difference has come from the variation in mix proportion, curing method and w/c ratio, and also to the changing cementitious material composition from CEM I to CEM II with different levels of cement replacement materials.

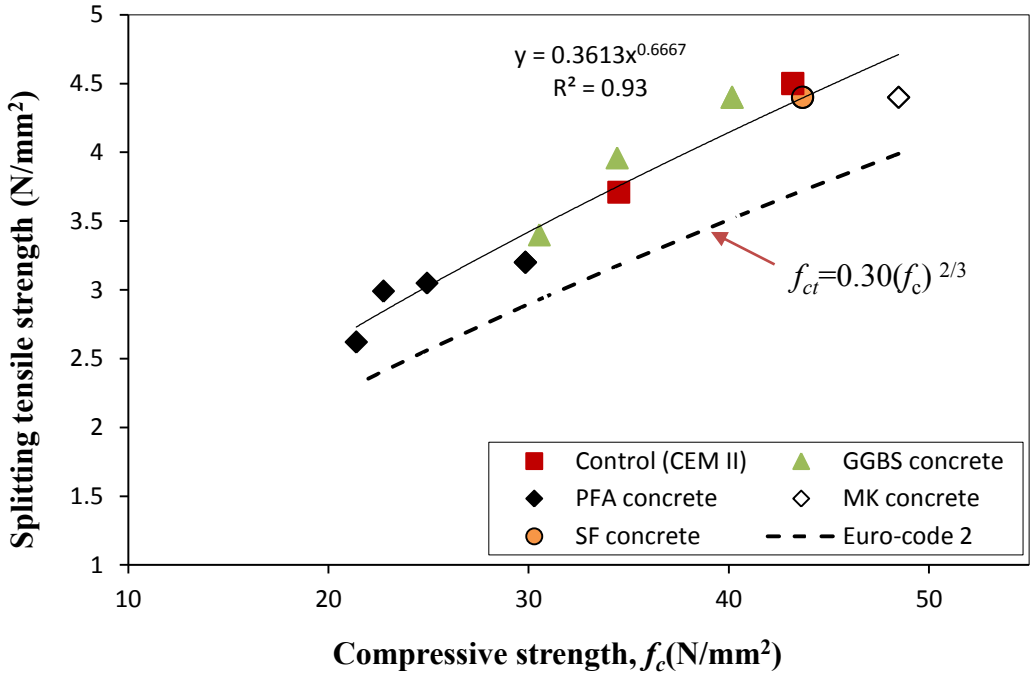

Figure 4.1: Relationship between splitting tensile and compressive strength in different concrete mixes at 28 days

4.3 Evolution of corrosion level with time and the effect of cement types

The accelerated corrosion of reinforcing bars embedded in different concrete mixes (i.e. CEMII, GGBS, PFA, MK and SF), which were subjected to different exposure times, i.e., 3, 7, 10, 14 and 20 days, was studied with constant current. The corrosion level was measured based on the weight loss method, as mentioned in section 3.5.4. Figure 4.2 shows the corrosion level of steel bars against the corrosion time for the concrete mixes (set-1). From Figure 4.2, the level of corrosion of the steel bar in the CEM II concrete ranged from 0.27 to 1.97%, with an increasing level of corrosion at all exposure times considered. This is due to the breakdown of the passive layer surrounding the steel bar as a result of chloride ion penetration. The corrosion level values of the steel bar in the concrete with 30% of PFA and 50% of GGBS ranged from 0.18 to 1.2% and 0.09 to 1.55%, respectively, which were lower corrosion levels than the control concrete at all exposure times. It is also apparent that the 50% GGBS exhibited slightly lower levels of corrosion at 3 and 7 days of exposure time compared to the 30% PFA mix, but thereafter the level of corrosion increased to exceed that of the 30% PFA mix at 10 days of exposure time.

The inclusion of GGBS in a concrete mix usually leads to a reduction in the mobility of chloride ions as a result of a change in the mineralogy of the cement hydrates, and this may explain why the GGBS concrete possesses a lower initial corrosion level than other mixes (Li and Roy, 1986). In the case of mix containing 10% MK cement replacement, the corrosion level values ranged from 0.42% to 1.2%, which was slightly higher in the initial exposure time compared to the control specimen, but at the end of the corrosion time (14 days), was approximately 39% lower than the CEM II concrete. This could be attributed to the difference in pore structure at an early age, which led to the chlorides

and oxygen penetrating easily to reach the steel bar, while with increased curing time the chloride ion penetration resistance was greater as a result of a reduction in pore size from continuing hydration of pozzolanic material. In the case of the concrete mix containing 10% SF cement replacement, the corrosion level was less than the other concrete mixes during the whole corrosion period, at between 0.02% and 0.25%, because the SF has low permeability and higher electrical resistivity and therefore enhanced corrosion resistance. This is in good agreement with Smith et al. (2004).

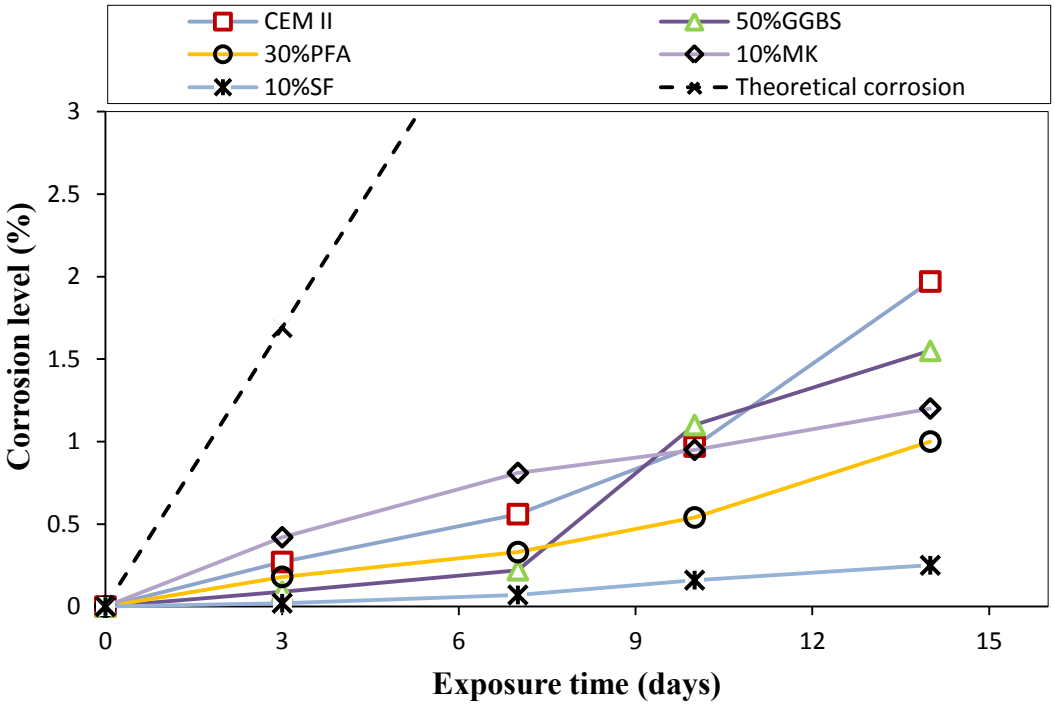

Figure 4.2: The corrosion level and exposure time (set-1)

Figure 4.3 plots the level of corrosion against the exposure time for the steel bars in the different concrete mixes for set 2. This set different percentage levels of GBBS and PFA cement replacement with different exposure time. It can be seen that the amount of corrosion of the steel bar embedded in the CEM II concrete varied from 0.65% to 2.4% in 3 to 20 days of exposure, respectively. When using 50% and 60% GGBS

replacement, the corrosion levels ranged from 0.69% to 2.53% and 0.90% to 2.50%, respectively. Figure 4.3 also indicates that the 50% GGBS mixes exhibited approximately 2.5 times the amount of corrosion up to 20 days of corrosion time compared to the control specimen, while the 60% GGBS concrete showed slightly higher levels of corrosion than the 50% GGBS mix. In the cases of 30%, 40% and 45% PFA replacement, the corrosion level of the steel bars was lower than the control mixes and the corrosion levels of steel bar in concretes (50% and 60% GGBS) concrete were measured as 0.18%-1.98%, 0.51%-0.78%, and 0.43%-0.85%, respectively. Dinakar et al. (2007) also reported that the corrosion rate of steel in cement containing pozzolanic materials (GGBS and PFA) was found to be lower than their CEM I control. Consequently, it can be concluded that the PFA concrete (30%, 40% and 45%) had lower corrosion values than other concretes at the same exposure time. This is attributed to the fact that PFA concrete has good permeability resistance and electronic resistivity compared with other concrete types.

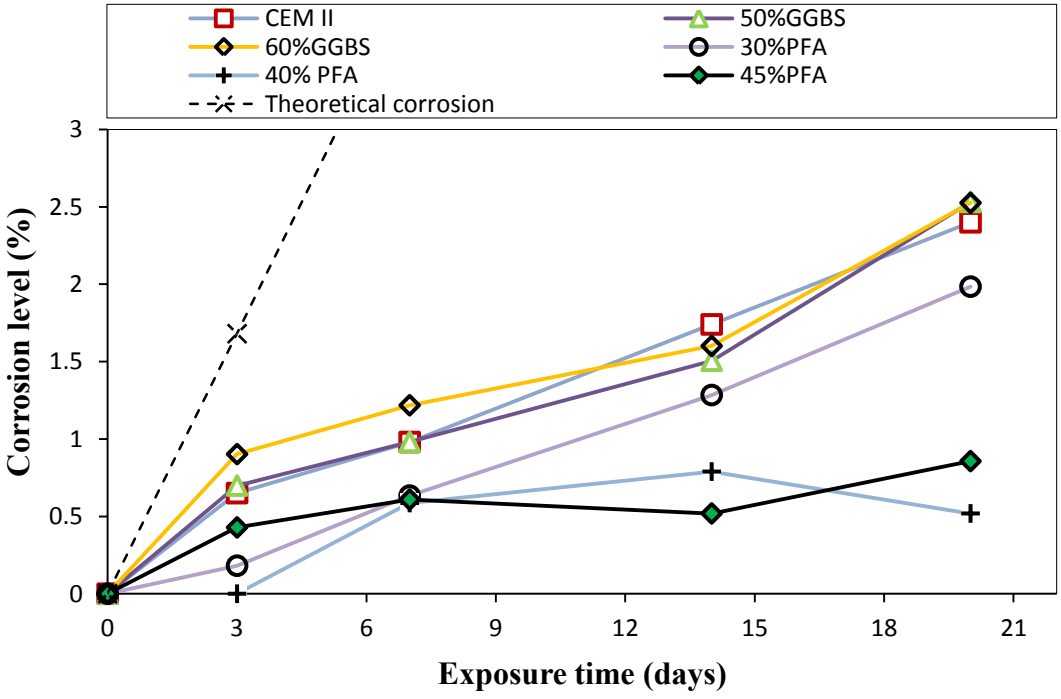

Figure 4.3: The corrosion level and exposure time (set-2)

In Figures 4.2 and 4.3, it is evident that the concrete made with replacement cement of SF and PFA had lower corrosion levels than other concrete mixes, which may be due to the influence of the SF and PFA on the concrete microstructure and the higher resistivity. In this study, it can be said that for the same exposure time, the corrosion level was lower for concrete made with different SCM's. The decreased permeability of concrete with pozzolanic cement probably decreased the corrosion of steel bars due to the denser microstructure of the concrete mix and also the electrical resistivity of concrete may be slowing the corrosion of steel (Khavat and Aitecin 1993). As expected, the corrosion level increases with increasing corrosion exposure times. These results agree with work reported in literature. Abosrra et al. (2011) found that high concrete strength had higher corrosion resistance and that corrosion increased with exposure time. Yalciner et al. (2012) also observed that the corrosion level increased with greater time and that the lower the water-to-cement ratio and the higher the concrete compressive strength, the higher the corrosion resistance.

As mentioned previously, the estimated corrosion level was calculated by using Faraday's law (equation 3.6) and the theoretical predicted corrosion was compared with the experimental corrosion level for both sets, as seen in Figures 4.2 and 4.3. These results indicated that the experimental corrosion level was less than the theoretical corrosion for all specimens. As shown in a previous study by Auyeung et al. (2000), the theoretical prediction of corrosion begins as soon as the electrical energy is applied, but corrosion of a steel bar in concrete starts when the oxygen and moisture reach the steel's surface. It was observed from the results that the corrosion estimated by Faraday's law was greater than the actual corrosion obtained from test results. This is because, in

Faraday's method, the steel bar is directly immersed in electrolyte solution without any protective cover.

4.4 Bond strength results

The detailed procedure for the pull-out test was previously discussed in chapter 3. The results obtained for the effect of corrosion of the ribbed bars embedded in concrete on the bond strength, as well as the control (un-corroded) and corroded specimens are presented in Table 4.3; all specimen tests were carried out at 46 days. After the prescribed period of corrosion, specimens were left under wet hessian until the time of testing. The ultimate bond strength is calculated using the equation 3.7 (section 3.5.5) and the average bond strength τ_m was measured according to BS EN 10080:2005 as the arithmetic mean of bond strength $\tau_{0.01,}$ $\tau_{0.1}$and $\tau_{1.0}$ at 0.01mm, 0.1mm and 1.0mm slip, respectively. The CEB-FIP Model Code 1990 defines the ultimate bond strength as being dependent upon the concrete strength, and therefore the cylinder compressive strengths have been calculated from the cube compressive strength results in this study using.

$f_c = f_{cu} \times 0.8$ (Eurocode 2, 2004) (4.1)

Table 4.3: Results of pull-out tests for concrete mixes at 46 days

Specimen	f_{cu} [a] **(46 day)**	f_{max} [b]	**Bond strength** τ_{max}	**Slip at Max Load**	τ_m [c]	τ/f_{cu}	**Failure mode**
	N/mm^2	kN	N/mm^2	mm	N/mm^2	-	-
00-CEM II-0	61.9	38.9	20.6	1.16	11.1	0.33	Pull-out
00-CEM II-0		33.0	17.5	1.60	8.0	0.28	Pull-out
00-CEM II-0		38.8	20.6	1.50	9.70	0.33	Pull-out
00-CEM II-3		45.5	29.1	0.69	17.2	0.47	Pull-out
00-CEM II-7		64.0	33.9	0.36	27.5	0.54	Pull-out
00-CEM II-10		68.8	36.5	0.39	30.9	0.59	Pull-out
00-CEM II-14		63.9	33.9	0.49	29.9	0.55	Pull-out
50-GGBS-0	51.6	35.3	18.7	1.25	8.5	0.36	Pull-out
50-GGBS-0		36.0	19.1	1.62	8.8	0.37	Pull-out
50-GGBS-0		29.6	15.6	0.66	7.1	0.30	Pull-out
50-GGBS-3		45.7	24.2	0.96	16.4	0.46	Pull-out
50-GGBS-7		50.5	26.8	0.91	20.3	0.52	Pull-out
50-GGBS-10		62.4	33.1	0.26	29.0	0.64	Pull-out
50-GGBS-14		65.9	34.9	0.15	30.1	0.67	Pull-out
30-PFA-0	40.2	21.6	11.4	1.38	6.0	0.28	Pull-out
30-PFA-0		20.84	11.0	1.48	4.1	0.27	Pull-out
30-PFA-0		19.45	10.3	1.06	6.3	0.26	Pull-out
30-PFA-3		29.2	15.5	1.02	10.2	0.38	Pull-out
30-PFA-7		37.1	19.0	0.73	15.4	0.47	Pull-out
30-PFA-10		44.7	23.7	0.53	19.2	0.59	Pull-out
30-PFA-14		50.0	26.5	0.10	21.5	0.66	Pull-out
10-MK-0	61.7	39.0	20.6	1.13	10.3	0.33	Pull-out
10-MK-0		41.00	21.8	0.86	12.24	0.35	Pull-out
10-MK-0		28.44	15.1	1.06	8.00	0.24	Pull-out
10-MK-3		50.5	26.8	0.87	22.5	0.43	Pull-out
10-MK-7		57.0	30.2	0.94	24.9	0.49	Pull-out
10-MK-10		64.8	34.4	0.69	29.4	0.56	Pull-out
10-MK-14		64.4	34.2	0.39	28.7	0.55	Pull-out
10-SF-0	59.7	42.7	22.6	1.32	12.5	0.38	Pull-out
10-SF-0		39.71	21.1	1.42	10.0	0.35	Pull-out
10-SF-0		48.28	25.61	1.24	13.61	0.43	Pull-out
10-SF-3		49.1	26.0	1.60	14.5	0.43	Pull-out
10-SF-7		54.5	28.9	1.43	18.7	0.48	Pull-out
10-SF-10		55.7	29.5	0.44	22.6	0.49	Pull-out
10-SF-14		61.4	32.6	0.76	21.7	0.54	Pull-out

Note: [a] f_{cu} = average compressive strength (cube, 100); [b] f_{max} = maximum pull-out load; [c] τ_m = the mean bond strength.

4.4.1 The influence of concrete strength on bond strength

Figure 4.4 demonstrates both the predicted and the experimental results of the bond strengths as function of the compressive strength of concrete for different concrete mixes. This Figure also includes results from Mawson (unpublished). As seen from Figure 4.4, the CEM II, GGBS, MK, and SF concrete mixes showed higher bond strengths and, consequently, the average concrete strength of these mixes was also higher than for the PFA concrete mix. Additionally, the results of these investigations revealed that increasing the compressive strength of concrete (41-50 N/mm^2) caused a consistently significant effect on the bond strength, which was shown to be about 39% to 50% of the bond strength of CEM II concrete. The maximum bond strengths derived from the expression in CEB-FIP Model Code 1990 (Equation 4.2) are also represented by the dashed line called MC90 alongside the corresponding test results in Figure 4.4. It can be observed from the experimental results that the pull-out specimens of CEM II, GGBS, MK and SF concretes had higher bond strengths than those calculated according to the MC90 because of the compressive strengths of these concretes being significantly higher. On the other hand, in the case of the PFA concretes, the bond strength values were much lower than those of the CEM II and other concrete mixes. This is attributed to the tensile strength of the concretes, which were significantly lower (Tables 4.1 and 4.2). This decrease in bond strength is therefore governed by the tensile strength of the concrete. Moreover, the compressive strength and type of concrete have been identified as key parameters in bond strength (Eligehausen et al., 1983). Figure 4.4 shows Mawson's unpublished results, wherein the bond strength was obtained based on test specimens having 16 and 32mm diameter steel bars in beams of various

compressive strengths (15-30 N/mm^2). It was observed that the bond strength results of concrete with 32mm diameter steel bar fitted well to the MC 90 results. This can be explained by the MC90 being based on Eligehausen's bond slip model, where the compressive strength is 30 N/mm^2. Another possible is different bar diameters, since it is known that the bond strength was affected by diameter of steel bar. The bond strength results obtained from concretes SF, GGBS and MK were higher because the compressive strength in tests presented here was higher than that used Eligehausen et al. (1983). Therefore, it can be expected that the influence of the compressive strength of concrete on the bond strength should be higher here.

It is believed that the reason for the variability in the bond strength of PFA concretes can be attributed to the influence of the tensile strength concrete on bond strength of concrete specimens with PFA replacement materials. Similar findings by Arel and Yazici (2012) support the results found in this study. They reported that the bond strength between concrete and steel bar increases as the mechanical properties of the concrete increase (i.e. compressive and tensile strength). However, the tensile and compressive strength play a major role in both pull-out and splitting failure (FIB, 2000).

In conclusion, it can be stated that the results of this study agree with previous findings, in that the bond strength is significantly affected by the tensile strength and the compressive concrete strength as well as the concrete type. It is believed that if PFA concrete is cast around a ribbed bar, the interaction zone between the steel bar and concrete is weaker and the concrete paste around the surface of the ribs because of the weakness of the bond strength between the aggregate and fly ash paste.

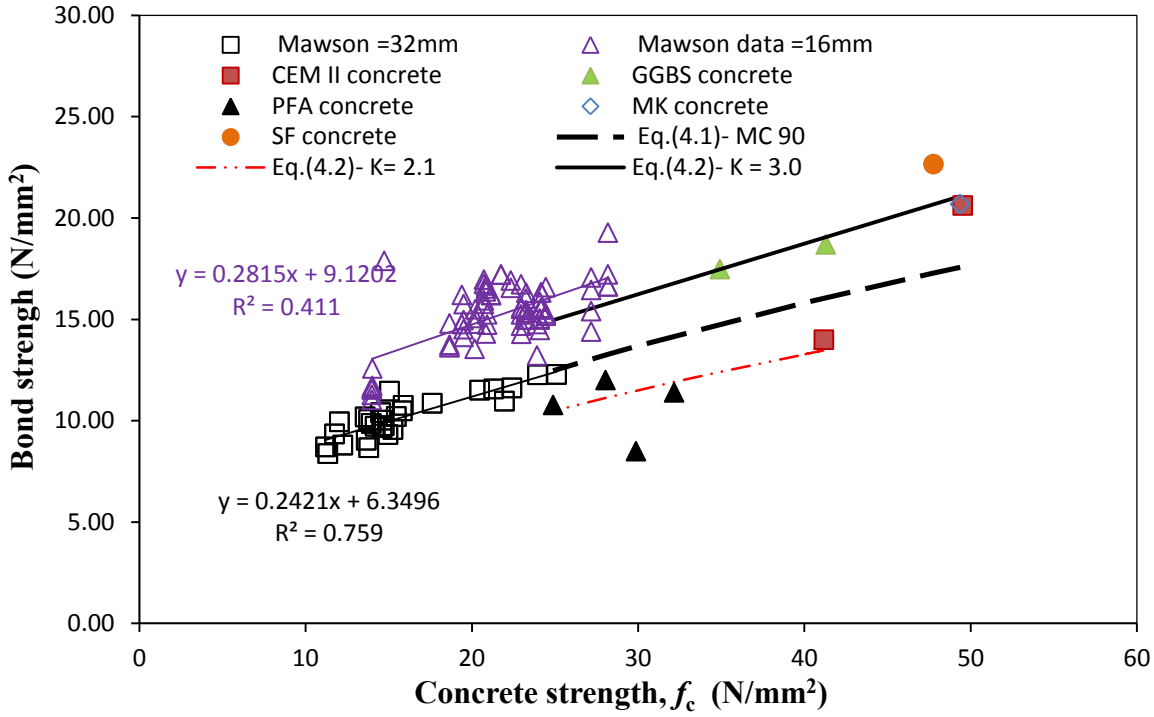

Figure 4.4: Bond strength vs. concrete strength for different concrete types

The CEB-FIP Model Code suggests that bond strength is a function of the square root of the compressive strength of concrete, as shown in equation 4.2:

$$\tau_{max} = 2.5\sqrt{f_c} \tag{4.2}$$

where τ_{max} is the maximum bond strength and f_c is the compressive strength of the concrete. The effect of splitting tensile strength on the bond capacity of the steel bar embedded in different concrete types is investigated to evaluate the maximum bond strength, by assuming the following equation:

$$\tau_{max} = k\,(f_c)^{\beta} \tag{4.3}$$

where β is taken as 0.5; τ_{max} is the maximum bond strength and f_c is the compressive strength of the concrete. In Eq. (4.3), the coefficient k was required to be 3.0 for the

high compressive strength concretes made with GGBS, MK and SF cement replacement in order to fit the bond strength data, while the coefficient *k* was only 2.1 for the PFA concretes.

4.5 The bond strength - slip relationships

Three bond strength–slip curves were generated for each control sample at 46 days. Figure 4.5 (a-e) shows the experimental results of bond strength versus slip for the five concrete mixes at 46 days, including the MC 90 curves. From these figures, it can be noted that the bond strength-slip behaviour comprises three stages. In the first stage, the bond strength increased until the chemical adhesion is exhausted, and slip starts between the steel and concrete. This stage is limited by the tensile strength of the concrete, and the bond strength- slip curve remains linear. This is lower up to about 15% (CEM II), 19% (50% GGBS), 24% (30% PFA), 21% (10% MK) and 19.50% (10% SF) of their average ultimate bond strength and this ascending branch is in good agreement with that obtained from MC 90 (dashed line), as illustrated in Figure 4.5 (a-e). In the second stage, when the applied load increases towards a critical value, the rate of slip starts to increase and the ascending branch of the curve becomes distinctly non-linear. This second stage corresponds to the occurrence of micro-cracking in the concrete matrix. In the third stage, the load reaches a maximum value and some longitudinal splitting cracks develop parallel to the steel bar. In this case, the bond-slip curve exhibits a very gradual drop in load with a rapidly increasing slip. Figure 4.5 also shows the prediction of bond stress-slip by the MC 90 and it can be seen that the MC 90 theory's predicted bond strengths are in very good agreement with the experimental results, with the exception of the PFA concrete which had consistently lower bond strength. The ascending branch of the

curve as defined by MC 90 matches with good accuracy the bond strength obtained from the experimental data.

Figure 4.5 a-e also illustrates the average curve of the bond strength–slip behaviour of all the tested specimens. However, it was also observed that the average experimental results for bond strength were closer to the theoretical bond strength of MC 90 for CEM II, GGBS and MK concretes. On the other hand, the average ultimate bond strength of the 10% SF concrete was higher than the MC90 predication by 25.10%, whereas the average ultimate bond strength of the 30% PFA concrete was lower than the prediction by 25.86%. The main reason for the higher bond strength of concretes made with 10% SF, 10% MK, and 50% GGBS cement replacement and CEM II can be attributed to their greater compressive and tensile strength, as discussed in section 4.4. Lundgren (2007) used a large concrete cover of 80 mm and a 20 mm bar size to analyse bond strength. It was found that the maximum bond strength was close to half the compressive strength (around 20 N/mm^2). In addition, the experimental results of this study indicated the average values of bond strength of CEM II, GBBS, PFA, MK and SF concrete which ranged from 18.60 to 21.40 N/mm^2. This is due to higher confinement which was provided by the large concrete cover (for cover more than 7.5d) associated with high compressive strength, where the compressive strengths of the concretes, f_c was greater than 32.5 N/mm^2. From the results presented in Figure 4.5 a-e, the specimens were failed by pull-out failure where the steel bar was pulled out with no apparent external cracks. These results show similar trends but with different level of bond strength, reflecting the variation in the concrete's mechanical properties.

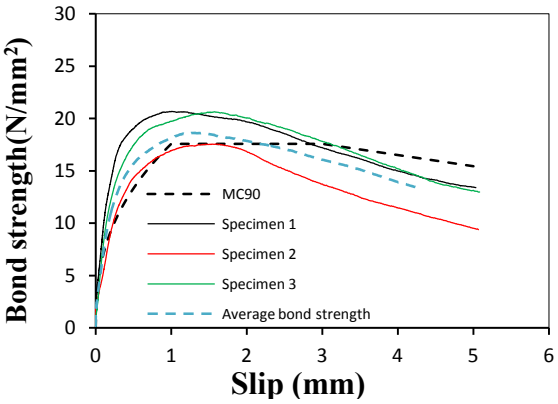

(a) Concrete with CEMII

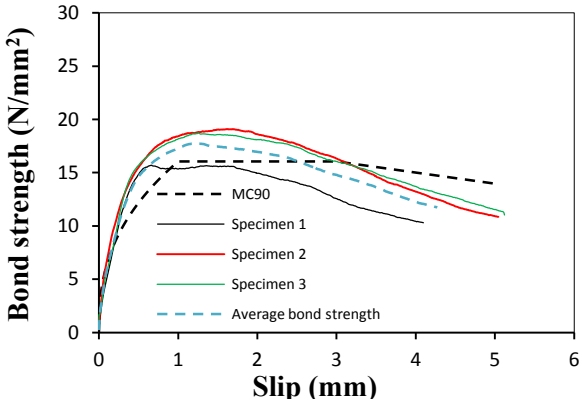

(b) Concrete with 50%GGBS

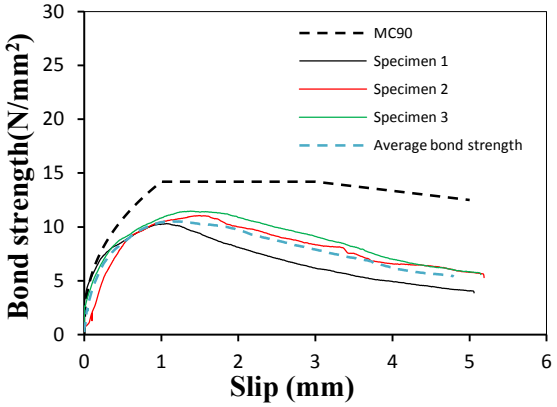

(c) Concrete with 30% PFA

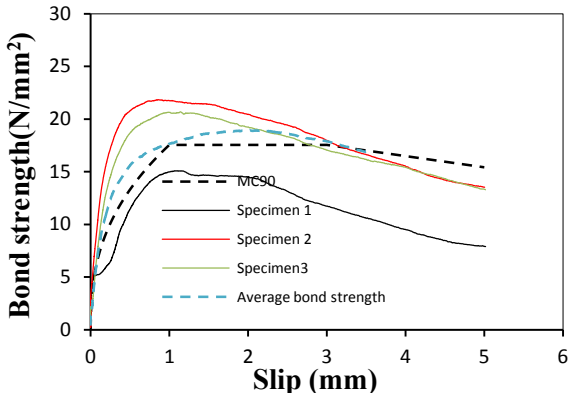

(d) Concrete with 10% MK

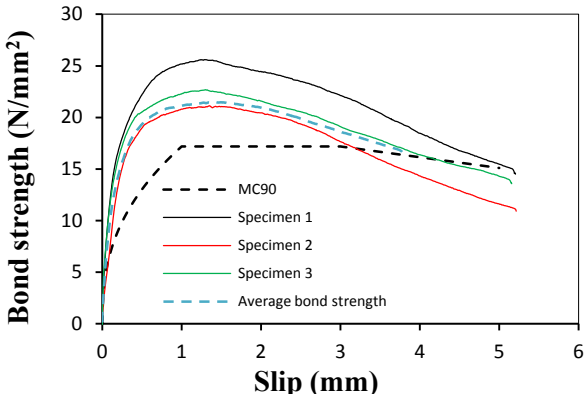

(e) Concrete with 10%SF

Figure 4.5: Bond strength versus slip for different concrete types (control specimens)

4.5.1 Influence of concrete type on the bond strength

Figure 4.6 presents the maximum bond strength and the mean bond strength as well as normalised bond strength (τ_u/f_{cu}) of control specimens for all mixes. As shown in Figure 4.6, the 10% SF mix had the highest maximum bond strength and mean bond strength which were 22.6 and 12.5 N/mm^2, respectively, while the normalised bond strengths (τ_u/f_{cu}) were found to be 1.15 and 1.8 times higher than that of the control mix, followed by the CEM II, 10% MK, and 50% GGBS mix. Comparing these results, it can be inferred that the control mix (CEM II) develops a maximum bond strength similar to that of the 50% GGBS and 10% MK mix, but the 50% GGBS and 10% MK concrete mixes had slightly lower mean bond strength than that of the control mix and the normalised values (τ_u/f_{cu}) were approximately 0.95 and 0.90 times lower than that of the CEM II mix.

Figure 4.6 also shows that both the maximum and the mean bond strengths were considerably lower for the 30% PFA mix, corresponding to a normalised bond strength (τ_u/f_{cu}) 0.85-0.81 times lower than the control mix. This can be explained by the cement replacement materials in the PFA mix which effect the interfacial zone (ITZ) between steel and concrete (Tanyildizi et al., 2008). In the cases of SF, MK and GGBS mixes have a higher compressive strength; concrete types apparently have similar bond strength, which is usually considered to be a function of chemical and micromechanical adhesion. It can be said that the SF concrete has a dense microstructure due to pore size reduction and the pozzolanic activity of the SF which can significantly improve the transition zone between the reinforcing bar and cement matrix leading to high bond strength. Gjorv et al. (1990) studied the influence of SF

on the bond strength capacity by using X-ray analyses and they reported that the silica fume was affected on interface zone between the steel bar and concrete, which made the transition zone denser. On the other hand, the bond strength of the 30% PFA mix was lower than that of the other concrete mixes. This is attributed to lower splitting tensile strength, as discussed previously. Arezoumandi et al. (2013) reported on the bond strengths of steel bar in high-volume fly ash concrete obtained for an FA cement replacement of 70%. They found that the bond strength of fly ash concrete was higher than the reference concrete because the cement replacement used in their study had more calcium oxide (Class C, fly ash). In contrast, this study the bond strength demonstrates that the bond strength of 45% of fly ash was lower than that of the control specimen due to the type of PFA (Class F), which affects concrete properties.

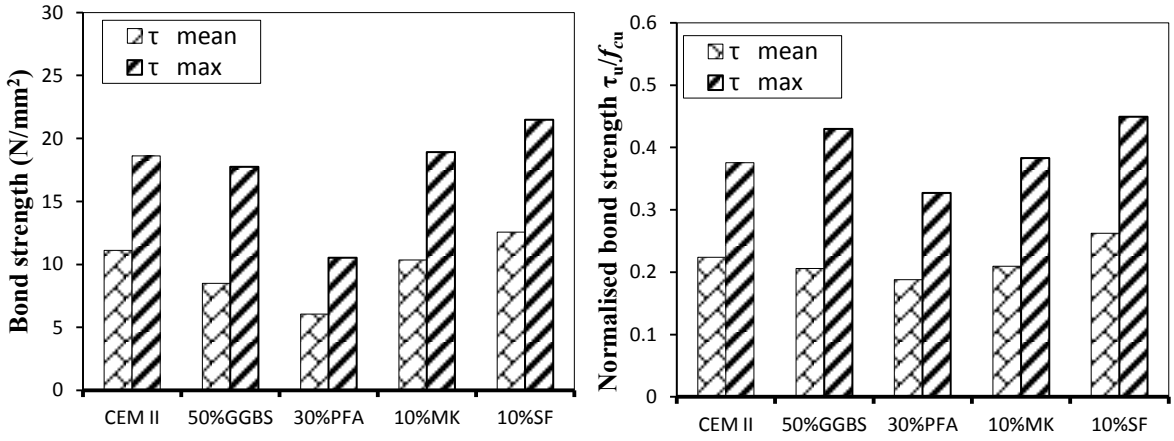

Figure 4.6: (a) bond strength and (b) normalised bond strength τ_u/f_{cu} for concrete mixes

4.5.2 Influence of corrosion levels on the bond strength

Figures 4.7 to 4.11 illustrate the bond strength-slip relationship for corroded and un-corroded samples for the five different concrete compositions, i.e., CEM II, 50% GGBS, 30% PFA, 10% MK and 10% SF.

Figure 4.7 shows typical bond strength versus slip curves for the CEM II concrete with different corrosion levels. The 00-CEM II-0 specimen is the control cube (without corrosion) and its maximum bond strength was 20.6 N/mm^2, corresponding to a slip of 1.16mm. After 3 days of corrosion, the bond strength of specimen 00-CEM II-3 was increased by 41.26% at a corrosion level of 0.27% but at a decrease in slip to 0.69mm. Specimens 00-CEM II-7 and 00-CEM II-10 exhibited corrosion levels of 0.56% and 0.97% with an associated increase in bond strengths by 64.5% and 77.18% compared with the control specimen, but at reduced levels of slip of 0.36mm and 0.39mm respectively. From Figure 4.7, it can be observed that a linear relationship between the bond strength-slip is obtained for the ascending branch of the corroded specimens. However, the initial response becomes stiffer since the degree of corrosion increases and improves the interface between the steel and the concrete. This phenomenon has been reported by other authors, such as Almusallam et al. (1996) and Chung et al. (2008), and is explained by an increase in friction between the reinforcing bar and the surrounding concrete as a result of the formation of small amounts of corrosion products. When the level of corrosion increased to 1.97% at 14 days, the maximum bond strength of the 00-CEM II-14 specimen was 7.12% (33.9 N/mm^2) lower than the ultimate bond strength of the 00-CEM II-10 specimen, and the slip was 0.49mm. The reason for the lower bond strength at 1.97% corrosion level was that the relative rib area of the reinforcing bars was reduced,

which led to a lower mechanical interlocking force. This was also confirmed after the corrosion products were removed from the steel bar.

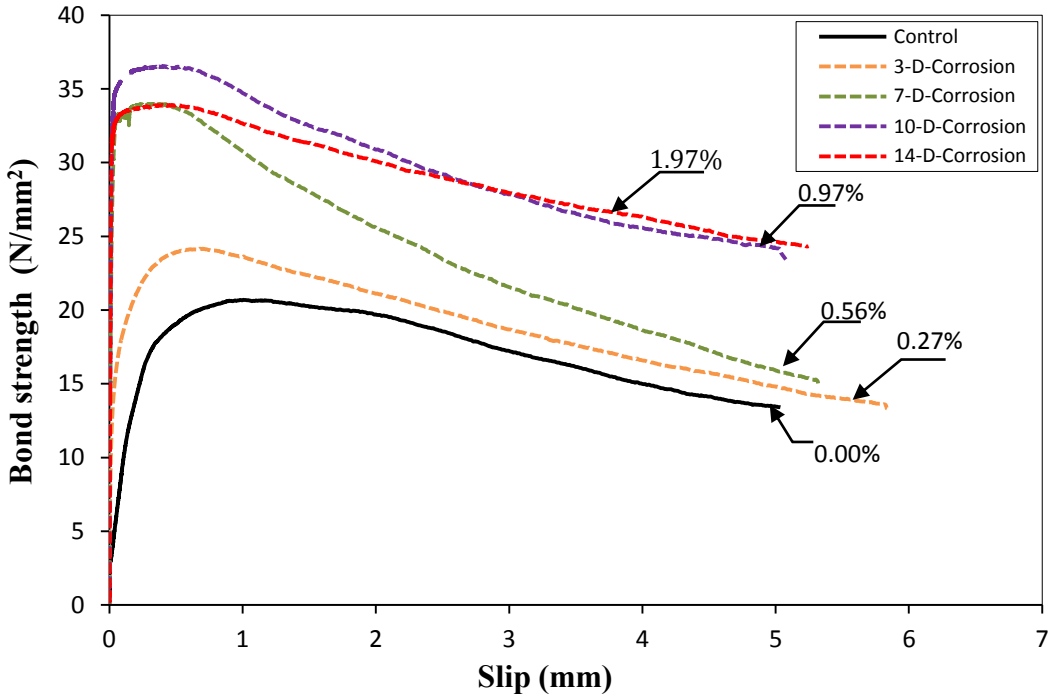

Figure 4.7: Bond strength versus slip curves for pull-out tests for CEM II concrete at different corrosion levels (%)

The typical bond strength versus slip curves of the 50% GGBS concrete were studied with the various corrosion levels, as shown in Figure 4.8. The maximum bond strength of the control sample (0% corrosion) was 18.7 N/mm^2 corresponding to a slip of 1.25mm. After 3 days of corrosion, the corrosion level was measured at 0.09% and the bond strength was 29.41% greater than the 50-GGBS-0 specimen, where the slip was also lower by 23.20% (0.96mm). Specimens corroded for 7 and 10 days illustrated corrosion levels of 0.22% and 1.10% and bond strengths that were 43.31% and 77% higher than that of the control (50-GGBS-0) respectively, but at decreased levels of slip of 0.91mm and 0.26mm respectively. For the corroded samples at 14 days, the corrosion level rose to 1.55%, while the bond strength value increased by a further 5.43% to 34.9 N/mm^2, compared with the 50-GGBS-10

specimen, with a slip level reduced to 0.15mm. Unlike the case with other cements, there is no reported data for bond strength using GGBS as cement replacement materials, which makes it difficult to compare the results to those of others.

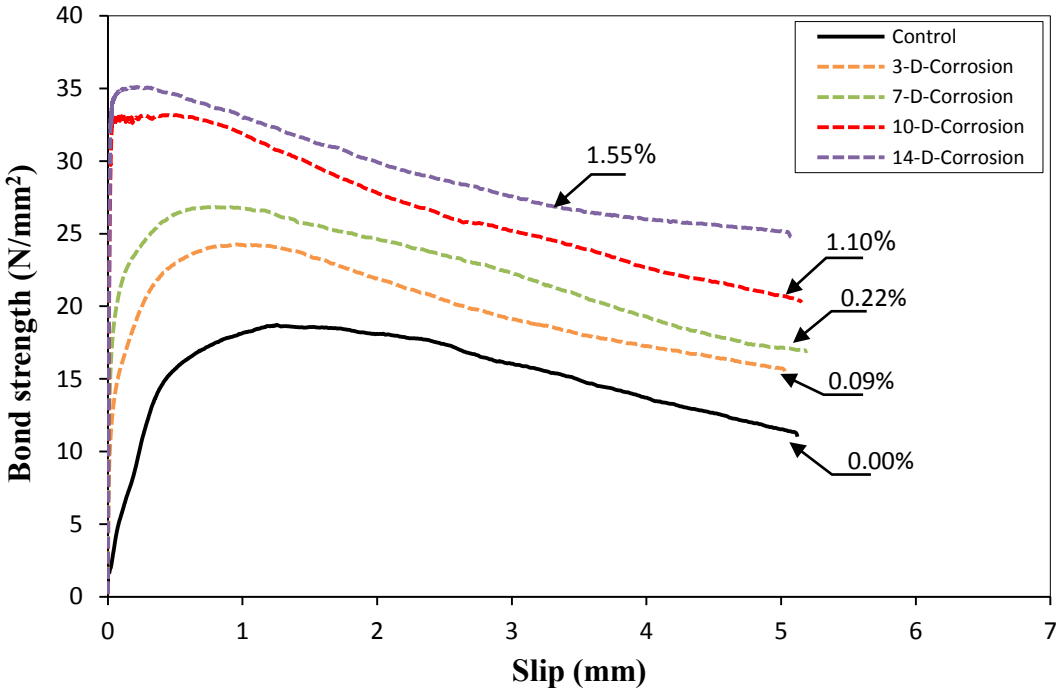

Figure 4.8: Bond strength versus slip curves for pull-out tests for concrete made with 50% GGBS cement replacement at different corrosion levels

Figure 4.9 shows typical bond strength versus slip curves for the 30% PFA concrete mix. It can be seen that the maximum bond strength of the control sample (0% corrosion) was 11.4 N/mm^2 at a slip of 1.38mm. After 3 days of corrosion, the corrosion level was measured at 0.18% and led to a 36% increase in bond strength but a decrease in slip from 1.38mm to 1.02mm. In addition, the 30-PFA-7 and 30-PFA-10 samples exhibited corrosion levels of 0.33% and 1.10% and bond strengths that were 66 % and 107.89 % higher than the un-corroded specimen, but at reduced levels of slip of 0.73mm and 0.53mm respectively. For the 30-PFA-14 sample, the corrosion level was increased to 1.0% whilst the ultimate bond strength increased by 11.81% to 26.5 N/mm^2. In a similar type of study, Cabrera (1996) also found that the

bond strength-slip of 30% fly ash (class C) concrete increased as the corrosion level increased. This is attributed to the very low amount of corrosion of the PFA specimens and as a result, the bond strength resistance was improved.

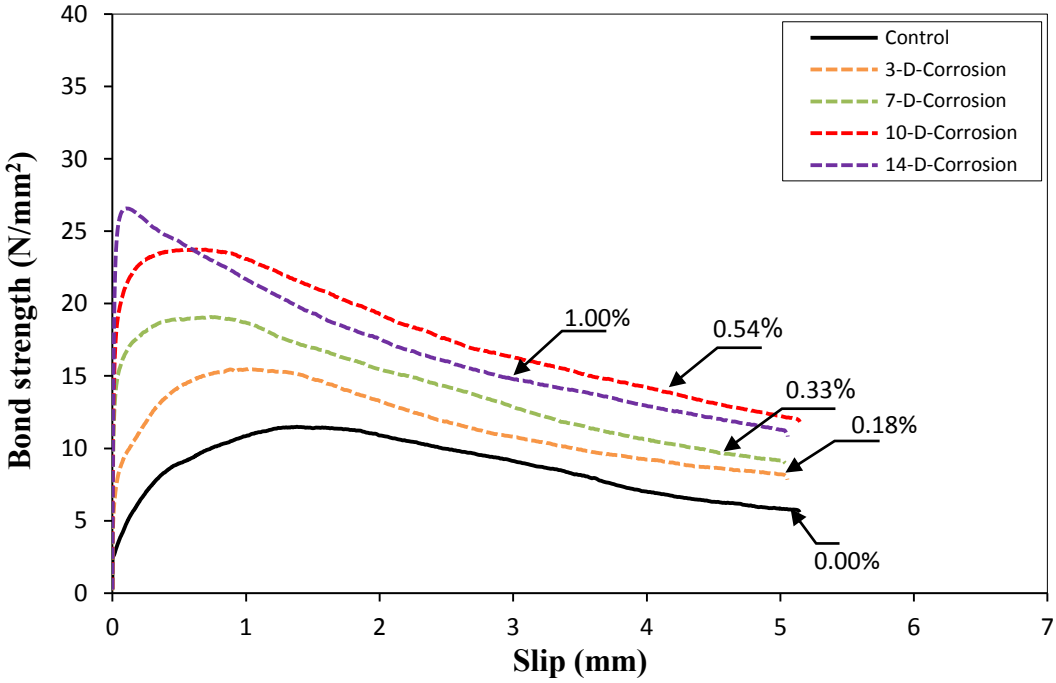

Figure 4.9: Bond strength versus slip curves for pull-out tests for concrete made with 30% PFA cement replacement at different corrosion levels

Figure 4.10 plots typical bond strength versus slip curves for concrete made with 10% MK. In this figure, it is noted that the maximum bond strength of the control specimen (10-MK-0) was 20.69 N/mm^2, corresponding to a slip of 1.13mm. After 3 days of corrosion, the corrosion level was measured at 0.42% and led to a 30.09% increase of bond strength capacity, but a decrease in the slip from 1.13mm to 0.87mm. However, specimens corroded for 7 and 10 days showed corrosion levels of 0.81% and 0.95% and the bond strength values were increased by 46.60% and 67% compared with the control sample, and there were reduced levels of slip of 0.94mm and 0.69mm respectively.

Figure 4.10 also displays up to 14 days of the exposure time, when the corrosion level increased to 1.20% while the bond strength value was slightly reduced by 0.58% to 34.2 N/mm^2 compared with that of the 10 days corroded (10-MK-10), and the slip decreased to 0.39mm. As can be seen in Figure 4.10, the corroded specimens at 10 and 14 days of exposure time demonstrated a linear behaviour in the pre-peak region (less than 1.5% corrosion level), which was high stiffness due to the corrosion products with the improvement the friction between the concrete and steel reinforcement.

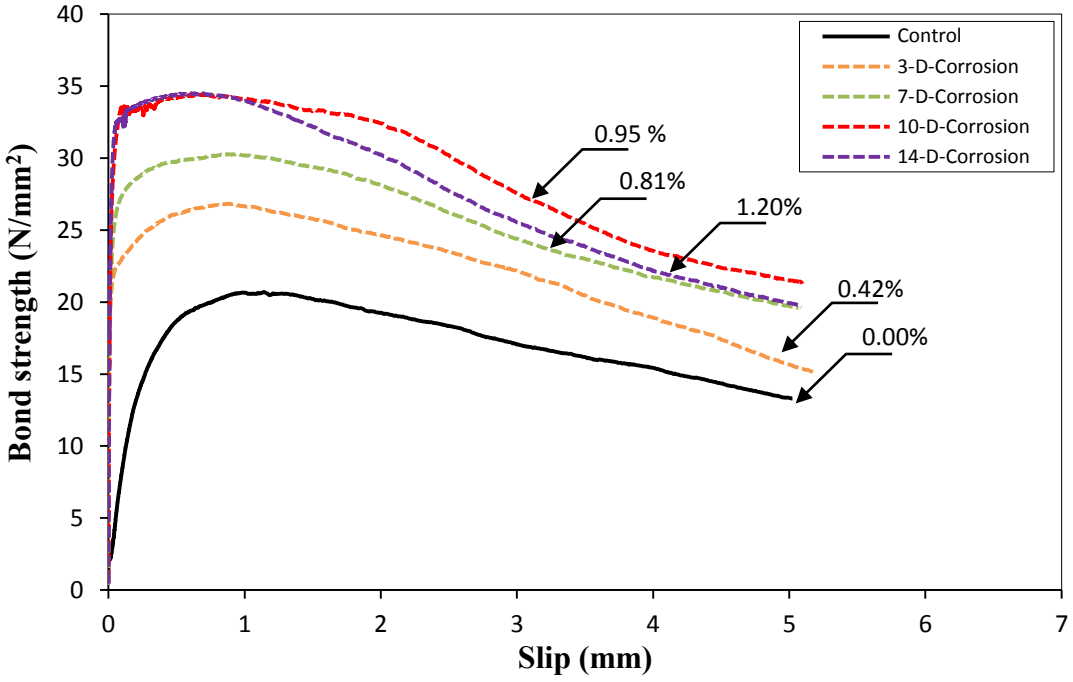

Figure 4.10: Bond strength versus slip curves for pull-out tests for concrete made with 10% MK cement replacement at different corrosion levels

The typical bond strength versus slip curves for steel bar in the 10% SF concrete with different degrees of corrosion are presented in Figure 4.11. It can be seen that the maximum bond strength of the uncorroded specimen (10-SF-0, control) was 22.60 N/mm^2, corresponding to a slip of 1.32mm. After extending the exposure time for 3

days, the corrosion level was 0.02% and led to an 18.09% increase in bond strength, but an increase in the slip from 1.32mm to 1.60mm. Meanwhile the corroded 10-SF-7 and 10-SF-10 specimens for 7 and 10 days displayed corrosion levels of 0.07% and 0.16% and the bond strength increased by 27.62% and 30.45% compared with that of the 10-SF-0 (control) sample, corresponding to slips of 1.43mm and 0.44mm, respectively. As shown in Figure 4.11, the 10-SF-14 sample was corroded up to 14 days of exposure, the corrosion level increased to 0.25%, whereas the bond strength value was 43.86% (32.6 N/mm^2) greater than that of the control specimen, in which the slip increased to 0.76mm. Furthermore, it was observed that the improvement of the bond strength is associated with low corrosion levels. This could be due to the low formation of corrosion products around the reinforcing bar. These results indicated that the silica fume has low permeability of concrete as known from previous studies (Güneyisi et al. 2012). Furthermore, it may be attributed to the reaction of the SF with calcium hydroxide during the hydration of products which leads to the filling of pores and packing of the fine particles pores between concrete/steel interface, which resulted to the reduction of chloride ion penetration in concrete.

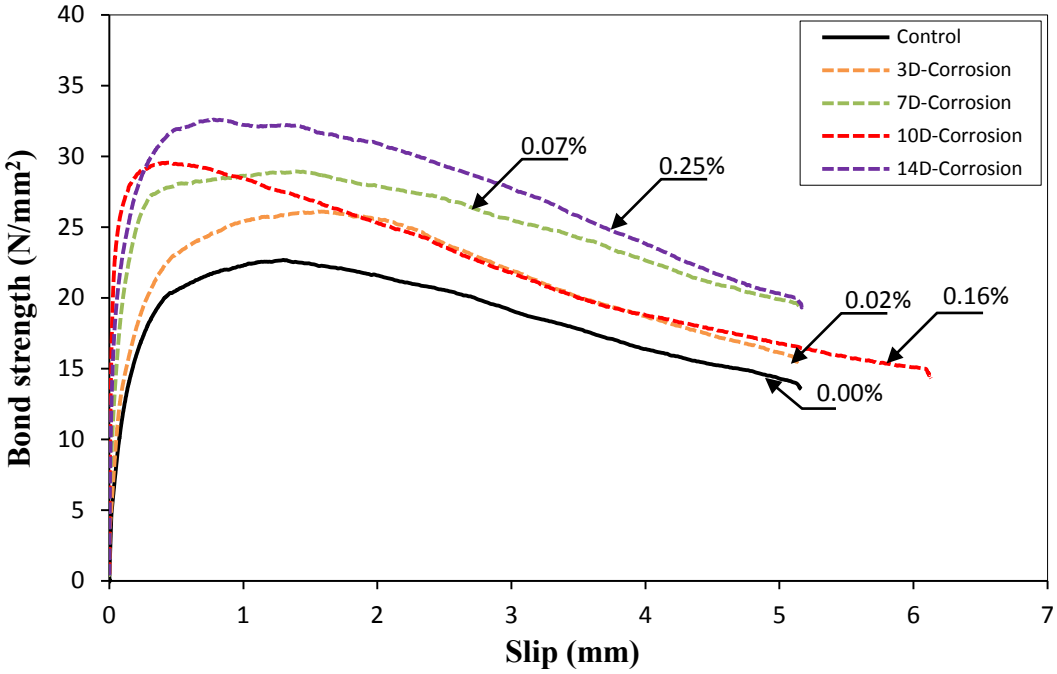

Figure 4.11: Bond strength versus slip curves for pull-out tests of concrete made with 10% SF cement replacement at different corrosion levels

Figures 4.7 to 4.11 present the results for the bond strength-slip curves for different corrosion levels for a reinforcing bar in concrete made with different cement replacement materials. They reveal that the bond strength increases as the corrosion level increases because of the roughness of the reinforcing bar, and this improves the friction between the steel and concrete interface. This phenomenon was reported by Chaung et al. (2008), Fang et al. (2004) and Lee et al. (2002). In addition, the bond strength was also affected by compressive strength; leading to high level of confinement causing an expansive mechanical pressure on the surrounding concrete. Figure 4.7 shows the bond strength of the CEM II gradually decreasing when the corrosion level was 1.97% after 14 days of corrosion, due to deterioration of the ribs of the steel bar and loss of the interaction between the steel and concrete at the interface. On the other hand, the bond strength of concrete made with pozzolanic materials (50% GGBS, 30% PFA, 10% MK and 10% SF) increased at the same

exposure time (14 days), which means that the corrosion levels of these concrete were lower by 21.3%, 49.2%, 39% and 87.3% when compared to the corrosion level of CEM II concrete, as shown in Figures 4.7 to 4.11. The difference in corrosion level observed can be attributed to the influence of pozzolanic material on the concrete microstructure used in this investigation, which leads to good impermeability and corrosion resistance compared with normal concrete. Overall, from these results it can be stated that low corrosion level was provided better the bond strength, and this is true irrespective of the cement replacement materials used or the compressive strength.

4.6 Results of bond strength with further corroded specimens

The exposure time of these specimens (chapter 3.1) was extended to give a further 20 days of corrosion exposure (6+14 days), with the aim of generating additional corrosion products and hence exploring their effects on bond strength. The individual cube sample was tested at each time of the pull-out test. The control mix was made with CEM II. Additionally, the GGBS concrete was made with two levels of replacement materials (50% and 60%) and the PFA concrete was made with three levels of replacement materials (30%, 40% and 45%). After the prescribed period of corrosion, specimens were left under wet hessian until the time of testing, when bond sample tests were carried out at 52 days. The results obtained for the effect of the corrosion of the steel bars embedded in concrete on bond strength are presented in Table 4.4.

Table 4.4: Results of pull-out tests for concrete mixes at 52 days

Specimen	f_{cu} [a] **(52 days)**	f_{max} [b]	**Bond strength** τ_{max}	**Slip at max Load**	τ_m [c]	τ_u/f_{cu}	**Failure Mode**
	N/mm^2	kN	N/mm^2	mm	N/mm^2	-	-
00-CEM II-0	50.0	26.5	14.1	1.87	7.7	0.28	Pull-out
00- CEM II-3		42.9	22.8	0.51	18.3	0.45	Pull-out
00- CEM II-7		59.3	31.5	0.16	26.3	0.63	Pull-out
00- CEM II-14		62.0	32.9	0.13	28.2	0.65	Pull-out
00- CEM II-20		59.7	31.7	0.02	20.0	0.63	Splitting
50-GGBS-0	51.4	26.3	14.0	1.06	6.6	0.27	Pull-out
50- GGBS-3		42.6	22.6	0.67	18.8	0.44	Pull-out
50- GGBS-7		43.7	23.2	0.45	19.9	0.45	Pull-out
50- GGBS-14		64.8	34.4	0.17	29.2	0.66	Pull-out
50- GGBS-20		49.9	26.5	0.01	20.0	0.51	Splitting
60-GGBS-0	43.6	32.9	17.4	1.08	8.8	0.39	Pull-out
60-GGBS-3		36.1	19.1	0.4	16.0	0.44	Pull-out
60-GGBS-7		52.8	28.0	0.1	22.2	0.64	Pull-out
60-GGBS-14		62.9	33.3	0.06	26.8	0.76	Pull-out
60-GGBS-20		62.2	33.4	0.05	27.5	0.77	Pull-out
30-PFA-0	37.3	16.0	8.5	1.39	4.7	0.23	Pull-out
30-PFA-3		36.7	19.5	0.73	14.3	0.52	Pull-out
30-PFA-7		46.9	24.9	0.19	19.6	0.67	Pull-out
30-PFA-14		58.8	31.2	0.074	24.5	0.83	Pull-out
30-PFA-20		61.2	32.5	0.17	24.4	0.87	Pull-out
40-PFA-0	35.0	22.6	12.0	1.01	7.3	0.34	Pull-out
40-PFA-3		26.8	14.2	1.28	9.6	0.40	Pull-out
40-PFA-7		27.0	14.3	0.59	11.4	0.41	Pull-out
40-PFA-14		32.0	17.0	0.49	13.3	0.48	Pull-out
40-PFA-20		45.7	24.2	0.24	18.3	0.69	Pull-out
45-PFA-0	31.1	20.3	10.7	1.02	5.3	0.34	Pull-out
45-PFA-3		30.2	16.0	0.36	12.9	0.51	Pull-out
45-PFA-7		35.9	19.0	0.31	15.4	0.61	Pull-out
45-PFA-14		26.0	13.8	0.63	11.5	0.44	Pull-out
45-PFA-20		36.5	19.4	0.30	16.4	0.62	Pull-out

Note: [a] f_{cu} = average compressive strength (cube, 100); [b] f_{max}=maximum pull-out load; [c] τ_m= the mean bond strength.

Figure 4.12 shows bond strength-slip curves of 5 individual pull-out specimens for different corrosion levels of steel reinforcements embedded in the CEM II concrete (set 2). As observed previously, the bond strength capacity increases relative to the amount of corrosion, which improved the roughness of the steel bar. Figure 4.12 also shows that the ultimate bond strength of the 00-CEM II-20 specimen was 3.64% less (31.7 N/mm^2) than that of the bond strength of the 00-CEM II-14 specimen after extending the exposure time to 20 days. The brittle failure obtained during the pull-out test of the specimen is a result of the internal cracks due to the expansion pressure created by the corrosion products exceeding the tensile strength of the concrete, which led to the formation of a longitudinal crack along the concrete cover. Finally, the bond strength suddenly dropped to about 4.2 N/mm^2 (see Figure 4.12) due to the loss interlocking action between steel bar and concrete.

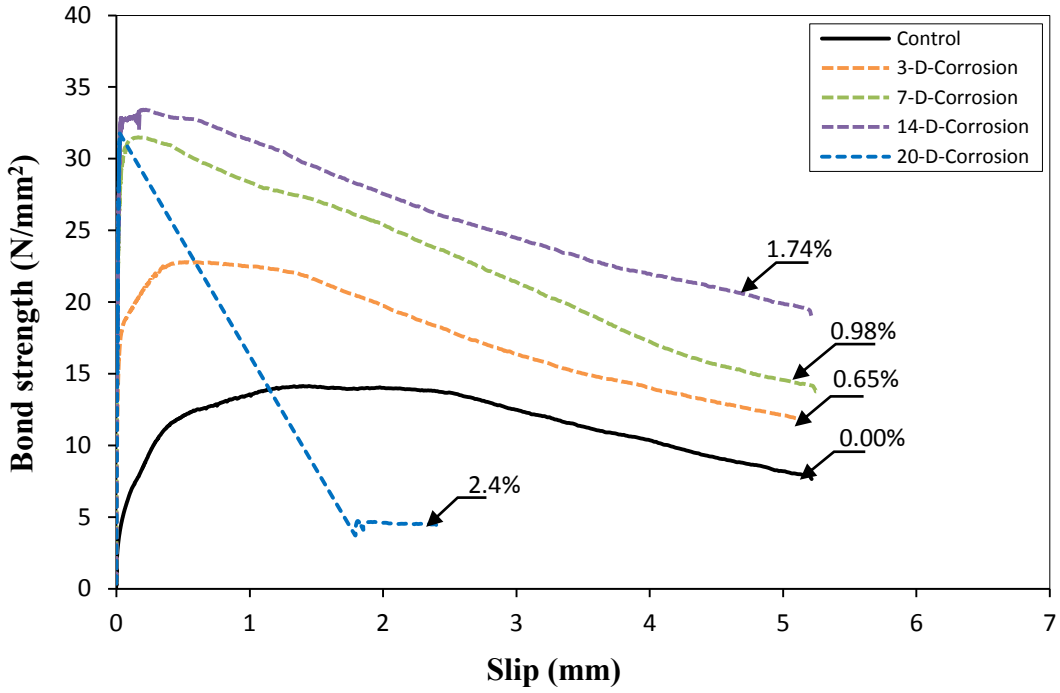

Figure 4.12: Bond strength versus slip curves for pull-out tests of concrete made with CEM II at different corrosion levels

Figures 4.13 and 4.14 show the bond strength-slip curves for steel bar in concrete mix with 50% and 60% GGBS replacement with varying corrosion levels. It can be seen that the bond strength achieved with increasing corrosion is between 61% and 145% of the bond strength of the control specimen, as shown in Figure 4.13. The bond strength increased when corrosion level was low (less than 2% of corrosion level), it can be attributed to the mechanical pressure on the surrounding concrete and hence, leading to increased mechanical interlocking as well as increased roughness of steel bar. When the exposure time is extended to 20 days, the 50-GGBS-20 specimen had a higher corrosion level and a bond strength 22.96% lower (26.5 N/mm^2) than the 50-GGBS-14 specimen. In this case, the maximum bond strength reduced as the corrosion progressed. This may be attributed to the degradation of the bond strength when the corrosion volume increased, leading to a loss of interlocking action between the steel bar and the concrete. The bond failure changed from a pull-out to a splitting failure (brittle) and cracking was observed on the side of the specimen. This finding is in good agreement with findings from previous studies (Chung et al., 2008). Additionally, the bond strength-slip curves for the steel bar for the 60% GGBS concrete are shown in Figure 4.14. The bond strength obtained for the control was 17.48 N/mm^2, but the bond strength of the corroded specimens increased gradually by 9.16%, 60.52% and 90%, corresponding to corrosion levels of 0.90%, 1.21% and 1.60% respectively. The bond strength of the 60-GGBS-20 sample decreased by 0.17% compared with the 60-GGBS-14 specimen because the corrosion product layer formed to affect the mechanical interlocking at the interface. From the use of both 50% and 60% GGBS concretes, it is concluded that the ultimate bond strength increased when increasing the corrosion exposure to 14 days. Additionally, the bond stiffness increased in first stage of the bond strength-slip curve due to an increase in the amount of corrosion around the steel bar.

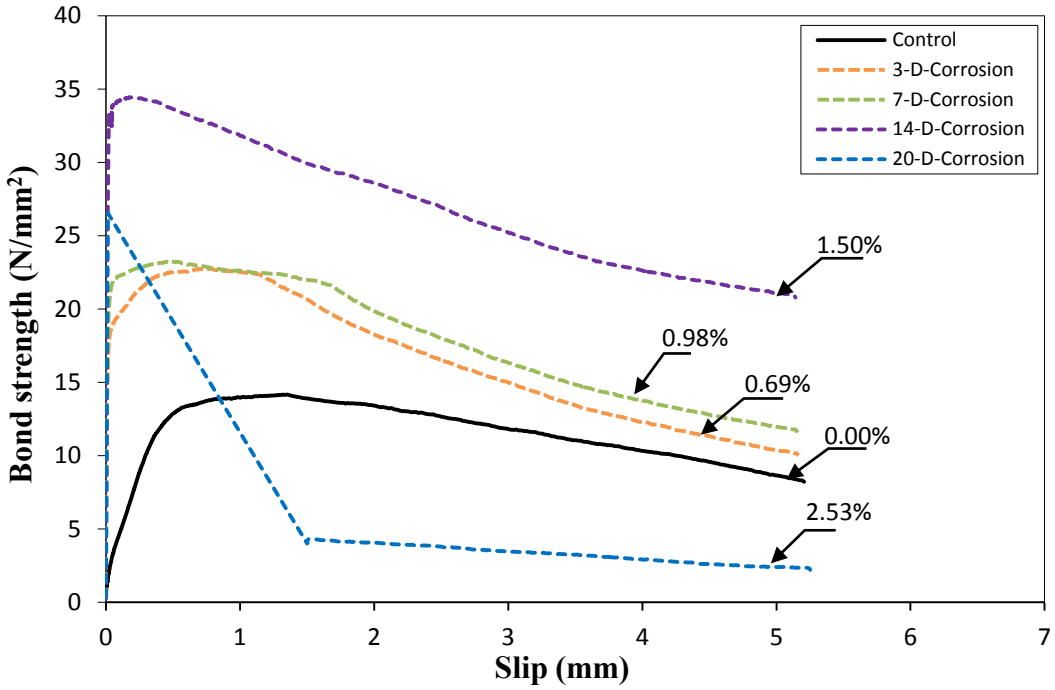

Figure 4.13: Bond strength versus slip curves for pull-out tests of concrete made with 50% GGBS cement replacement at different corrosion levels

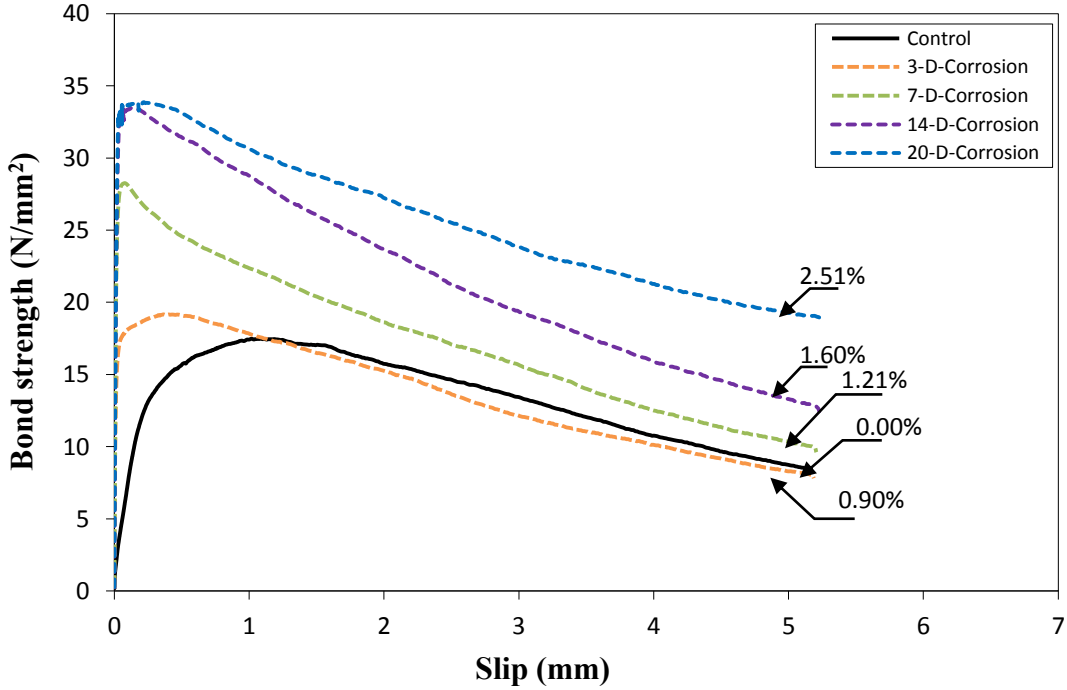

Figure 4.14: Bond strength versus slip curves for pull-out tests for concrete made with 60% GGBS cement replacement at different corrosion levels

Figures 4.15 to 4.17 show the bond strength-slip curves for various levels of corrosion of steel bars in the concrete containing 30%, 40% and 45% PFA. It can be seen from Figure 4.15 that, when using the 30% PFA concrete, the maximum bond strength of the 30-PFA-0 specimen was 8.5 N/mm^2 (0%, control), whereas the corrosion of steel reinforcement of specimens 30-PFA-3 and 30-PFA-7 increased to 0.18% and 0.63%, and hence the maximum bond strength was 129.9% and 192.9% greater than the bond strength of 30-PFA-0 after an exposure time of 3 and 7 days, respectively. In addition, the bond strength of specimens 30-PFA-14 and 30-PFA-20 had high corrosion levels of steel bars after 14 and 20 days of corrosion time with greater bond strength (31.2 and 32.5 N/mm^2) compared with sample 30-PFA-7. Figure 4.15 shows that the stiffness of corroded specimens increased with the increasing degree of corrosion caused by the increasing roughness of the steel bar. This is because the increase in the steel bar's roughness enhances the friction between the steel bar and concrete. This phenomenon has also been observed by other researchers (Cabrera, 1996; Almusallam et al., 1996; Abosrra et al., 2011). Figure 4.16 indicates the bond strength-slip curves of 40% PFA concrete and the values of bond strength obtained were approximately 18.5% - 102% higher than the control specimens. As can be seen in Figure 4.17, the bond strength-slip curves for the steel bar embedded in the concrete containing 45% of PFA at different corrosion levels demonstrate that the ultimate bond strength obtained for specimen 45-PFA-0 was 10.78 N/mm^2, but the ultimate bond strength of corroded specimens at 3 and 7 days of exposure time increased by 52.95% and 81.96%, respectively, while the corroded specimen for 14 days (45-PFA-14) of exposure had a bond strength 45% less than that of 45-PFA-7, which exhibited a lower corrosion level (0.51%). For the specimen corroded up to 20 days, as the amount of corrosion increased (i.e., 0.85%), there was an increase in bond strength (19.40 N/mm^2), greater than the bond strength of the control specimen by about 80% and the value of slip was 0.30 mm.

From Figures 4.15 to 4.17, it can be clearly seen that the concrete containing high values of PFA (40% and 45%) had higher corrosion resistance than the concrete containing 30% PFA. It would appear that bond strengths for these mixes may be lower due to the variation in mechanical properties of these concretes, as mentioned earlier. For example, for the specimen with 30% PFA at 14 days of exposure time, the corrosion level was 1.28%, whereas both 40% and 45% PFA concretes had corrosion levels that were about 2.20 and 2.13 times lower respectively at the same exposure time. Both mixes of 40% and 45% PFA take longer to achieve approximately the same corrosion level of the 30% PFA mix at 14 days of exposure time. This can be explained by the fact that the concretes made with 40% and 45% PFA became more impermeable than concrete have 30% PFA. In addition other reason may be the high resistance of these concrete to chloride penetration as pozzolanic reaction causes formation of products more CSH gel the refinement of the pore structure. An incremental increase in the fly ash percentage in the concrete improved the corrosion resistance, as reported by Chalee et al. (2009). The findings from this comparison indicate that the different types of concrete used in this study have different microstructures and systems of pores sizes, which affected the corrosion level.

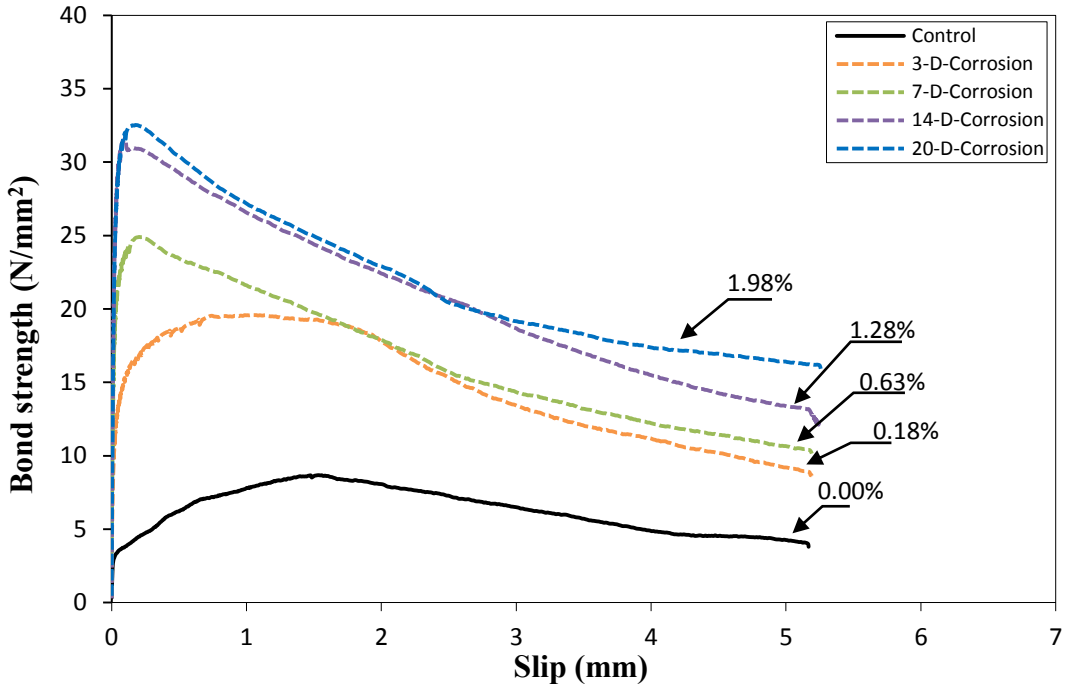

Figure 4.15: Bond strength versus slip curves for pull-out tests for concrete made with 30% PFA cement replacement at different corrosion levels

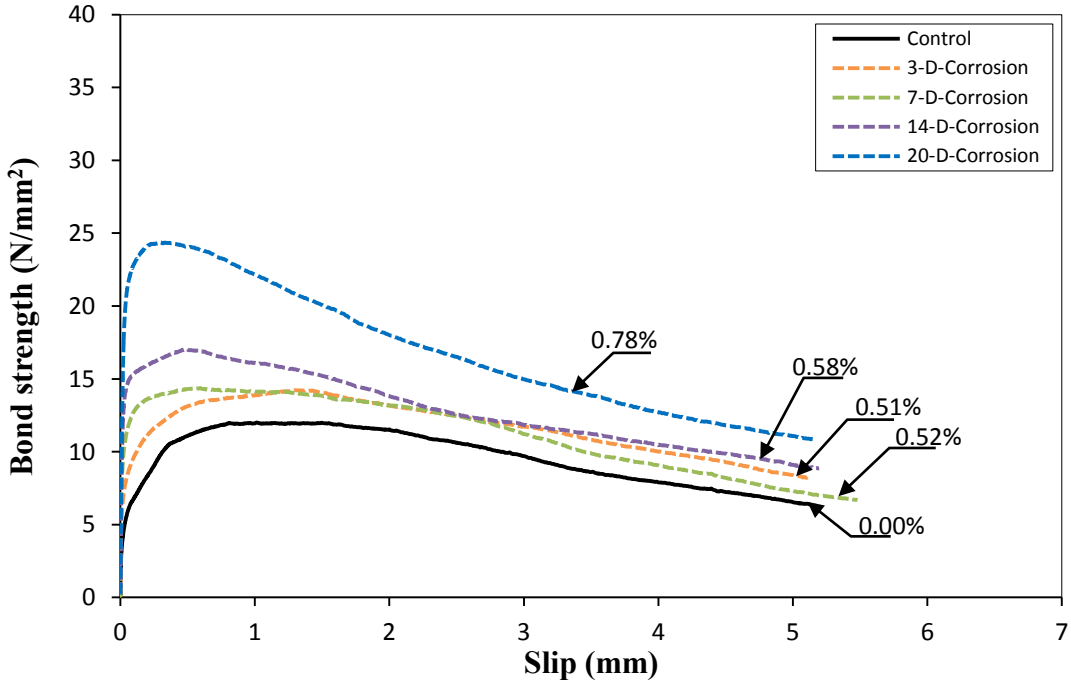

Figure 4.16: Bond strength versus slip curves for pull-out tests for concrete made with 40% PFA cement replacement at different corrosion levels

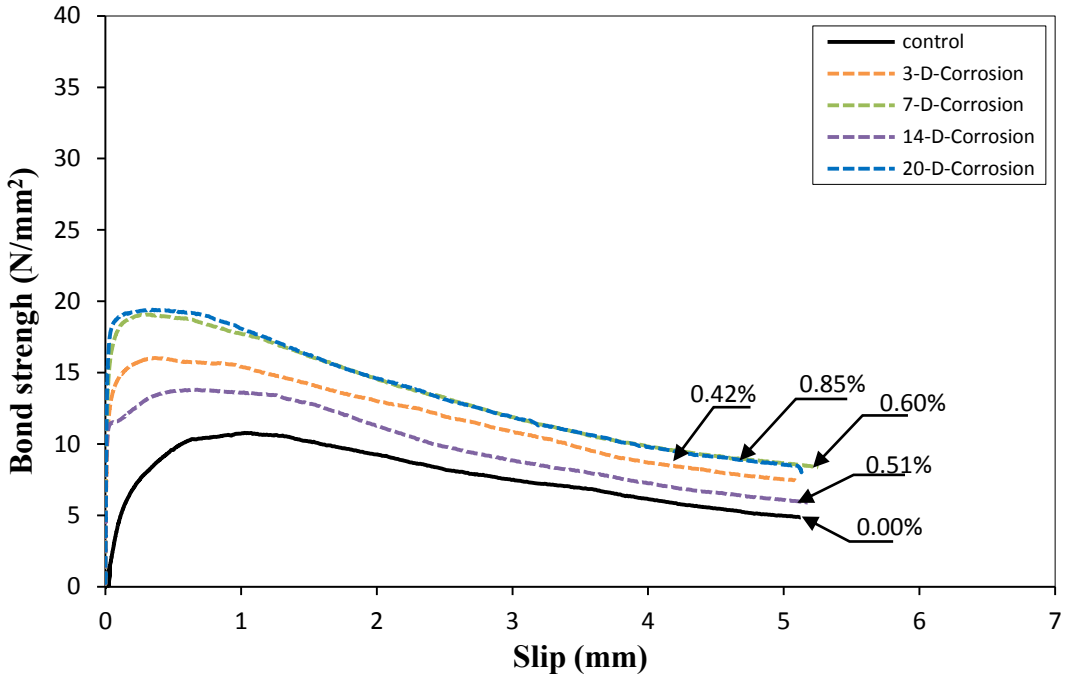

Figure 4.17

Figure 4.17: Bond strength versus slip curves for pull-out tests for concrete made with 45% PFA cement replacement at different corrosion levels

4.7 Bond failure modes

There are two important modes of failure corresponding to the bond failure. From the experimental results, it can be observed that the bond failure behaviour for all the control specimens (un-corroded) was similar for all mixes, as presented by Figure 4.4(a-e), and visual observation did not any reveal any splitting cracks during the pull-out test. This is because the concrete cube specimen had sufficient concrete cover depth (94mm), which is greater than three times the reinforcing bar diameter to provide confinement of the steel bar during the pull-out testing to result in pull-out failure (Figure 4.18(a)). Furthermore, all corroded specimens had similar failure modes as a result of the low corrosion levels, with the exception of two specimens corroded up to 20 days (00-CEM II-20 and 50-GGBS-20), where bond failure occurred by splitting rather than pull-out (Figure 4.18(b)). The reason for this change in the failure from ductile to brittle is due to

the high quantity of corrosion products on the steel surface, which led to longitudinal cracks and damaged the concrete, signifying that the transfer of forces from the steel to the concrete can no longer take place.

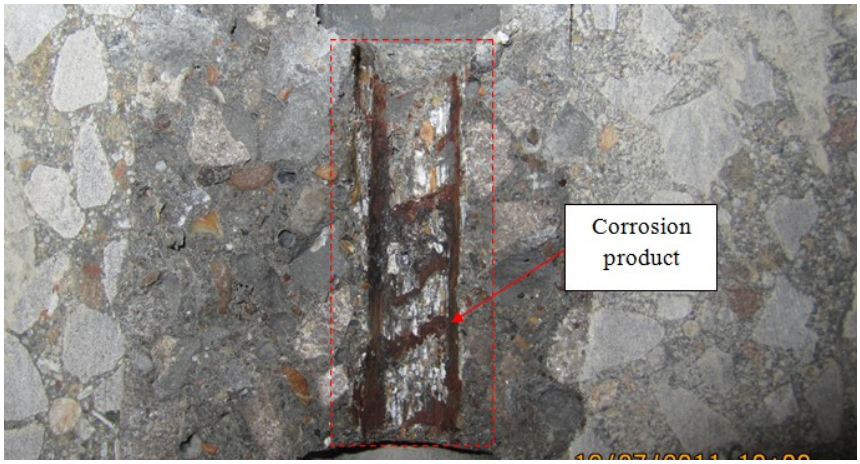

(a)

(b)

Figure 4.18: (a) Photograph of steel bar after artificial corrosion and pull-out test; (b) Splitting of concrete due to corrosion (50-GGBS-20)

4.8 Influence of the corrosion levels on slip

Figure 4.19 shows the value of slip with respect to the maximum bond strength for every specimen plotted against corrosion level for all of the different concretes. It is evident that the relationship between slip and the level of corrosion of the bar is consistent in all cases. From the results reported in Tables 4.4 and 4.5, it is observed that the slip of the control specimens of all concrete mixes was higher than that of the corroded specimens. When the corrosion level increased to 20 days; the slips of specimens 00-CEM II-20 and 50-GGBS-20 were reduced by 99% (0.02 mm, 0.01 mm) respectively of the control specimens due to higher quantities of the corrosion products. It can be said that the slip corresponding to the maximum bond strength decreased with an increasing corrosion level within the range considered. As the tension in specimen was increased due to the formation of the corrosion layer between the steel bar and concrete interface and therefore the confinement was increased. The value of slip at the 1.74% corrosion level was less than 0.13 mm for 00-CEM II-14 specimen. This represents about a 14-fold decrease compared to uncorroded steel bar specimens. In addition, it appears that there is a reduction in slippage for specimens with increasing degrees of corrosion; this could be due to the influence of the corrosion formation on bond properties at the interface of the steel and the concrete. Similar findings were reported by Auyeung et al. (2000), in that the slip at failure decreased as the level of corrosion increased. They observed that at a corrosion level of 0.98%, the slip of the steel bar at failure was roughly 0.33 of that of the uncorroded steel bar.

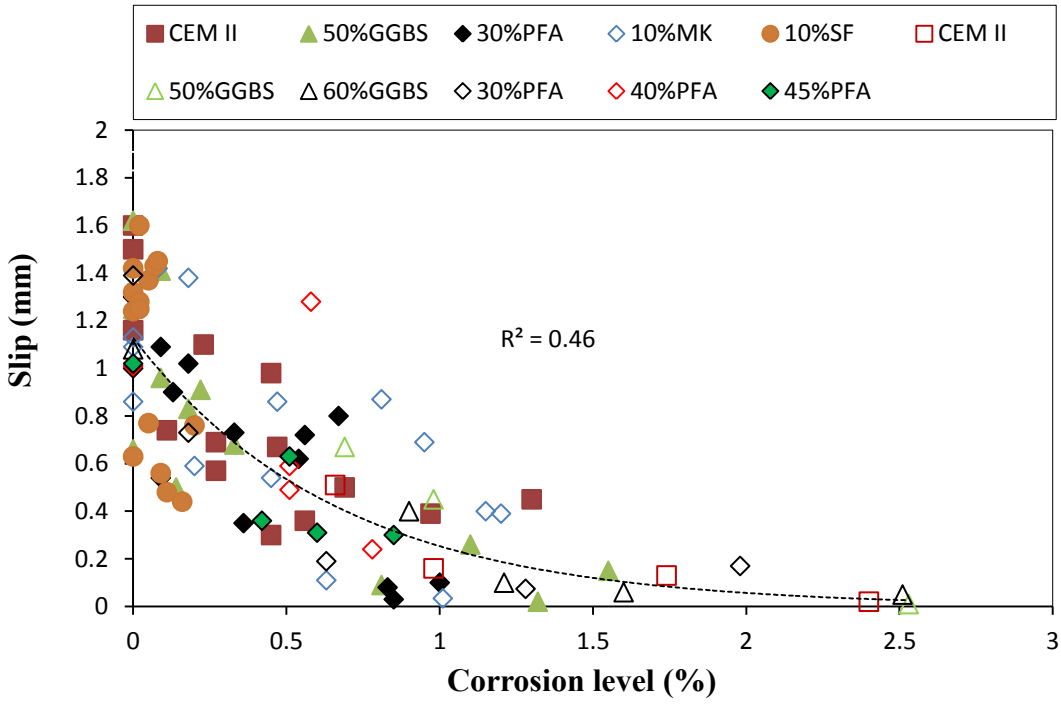

Figure 4.19: Slip and corrosion levels for all the concrete types

4.9 Empirical models of bond strength for corroded reinforcement bars

Figure 4.20 shows the bond strength ratio ($\tau_{u,corrosion}/\tau_{u,control}$) for the experimental results of CEM II concrete, which were obtained in the corrosion level range from 0% to 1.97% in this research and those obtained in the work of various authors (Al-Sulaimani et al, 1990; Cabrera, 1996; Almusallam et al; 1996; Auyeung et al; 2000; Lee et al, 2002; Chung et al., 2008). It is worthwhile to note that the results reported by these authors were from a wider range of corrosion levels compared to the study presented in this chapter. Based on the experimental results, Eq. (4.4) was obtained using nonlinear regression analysis to predict the bond strength as a function of corrosion when the corrosion level is less than 2%, but the experimental results do not extend to high levels of corrosion. When the corrosion level is greater than 2%, an empirical equation (4.5) developed by Chung et al. (2004) can be used to predict bond strength:

$$\tau_u = -4.760\, cl^2 + 14.219 cl + 23.635 \quad (4.4)$$

for $cl < 2.0\%$

$$\tau_u = 2.09\, cl^{-1.06} \quad (4.5)$$

for $cl \geq 2.0\%$

where τ_u is the bond strength and cl is the corrosion level of the steel bars.

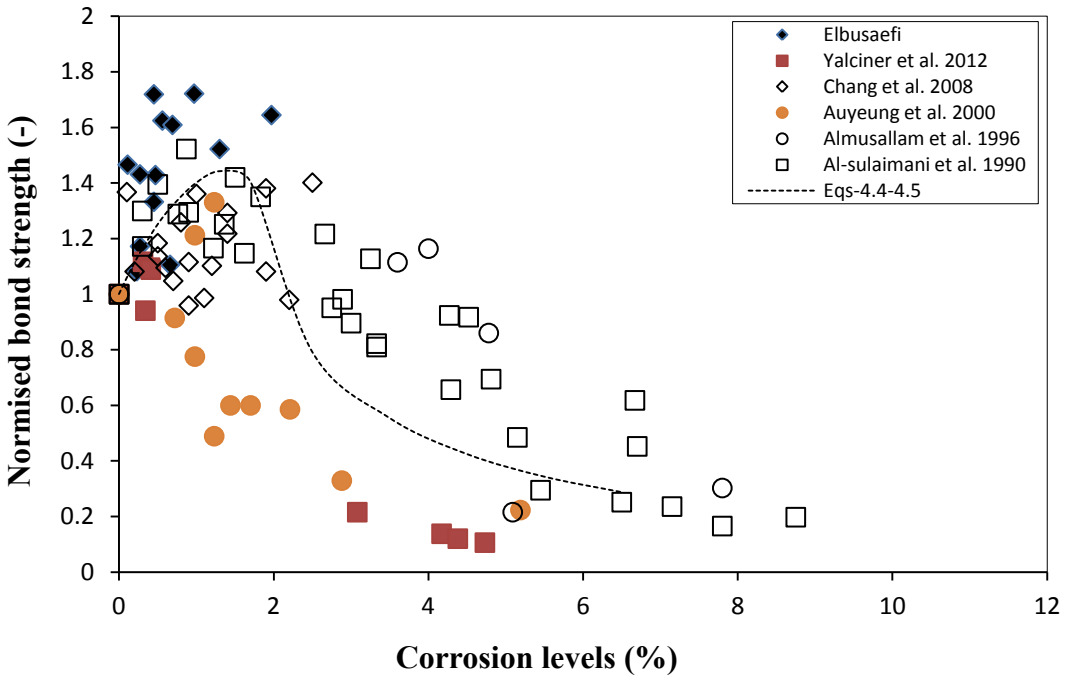

Figure 4.20: Normalised bond strength as a function of corrosion level

Figure 4.21 shows the comparison of experimental results and the bond strength equation model in Eqs. (4.4) and (4.5), and the empirical bond strength model developed by other researchers (Cabrera., 1996; Lee et al., 2002; Bhargava et al., 2007; Chung et al., 2004). It can be seen from the same figure that the previous empirical models exhibit a linear decrease in bond strength when the level of corrosion increases. The reason for this may be the very high current densities (i_{corr}) from 2000 to 4000 μA/cm^2 used in these studies, as evidenced by the higher corrosion levels and higher deterioration of steel bar. On the other hand, the results obtained show significant differences to the predicted bond capacity, as they were greater than the other predicted

results because the corrosion level was smaller than 2% and current density used in this study was low, at 0.53 μA/cm^2. Moreover, the concrete cover to diameter ratio used in this study is 7.83 (94mm/12mm) which is higher than previous studies, which used slightly lower (ranging from 3 to 5.75d_b), thus leading to higher confinement of the concrete cover and an improvement in the bond strength.

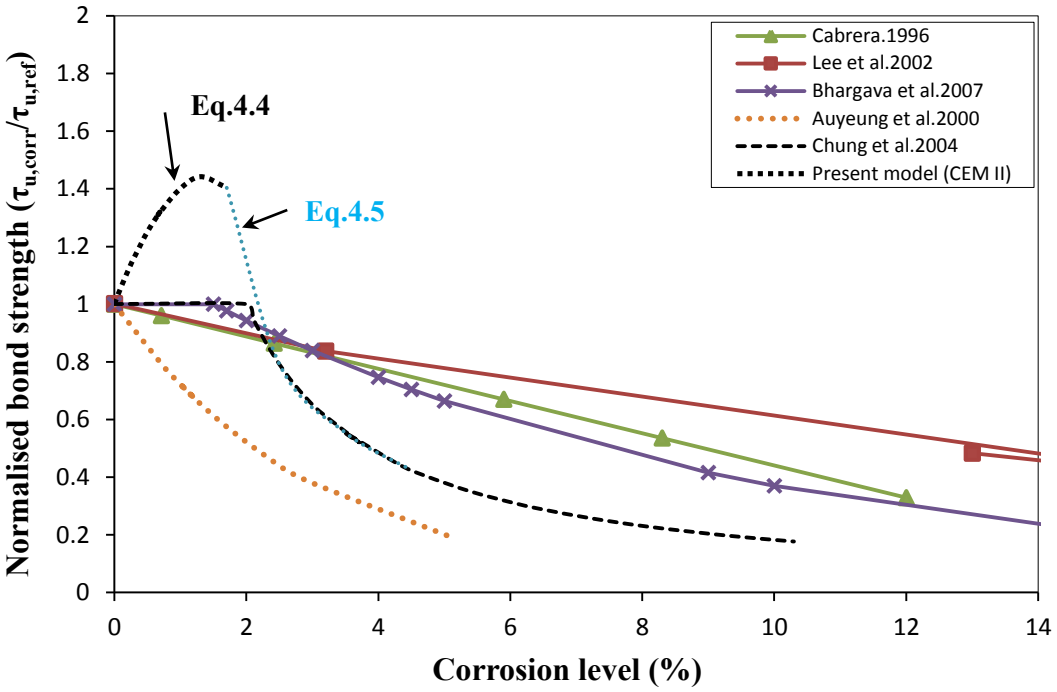

Figure 4.21: Normalised bond strength as a function of corrosion level

4.10 Effect of varying levels of corrosion on the bond strength

From the results which have been presented, it is clear that there is a general relationship between both bond strength and the level of corrosion and slip and the level of corrosion. To explore the former relationship further, Figures 4.22 and 4.23 have been plotted in which both the maximum bond strength and the mean bond strength of all test specimens have been non-dimensionalised by dividing them by the compressive strength of the mix from which they were taken. The mean bond strength is that obtained by averaging the strength recorded at slips of 0.01mm, 0.1mm and 1.0mm, as defined by BS EN 10080:2005.

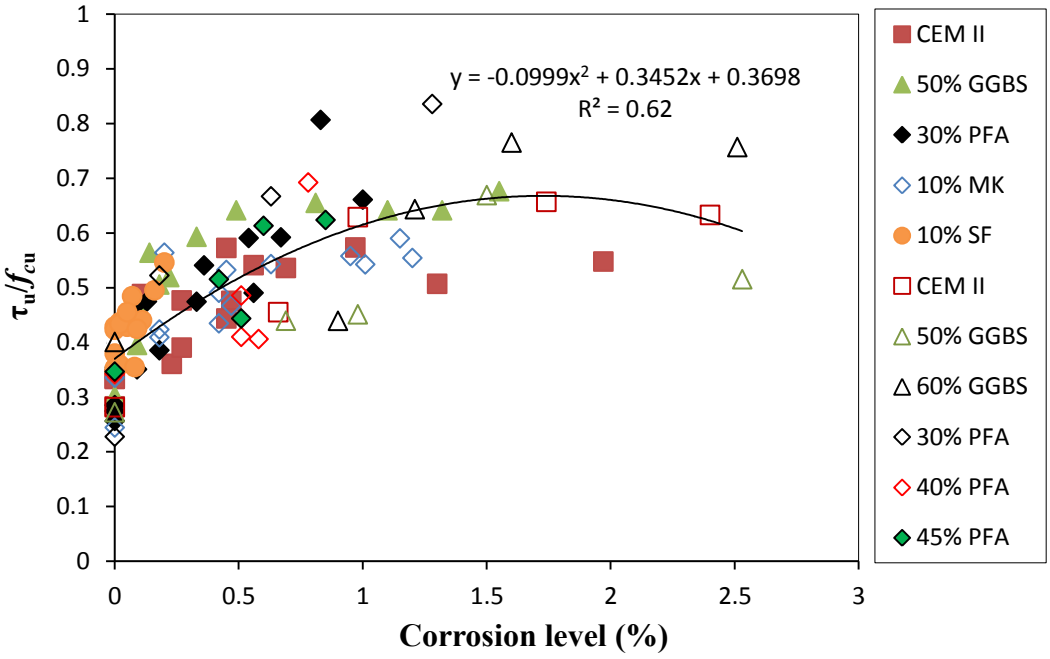

Figure 4.22: Normalised maximum bond strength versus corresponding corrosion level for different concrete types

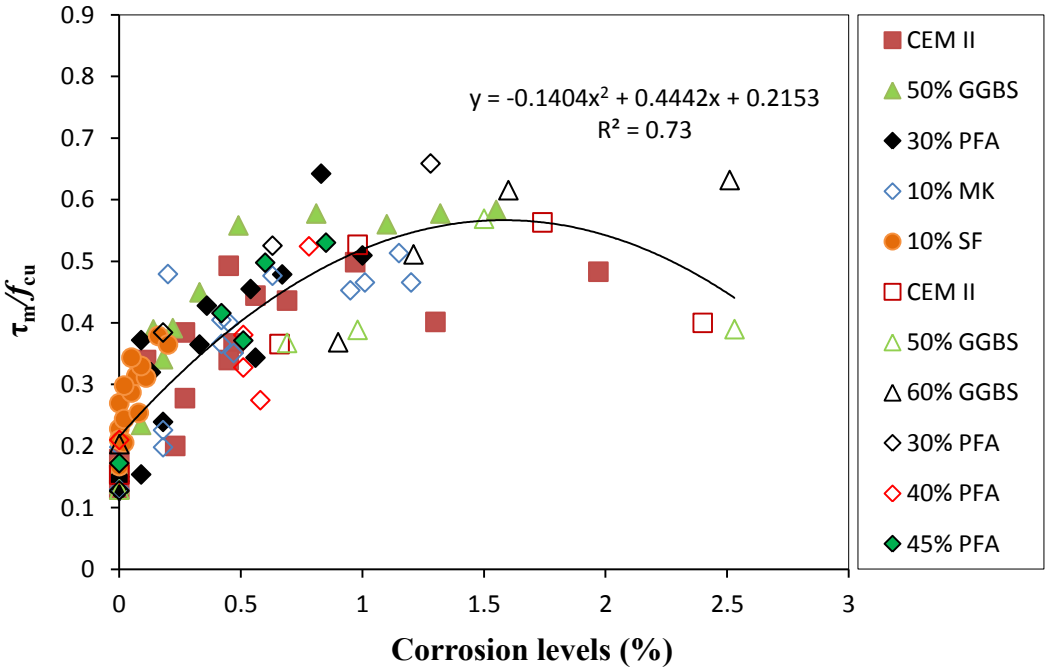

Figure 4.23: Normalised mean bond strength versus corresponding corrosion level for different concrete types

Both of these figures suggest a clear relationship between bond strength and the level of corrosion, in which the strength increases up to a corrosion level of approximately 1.74%, after which it starts to decrease. It is suggested that this is because, at low levels of corrosion, the rust that is formed expands and exerts pressure on the surrounding concrete, which therefore behaves like a thick cylinder under internal pressure (Balafas and Burgoyne, 2010). This radial pressure has the effect of confining the concrete which surrounds the steel bar and therefore the bond strength is enhanced. However, when the expansive stress of the corrosion eventually reaches the tensile strength of the concrete, the concrete cracks, the confinement is then released and the bond strength starts to fall. It is this cracking which eventually propagates to the surface of the specimen and manifests itself in the longitudinal cracks that are typically associated with high levels of corrosion. At this point the bond strength is significantly reduced and the mode of failure changes from pull-out to splitting of the concrete. To confirm this, the behaviour at higher levels of corrosion was observed for 20 days of corrosion for two binder types, CEM II and 50% GGBS, which led to cracking of the concrete cover. It can be said that, other than in the strength of the concrete, the binder type has an influence on the behaviour described above and therefore the extent and magnitude of both the confinement and the cracking that is generated by the corrosion of the steel bar. However, it is possible to anticipate, as is evident from the raw data from which these results have been obtained, the rate of corrosion and therefore the time to the critical level of corrosion as a function of the binder type. This difference can be attributed to the variation in the permeability of the concrete (i.e. microstructure, porosity system) for all concrete mixes, with the control mix being more permeable, followed by GGBS and MK, then the SF and PFA concrete. As observed in other studies (Yuan and J i, 2009), the high porosity in the transition zone (ITZ) offers more space for corrosion products and the corrosion rate increases as the expansive force increases, improving the stress surrounding the steel bar and leading

to cracking. This cracking induction was similarly observed by Wong et al. (2010). In addition, the low capillary porosity in the concrete plays an important role in the corrosion penetration. These results will be further commented on in Chapter 5 for concrete permeability with the different concrete mixes and its variation with time.

4.11 Conclusions

The bond strength of steel reinforcement in concrete containing CEM II, GGBS, PFA, MK and SF was investigated experimentally using pull-out tests in which steel reinforcement was artificially corroded for different exposure times of 3, 7, 10, 14 and 20 days. Based on the results presented in this chapter, the following conclusions and observations about what has been found in the literature can be made:

- The compressive strength and splitting strength of concrete for all concrete mixes were affected by the cement replacement material, this is also confirmed by Megat Johari et al. (2011) and the influence of further cement hydration on the concrete strength increase with curing age.
- The corrosion levels of the steel bar in different concrete mixes appear to follow a similar trend, where an increase in corrosion level was observed with increasing corrosion exposure time, as said by Abosrra et al. (2011) and the magnitude of increase in corrosion level for the SF and PFA mixes was less than the other concrete mixes due to a more dense concrete and high electrical resistivity.
- It was found that the bond strength of the corroded specimens depended on the corrosion level and the concrete strength. The higher the compressive strength, the higher the bond strength and there was no significant influence of the presence of cement replacement materials on the bond strength as confirmed by Fang et al. (2006).

From the experimental work in this chapter it can be concluded that:

- The magnitude of the corrosion level of the steel bars was dependent on the cement and cement replacement types and exposure time of artificial corrosion, with increasing exposure time leading to increased corrosion levels. The actual corrosion was less than that predicted by Faraday's equation as a result of the additional corrosion resistance afforded to the bar by the cover concrete

  The ultimate bond strength of the control specimens for all concrete mixes was directly related to the compressive and tensile strength of the concrete. The average value of bond strength was compared to the CEB-FIP Model Code 1990. The bond strength for the GGBS and MK mixes was similar to that predicted by the model code. The PFA mix bond strength was approximately 34% lower than the model code, whilst that of the SF mix was considerably higher (44%) than the model code.
- The results clearly show that the control specimens of all concrete mixes (without corrosion) failed in a pull-out failure mode due to the high confinement associated with a concrete cover greater than three times the reinforcing bar diameter.
- It was found that the bond strength of the corroded specimens depended on the corrosion level and the concrete strength. The higher the compressive strength, the higher the bond strength and there was no significant influence of the presence of cement replacement materials on the bond strength.
- The slip reduced with increasing corrosion levels in all concrete mixes and the slip levels were 14 times less than the slip of the control specimens when corrosion level was exceeded by 2%.
- When the corrosion level was increased, the corroded specimens 00-CEM II-20 and 50-GGBS-20 showed brittle failure compared to other corroded specimens.

- In all the concrete mixes studied, the ultimate bond strength was affected by the corrosion level and was different across all concrete types, varying with the concrete microstructure. This suggests that the increased bond strength is due to the enhanced confinement which results from the expansive pressure caused by the corrosion products on the surrounding concrete. Once corrosion levels exceeded approximately 1.74%, the bond strength began to decline slightly.

This chapter investigated the influence of the corrosion level on bond strength with the different concrete types, but without investigating the effects of their permeability variations. To investigate this further, the permeability of different concrete mixes, its variation with time and the relationship between the permeability and corrosion level will be discussed in the next chapter.

CHAPTER 5

GAS PERMEABILITY AND ITS RELATIONSHIP WITH CORROSION RATE

5.1 Introduction

The deterioration of reinforced concrete is of major concern. Much of the damage that occurs is a consequence of steel bar corrosion. Concrete permeability is an important factor in controlling the movement of chloride ions through the concrete towards the reinforcing bar. Therefore, the permeability of concrete comprising different cement replacement materials (i.e. PFA, GGBS, MK and SF) with various percentage levels of cement replacement, to improve the durability of concrete by decreasing the permeability, was investigated.

The effect of different cement replacement materials on the corrosion of steel bar in concrete was investigated in Chapter 4 with limited reference to concrete permeability. In this chapter the effect of cement replacement materials on gas permeability of those concrete mixes for different curing times is described. Achieving low permeability concrete is useful for improving concrete durability where corrosion protection is necessary. Thus, this chapter will discuss the experimental results obtained from gas permeability tests and its influence over time as well as the corrosion rate of steel, associated with the use of replacement cement materials.

5.2 Effect of concrete strength on permeability

Table 5.1 presents measurements of the gas permeability coefficient of concrete mixes, along with their compressive strength. The relationship between the gas permeability coefficient of the concrete mixes after 28 days of curing and compressive strength of concrete is illustrated in Figure 5.1. The results clearly showed that the gas permeability value of the CEM II concrete was 9.36×10^{-17} m^2 at a compressive strength of 53.9 N/mm^2. However, for the 10% MK and 50% GGBS concretes the higher the compressive strength, the higher the gas permeability coefficients (which were 1.7 and 2.4 times higher than the control mix, respectively). For the 10% SF concrete the compressive strength was higher, but the gas permeability was 0.89 times lower than the value obtained from the CEM II concrete. Conversely, the concrete made with 30% PFA, exhibited a lower concrete strength and provided relatively lower gas permeability when compared to the other concrete mixes in this investigation.

The variability of gas permeability measurements can be attributed to the differences in the microstructure of the concretes containing the cement replacements materials which were used in this investigation. In this work, it is also important to note that this relationship between the gas permeability coefficient and compressive strength was found at age of 28 days. It can therefore be concluded that the compressive strength of concrete has no significant effect on the gas permeability coefficient. The variations in scatter (in Figure 5.1) can be attributed to the relative composition of these concretes in terms of the fineness replacement materials as well as pozzolanic reaction. In a similar investigation, Chindaprasirt et al. (2007) found that the relationship between

permeability of concrete and compressive strength at 28 days was more scattered, and they linked this to the effects of the different cementitious materials (namely fly ash, Palm fuel ash, and ground rice husk ash) on permeability of concrete.

Table 5.1: Intrinsic gas permeability and concrete strength at 28 days

Concrete mixes	**[a] Average of f_{cu} (N/mm^2)**	**[b] Mean $t_{1/2}$ (min)**	**C.O.V %**	**[c] Average of k_{ef} (m^2)**	**C.O.V %**
CEM II (control)	53.9	48.5	12.2	9.36×10^{-17}	11.9
CEM II+50% GGBS	50.2	20.4	11.4	2.23×10^{-16}	11.2
CEM II+30% PFA	37.3	59.2	13.1	7.71×10^{-17}	14.5
CEM II+10% MK	60.6	29.5	7.1	1.65×10^{-16}	7.5
CEM II+10% SF	55.8	53.0	7.5	8.34×10^{-17}	10.6

Note: [a] f_{cu} = cube compressive strength; [b] $t_{1/2}$ = mean time to reach $P_{1/2}$; [c] k_{ef} = intrinsic gas permeability.

From the results reported in Table 5.1, it could be noticed that the highest coefficient of variation of gas permeability coefficient was obtained for the PFA mix (14.5%), at 28 days and the compressive strength of this concrete, whereby the coefficient of variation for average of k_{ef} value was about 1.2 times, greater than the coefficient of variation of the other concretes, indicating spread of the gas permeability results because of the slow reaction of the PFA concrete.

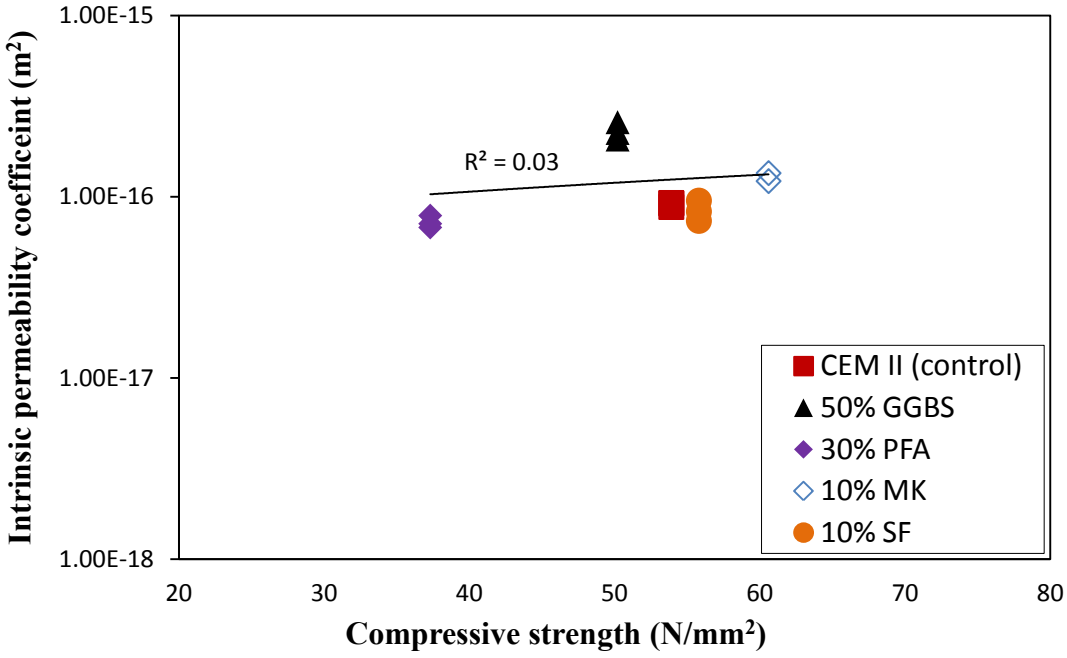

Figure 5.1: Relationship between intrinsic permeability coefficients and concrete strength for different mixes at 28 days curing

5.3 Effect of material composition on permeability

The relationship between the results of the gas permeability tests obtained after drying specimens at 105˚C for different concrete mixes is shown in Figures 5.2 and 5.3 and is reported in Table 5.2. From Figure 5.2, it can be seen that the CEM II concrete had a gas permeability coefficient at 28 to 52 days of 2.05×10^{-16} m^2 to 1.23×10^{-16} m^2, respectively. The gas permeability coefficient of 30% PFA concrete at 28 to 52 days was lower by approximately 3.3 to 2.2 times as compared to the control concrete. Hassan et al.(2000) found that the gas permeability (using oxygen) of 30% PFA concrete exhibited considerable reduction with curing age, which was lower by about 2.85×10^{-18} m^2 at an age of 50 days. The gas permeability coefficient concrete mixes of 40% and 45% PFA were lower than that of the CEM II concrete by about 2.3 and 2.4

times (respectively) at 28 days, and then lower to 2.2 and 2.4 times by 52 days. This can be attributed to the pozzolanic reaction of concrete at a later age and the formation of hydration products which produce additional C-S-H gel, leading to a more dense microstructure which ultimately reduces the permeability of the concrete. From the literature, concrete containing 15-30% PFA cement replacement has been reported to reduce the gas permeability below that of normal concrete (Shi et al., 2008; Thomas and Matthews, 1992). In the case of 50% GGBS concrete, lower gas permeability was observed compared to the CEM II concrete, with much lower values by 52 days (1.84×10^{-16} m^2 compared to 9.85×10^{-17} m^2 respectively, as shown in Figure 5.3). On the other hand, the high replacement percentage of 60% GGBS concrete had the highest measured gas permeability coefficient (3.16×10^{-16} m^2 and 2.34×10^{-16} m^2 at 28 to 52 days respectively) when compared to the CEM II concrete. This can be explained by the formation of more voids due to insufficient compaction during casting process because the GGBS reduces the workability of fresh concrete (Table 3.3) compared to the control concrete, and this low workability leads to improper compaction. This result indicated the highest intrinsic gas permeability values.

Comparison of the results for all the concrete mixes presented in both Figures 5.2 and 5.3, exhibits that the concrete containing PFA (i.e. 30%, 40% and 45% PFA) had superior gas permeability than those of GGBS (i.e. 50%, 60%) concrete mixes and the CEM II concrete at all testing ages because of its lower connectivity of the pores. The use of PFA can enhance the capillary pore structure in concrete through its physical, chemical and pozzolanic influence during hydrating states (Uysal and Akyuncu, 2012). Furthermore, the gas permeability coefficients of all PFA concretes were close to each

other at 52 days. The age of concrete was found to be an important factor affecting the measurements of gas permeability coefficient, where an increased concrete age leads to a reduction in gas permeability coefficient. This can be explained by the pozzolanic cement containing a greater quantity of hydrated products, causing a reduction in the number of pores present in its microstructure (Silva, 1995).

The conclusion can be drawn that the variation of gas permeability coefficient obtained from these results (see Table 5.2) is related to differences in the microstructure of concrete mixes, and in particular, the influence on microstructure caused by the use of cement replacement materials. In Figures 5.2 and 5.3, the error bars show that the variability of the three replicated samples tested was as much as the influence of using different cements replacement materials in some cases. From these results, it can also be observed that the concrete containing PFA and GGBS replacement materials were sensitive to a change in the microstructure of cement paste. The increase in curing age is associated with the on-going secondary reaction between $Ca(OH)_2$ and pozzolanic material producing more C-S-H gel, which in turn, filling up pores. This is one of the main reasons why there were variations in the gas permeability coefficient. Similar findings were reported by Dhir et al. (1998) and Naik et al. (1995). In addition, another possible reason for the differences in gas permeability is due to the deterioration of the pore structure resulting from oven-drying at 105 ºC. Gardner (2005) reported that drying temperature at 105 ºC induced cracks in the microstructure of the concrete forming wider pores structures allowing the gas to permeate through. Shafiq and Cabrera (2004) also found that the gas permeability of fly ash concrete depends not only on the composition of blended cement but also on the curing conditions.

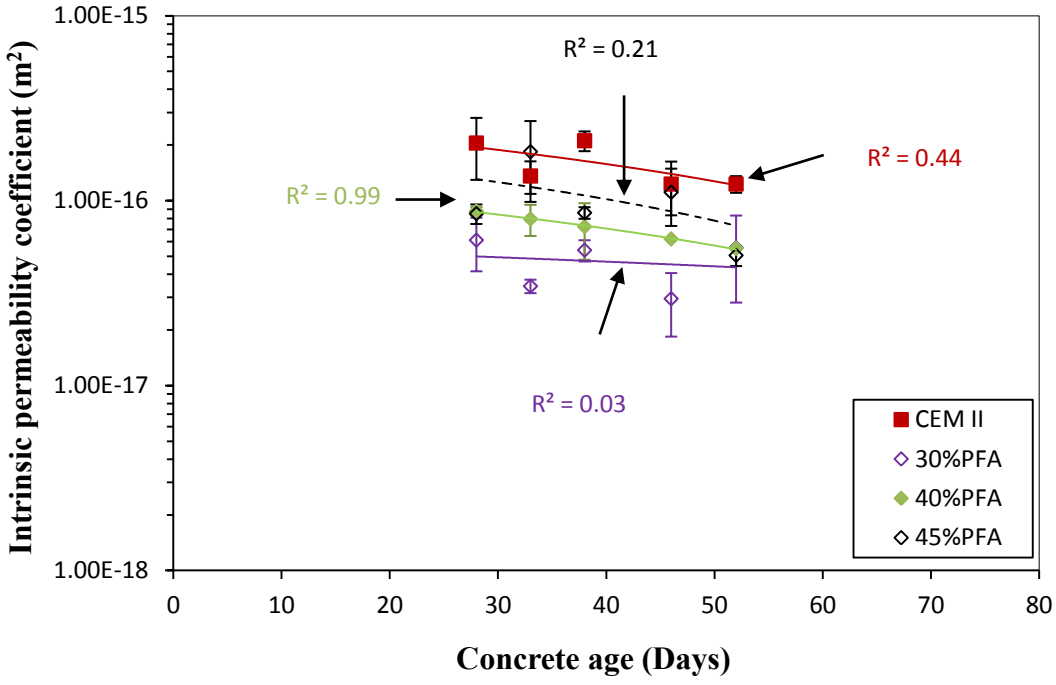

Figure 5.2: Variation of intrinsic permeability coefficient with time for CEM II and PFA concretes

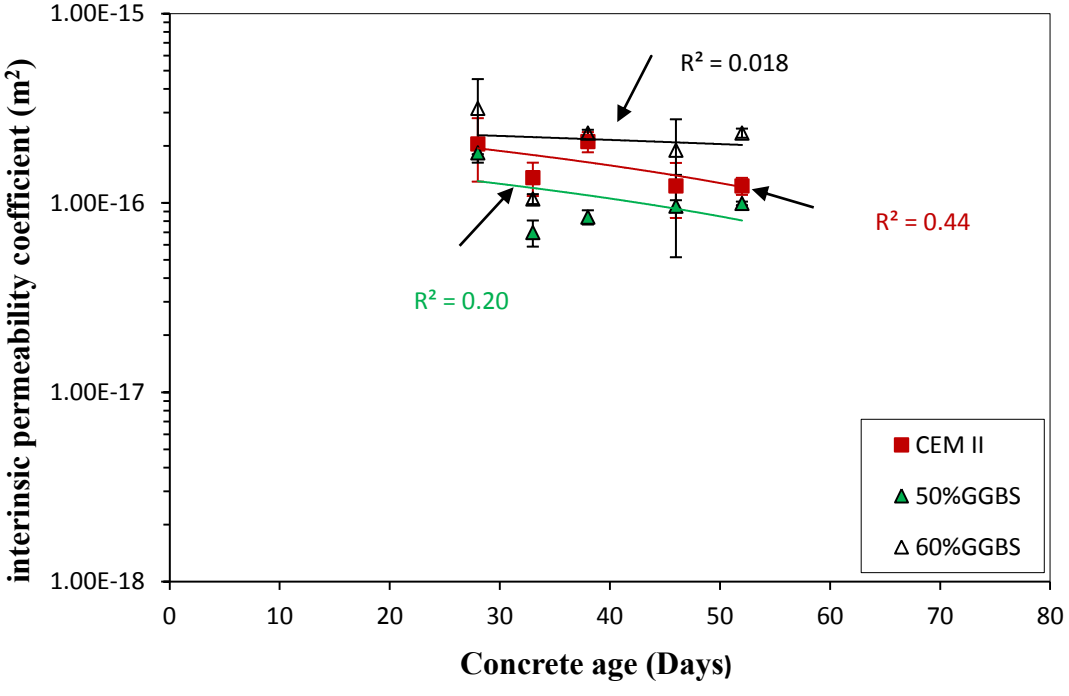

Figure 5.3: Variation of intrinsic gas permeability coefficient with time for CEM II and GGBS concretes

Table 5.2: Gas Permeability Test Results

Concrete mixes	**Age (Days)**	**[a] Mean $t_{1/2}$ (min)**	**C.O.V of $t_{1/2}$ (%)**	**[b] Average of (k_{ef}, m^2)**	**C.O.V of k_{ef} (%)**
CEM II (control)	28	24.7	46.4	2.05×10^{-16}	36.8
	33	34.2	19.5	1.36×10^{-16}	20.0
	38	20.4	12.0	2.11×10^{-16}	11.6
	46	38.8	28.7	1.23×10^{-16}	32.2
	52	36.7	10.3	1.23×10^{-16}	10.3
CEMII + 50% GGBS	28	24.5	10.6	1.84×10^{-16}	11.3
	33	64.9	15.3	6.98×10^{-17}	15.8
	38	53.5	8.6	8.42×10^{-17}	8.6
	46	52.9	37.7	9.62×10^{-17}	47.5
	52	45.2	1.9	9.95×10^{-17}	2.2
CEMII + 60% GGBS	28	16.4	49.9	3.16×10^{-16}	42.7
	33	43.0	5.8	1.05×10^{-16}	6.0
	38	49.6	10.8	2.34×10^{-16}	33.9
	46	27.0	44.0	1.90×10^{-16}	45.5
	52	19.2	5.6	2.34×10^{-16}	5.5
CEMII + 30% PFA	28	79.9	38.3	6.12×10^{-17}	32.2
	33	130.8	8.3	3.45×10^{-17}	8.4
	38	84.1	13.3	5.40×10^{-17}	13.1
	46	170.3	42.4	2.95×10^{-17}	37.7
	52	94.8	46.7	5.56×10^{-17}	49.5
CEMII + 40% PFA	28	52.7	5.3	8.78×10^{-17}	5.2
	33	51.8	16.9	7.97×10^{-17}	16.2
	38	67.4	29.7	7.24×10^{-17}	34.3
	46	72.6	9.0	6.21×10^{-17}	0.53
	52	81.2	0.6	5.53×10^{-17}	0.64
CEMII + 45% PFA	28	54.8	16.1	8.51×10^{-17}	12.2
	33	28.3	40.3	1.84×10^{-16}	42.6
	38	52.3	7.0	8.60×10^{-17}	7.2
	46	44.8	42.3	1.11×10^{-16}	34.3
	52	89.4	11.6	5.06×10^{-17}	12.1

Note: [a] $t_{1/2}$ = Mean time to reach $P_{1/2}$; [b] k_{ef} = Intrinsic gas permeability.

5.4 Effect of time on corrosion rate and permeability of concrete

The effect of curing age on the corrosion rates (related to the permeability of concrete) is shown in Figures 5.4 to 5.9 for different concrete mixes. The corrosion rates can be obtained based on weight loss by using the following equation (5.1), (Thangavel and Rengaswamy, 1998) which converts the weight loss due to corrosion to an average corrosion rate.

$$(C_R) = \frac{534\,w}{DAT} \tag{5.1}$$

Where C_R is the average corrosion rate (mils penetration per year, mpy); w is the weight loss (g), D is the density of steel (g/cm^3), A is the area and T is the exposure time (h).

Figure 5.4 illustrates the change of corrosion rate for steel bars and the gas permeability of the CEM II concrete specimens at the different curing ages. It can be seen that the corrosion rate of the steel bar decreased as curing age increased from 33 to 52 days. Also, the gas permeability was slightly decreased with increasing curing. The highest value of gas permeability coefficient was obtained at 28 days. As seen from Figure 5.4, the corrosion rate value of CEM II specimen was the highest (0.156 mpy) at the beginning of exposure time (33 days of the age). This is due to the high permeability associated with the start of the hydration process of concrete. However, the corrosion rate of the CEM II specimen progressively decreased as the curing age increased to 52 days (20 days of exposure time) by which point it was 78.2% (0.034 mpy) lower than that at the age of 33 days. This is because as the hydration process progresses, the pore

structure becomes denser which inhibits the chloride ions and moisture from reaching steel bar.

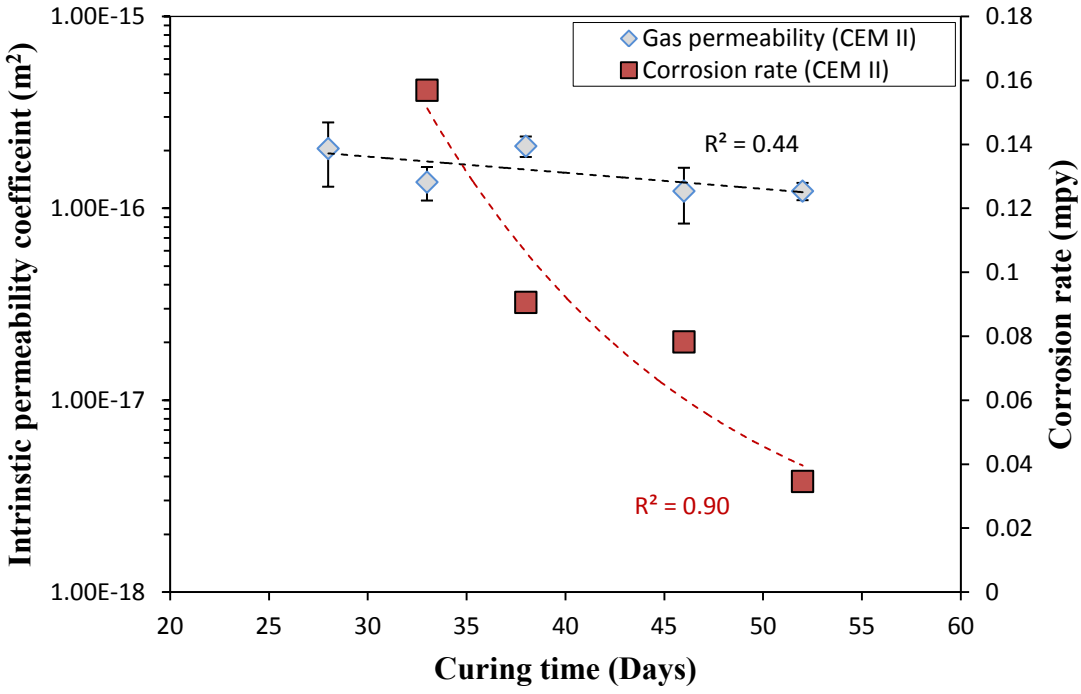

Figure 5.4: The intrinsic permeability coefficient and corrosion rate of steel bar in CEM II concrete as function of time

Figures 5.5 and 5.6 illustrate that the corrosion rate of reinforcing bars in concrete made with GGBS cement replacement material and gas permeability with time. Figure 5.6 shows the gas permeability of 60% GGBS concrete slightly decreased as the curing age increased. It is also noted that the gas permeability coefficient at 28 days equals about 1.3 times the permeability coefficient at 52 days (20 days of exposure time) due to the hydration process is not completed and as mentioned in previously section 5.2. It can be seen that the steel bars embedded in GGBS concrete (both 50% and 60%) had lower corrosion rates than the CEM II concrete. Furthermore, in the case of 33 days, the corrosion rates of the steel bars were 0.099 and 0.128 mpy for 50% and 60% GGBS

concrete, respectively, which reduced to 0.053 and 0.054 mpy after 52 days (20 days of exposure time). This is mainly due to an increase in age reflecting the influence of GGBS cement on intrinsic gas permeability of the specimens. This can also be explained by the fact that the GGBS cement reacts with water and then $Ca(HO)_2$ forming cement hydration product through pozzolanic reaction as well as forming more C-S-H, it is effective in refining the pores in concrete and improving the resistance to liquid penetration (Chloride ion). In line with the findings presented here, Cheng et al. (2005) reported that the incorporation of GGBS in concrete modified the pores structure in hardened cementitious materials. In their study, the capillary pores of GGBS concrete were (10 to 50 nm) smaller than the OPC specimen. The results showed the higher GGBS replacement content led to a denser microstructure which prevented water and chloride ions penetration into concrete.

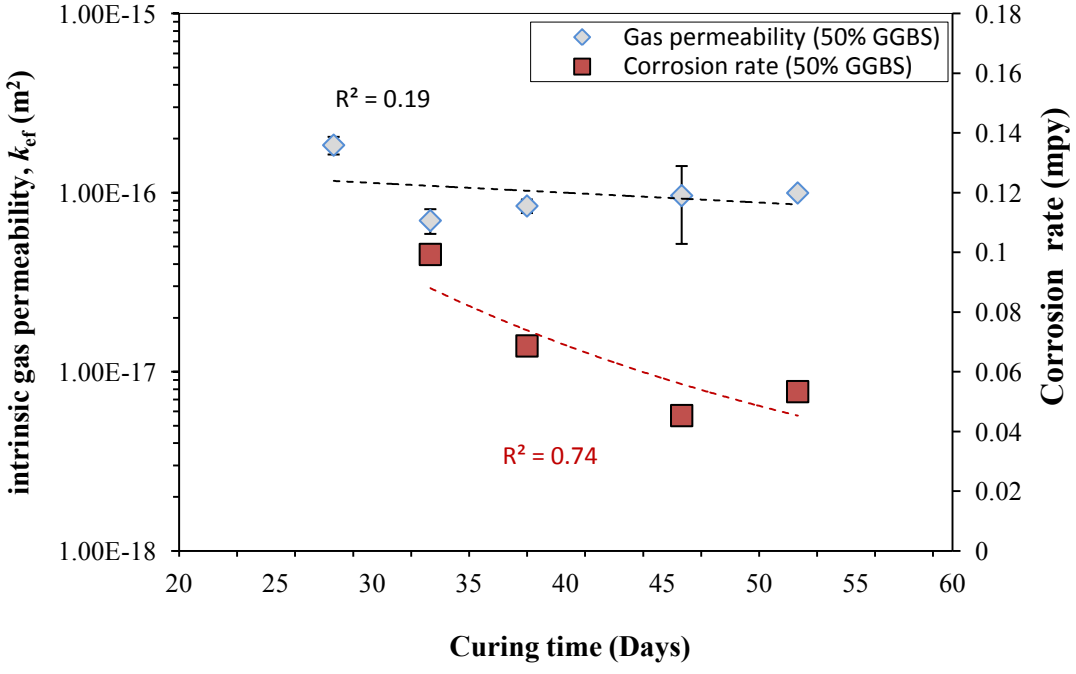

Figure 5.5: The intrinsic permeability coefficient and corrosion rate of steel bar in 50% GGBS concrete as function of time

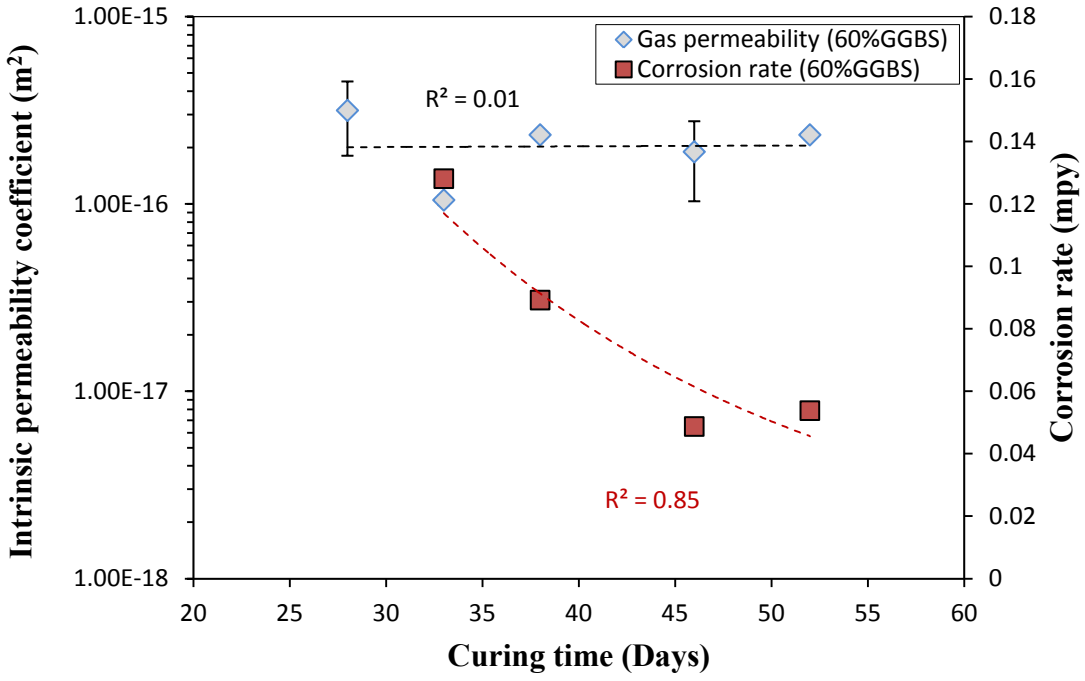

Figure 5.6: The intrinsic permeability coefficient and corrosion rate of steel bar in 60% GGBS concrete as function of time

Figure 5.7 shows the evolution of gas permeability and corrosion rate of the steel bars embedded in the 30% PFA with time. The gas permeability of concrete containing 30% PFA cement decreased with increasing age, by a magnitude of the results of gas permeability and hence the corrosion rates of steel decreased to 0.038 mpy compared with 0.057 mpy at 33 days. As seen in Figures 5.8 and 5.9, the corrosion rates of both 40% PFA and 45% PFA concretes decreased from 0.083 mpy to 0.011 mpy and from 0.060 mpy to 0.018 mpy at 33 and 52 days, respectively, indicating an approximate 66 to 70% reduction in the 33-day corrosion rate. The 40% PFA concrete resulted in greater correlation between corrosion rates and curing age, with a correlation coefficient of 0.98. It can also be observed that PFA cement replacement had a significant influence on corrosion rate with curing age for concrete mixes investigated, and that specimens

had lower corrosion rate than that of CEM II concrete for all ages, as expected. This was more pronounced for 40% PFA concrete specimens. Similar findings have been reported by Scott and Alexander (2007) regarding the effect of blended cement (PFA and GGBS) on the corrosion rate. They concluded that the corrosion rate of steel in concrete product with blended cement was decreased by about 50% as compared with Portland cement. On the other hand, there may be other possible reasons for the reduction in the corrosion rate of steel bar in concrete namely chloride diffusion which is not included in this research. However, in the literature Dhir et al. (1999) found that the coefficient of chloride diffusion was sharply reduced when the PFA content increased to 50% and this was dependent on both the intrinsic permeability of concrete and the ability of its cement paste to bind chlorides.

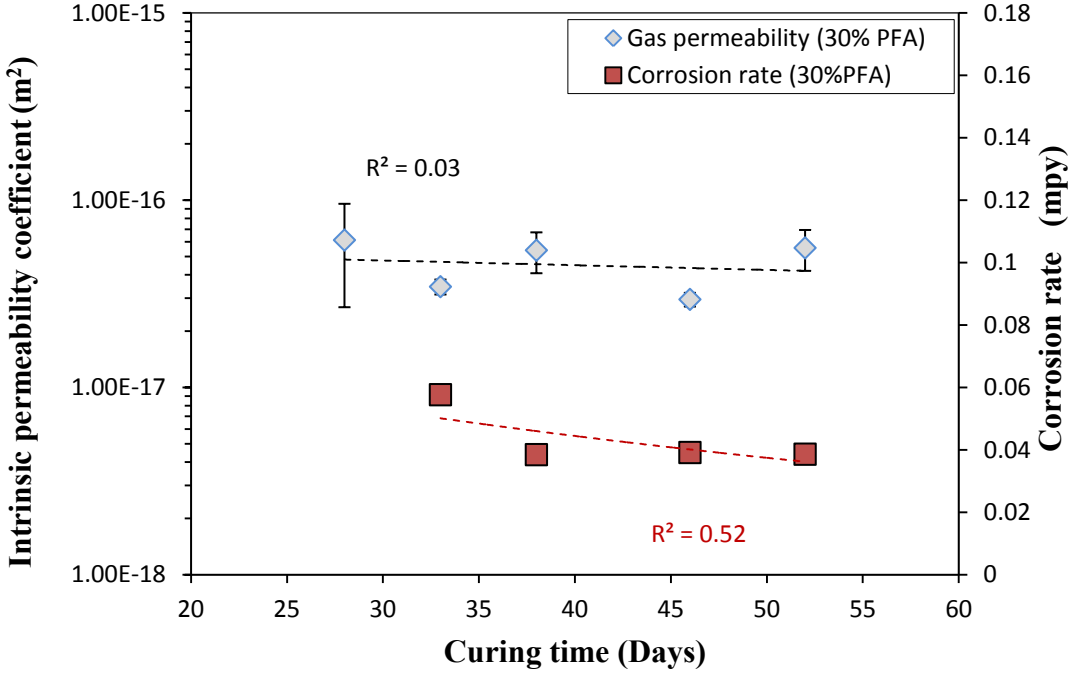

Figure 5.7: The intrinsic permeability coefficient and corrosion rate of steel bar in 30% PFA concrete as function of time

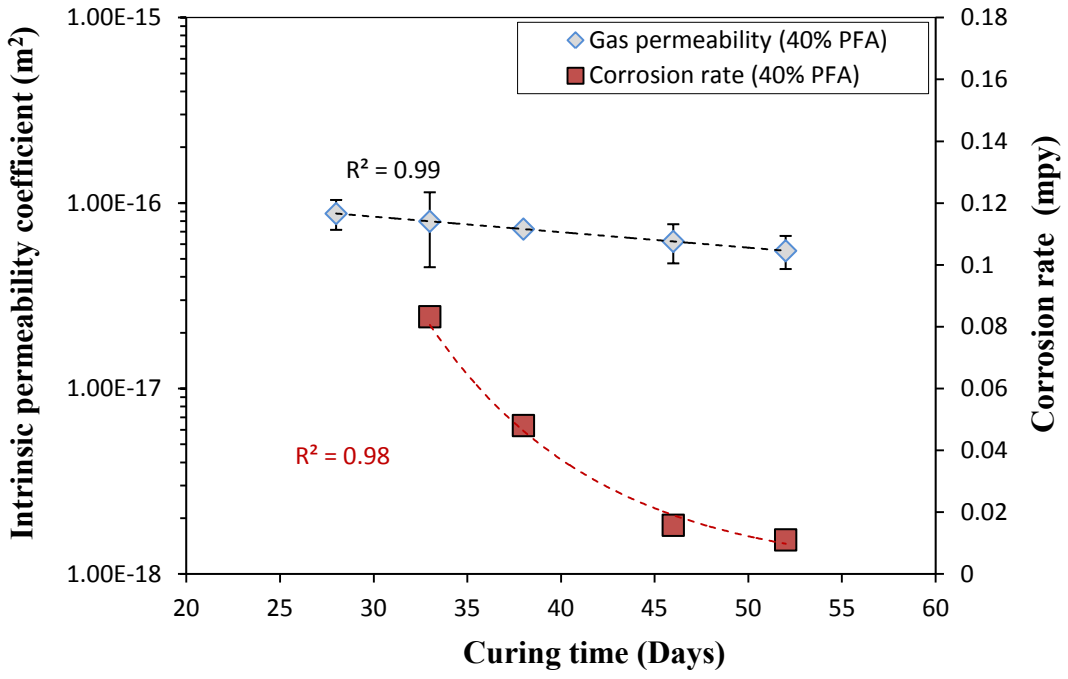

Figure 5.8: The intrinsic permeability coefficient and corrosion rate of steel bar in 40% PFA concrete as function of time

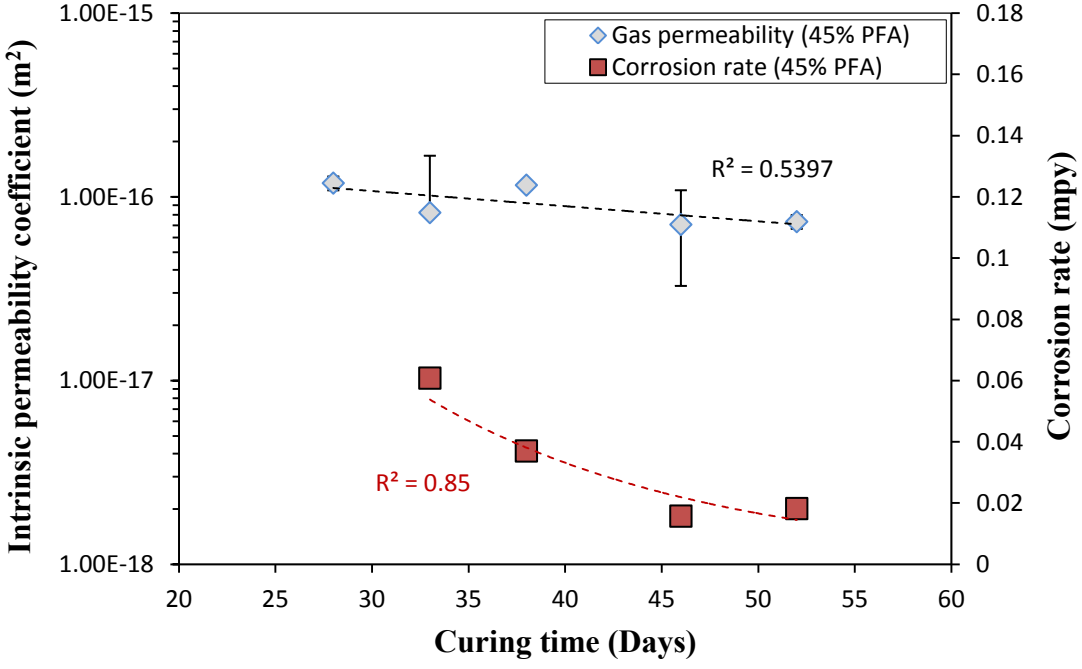

Figure 5.9: The intrinsic permeability coefficient and corrosion rate of steel bar in 45% PFA concrete as function of time

The results presented in Figure 5.4 through 5.9 illustrate that the inverse exponential best fit line satisfactorily represents the relationship between corrosion rate and time for different mixes. Additionally, the difference in the coefficient of gas permeability was accounted for by an exponential decay with time. It can be observed that there is good correlation between corrosion rates with time for all concretes and the following equations were obtained and presented in Table 5.3.

The results clearly revealed that time significantly affected corrosion rate of steel bar in pozzolanic concrete (PFA and GGBS). This suggests that as the curing age is increased there is a reduction in corrosion rate because the concrete becomes more dense leading to enhancement of the pore structure.

Table 5.3: Regression between corrosion rate and time

Concrete mixes	**Corrosion rate**	
	Exponential	R^2
CEM II (control)	$CR = 1.554e^{-0.071x}$	0.90
CEM II+50% GGBS	$CR = 0.278e^{-0.035x}$	0.74
CEM II+60% GGBS	$CR = 0.600e^{-0.05x}$	0.85
CEM II+30% PFA	$CR = 0.088e^{-0.017x}$	0.52
CEM II+40% PFA	$CR = 3.127e^{-0.011x}$	0.98
CEM II+45% PFA	$CR = 0.525e^{-0.069x}$	0.85

From Figures 5.4 to 5.9, it can be observed that the CEM II concrete had a higher corrosion rate than all other specimens. The curing time had a significant effect on the corrosion rate of steel bars when using the PFA replacement material. In these cases the corrosion rates show the same trend but with a different magnitude and good correlation were found between corrosion rate and time using cement content of 40% PFA. These

results indicate that the corrosion rate of steel bar decreases with age due to the current flow, and the ingress of chloride ions to the steel bar interface was affected by the changing microstructure of concrete mixes. This could be attributed to the secondary reaction taking place as the age of specimen is increased, which leads to more C-S-H gel filling the voids. This also confirms the earlier observation of section 5.2 reduced gas permeability of the concrete composition.

5.4.1 The relationship between gas permeability and corrosion rate

The relationship between the measured gas permeability and the corrosion rates at days 33, 38, 46 and 52 for the six investigated concrete types is plotted in Figure 5.10. It can be seen clearly from this figure that the corrosion rate decreases as the gas permeability value decreases. Moreover, some scattered data points were observed at the higher corrosion rate for concretes containing CEM II and 60% GGBS, particularly at high gas permeability values. For instance, the concrete with 30% PFA had a corrosion rate of around 0.044 mpy, with a gas permeability of 1.23×10^{-16} m^2. These values are respectively 13.50% and 76% lower than the control concrete at a similar age. As shown in Figure 5.10, there was a relationship between gas permeability and corrosion rate for different concrete mixes with a correlation factor of 0.53. This suggests that the relationship between corrosion rate and gas permeability can be affected by different cement replacement levels. Consequently, it can be concluded from these observations that the low gas permeability of PFA concretes yields lower corrosion rates, and as a result, the gas permeability of PFA concretes were found to be lower than that of the control concrete. This lead to lower corrosion rate of PFA concretes. This can be

explained by the fact that the addition of pozzolanic materials in the concretes improves the physical characteristics of the paste matrix, resulting in lower chloride ingress.

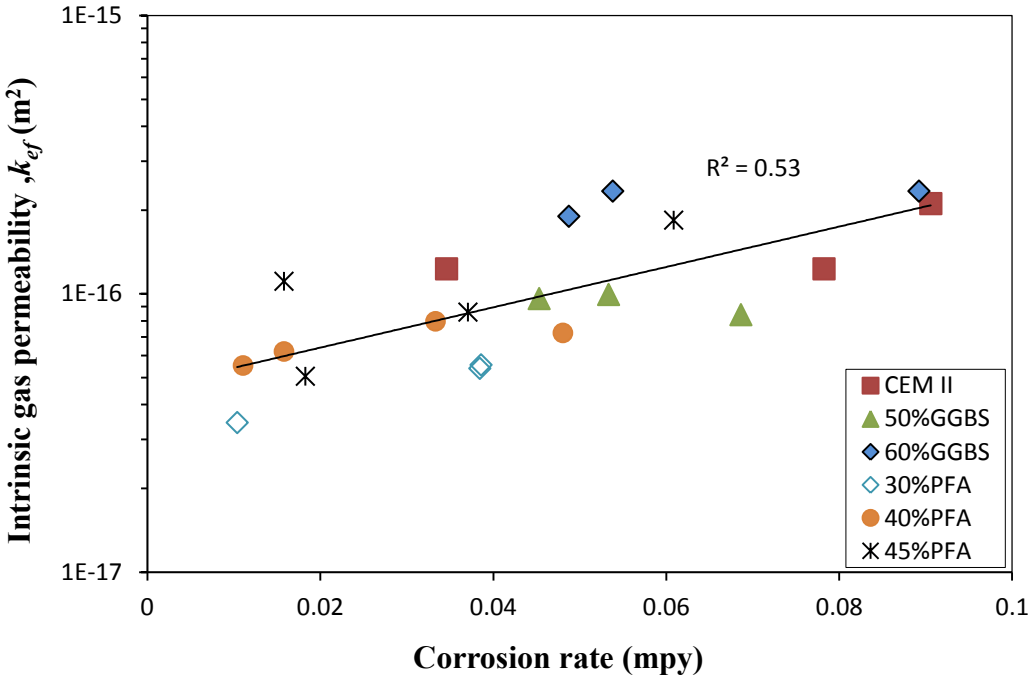

Figure 5.10: The relationship between intrinsic gas permeability on corrosion rate of steel bar in different concrete mixes

5.5 Results of gas permeability with further curing time

In the previous section, the effect of cement replacement material on the gas permeability was investigated. In this section the long term effects on the gas permeability of six different concrete mixes with similar mix proportions and different cement replacement levels are evaluated. This enabled a comparison to be made between the curing ages of different concrete mixes. The coefficients of gas permeability were determined at the ages of 28, 52, 70, 90, and 180 days. In general, the gas permeability coefficient results of these concrete mixes are reported in Table 5.4.

The full experimental pressure decay profiles for the specimens used in this study are provided in Appendix B.

Table 5.4: Gas permeability test results for increased duration.

Concrete mixes	Age (Days)	[a] Mean $t_{1/2}$ (min)	C.O.V of $t_{1/2}$ (%)	[b] Average of (k_{ef}, m^2)	C.O.V of k_{ef} (%)
CEM II (control)	28	36.5	25.6	1.29×10^{-16}	26.6
	52	44.6	3.1	1.01×10^{-16}	3.1
	70	40.4	12.2	1.12×10^{-16}	11.9
	90	48.8	2.7	9.21×10^{-17}	ˣ2.6
	180	45.5	5.8	1.03×10^{-16}	13.2
CEMII + 50% GGBS	28	17.2	7.5	2.60×10^{-16}	7.7
	52	23.4	25.7	2.00×10^{-16}	24.1
	70	21.7	24.8	2.15×10^{-16}	24.1
	90	23.1	8.2	1.94×10^{-16}	7.9
	180	41.9	6.8	1.07×10^{-16}	6.3
CEMII + 60% GGBS	28	17.1	10.8	2.65×10^{-16}	11.3
	52	20.3	11.8	2.23×10^{-16}	12.8
	70	22.8	21.0	2.02×10^{-16}	19.8
	90	25.1	11.5	1.80×10^{-16}	10.5
	180	19.6	11.9	2.63×10^{-16}	12.3
CEMII + 30% PFA	28	63.1	8.6	7.14×10^{-17}	ˣ8.6
	52	74.0	23.2	6.27×10^{-17}	20.9
	70	56.3	9.3	8.01×10^{-17}	9.5
	90	66.1	9.5	6.82×10^{-17}	10.0
	180	62.9	1.6	7.12×10^{-17}	1.6
CEMII + 40% PFA	28	67.1	23.4	6.88×10^{-17}	ˣ23.4
	52	68.9	41.7	7.44×10^{-17}	46.4
	70	54.9	2.0	8.17×10^{-17}	ˣ1.9
	90	74.7	26.9	6.27×10^{-17}	23.6
	180	64.4	14.5	7.07×10^{-17}	15.8
CEMII + 45% PFA	28	48.8	18.3	1.19×10^{-16}	16.7
	52	45.5	11.1	8.22×10^{-17}	11.7
	70	39.2	12.6	1.16×10^{-16}	13.7
	90	64.6	17.9	7.08×10^{-17}	17.2
	180	61.5	9.7	7.34×10^{-17}	9.3

Note: [a] $t_{1/2}$ = mean time to reach $P_{1/2}$; [b] k_{ef} = Intrinsic gas permeability; ˣ = coefficient of variation based two values

5.5.1 The effect of PFA and GGBS on compressive strength

Figure 5.11 presents the compressive strength results of different concrete mixes at their testing age (i.e. 28, 52 70, 90 and 180 days) with curing age. As seen in the figure, the CEM II concrete had the greatest compressive strengths from 28 to 180 days which ranged from 47.8 to 62.5 N/mm^2. In the cases of concretes containing PFA and GGBS cement replacement the compressive strengths were lower, ranging from 28.1 to 45.2 N/mm^2 and from 38.6 to 54.1 N/mm^2, respectively. From Figure 5.11, it can be seen that the gain in strength between 28 and 180 days for the CEM II concrete was increased by 30.8%, whereas the rate for concretes having 30%, 40% and 45% PFA cement replacement was increased by 36.7%, 38.8% and 42.6%, respectively. The figure also shows that the compressive strength of 30% PFA concrete at 180 days was found to be equivalent to the CEM II compressive strength at 28 days, which suggests that the class F fly ash content in the concrete did not play a significant role in the development of compressive strength because the slow degree of hydration in concrete. However, it was also found by Papadakis (2000) that the concrete strength of 30% PFA concrete exceeded the control concrete after 360 days. In addition, the compressive strengths of 50% and 60% of GGBS concrete were 49.09 N/mm^2 and 38.69 N/mm^2, at 28 days ages, respectively. For instance, the 180 day compressive strength of 50% GGBS concrete displayed a 17.37% increase with respect to the strength at 28 days, while this increment was 30.34% for the 60% GGBS concrete. It was observed that the compressive strengths of the concretes produced with cement replacement by PFA and GGBS were lower than the CEM II concrete up to 180 days in this investigation. Oner and Akyuz (2007) reported that the strength of concrete containing GGBS exceeded the compressive strength of control concrete after 365 days ages due to the fact that the

pozzolanic reaction is slow and the strength gain takes a longer time for GGBS concrete.

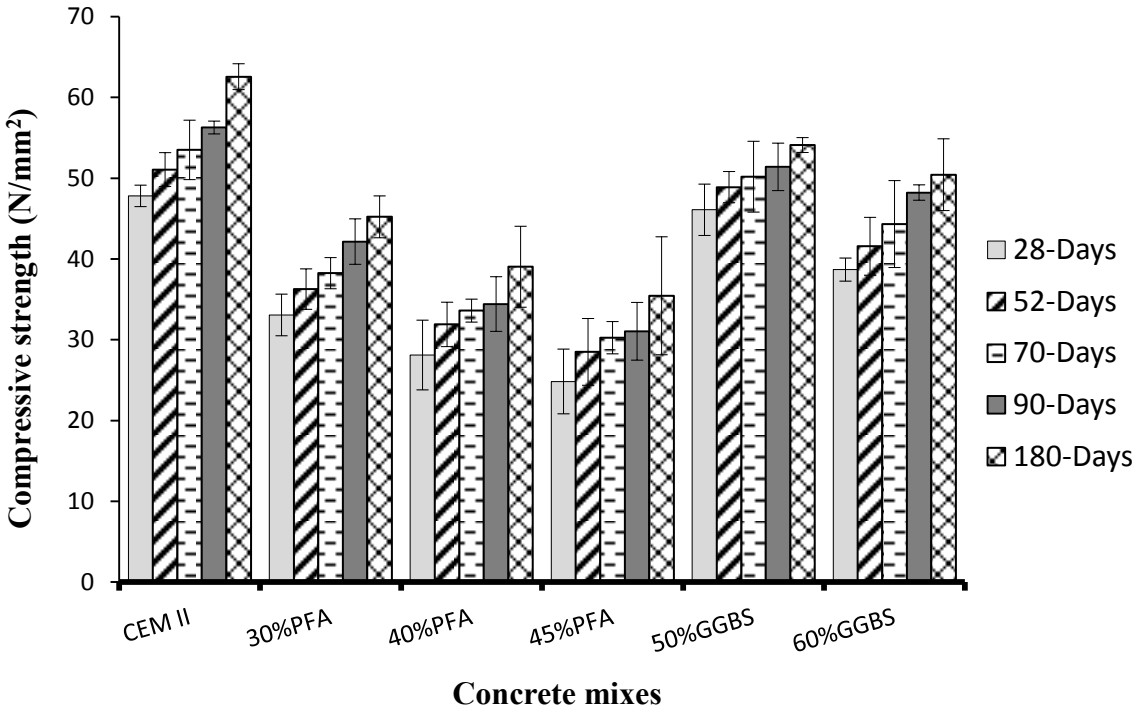

Figure 5.11: Compressive strength of concrete with different cement replacement levels at different curing times

Figure 5.11 shows the difference in the compressive strength of the CEM II concrete compared to PFA cement and GGBS cement concrete. In summary, the compressive strength of these concretes steadily increases with increasing curing time. This is due to the fact that the pozzolanic reaction of blended cement is slow at early age but at later ages the pozzolanic reaction accelerated leading to an increased content of C-S-H and consequently an improvement in the gain in strength of concrete. Also, for the concrete mixes made with PFA cement replacement, the cement particle size is higher compared to that of GGBS, and the pores in the cement paste are not completely filled. Furthermore, the 30% PFA concrete exhibited significantly higher concrete strength than those concretes with higher PFA content (40% and 45%) at the same curing time. This may be attributed to an increase in the PFA content, so that there is simply less

cement in the mix to hydrate, leading to lower compressive strength. The strength gain can be attributed to the improvement of the hydration process under curing time. This result is in agreement with results which were reported elsewhere (Papadakis 2000 and Sumer 2012). Similarly, Shi et al. (2009) found that compressive strength of concrete with fly ash (PFA) increased with increases of PFA content up to 30%, after that the concrete strength significantly decreases due to the increase in the PFA content.

5.5.2 The influence of f_{cu} on gas permeability of concrete

The relationships between the intrinsic permeability coefficient (k_{ef}) and the compressive strength of concrete made with different cement replacement levels of PFA and GGBS are shown in Figure 5.12. From the results presented in Figure 5.12, it can be seen that the values of gas permeability coefficient of the CEM II concrete mixes decreased slightly as the compressive strength increased. On the other hand, in the case of both the 30% and 40% PFA concretes, the compressive strength does not appear to influence gas permeability coefficient. For example, the case of 40% PFA had the compressive strength of 39.0 N/mm^2 and the gas permeability was around 7.07×10^{-17} m^2 at 180 days, whilst the CEM II concrete had the compressive strength of 62.5 N/mm^2 and the gas permeability value at the same age was 1.03×10^{-16} m^2. Therefore, the gas permeability coefficient of both 30% and 40% PFA concrete were about 30%-31.5% lower than the gas permeability obtained from the CEM II concrete. This can be explained by the reduction in gas permeability in PFA cement concretes due to the formation of secondary calcium silicate hydrates by the pozzolanic reaction, which decreases the pore size and leads to a denser microstructure. It can be seen from Figure 5.12 that the concrete having 30% and 40% PFA cement replacement had lower compressive strength and lower gas permeability as expected. Another important observation from the compressive strength versus the gas permeability coefficient is that

a very low gas permeability is indeed obtained at the low compressive strength. Therefore, it can be said that concrete made with PFA is the most impermeable. In other words, the 45% PFA concrete in this investigation had the highest gas permeability (1.19×10^{-16} m^2) at 28 days, but at 180 days the compressive strength increased up to 35.44 N/mm^2, the gas permeability was around 7.34×10^{-17} m^2, which is attributed to the slower pozzolanic reaction of PFA cement and the long-time duration associated with the formation of calcium silicate hydrate.

Figure 5.12 also shows the relationship between compressive strength and the intrinsic permeability coefficient of GGBS concrete mixes with different cement replacement levels. It can be seen that the gas permeability coefficient of 50% GGBS concrete was much higher than that of the CEM II concrete, while their compressive strengths were approximately 2.5% lower. However, the gas permeability of the 50% GGBS concrete decreased as the compressive strength increased up to 180 days. The gas permeability coefficient of 60% GGBS concrete was higher and the compressive strength increased greatly.

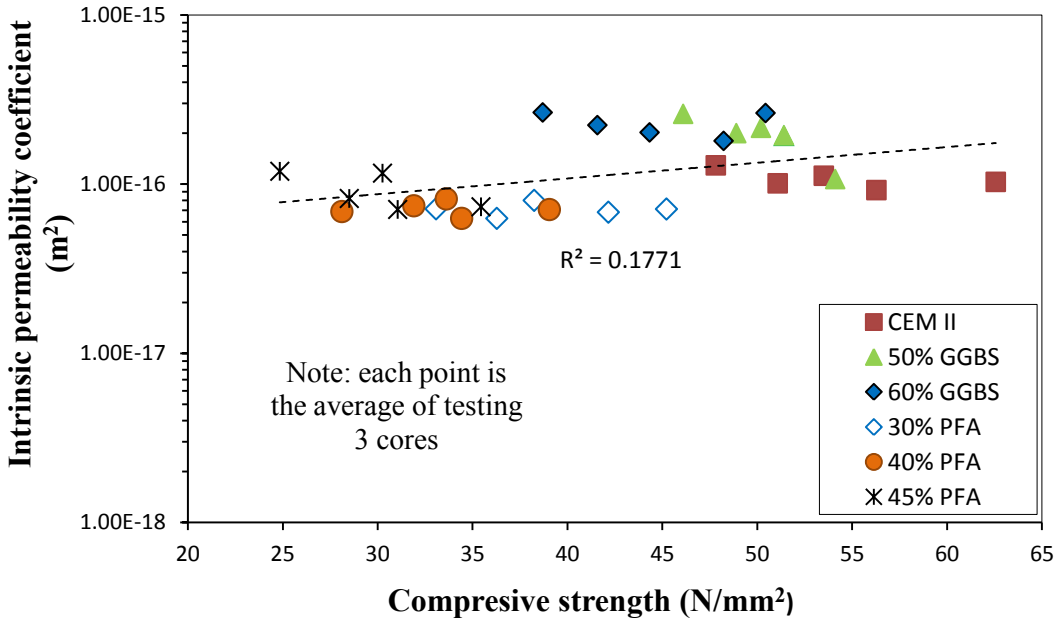

Figure 5.12: The relationship between intrinsic gas permeability and compressive strength for different concrete mixes

The results plotted in Figure 5.12 revealed that the compressive strength of these concretes does not influence the gas permeability coefficient. There was poor correlation between the intrinsic gas permeability coefficient and the concrete compressive strength. A similar study by Dellinghausen et al.(2012) reported that the oxygen permeability values of GGBS concrete were differed with the same level of compressive strength. In contrast, the results reported by Shi et al. (2009) for the nitrogen gas permeability of concrete with GGBFS were significantly affected by the compressive strength. However, they found the compressive strength of GGBFS concrete was linearly correlated to gas permeability. This is dependent on w/c ratio and replacement materials (mineral admixtures).

By comparing the results obtained in Figure 5.12, it can be suggested that cement replacement by PFA has been useful in decreasing the gas permeability of concretes which is attributed to the role played by its influence on the concrete microstructure. On the other hand, the compressive strength of these concretes had little influence and did not affect the coefficient of gas permeability.

5.5.3 Effect of time on gas permeability

The intrinsic gas permeability coefficients for different concrete mixes at 28, 52, 70, 90 and 180 days are shown in Figure 5.13 and reported in Table 5.4. From this Figure, it can be seen that the control concrete mix (CEM II) had a higher value of gas permeability at 28 days (1.29×10^{-16} m^2) than when the curing age was increased up to 180 days, which resulted in the coefficient of gas permeability being decreased slightly, to 1.03×10^{-16} m^2, about 20% less than that at the age of 28 days. The gas permeability coefficients measured for both the 30% and 40% PFA concretes were significantly lower than that of the CEM II mix over the full 28 to 180 days, whereas for concrete containing 45% of PFA, the gas permeability was found to be similar to the control

concrete at ages up to 70 days. It can therefore be stated that the 45% PFA does not significantly influence the gas permeability of concrete up to 70 days. However, beyond an age of 70 days, the 45% PFA concrete exhibits a lower gas permeability coefficient, though the values were still not as low as those of the 30% and 40% PFA concrete, as shown in Figure 5.13.

It was also observed that the concretes made with the addition of PFA cement replacement (30% and 40%) had lower gas permeability coefficients than the control concrete in the first 28 days and became stable at a later age. This can be explained by the fact that the pozzolanic reaction of PFA concrete proceeds further as curing age increases which leads to the formation of more C-S-H gel. As a result the interconnected pores were blocked and a reduction in gas permeability coefficient was observed.

For the concrete made with 50% GGBS cement replacement, the gas permeability was higher (about 50.83% at 28 days) than that of the CEM II concrete. As a result, the increased curing time appears to cause a decrease in gas permeability coefficients, which were similar to those of the control concrete at the same ages (1.07×10^{-16} m^2, 180 days). On the other hand, the addition of GGBS did not improve the performance of 60% GGBS at 180 days, but it reduced the gas permeability coefficient between 28 and 90 days which was 30 % lower than the 28 days specimen. The 60% GGBS specimen at 180 days had higher gas permeability coefficient than the specimen at 90 days but a similar gas permeability coefficient at 28 days. This may be related to the complete drying of the specimens, which results in a change in the pore structure and the possibility of cracking. This phenomenon were reported by Cabrera and Lynsdale

(1988), who found that the complete drying of a specimen at 105℃ resulted in shrinkage cracking which modifies the pores and leads to higher gas permeability.

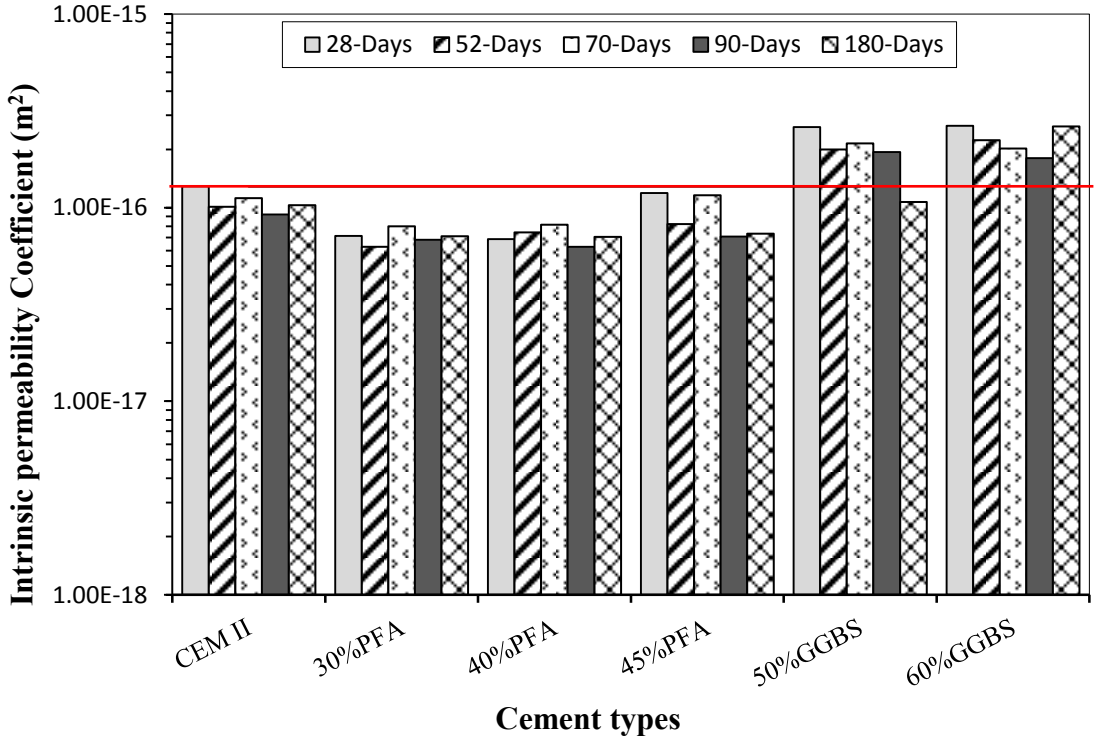

Figure 5.13: The effect cement replacement on gas permeability of concrete at different ages

Comparing the results from the different concrete mixes, the most obvious similarities are the relationships between gas permeability and curing time. The results show that the concrete made with PFA cement replacement had more positive effect on gas permeability than for CEM II and GGBS concretes. This is attributed to the improved pores structure of paste with a denser matrix due to increased age of curing. This is in agreement with McCarthy and Dhir (2005).

These results also correspond to Chindaprasirt et al. (2007), who reported that the blended cement paste containing PFA has smaller pores size than control concrete. They found the pore size of the PFA concrete with 40% PFA was lower than the 20% PFA

concrete. Also, the pore sizes were influenced significantly by increasing the curing time. The pozzolanic reaction may cause a lower number of capillary pores and lower interconnectivity between pores, which decreases the gas permeability coefficient (Li and Roy 1986). Although PFA concrete mixes had lower compressive strengths (seen in Figure 5.11), these concretes had superior coefficients of gas permeability due to microstructure modifications caused by increasing the curing age of the PFA. Elahi et al. (2010) reported similar observations with the use of fly ash cement replacement. They concluded that the air permeability decreased as curing time increased. The concrete containing GGBS cement had higher gas permeability for both levels of replacement (50% and 60%), but showed a decrease in gas permeability with an increase in curing time. It is observed that concrete mixes made with pozzolanic material showed a decrease in intrinsic permeability coefficient, from 3 to 26 times lower than that of the control CEM II mix, as the age of curing was increased.

5.6 Conclusions

In this chapter, the gas permeability coefficients of different types of concrete were investigated experimentally using different cement replacement materials (i.e. PFA and GGBS) and varying replacement levels. Moreover, the influence of cementitious materials and curing time on the corrosion rates was also investigated. From the results that have been presented in this chapter the following observations can be made:

In confirmation of what has been reported in the literature:

- Permeabilities depended on curing time, pozzolanic reaction and cement replacement levels, with the PFA having the lowest permeability compared to the other two types of cement as this confirmed by McCarthy and Dhir (2005).

The difference in gas permeability of concrete corresponds to differences in the microstructure. The gas permeability coefficient of GGBS concrete was higher than that of the PFA concrete mixes as a result of a change in the morphology of the cement hydrates.

From the experimental work reported in this chapter it was found that:

- The compressive strength of all concrete mixes increased as the curing age increased, with that of the CEM II concrete being significantly higher than that of the blended cement concretes. While the water content was kept constant, the compressive strength was affected by the cement replacement with both PFA and GGBS at all ages. In addition, the GGBS and PFA concretes had low workability compared to the control concrete at the same w/c ratios. This confirms the earlier observation in section 3.3.

- The cement replacement materials exhibited at least a 57 % lower gas permeability coefficient than the CEM II concrete used in this study. Of all concrete mixes, the PFA mixes exhibited the best improvement (reduction) in the gas permeability coefficient. For instance, the gas permeability decreased by approximately 23% as the cement replacement level increased from 30% to 40% of PFA cement.

- A strong correlation coefficient was observed between the corrosion rate of steel bar and the age of the concrete. As the curing time increased the corrosion rate decreased indicating that the microstructure of PFA and GGBS had changed with time due to the formation of C-S-H gel which filled the concrete pores limiting the chloride ions and Nitrogen penetration.

- Corrosion rate and gas permeability observed in concretes with different cement replacement levels were seen to significantly decrease as the concretes matured. There was a decrease in the corrosion rate with age for all concrete mixes. Concrete consisting of 40% PFA cement replacement illustrates a stronger improvement in gas permeability and corrosion rate. As a result it is beneficial to employ PFA as a replacement additive at 40% of cement weight for a strong reduction in concrete permeability.

- Gas permeability of concrete correlates with the corrosion rate, where a concrete with lower gas permeability exhibited a lower corrosion rate. The concretes with PFA had lower values of gas permeability and corrosion rate compared with others at the same w/c ratio. This can be attributed to changes in the pore structure of paste within the concrete. Therefore, corrosion rate is directly dependent on the gas permeability of concrete, which varies according to concrete type.

- There was a decrease in gas permeability with age for all concrete mixes. PFA was more effective at improving the gas permeability at 180 days. The 40% PFA with CEM II improved the gas permeability at 180 days, and similarly, the 45% PFA with CEM II improved the gas permeability at 180 days. It was found that an addition of 60% GGBS was not sufficient to improve gas permeability at a similar age.

- The influence of the compressive strength on the gas permeability of concretes was insignificant and it was found to be dependent upon the cement replacement levels. Moreover, the PFA concretes exhibit a lower compressive strength and

lower gas permeability coefficient when compared to the GGBS concretes. They also have higher compressive strength and higher gas concrete permeabilities.

The results obtained from the concrete permeability tests associated with cement replacement materials in this chapter have proven that the permeability plays a significant role in determining the durability of concrete. As discussed earlier in Chapter Four, the cement replacement materials had an influence on both the corrosion level and bond strength of concrete. From the investigation in this chapter, the permeability of concrete was shown to be governed by both the curing age and concrete type, and it was found that there appears to a direct relationship between gas permeability and corrosion rate. Low concrete permeability is associated with a reduction of the chloride ion and gas ingress in concrete and this is dependent on type and percentage of cementitious materials used. Although there is no direct relationship between permeability and bond strength, the latter is affected by corrosion rate, which is dependent on concrete permeability as discussed.

CHAPTER 6

NUMERICAL ANALYSIS OF BOND BETWEEN STEEL-CONCRETE

6.1 Introduction

The finite element method (FEM) has become a widely used numerical technique for solving a range of problems in engineering. The basic concept involved in FEM is the discretisation of a structure into a finite number of elements connected by nodes (Cook et al., 2002). The use of FEM analysis has increased significantly as personal computers have become more readily available. Some of the various commercial engineering finite element modelling packages available are ANSYS, ABAQUS, ADINA, LUSAS etc. In this present study, non-linear finite element analysis (NLFEA) has been implemented to study the bond between steel bars and concrete using the commercially available FEM packages LUSAS version 14.7 (LUSAS, 2006) and ABAQUS 6.11 (ABAQUS, 2011). In the first instance LUSAS was used to model the perfect bond and interface bond-slip behaviour between steel bar and concrete using the Joint Element Method (JEM). In the second instance ABAQUS was used to model the bond-slip relation via a cohesive zone method (CZM). This chapter will describe the available materials models for concrete, steel reinforcement and modelling of the steel bar-concrete interface.

The aim of the study presented in this chapter is to numerically predict the bond-slip behaviour and the numerical model will then be compared with experimental results of pull-out test specimens (control specimen) as well as the results obtained by Model Code 1990 as described in Chapter Four.

6.2 Material modelling

6.2.1 Concrete constitutive model

Concrete is a quasi-brittle material, having different properties in compression and tension. The uniaxial tensile strength of concrete is typically 8-15% of the compressive strength (Karihaloo, 1995; Bazant, 2002). The Elastic-Plasticity theory is able to simulate many aspects of concrete behaviour and is one of the earliest multi-axial plasticity based models for concrete when the principal stress components are dominant (William and Warnke, 1975, Cook et al., 2002).

6.2.1.1 Concrete model using LUSAS

Several constitutive models which can predict the behaviour of concrete under different loading conditions are available (Chen and Han, 1988). By using LUSAS the concrete was modelled by Multi-crack concrete (MC 94). This model is a plastic-damage-contact model in which damage planes form according to a principal stress criterion and then develop embedded rough contact planes which were developed by Jefferson (1999) and have been incorporated into the LUSAS software program (LUSAS Manual 2006).

6.2.1.2 Concrete model using ABAQUS

The ABAQUS program has two approaches to predicting concrete behaviour which are the concrete damage plasticity (CDP) model and the smeared crack model (Chen and Han, 1988). The CDP model was chosen for this present study, since it has higher potential for convergence as compared to the smeared crack model (Obaidat et al., 2010). The concrete damage plasticity model depends on the two main concrete failure mechanisms which are the compressive crushing and tensile cracking of concrete (Lee and Fenves, 1998). The plastic damage model requires the values of elastic modulus, Poisson's ratio, the plastic damage parameters and descriptions of compressive strength

and tensile behaviour. The values of the plastic damage parameters recommended by the ABAQUS documentation are presented in Table 6.1.The dilation angle was assumed to be 38˚and the Poisson's ratio for concrete was to be as 0.2 which was suggested by the CEB-FIP- Model Code1990.

Table 6.1: Material parameters of concrete damage plasticity (CDP)

Parameters	**Values**
Flow potential eccentricity (m)	0.1
Initial equibiaxial / initial uniaxial (σ_{c0}/σ_{b0})	1.16
The ratio of second stress invariant on the tensile meridian(k_c)	0.67
Viscosity parameter (μ)	0.0

The curve defining the stress-strain behaviour of concrete in uniaxial compression was determined from Eqs. (6.1), (6.2) and (6.3), according to BS EN 1992-1-1.

$$\frac{\sigma_c}{f_{cm}} = \frac{k\eta - \eta^2}{1 + (k-2)\eta} \tag{6.1}$$

Where:

σ_c = compressive stress in the concrete

$$\eta = \frac{\varepsilon_c}{\varepsilon_{c1}} \tag{6.2}$$

ε_c = compressive strain in the concrete

ε_{c1} = strain in the concrete at the peak stress f_c, usually considered to be 0.0022

$$k = 1.1E_C \times \frac{\varepsilon_{c1}}{fc} \tag{6.3}$$

According to BS EN 1992-1-1, the ultimate strain (ε_{c1}) for the concrete compressive strength of 12-50 N/mm^2 can be taken as 0.0035. The stress-strain relationship for the nonlinear response of concrete is presented in Figure 6.1.

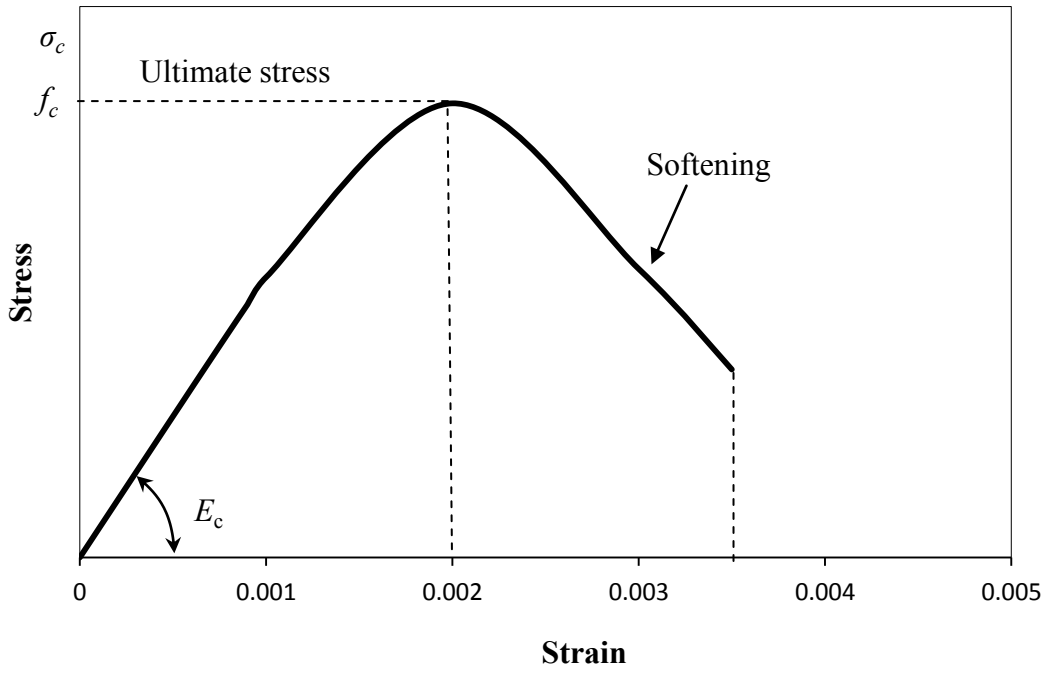

Figure 6.1: Stress-strain curve for concrete in compression

The behaviour of concrete under tension is considered to be a linear elastic system until concrete cracking is initiated at a tensile strength, f_{ct}. After cracking has occurred, the softening behaviour will gradually begin. Therefore, in this study, the tensile behaviour of concrete was described though the tensile stress-strain relationship as shown in Figure 6.2, which was determined from Eqs. (6.4) and (6.5).

$$f_{ct} = \mathrm{E_C} \times \varepsilon_t \tag{6.4}$$

$$\mathrm{f_{ct}} = \mathrm{f_r} \left(\frac{\varepsilon_r}{\varepsilon_t}\right)^{0.4} \tag{6.5}$$

Where f_{ct} and ε_t are the tensile stress and strain of concrete, respectively, f_r $\left(0.62\sqrt{f_c}\right)$ and ε_r are the tensile strength and corresponding tensile strain as seen in Figure 6.2. Experimental results are not available for the fracture energy, G_F. In this case, it is recommended to derive them by using CEB-FIP Model Code 1990 (CEB-FIP 1993), depending on the compressive strength and which coarse aggregate was used in this study.

$$G_f = (0.0469\, d_a^2 - 0.5 d_a + 26)\left(\frac{f_c}{10}\right)^{0.7} \tag{6.6}$$

Where d_a is the maximum aggregate size. In this study is 10mm. It should be noted that in Eq. (6.6), f_c is compressive strength of concrete.

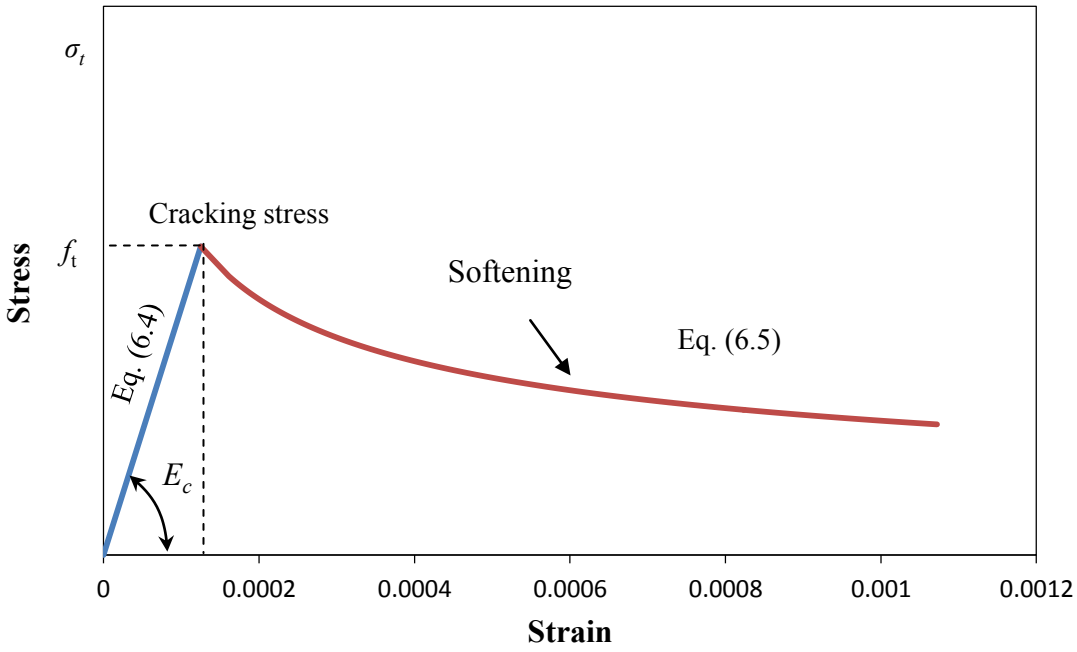

Figure 6.2: Stress-strain curve for concrete in tension

6.2.2 Steel reinforcement model

The steel reinforcement responds as a linear material up to the initial yield stress. The steel for the finite element models is assumed to be an elastic-perfectly plastic material in both tension and compression. The elastic modulus, E_s, and yield stress, f_y, of the

steel reinforcement were used in the FE model, which was programmed with the same material properties used in the experimental investigation as summarised in Chapter 3 (see Table 3.2). In addition, the Poisson's ratio was assumed to be 0.3 in this study. The stress-strain curve of the reinforcement steel is plotted in Figure 6.3 and the curve shows a liner-elastic region for stress below the initial yield stress.

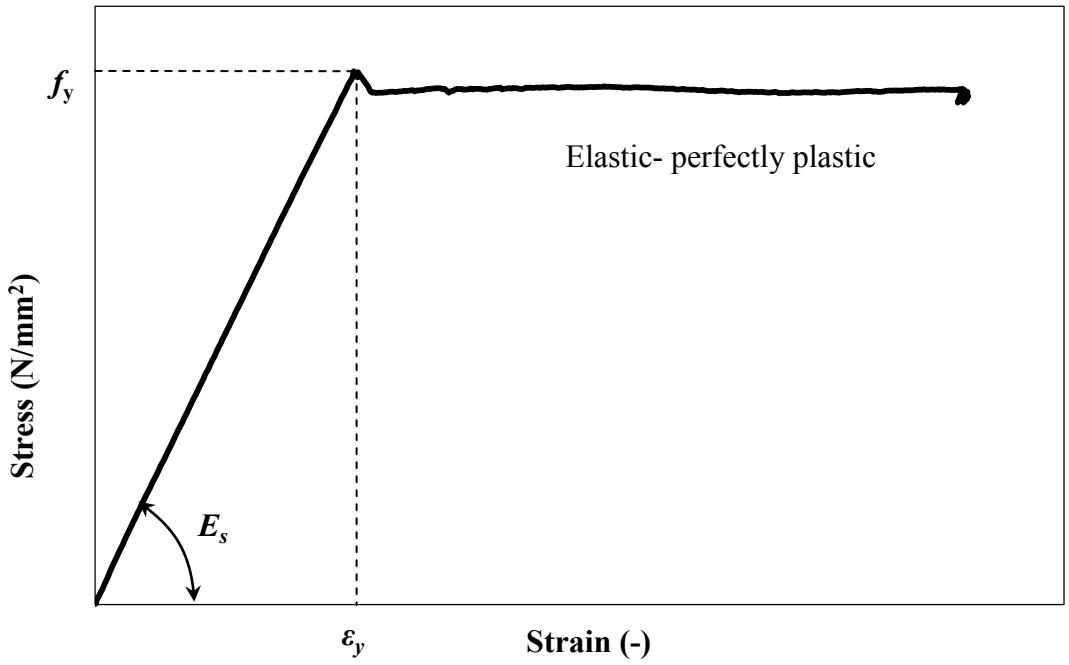

Figure 6.3: Stress-strain curve for steel reinforcement

6.3 Steel-concrete interface

The interface between the steel bar and concrete is of particular importance. There are different methods which are considered to model the interaction between the two different materials. Firstly, the interface was modelled as a perfect bond, as is used in many different finite element analysis packages, and the joint element method which were modelled by the LUSAS program. Secondly, the bond behaviour between the steel

and concrete was also modelled using the cohesive zone method (CZM). This method is available in the ABAQUS program, and is explained in the following section.

6.4 Cohesive zone model

The cohesive zone model (CZM) is commonly used to simulate fracture processes in a number of homogenous material systems. The models are typically expressed as a function of the tractions τ and the displacement δ in the interface, and the damage evolution can be defined in order to model the behaviour of the bond stress after the loss of elasticity.

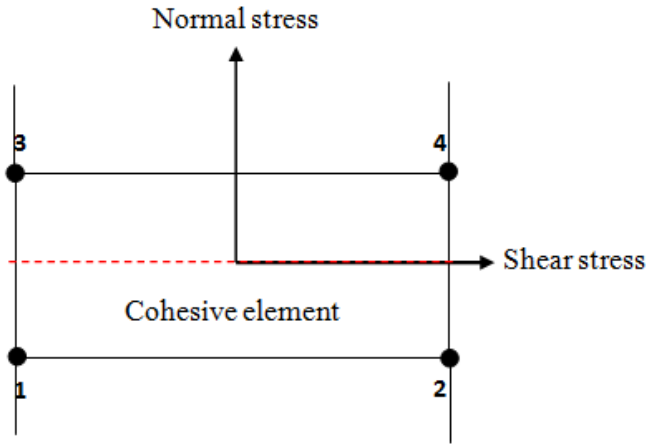

Figure 6.4: Local direction for 2-D interface element

In this research, a bilinear traction-separation law (see Figure 6.5) was assumed to model the bond-slip behaviour, of which the damage initial response is the ascending branch, and the damage evolution follows the descending branch. The damage evolution is governed by the damage at the contact point which ranges from 0 (undamaged) to 1 at full degradation (ABAQUS, 2011). The characteristic form of the damage evaluation of the curve can be defined from experimental results (pull-out test). Equation 6.7 indicates

the full constitutive stiffness relationship for a 2-dimensional problem which defines the stiffness of the bond in matrix form that relates the normal stress to the displacement.

$$t = K.\delta = \begin{Bmatrix} \tau_n \\ \tau_s \end{Bmatrix} = \begin{bmatrix} k_{nn} & 0 \\ 0 & k_{ss} \end{bmatrix} \begin{Bmatrix} \delta_n \\ \delta_s \end{Bmatrix} \quad (6.7)$$

Where:

τ = Traction vector

K = Elastic constitutive stiffness

δ = Separation vector

The normal stiffness, k_{nn} was assumed to be two orders of magnitude larger than the shear stiffness (k_{ss}) in the present study, whereas the shear stiffness was obtained from following Eq. (6.8), according to Gan (2000) and Heneriques el al. (2013). More details about the cohesive zone method input data are presented in Appendix C.

$$k_{ss} = \frac{\tau_{max}}{S_1} \quad (6.8)$$

Where τ_{max} = the maximum bond strength; S_1 = the slip at maximum bond strength.

In the damage initiation stage the user defines maximum stresses or maximum displacements which can be allowed without damage occurring. Several damage initiation criteria are available in ABAQUS. This study used the quadratic nominal stress criterion in all the examples, as expressed in Eq (6.9).

$$\left(\frac{\sigma}{\sigma_n}\right)^2 + \left(\frac{\tau}{\tau_s}\right)^2 = 1 \quad (6.9)$$

Where σ_n is the normal strength, this was assumed to be the tensile strength of concrete and τ_s is shear strength (Mohamadi and Wan, 2013 and Obainat et al., 2010).

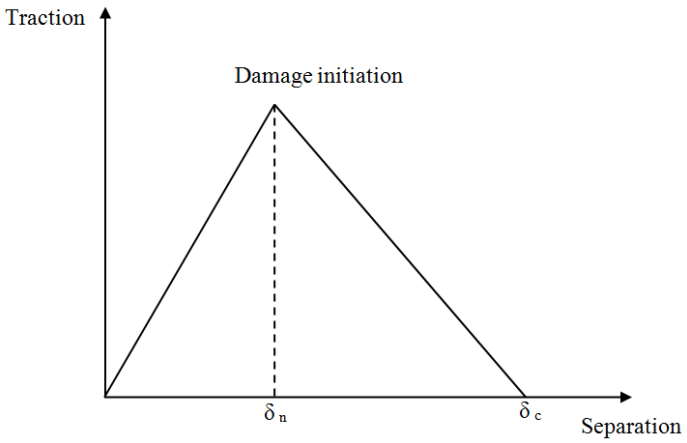

Figure 6.5: Bilinear traction- separation for cohesive zone model

6.5 Finite element modelling

6.5.1 Model geometry and boundary conditions using LUSAS

The geometry of the pull-out specimens was developed by assuming half symmetry. The cube of concrete and the steel bar were modelled as separate parts, and the parts were assembled together to complete the model for the pull-out specimen. The element library of the finite element software LUSAS program (LUSAS, 2006) has many different types of quadrilateral plane stress elements. The concrete cube was modelled using 8-noded quadrilateral plane stress elements (QPM8), each node having two degrees of freedom (DOF). A non-linear cracking and crushing concrete model (multi-crack model, Model 94) was selected for the plane stress element. The line mesh (BAR2) with 2-D structural bar element was selected to model the steel reinforcement element, and the Von Mises plastic material model was used for the steel reinforcement. The connections between the reinforcing bar and the concrete were modelled by the joint element method (JNT3), available in the LUSAS program. The use of the joint element method ensures that adjacent nodes are connected by springs in the non-linear analyses and enables the realistic modelling of hardening elasto-plastic behaviour.

In order to reduce the computational time, the coarse mesh was used as the overall size, in this model, two groups of boundary condition were given to the model as shown by the green arrows in Figure 6.6 (a). One was applied at the bottom of the cube of concrete which was fully restrained, with no translation in the X and Y directions, while the other was applied on the reinforcement steel which was only restrained in the X direction, allowing only vertical displacement. The boundary conditions were similar to those in the experimental set up, as shown in Figure 6.6 (a). In LUSAS, the load was applied at the end of the reinforcement bar and the load was applied incrementally beginning from 1N until the concrete failed. The starting load factor was set to 100 which multiplies the applied loading by a factor of 100 on the first load increment or the maximum number of increments until convergence is achieved.

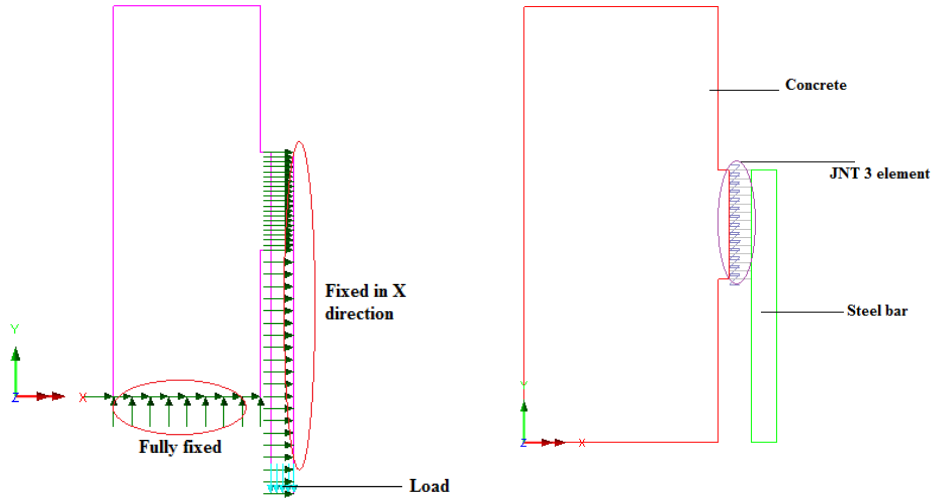

Figure 6.6: **(a)** Boundary conditions of model; (b) Joint element JNT3 employed in the model

6.5.2 Model Geometry and Meshing using ABAQUS

The geometry of the full specimen was represented by a 2 dimensional axisymmetric partial specimen, which was developed using ABAQUS 6.11. This was done by

defining boundary conditions along the line of symmetry which restricted movement in this direction. Figure 6.7 illustrates the simple diagram of the model geometry and the concrete and the steel reinforcement which were modelled as separate parts and then the parts were assembled together to complete the model.

The concrete part was modelled with 4-node bilinear quadrilateral element (CAX4) available in the ABAQUS element library because it is a suitable element for a 2-dimension axisymmetric arrangement. This element type has reduced integration stiffness (Ngo and Scordelis, 1967). This element can be used for nonlinear analysis including that of contact.

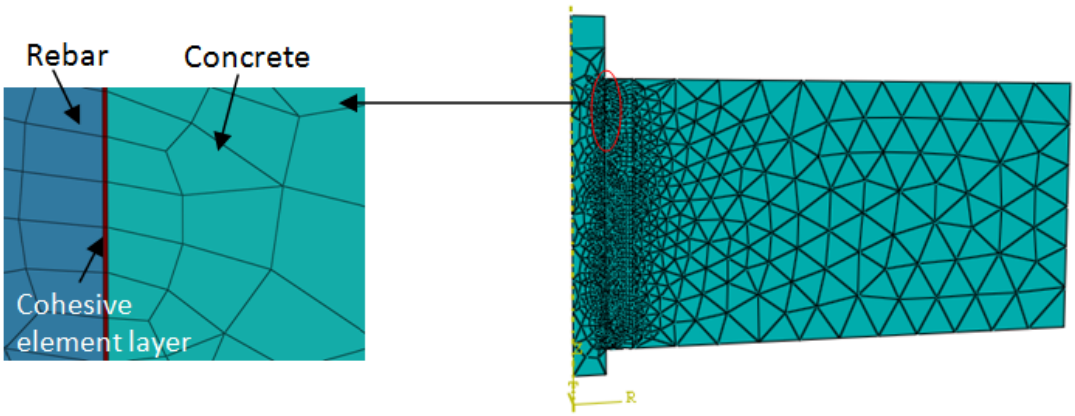

Figure 6.7: Geometry of the model for FE model

The steel reinforcement was also modelled with the element CAX4. On the other hand, a thin cohesive layer of 0.02mm thickness was placed between the reinforcement and the concrete as shown in Figure 6.7, while one surface of the cohesive layer was tied to the reinforcement and the other surface was tied to the concrete. The cohesive layer between the steel and concrete was meshed with a 4-node cohesive element COH2D4 (see Figure 6.4). In order to reduce the computational time, the fine mesh was used in the cohesive layer and its surrounding concrete to achieve accurate results, but the coarse mesh was applied to the area away from the cohesive layer, where the element

size of the cohesive element was selected as 0.2mm. Furthermore, the mesh has an element size of 0.2mm for both the concrete part and the steel bar part close to the cohesive layer and larger element size of 5mm was used for regions far away from the bonding area of the reinforcement and concrete.

6.5.3 Load and Boundary Conditions

The pull-out test configuration shown in Figure 6.8 was modelled as plane stress and a partial cube was built and simulated in ABAQUS to reduce the subsequent processing time by taking advantage of the structural symmetry of the cube. In the FE model, the boundary condition at the bottom and top of the concrete part was restrained in the vertical direction Y while the steel reinforcement was only restrained in the X direction and slip along the Y-direction was allowed to be similar as in the experimental set up, as illustrated in Figure 6.8. In the ABAQUS finite element model, the Newton-Raphson Method was used to model the nonlinear FE model behaviour and the slip was applied instead of the load at the end of the steel bar to the location corresponding to the experimental test.

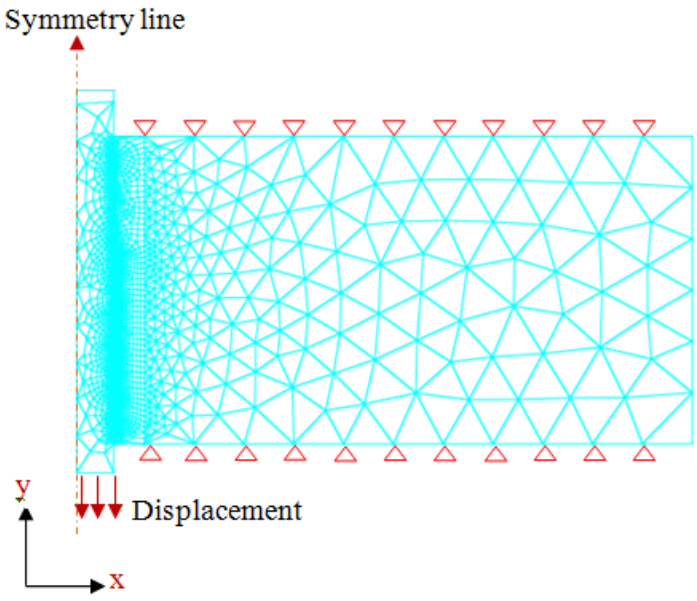

Figure 6.8: Loading and boundary conditions

6.6 Numerical results and discussion

6.6.1 Bond-slip curve using LUSAS model

This section presents the numerical results of the Joint Element Method (JEM) used to investigate the bond-slip response. The finite element modelling of the bond-slip was performed using the LUSAS 14.3 program (LUSAS, 2006), which was used to validate the experimental results. The numerical results of the bond-slip curve for perfect bond were compared with the test results.

Figure 6.9 shows that the comparison between the bond-slip curves that were obtained from the LUSAS analysis and experimental results for the CEM II specimen. It can be seen that the specimen (dashed line) was assumed to have perfect bond which is characterised by the linear behaviour at the beginning of the elastic region. Consequently, the bond-slip relation becomes highly nonlinear as numerous cracks develop and the slip increases considerably. This is due the rigid connection to the steel reinforcement and concrete having the same nodes and the same degrees of the freedom which increased the bond strength up to 29.2 N/mm^2 leading to the deformation in the interface. The peak bond value (perfect bond) was higher by 45% compared to the experimental results. The stiffness of the finite element model was again higher than that of the experimental results. This may be attributed to the perfect bond between the concrete and steel bar assumed in the FE model, but the assumption would not be true for the experimental results. Figure 6.9 also shows that the bond-slip relation obtained from the joint element method (JEM, dotted line) was less than the experimental result which was lower about 37.65% of the peak bond strength. It can be seen that when using JME, there was a good fitted the test result in the ascending branch up to 9.37 N/mm^2 of bond strength. After that, the LUSAS analysis was terminated due to cracking concrete occurring at this point. Therefore, depending on the numerical results obtained

from LUSAS (Figure 6.9), it can be concluded that the joint element method used to model the bond-slip curve was not a suitable method due to inability of LUSAS to incorporate the shear stiffness of bond into the models. In addition, the LUSAS software package does not support the use of interface finite elements to define the bond - slip behaviour based on the joint element interface approach.

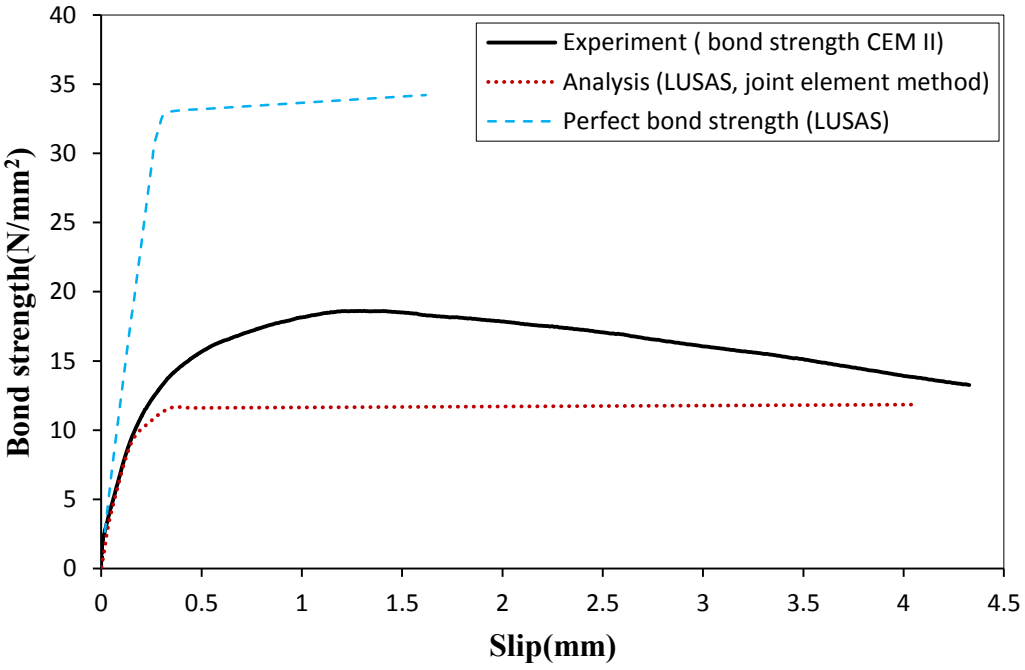

Figure 6.9: Relationship between bond-slip for the CEM II specimen

6.6.2 Validation of the numerical model

In this section, the numerical results of bond-slip for different concrete specimens (without corrosion) are presented and compared with available experimental results as described in Chapter 4 (section 4.5). All the specimens were modelled with the FE package ABAQUS/Standard, wherein the present bond-slip model has been implemented.

Figure 6.10 depicts the bond-slip response of the numerical results, along with the analytical results obtained from MC90 of the CEM II specimen. The experimental

results of three specimens were included for validation. It can be seen from the figure that the numerical prediction of the bond-slip curve was higher than one of the test results, but very the close to the other experimental bond-slip responses. Figure 6.10 also illustrates that the ascending and descending branch of the numerical curve exhibited reasonably good agreement with the experimental results. It can be noted that the peak bond strength of the experimental results ranged from 17.52 N/mm^2 to 20.05 N/mm^2, whereas the peak bond strength in the numerical result was 20.63 N/mm^2. Furthermore, the numerical results were compared with the bond-slip curve derived from CEB-FIP Model Code 1990. The numerical result was higher by 18.22% than the analytical results. It was hence determined that direct comparison between numerical and experimental results provides validation and justification for the use of the CZM interface between steel and concrete.

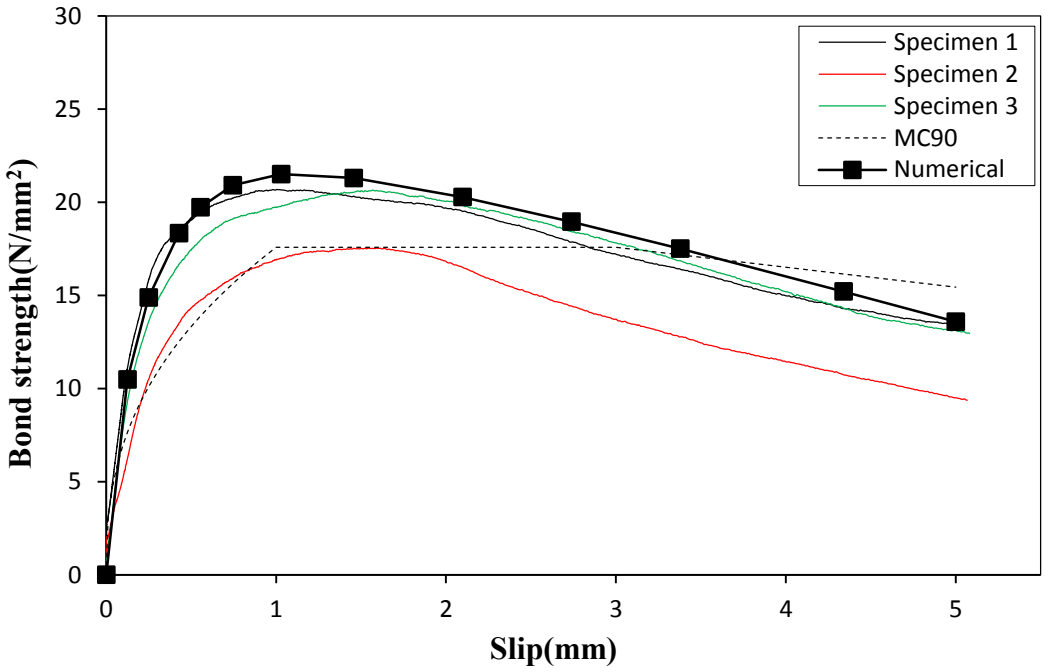

Figure 6.10: Comparison between numerical and experiment results of bond-slip for CEM II concrete specimen

The bond-slip curves obtained from the experimental, analytical and numerical results in the case of the GGBS specimens are shown in Figure 6.11. It can be seen from the figure that the numerically calculated bond-slip response give results in good agreement with experimental data. However Figure 6.11 also shows that the bond strength predicted by MC90 did not reach the bond strength of the numerical model, and was found to be approximately 10.25% lower. Moreover, the results demonstrate that the numerically determined bond-slip curve is stiffer in the pre-peak region and tends to have a higher peak bond level than that of the analytical results (MC90 value). Nevertheless it still represents a good agreement with several of the experimental results.

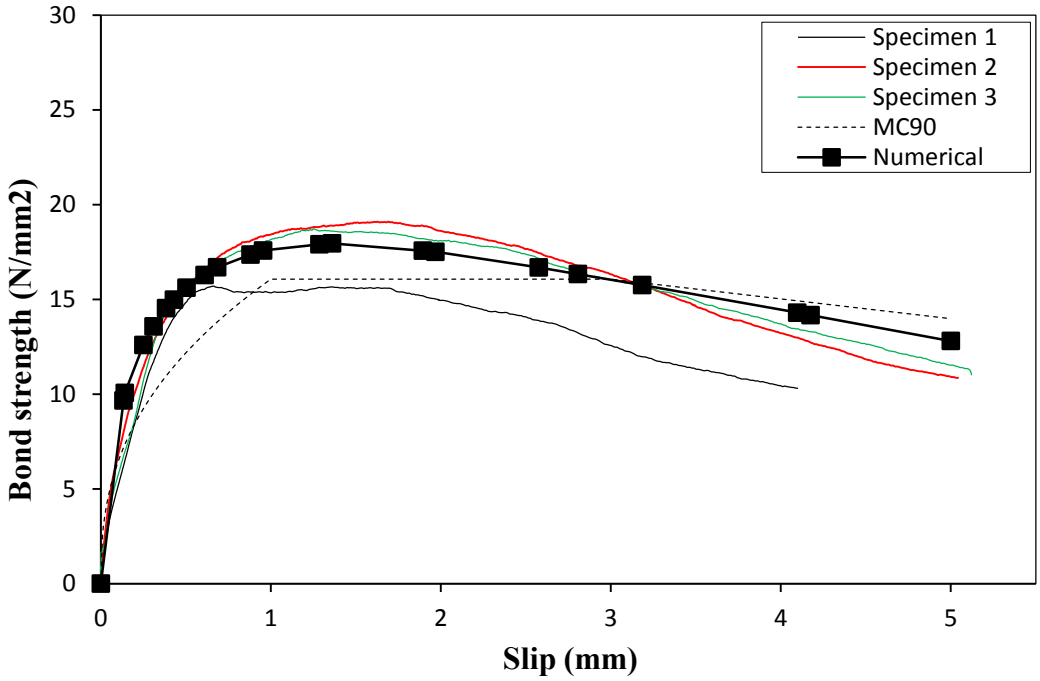

Figure 6.11: Comparison between numerical and experiment results of bond-slip for GGBS concrete specimen

Figure 6.12 presents the bond-slip response of the experimental results for the PFA specimens, which was compared with the bond-slip curve obtained from both the numerical model and the analytical model predicted using MC90. It can be noted from

this figure that the bond strength obtained from experimental results as shown did not reach the bond strength value of the numerical model, generally being lower by 25 %. It appears from Figure 6.12 that the numerical bond-slip response agreed well with actual experimental data up to 7.50 N/mm^2. However, the bond-slip curve of the numerical model exhibits higher stiffness of ascending branch due to the initial cracking occurring at a later stage. In addition, the compressive strength of concrete was modelled in accordance to BS EN 1991-1-1, which may have a slight difference to the actual stress-strain characteristic of the concrete used in the test results. Another explanation for the deviation of the numerical and MC90 model results from the experimental data may be the weak interface bond between the PFA paste and the steel bar (chemical adhesion), which affects the experimental results but is not reflected in the interface models.

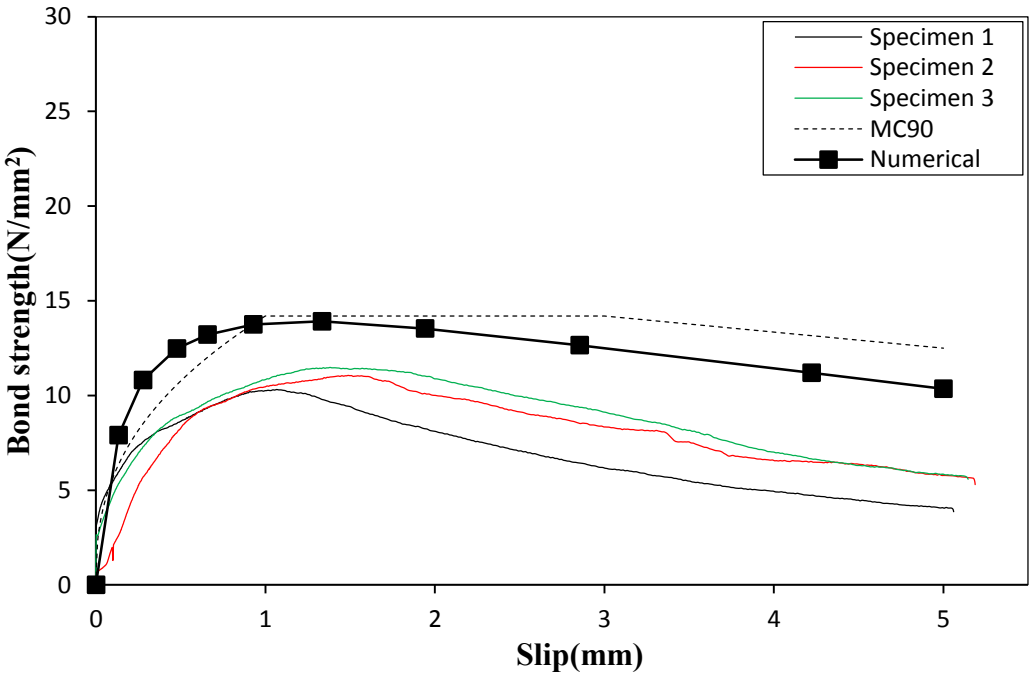

Figure 6.12: Comparison between numerical and experiment results of bond-slip for PFA concrete specimen

Figure 6.13 compares the bond-slip curves obtained from the experimental tests, the analytical models, and numerical results using the MK specimens. The results show that

the numerical data fits the experimental results with reasonable accuracy in the ascending part of the curve, where the bond strength is below 18.20 N/mm^2. The peak bond of the numerical model was 23.78 N/mm^2, which was higher than that of the experimental results (20.5 N/mm^2). Beyond this point, the bond strength decreased gradually, with the calculation terminating at around 22.2 N/mm^2. As can be seen from Figure 6.13, the bond-slip response of the analytical result obtained from the Model Code 1990 was lower by 36.34% at peak bond compared to that of the numerical result. It can therefore be concluded that the differences between the results predicted by the FE model and those obtained experimentally may be attributed to the different interface properties (cohesive element). Here, the normal and shear stiffness depends on the maximum peak bond strength of the test results, where in this case the peak bond strength was calculated as the average of three bond-slip curves. Again the reason behind the difference between numerical and experimental results may be due to different mechanical properties of concrete used in the modelling of the finite element method (such as tension and compressive strength). This could introduce a considerable uncertainty in the analysis.

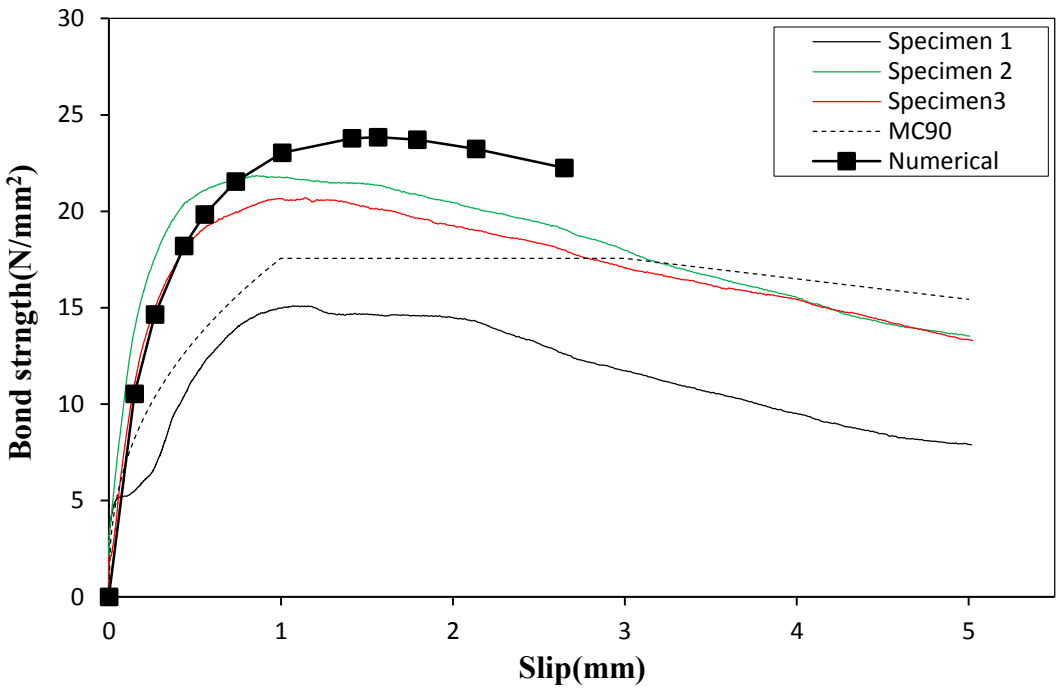

Figure 6.13: Comparison between numerical and experiment results of bond-slip for MK concrete specimens

The experimental bond-slip curves of SF specimens in the presented study are compared against analytical and numerical mode results in Figure 6.14. It can be seen from the figure that the bond-slip curve obtained from the numerical model matches well with one experimental result in terms of peak bond strength. The two remaining experimental specimens had bond-slip curves which had higher bond strength (by about 7.5-23%) in comparison to the numerical model. Conversely, the analytical model obtained by MC90 was found to underestimate the bond strength by 17.20% compared to numerical model predictions. In general, the test results and numerical results exhibit similar trends of behaviour. The two experimental results exhibited higher bond strength than the numerical prediction of the bond-slip curves. This can be mainly attributed to the chemical adhesion between steel and concrete which was stronger in the experimental results. Furthermore, the chemical adhesion may be destroyed at low levels of loading, and the contribution of the frictional resistance to the bond strength

depends on the calculated stress state at the interface to a great extent. In addition, the interface properties of the FE model were different because they were derived from the average value of results. Another possible reason the differences between the test results and the numerical model is that the ribs of the deformed bar were not modelled discreetly as part of the model geometry and the ribs of the bar induce large bearing stresses in the concrete.

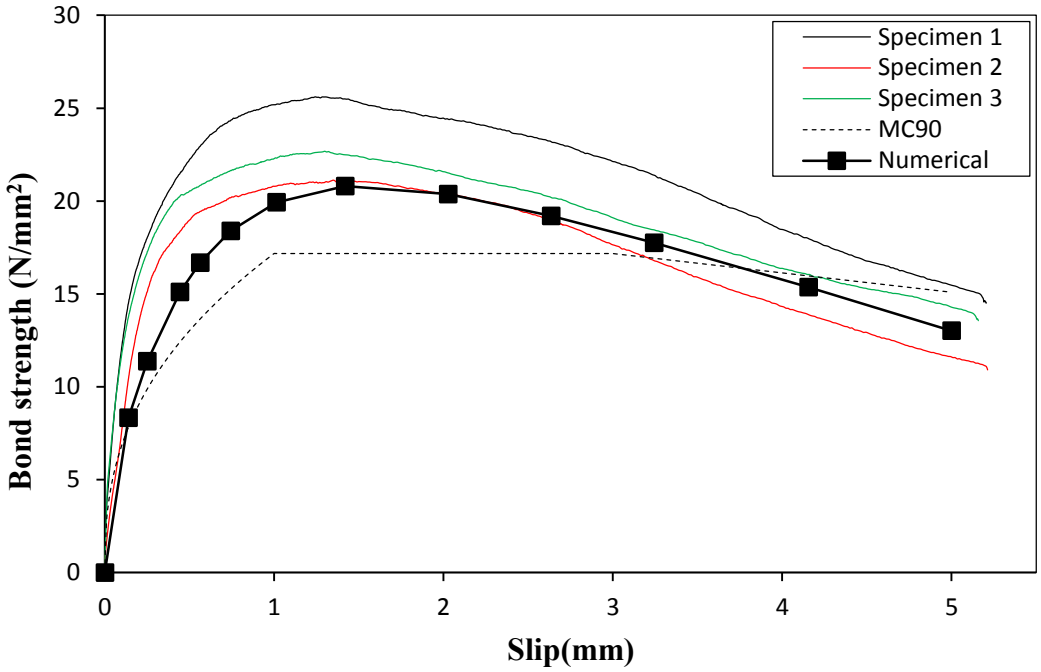

Figure 6.14: Comparison between numerical and experimental results of bond-slip for SF concrete specimens

Table 6.2: Comparison between bond-slip from experimental, numerical and analytical (MC 90)

Specimens	Bond strength (N/mm²)			$\tau_{,exp}/\tau_{,num}$	$\tau_{,mc90}/\tau_{,num}$
	$^{*}\tau_{max,exp}$	$\tau_{max,num}$	$\tau_{max,mc90}$		
00-CEM II-0	18.61	21.51	17.59	0.87	0.82
50-GGBS-0	17.73	17.95	16.06	0.99	0.89
30-PFA-0	10.51	13.95	13.69	0.75	0.98
10-MK-0	18.19	23.84	17.56	0.76	0.74
10-SF-0	21.45	20.80	17.17	1.03	0.83

* Average value of three specimens

Comparisons between bond-slip curves of different concretes obtained from numerical results using the cohesive zone method and the actual experimental results is presented in Figures 6.10 to 6.14 and Table 6.2. It can be seen that good agreement has been achieved between the experimental and numerical results for most of the bond-slip curve. Furthermore, it was observed that although the numerical results and experimental results match well, with a variation ranging from 13.19% to 23%, the numerical results did not compare well with the MC90 calculations (see Figures 6.10 to 6.14). It can hence be noted that the numerical results slightly overestimated the bond in comparison to the analytical results. This is attributed to the difference in the stress-strain behaviour of concrete and stiffness of interface element. Moreover, the specimens with GGBS and PFA concrete exhibit similar global bond-slip behaviour, while some similarity also exists between CEM II and SF concrete specimens. In general, the GGBS and PFA concrete specimens have lower bond strength than the CEM II and SF.

This result appears to be a direct consequence of the mechanical properties of the material. From these figures, it can be concluded that the numerical models exhibit a good agreement with the experimental results for both ascending and descending branches of the curve. Also, the difference in stiffness of interface element may be a reason that effects the numerical results as the stiffness values of the model were dependent on the peak bond strength. Therefore, the cohesive element model is suitable for the predictions of bond strength-slip behaviour subjected to monotonic loading.

6.6.3 **Effect of compressive strength of concrete on bond strength**

Figure 6.15 shows the relationship between the bond strengths and the concrete strengths of concrete containing different pozzolanic materials. In this figure, bond strengths obtained from the numerical model and analytical results obtained from MC90 are plotted in comparison with the measured data. It can clearly be seen that an increase

in the concrete compressive strength was found to be associated with an increase in both the predicted and experimental bond strength. Moreover, the compressive strength up to 50 N/mm^2 has a more pronounced effect on the peak bond strength. The bond strength of numerical and experimental results matched closely for concrete made with GGBS and SF cement (average values of three specimens), while the predicted PFA, CEM II and MK concretes gave values higher than the test results. Furthermore, a maximum difference of 32.5% was observed between the numerical results and the test results for the compressive strength of 32.5 N/mm^2 (see Figure 6.15). This may be due to variations in the stress-strain relationship of the numerical results (obtained from BS EN 1992-1-1) as compared to the actual results. This can be explained by the failure mechanisms associated with different tensile strength of the concrete as mentioned in section 4.4. In the same figure, best fit lines were plotted and good correlation can be seen between bond and concrete strength. It can be concluded that the concrete compressive strength has an important effect on the bond strength, as expected in this study.

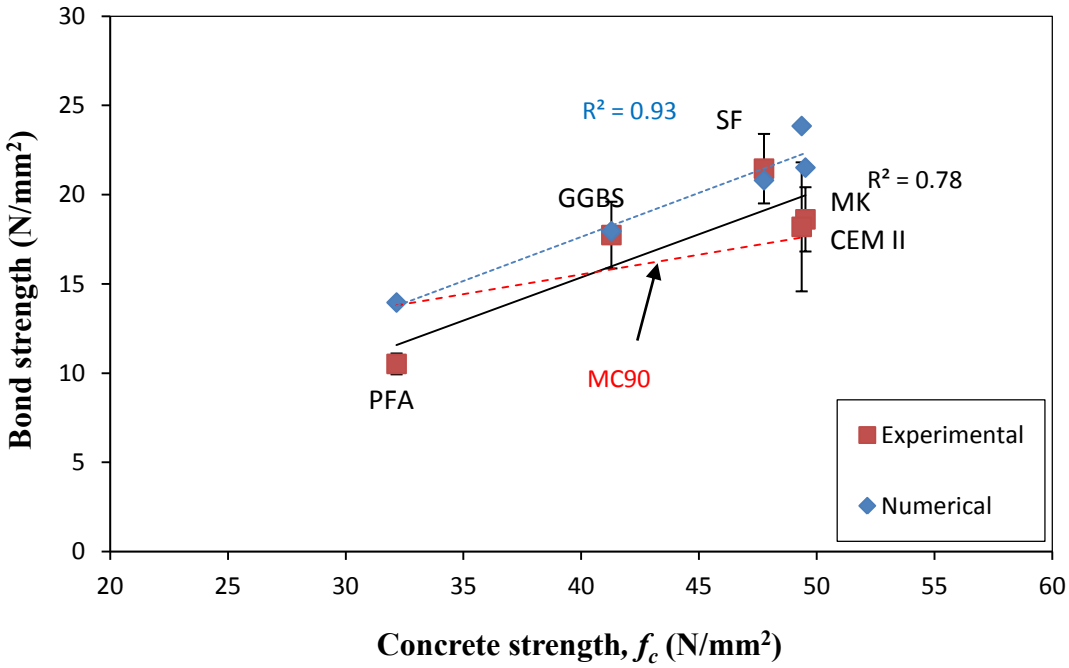

Figure 6.15: Influence of concrete strength on bond strength for different concretes

6.7 Conclusions

In this chapter, the bond-slip relations of different concretes for un-corroded specimens were investigated by using commercially available finite element packages, in this case LUSAS and ABAQUS. The experimental results of control specimens were used for validation of the numerical results. The cohesive zone model was also used to address the interfacial behaviour between the reinforcing bar and the surrounding concrete. Based on the results described the following conclusions may be drawn:

- The FE model software LUSAS was used in this study and was found not to be an appropriate tool for the analysis of bond-slip behaviour. This is due to the fact of LUSAS not including a constitutive interface model between the steel and the concrete, the joint element method lacking shear stiffness as a parameter.
- FE analysis of pull-out tests has been carried out using interface method (cohesive zone element). The obtained results have shown good agreement to the experimental results of CEM II, GGBS and SF concrete specimens, with the exception of the numerical results of PFA, whose numerical bond-slip predictions was higher than the experimental values. Moreover, the bond-slip curves predicted by using numerical model were higher than the bond-slip curves calculated using the CEB-FIP Model Code 1990.
- The cohesive zone element was used, and proved to be able to represent the bond-slip behaviour between steel reinforcement and concrete. The numerical predicted bond in both the ascending and the descending modes were consistent with the experimental results.
- Based on the comparison between the numerical and experimental results for CEM II, GGBS and MK concrete specimens under pull-out tests, it is observed

that the numerical model gives good results in the pre-peak for bond-slip relationships.

- The bond-slip relations of all concrete specimen, calculated through numerical simulations, were found to exhibit a similar failure mode to that of the experimental results.

The finite element modelling developed in this chapter predicted the bond strength for control specimens (0% corrosion) of the different concrete types using cohesive element method. The predicted results were compared against the pull-out test specimens. However, the bond-slip responses for corroded pull-out test specimens as discussed in Chapter Four are not investigated in this study. Therefore, further research is required to model the effect of corrosion rate (corrosion penetration as function of time) on the bond-slip behaviour and to predict the bond strength of reinforcing bar embedded in concrete containing pozzolanic materials.

CHAPTER 7

CONCLUSIONS AND RECOMMENDATIONS FOR FUTURE WORK

7.1 Introduction

This thesis has investigated the bond strength of corroded steel reinforcing bar embedded in concrete containing CEM II, GGBS, PFA, MK and SF which were immersed in chloride ion solution. Specifically, testing was conducted using pull-out tests and concrete permeability measurements. The steel reinforcement was artificially corroded for different exposure times of 3, 7, 10, 14 and 20 days. The pull-out test was used to investigate the impact of corrosion level, cement type and the compressive strength on bond strength. The nitrogen gas permeability test was used to investigate the permeability coefficient of these types of concrete. The FE models were validated against the experimental and analytical results of CEB-FIP Model Code 1990. In addition, the cohesive model was used to address the interfacial behaviour between steel and concrete.

The conclusions of the experimental and the numerical studies have been presented in chapters 4 to 6. The most significant conclusions are summarised below.

7.2 Conclusions

The main findings in this study were that the following conclusions can be drawn:

- The compressive strength and splitting strength of concrete for all concrete mixes were affected by the cement replacement material.
- The compressive strength was affected by the quantity of both PFA and GGBS cement replacement materials and the effect of further cement hydration on the concrete strength was an increase with curing age.
- The ultimate bond strength of the control specimens for all concrete mixes was directly related to concrete properties, namely the compressive and tensile strength of the concrete. The average value of bond strength was compared to the CEB-FIP Model Code 1990. The bond strength for the GGBS and MK mixes was similar to that predicted by the model code. All concrete mixes for concrete specimens (uncorroded) failed in a pull-out failure mode due to the higher confinement associated with a concrete cover greater than three times the reinforcing bar diameter.
- The corrosion levels of the steel bar in different concrete types appear to follow a similar trend, where concretes containing PFA and SF had lower steel bar corrosion levels. The magnitude of the corrosion level of the reinforcing bars was dependent on the concrete type and exposure time of the artificial corrosion.
- In all the concrete mixes studied, the bond strength of the corroded specimens depended on the corrosion levels and was different across all concrete types, varying with the concrete microstructure. The corrosion products cause an expansive pressure on the surrounding concrete leading to enhanced confinement which results in an increase in bond strength at low levels of

corrosion. However, as the corrosion level exceeded approximately 1.74%, the bond strength began to decline slightly.

- Permeabilities depended mostly on curing time, pozzolanic reactions and cement replacement levels, with the PFA having the lowest permeability compared to the other two types of cement. The difference in the gas permeability of the concrete corresponds to differences in the microstructure. The gas permeability coefficient of the GGBS concrete was higher than that of the PFA concrete mixes as a result of a change in microstructure.

- The concrete made with cement replacement materials had a lower gas permeability coefficient compared to the CEM II concrete which is dependent upon quantity of cement replacement. Amongst all concrete mixes, PFA mixes exhibited the best improvement (reduction) in the gas permeability coefficient.

- In all the concrete mixes, the gas permeability decreased with the increasing curing age. PFA was more effective in improving the gas permeability at 180 days. Both the 40% and 45% PFA with CEM II improved the gas permeability at 180 days. On the other hand, an addition of 60% GGBS had highest the gas permeability at a similar age.

  The influence of the compressive strength on the gas permeability of concretes was insignificant but is dependent upon the cement replacement levels. The CEM II and GGBS concretes exhibited higher compressive strength, but the gas permeability of these concretes was also higher. The PFA concretes exhibited a lower compressive strength at the same curing age, and the gas permeability coefficients were lower.

- There is a significant decrease in both the corrosion rate and gas permeability of concretes with different cement replacement levels as the age of these concretes is increased. It is beneficial to employ PFA as a replacement additive at 40% of the cement weight as it exhibited a stronger improvement in gas permeability and corrosion rate.

- A strong correlation coefficient was observed between the corrosion rate of steel bars and the age of curing. As the curing time increased the corrosion rate decreased due to pozzolanic reactions of PFA and GGBS. This resulted in the formation of C-S-H gel, which refined the pores and changed the concrete microstructure, limiting the ingress of chloride ions during the accelerated corrosion process.

- Gas permeability of concrete correlates with the corrosion rate, where the concretes with lower gas permeabilites had lower corrosion rates. The concretes with PFA had lower values of gas permeability and corrosion rate compared with others at the same w/c ratio. This can be attributed to change in pores structure of paste in concretes. Therefore, corrosion rate is directly dependent on gas permeability of concrete which varies according to concrete types.

- The FE model software LUSAS was used in this study and was found to be unsuitable for the analysis of bond-slip behaviour. For this reason, the cohesive zone model within the ABAQUS program was used to represent the bond-slip behaviour between steel bar and concrete.
- FE analysis of pull-out tests has been carried out using the interface method (cohesive zone element) and the obtained results were found to be in good agreement with the numerical modelling and the experimental results of CEM II,

GGBS and SF concrete specimens except in the case of PFA where the numerical result was found to be overestimated.

- The agreement between the results obtained by the numerical model and the experimental tests proves that the cohesive element method can be used reliably to model the interface between steel and concrete.

7.3 Recommendations for future work

Based on the conclusions of this thesis, the following topics can be recommended for future work:

1. Experimental study

- Further research is needed to investigate the effect of corrosion inhibitors (such as calcium nitrate, CN) in concrete mixes made with cement replacement materials. This would allow an examination of their effect on corrosion resistance. More experimental studies involving pull-out testing are required to evaluate the bond strength of corroded reinforcements embedded in concrete containing cementitious materials which have different concrete cover depths and different water-to-cement ratios.
- Cement replacement materials in concrete should be studied further, with particular emphasis toward the influence of the concrete microstructure on the interface of steel/matrix. Micro-cracking caused by corrosion expansion should also be explored using the scanning electron microscope (SEM) which can reveal the cracking characteristics at the interface between steel and concrete.
- The rapid chloride permeability method can be used to assess the chloride permeability of concrete for different concrete types at different times of curing.

This would enable a better comparison of the corrosion rate of steel in concrete over time since similar transport properties are employed both tests.

- Further work is needed in order to evaluate the influence of different compressive strengths of concrete the gas permeability of concrete with different w/c ratios for cement replacement materials such as PFA and GGBS over a long time curing time.
- The pull-out test specimens showed that lowest the bond strength of the reinforcing bar embedded in the PFA concrete. Therefore, further to this research, it is recommended to investigate the effect of using PFA cement replacement on the bond strength behaviour while varying other parameters such as the compressive strength, age of concrete and bar diameter. All these variables will help to explain the bond-slip behaviour of a steel bar in concrete made with cement replacement materials.

2. Numerical model study

- Further study is required to develop the numerical model of corroded specimens; the issue requires an appropriate bond model to predict the bond strength of corroded steel reinforcement in different concrete types having different parameters such as concrete strength and corrosion rates etc. As a basis for the implementation of the numerical investigation, a 3-dimensional nonlinear ABAQUS finite element model could be used. Numerical modelling investigation of the bond of corroded steel bar in concrete is currently a major challenge. The core idea of this model is its dependence on the corrosion rate of the bar and the resulting expansion effect of the corrosion products, and therefore it has to be accounted for. Two different numerical models may be

developed to address the question of the effect of corroded steel on its bond strength. The first model is based on the interface between the corroded steel bar and concrete implemented in the FE program composite model. In this model, the cohesive elements with corrosion products can be assigned using a subroutine code to represent the interaction layer between the corroded steel bar and the surrounding concrete. This would allow a better understanding of bond stress behaviour at steel/concrete interfaces. In addition, the developed FE models can be used further to compare with experimental results obtained from pull-out test under monotonic loading.

The second model is a corrosion model that was developed by Lundgren (2000) and which was further calibrated with several tests in Lundgren (2005b). In the corrosion model, the influence of corrosion is represented as the volume increase of the corrosion products (see Figure 7.1) compared with the original reinforcing bar. Here, corrosion product penetration is an important parameter. The most important details for this corrosion model are summarised in Appendix C.

- FORTRAN may be used to create a code which supports the interface cohesive method in the ABAQUS programme. In addition, more attention should be applied to creations of code which supports the interface cohesive method in the ABAQUS programme. More experimental pull-out testing is required with different cement replacement materials in order to further investigate the corresponding effect on bond strength-slip behaviour. Concrete mix proportions similar to those used in this research should be employed again to allow comparison. The FE model will then be validated with the experimental results to assess the effect of different variables of corrosion level on the bond strength.

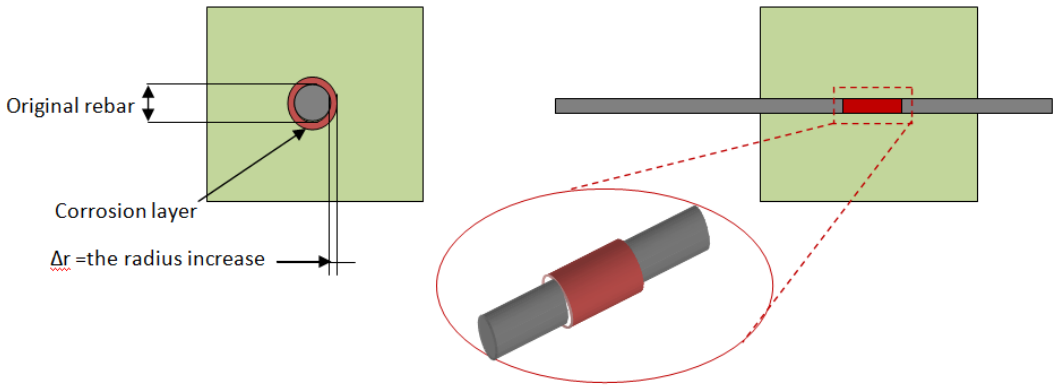

Figure 7.1: Example of pull-out specimen shows for corroded layer (corrosion penetration surrounding the steel bar concrete)

Once validated there is also potential for the FE model to be used as a tool by asset managers to predict, on the basis of concrete component materials and exposure conditions, the likely corrosion level of the steel reinforcement in the RC structure. Using this information, further assessments of residual structural longevity as a function of residual bond strength may be made. Whilst it is appreciated that this is a significant undertaking for the future, the current FE model shows promise in facilitating this transition from laboratory based experimentation and validation to practical implementation and application.

REFERENCES

ABAQUS *standard user's manual*, version 6.11. Hibbitt, Karlson, and Sorensen, Inc. Pawtucket, RI, USA; 2011.

Abosrra, L. 2010. *Corrosion of steel reinforcement in concrete*. PhD Thesis. Bradford University, UK.

Abosrra, L., Ashour, A. F. and Youseffi, M. 2011. Corrosion of steel reinforcement in concrete of different compressive strengths. *Construction and Building Materials* 25 (10), pp. 3915-3925.

ACI Committee 222. 2001. Protection of Metals in Concrete against Corrosion. *American Concrete Institute*, pp. 41.

ACI Committee 408. 2003. Bond and Development of Straight Reinforcing Bars in Tension, *American Concrete Institute***,** pp. 49.

Ahmad, S., Azad, A. K. and Loughlin, K. F. 2005. A study of permeability and tortuosity of concrete. *30th Conference on Our World in Concrete and Structures:* 23-24 August 2005, Singapore.

Ahmed, S. 2003. Reinforcement corrosion in concrete structures, its monitoring and service life prediction - a review. *Cement and Concrete Composites,* 25**,** pp. 459-471.

Al-Amoudi, O. S . R., Maslehuddin, M. and Al-Mana, A. I. 1993. Prediction of Long-Term Corrosion Resistance of Plain and Blended Cement concretes. *ACI Materials Journal,* 90**,** pp. 564-570.

Almusallam, A., Al-Gahtani, A. S., Aziz, A. R. and Rasheeduzzafar A .1996. Effect of reinforcement corrosion on bond strength. *Construction and Building Materials,* 10**,** pp.123-129.

Alonso, C., Andrade, C., Rodriguez , J. and Diez, M. 1998. Factors controlling cracking of concrete affected by reinforcement corrosion. *Materials and Structures,* 31**,** pp. 435-441.

Al-Sulaimani. G. J., Kaleemullah, M., Basunbul, I. A. and Rasheeduzzafar, A. 1990. Influence of corrosion and cracking on bond behavior and strength of reinforced concrete members. *ACI Structural Journal,* 87, pp. 220-231.

Amleh, L. 2000. *Bond deterioration of reinforcing steel in concrete due to corrosion.* PhD Thesis, University of Montreal, Canada.

Amleh, L. and Ghosh, A . 2006. Modeling the effect of corrosion on bond strength at the steel-concrete interface with finite-element analysis. *Canadian Journal of Civil Engineering,* 33(6)**,** pp. 673-682.

Amleh, L. and Mirza, M. S .1999. Corrosion influence on bond between steel and concrete. *ACI Structural Journal,* 96, pp. 415-423.

Ann, K. Y. and Song, H. W. 2007. Chloride threshold level for corrosion of steel in concrete. *Corrosion Science,* 49(11), pp. 4113-4133.

Arel*,* H. S. and Yazici*,* S. 2012. Concrete reinforcement bond in different concrete classes. *Construction and Building Material,* 36, pp. 78-83.

Arezoumandi, M., Wolfe, M. H. and Volz, J. S. 2013. A comparative study of the bond strength of reinforcing steel in high-volume fly ash concrete and conventional concrete. *Construction and Building Materials,* 40, pp. 919-924.

Arya, C. and Xu, Y.1995. Effect of cement type on chloride binding and corrosion of steel in concrete. *Cement and Concrete Research,* 25(4), pp. 893-902.

Auyeung, Y., Balaguru, P. and Chung, L. 2001. Bond behavior of corroded reinforcement bars. *ACI Materials Journal,* 97(2), pp. 214-220.

Azad, A. K., Ahmad, S. and Azher, S. A .2007. Residual strength of corrosion-damaged reinforced concrete beams. *ACI Materials Journal,* 104, pp. 40-47.

Baingo, D. 2012. *A framework for stochastic finite element analysis of reinforced concrete beams affected by reinforcement corrosion*. PhD thesis, University of Ottawa, Canada.

Balafas, I. and Burgoyne, C. J. 2010. Environmental effects on cover cracking due to corrosion. *Cement and Concrete Research,* 40, pp. 1429-1440.

Ballim,Y. and Reid, J. C. 2003. Reinforcement corrosion and the deflection of RC beams- an experimental critique of current test methods. *Cement and Concrete Composites,* 25**,** pp. 625-632.

Bamforth, P. B. 1991. The water permeability of concrete and its relationship with strength. *Magazine of Concrete Research,* 43(157), pp. 233-241.

Bamonte, P. and Gambarova, P. G. 2007. High-Bond Bars in NSC and HPC: Study on Size Effect and on the Local Bond-Stress Stress-Slip Law, *ASCE - Journal of Structural Engineering,* 133(2), pp. 225-234.

Bamonte, P., Biancini, S. and Lo Monte, F. 2012. Preliminary Results on Tension Stiffening in Heat-exposed R/C Tension Members: *Proceeding of the 4th international conference Bond in Concrete*. Brescia, Italy, pp. 559-565.

Batis, G. and Rakanta, E. 2005. Corrosion of steel reinforcement due to atmospheric pollution. *Cement and Concrete Composites,* 27(2), pp. 269-275.

Bazant, Z. P. 2002. Concrete fracture models: testing and practice. *Engineering Fracture Mechanics,* 69, pp. 165-205.

Berra, M., Castellani, A., Coronelli, D., Zanni, S. and Zhang, G. 2003. Steel-concrete bond deterioration due to corrosion: finite-element analysis for different confinement levels. *Magazine of Concrete Research,* 55(3), pp. 237-247.

Bhargava, K., Ghosh, A. K., Mori, Y. and Ramanujam, S. 2007. Corrosion-induced bond strength degradation in reinforced concrete-Analytical and empirical models. *Nuclear Engineering and Design,* 237(11), pp. 1140-1157.

Bingöl, A. F. and Gül, R. 2009. Residual bond strength between steel bars and concrete after elevated temperatures. *Fire Safety Journal*, 44, pp.854-859.

British Standards Institution BS 1881: Part 208: 1996. Testing concrete - Recommendations for the determination of the initial surface absorption of concrete. London. BSI.

British Standards Institution BS 6699:1992. Specification for ground granulated blastfurnace slag for use with Portland cement. London. BSI.

British Standards Institution BS EN 10080: 2005. Steel for the reinforcement of concrete-Weldable reinforcing steel-General. London. BSI.

British Standards Institution BS EN 12390-3:2009. Testing hardened concrete. Compressive strength of test specimens. London. BSI.

British Standards Institution BS EN 12390-6: 2000.Testing hardened concrete. Tensile splitting strength of test specimens. London. BSI.

British Standards Institution BS EN 12620. 2002. Aggregate of concrete. London. BSI.

British Standards Institution BS EN 197-1:2000. Cement Composition, specifications and conformity criteria for common cements. London. BSI.

British Standards Institution BS EN 1992-1-1. 2004. Eurocode 2: design of concrete structures: part 1-1: general rules and rules for building. London. BSI.

British Standards Institution BS EN 933-1: 1997. Tests for geometrical properties of aggregates. Determination of particle size distribution. Sieving method. London. BSI.

British Standards Institution BS EN12350-2: 2009.Testing fresh concrete. Slump-test. London. BSI.

British Standards Institution BS4449: 2005. Steel for the reinforcement of concrete. Weldable reinforcing steel. Bar, coil and decoiled product. Specification. London. BSI.

Broomfield, J. P. 2007. *Corrosion of Steel in Concrete: Understanding, Investigation and Repair*.Taylor & Francis, New York .USA.

Cabrera, J. G. and Lynsdale, C. J. 1988. New gas permeameter for measuring the permeability of mortar and concrete. Magazine of Concrete Research, 40(144), pp. 177-182.

Cabrera, J. G.1996. Deterioration of concrete due to reinforcement steel corrosion. *Cement and Concrete Composites,* 18(1)**,** pp. 47-59.

Cairns, J. and Abdullah, R. 1995. An evaluation of bond pullout test and their relevance to structural performance. *The Structural Engineer,* 73(11), pp.179-185.

Castel, A., Francois, R. and Arliguie, G. 2000. Mechanical behaviour of corroded reinforced concrete beams-Part 1: Experimental study of corroded beams. *Materials and Structures,* 33(9)**,** pp. 545-551.

CEB-FIP. Model code 90, first draft. committee euro-international du beton, Bulletin d'information, No.195-196, 1990.

Chalee, W., Jaturapitakkul, C. and Chindaprasir, P. 2009. Predicting the chloride penetration of fly ash concrete in seawater. *Marine Structures,* 22(3), pp.341-353.

Chan, C. H. S. 2012. *Bond and Cracking of Reinforced concrete*. PhD Thesis. Cardiff University, UK

Chana, P. S. 1990. A test method to establish realistic bond stresses. *Magazine of Concrete Research,* 42(151), pp. 83-90.

Chen, W.F. and Han, D. J. 1988. *Plasticity for Structural Engineers*. New York : J. Ross.

Chen, Z. J. 2004. Effect of Reinforcement Corrosion on the Serviceability of Reinforced Concrete Structures, MSc Thesis. University of Dundee, UK.

Cheng, A., Huang, R .,Wu, J. K. and Chen, C. H . 2005. Influence of ground granulated blast furnace slag on durability and corrosion behaviour of reinforced concrete. *Material Chemical Physical,* 93, pp. 404-411.

Chindaprasirt, P., Homwuttiwong, S. and Jaturapitakkul. C. 2007. Strength and water permeability of concrete containing palm oil fuel ash and rice husk-bark ash. *Construction and Building Materials,* 21(7), pp. 1492-1499.

Chindaprasirt, P., Jaturapitakkul, C and Sinsiri, T. 2005. Effect of fly ash fineness on compressive strength and pore size of blended.*Cement and Concrete Composite,* 27(4), pp. 425-428.

Choi, Y. S., Kim, J. G. and Lee, K. M. 2006. Corrosion behavior of steel bar embedded in fly ash concrete. *Corrosion Science,* 48(7), pp. 1733-1745.

Chung, L., Ho Cho, S., Jay Kim, J. H. and Yi, S. T . 2004. Correction factor suggestion for ACI development length provisions based on flexural testing of RC slabs with various levels of corroded reinforcing bars. *Engineering Structures,* 26**,** pp.1013-1026.

Chung, L., Jay Kim, J. H. and Yi, S. T. 2008. Bond strength prediction for reinforced concrete members with highly corroded reinforcing bars. *Cement and Concrete Composites,* 30, pp. 603-611.

Chung, L., Najm, H. and Balaguru, P . 2008. Flexural behavior of concrete slabs with corroded bars. *Cement and Concrete Composites,* 30**,** pp.184-193.

Collins, J. F. 1987. *Permeability of concrete mixtures.* PhD Thesis. Institute of Technology, New Jersey, USA.

Cook, R. D. Malkus, D. S. Plesha, M. E. and Witt, R. J. 2002. *Concepts and Applications of Finite Element Analysis*. New York: John Wiley and Sons INC.

Dahou, Z., Mehdi Sbartaï, Z., Castel, A. and Ghomari, F. 2009. Artificial neural network model for steel-concrete bond prediction. *Engineering Structures,* 31(8), pp. 1724-33.

Darwin, D. and Graham, E. 1993. Effect of Deformation Height and Spacing on Bond Strength of Reinforcing Bars. *ACI Structural Journal,* 90(6), pp. 646- 657.

De Groot, A. K., Kusters G. M. A. and Monnier, T. 1981. Numerical modelling of bond-slip behaviour. *Concrete Mechanics*, 26(1B), pp. 6-38.

De Larrard, F., Schaller, D. and Fuchs, J. 1993. Effect of bar diameter on the bond strength of passive reinforcement in HPC. *ACI Material Journal,* 90(4), pp.333-339.

Dellinghausen, L. M., Gastaldini, A. L. G., Vanzin, F. J. and Veiga, K.K.2012. Total shrinkage, oxygen permeability, and chloride ion penetration in concrete made with white Portland cement and blast-furnace slag *Construction and Building Material*, 37 , pp.652-659.

Dhir, R. K. and Jones, M. R.1999. Development of chloride -resisting concrete using fly ash .*Fuel,* 78(2), pp.137-142.

Dhir, R. K., El-Mohr, M. A. K. and Dyer, T. D. 1997. Developing chloride resisting concrete using PFA. *Cement and Concrete Research*, 27(11), pp. 1633-163.

Dinakar, P., Babu, K. G. and Santhanam, M. 2007.Corrosion behaviour of blended cements in low and medium strength concretes. *Cement and Concrete Composites,* 29(2), pp. 136-145.

Elahi, A., Basheer, P. A. M, Nanukuttan, S. V. and Khan, Q. U. Z. 2010. Mechanical and durability properties of high performance concretes containing supplementary cementitious materials. *Construction and Building Materials,* 24, pp. 292-299.

El-Hacha, R., El-Agroudy, H. and Rizkalla, S. H. 2006. Bond characteristics of high-strength steelreinforcement. *ACI Structural Journal,* 103(6), pp. 771-782.

Eligehausen, R., Bertero, V. V. and Popov, E. P.1983. Local bonds stress-slip relationships of deformed bars under generalized excitations: Tests and analytical model. Technical Report UCB/EERC-83. *Earthquake Engineering Research Centre.* University of California, Berkeley.

Elshab, A. A. 1997. *The permeability of high strength concrete.* PhD Thesis. Cardiff University, UK.

Fang, C., Lundgren, K., Chen, L. and Zhu, C. 2004. Corrosion influence on bond in reinforced concrete. *Cement and Concrete Research,* 34, pp. 2159-2167.

Fang, C., Lundgren, K., Plos, M. and Gylltoft, K . 2006. Bond behaviour of corroded reinforcing steel bars in concrete. *Cement and Concrete Research,* 36(10)**,** pp.1931-1938.

Ferguson, P. M., Turpin, R. D. and Thompson, J. N. 1955. Minimum bar spacing as a function of bond and shear strength. *American Concrete Institute Journal,* 50(10), pp. 869-888.

FESI. 2012. Hammersmith Flyover Corrosion Problems [Online]. Available at: http:// http://www.fesi.org.uk/fesi-news.html [Accessed: 12 September 2012].

FIB Bulletin 10 . 2000. Bond of Reinforcement in Concrete *Fédération Internationale du Béton, Lausanne, Switzerland.*

Francois, R .and Arliguie, G. 1998. Influence of Service Cracking on Reinforcement Steel Corrosion. *Journal of Materials for Civil Engineering,* 10(1), pp.14-20.

Fu, X. and Chung, D. D . L.1997. Effect of corrosion on the bond between concrete and steel rebar. *Cement and concrete research,* 27(12)**,** pp.1811-1815.

Gambarova, P. G. 2012. Bond in reinforced concrete: where do we stand today?: *Proceedings of the 4th international conference Bond in Concrete.* Brescia, Italy pp.1-13.

Gan Y. 2000. *Bond stress and slip modeling in non-linear finite element analysis of reinforced concrete structures*. MSc Thesis, University of Toronto.

Gardner, D. R. 2005. *Experimental and Numerical studies of the permeability of concrete*. PhD Thesis, Cardiff University, UK.

Gardner, D. R., Lark, R. J. and Barr, B. 2005. Effect of conditioning temperature on the strength and permeability of normal- and high-strength concrete. *Cement and Concrete Research,* 35(7), pp.1400 -1406.

Gardner, D. R., Lark, R. J. and Jefferson, A. D. 2007. An experimental, numerical and analytical investigation of gas flow characteristics in concrete. *Cement and Concrete Research,* 38, pp. 360-367.

Gencel, O., Koksal, F., Ozel, C. and Brostow, w. 2012. Combined effects of fly ash and waster ferrochromium on properties of concrete. *Construction and Building Materials,* 29, pp. 633-640.

Gjorv, O. E., Monteiro, P. J. M. and Mehta, P. K. 1990. Effect of condensed silica fume on the steel-concrete bond. *ACI Materials Journal,* 87(6), pp. 573-580.

Glass, G. K. and Buenfeld, N. R. 2000. The influence of chloride binding on the chloride induced corrosion risk in reinforced concrete. *Corrosion Science,* 42(2), pp.329-344.

Gunevisi, E., Gesoglu, M., Ozturan, T. and Ozbay, E. 2009. Estimation of chloride permeability of concretes by empirical modeling: Considering effects of cement type, curing condition and age. *Construction and Building Materials,* 23(1), pp. 469-481.

Güneyisi, E., Gesoğlu, M., Karaoğlu, S. and Mermerda, K. 2012. Strength, permeability and shrinkage cracking of silica fume and metakaolin concretes. *Construction and Building Materials,* 34, pp.120-130.

Ha, T. H., Muralidaran, S. Bae, J. H., Ha, Y.C., Lee, H. G., Park, K. W. and Kim, D. K. 2007. Accelerated short-term techniques to evaluate the corrosion performance of steel in fly ash blended concrete. *Building and Environment,* 42(1), pp. 78-85.

Haddad, R. H., Al-Saleh, R. J. and Al-Akhras, N. M. 2008. Effect of elevated temperature on bond between steel reinforcement and fiber reinforced concrete. *Fire Safety Journal,* 43(5), pp. 334-343.

Hadj-sadok, A., Kenai, S., Courard, L. and Darimont, A.2011. Microstructure and durability of mortars modified with medium active blast furnace slag. *Construction and Building Materials,* 25, pp. 1018-10125.

Hanson. 2013. Rugen GGBS [Online]. Available at: http://www.heidelbergcement.com/uk/en/hanson/products/cements/ggbs_and_related_products/regen-ggbs.htm [Accessed: 10 January 2013].

Haque, M. N. and Kayali, O. 1998. Properties of high-strength concrete using a fine fly ash. *Cement Concrete Research*, 28, pp. 1445-1452.

Hassan, K. E., Cabrera, J. G. and Maliehe, R.S. 2000.The effect of mineral admixtures on the properties of high-performance concrete. *Cement and Concrete Composites*, 22(4), pp. 267-271.

Heneriques, J., Da Sliva, L. S. and Valent, I. S. 2013. Numerical modeling of composite beam to reinforced concrete wall joints. *Engineering Structures,* 52, pp.747-767.

High Strength Concrete. FIP/CEB State of the Art Report. Bulletin d'Information, No.197, August 1990.

Huang, R., Chang, J. J. and Kuo Wu, J . 1996. Correlation between corrosion potential and polarization resistance of rebar in concrete.*Material Letters,* 28, pp. 445-450.

Ichinose, T., Kanayama, Y., Inoue, J. E. and Bolander, J. R. 2004. Size effect on bond strength of deformed bars. *Construction and Building materials*, 18(7), pp. 549-558

Jefferson, A. D. 1999. A multi-crack model for the finite element analysis of concrete. *Proceedings of BCA Concrete Conference*, pp. 275-286.

Jiang, D. H., Shah, S. P., Andonian, A. T. 1984. Study of the transfer of tensile forces by bond. *ACI Journal,* 81(4), pp. 251-259.

Kankam, C. K. 2003. A routine method for measuring bond stress, steel strain and slip in reinforced concrete at service loads. *Magazine of Concrete Research,* 55(1), pp. 85-93.

Karihaloo, B. L. 1995. *Fracture mechanics and structural concrete*. Longman Scientific and Technical, England.

Kasai, Y., Matsui, I., Fukushima, Y. and Kamohara, H. 1983. Air permeability and carbonation of blended cement mortars, ACI Special Publication SP-29, pp.435-451.

Kayali, O. and Sharfunddin, M. A. 2013. Assessment of high volume replacement fly ash concrete-concept of performance index. *Construction and Building Materials,* 39, pp. 71-76.

Kermani, A. 1991. Permeability of stressed concrete. *Building Research and information*, 19(6), pp 360-366.

Khalfallah, S. 2008. Modeling of bond for pull-out tests. *Building Research Journal,* 56, pp. 37-48.

Khana, M. I. and Lynsdaleb, C. J. 2002. Strength, permeability, and carbonation of high-performance concrete. *Cement and Concrete Research*, 32, pp.123-131.

Khayat, K. H., and Aitcin, P. C. 1993. *Silica fume –A unique supplementary cementitious material. Mineral Admixtures in Cement and Concrete*. In S.N Ghosh (ed) vol. 4: 227-265. ABI Books Private Limited.

Kivell, A., Palermo, A. and Scott, A. 2011. Effects of bond deterioration due to corrosion in reinforced concrete: *Proceeding of the 9th Pacific Conference on Earthquake Engineering* (PCEE), Auckland, New Zealand, pp. 081-088.

Lee, H. S., Noguchi, T. and Tomosawa, F. 2002. Evaluation of the bond properties between concrete and reinforcement as a function of the degree of reinforcement corrosion. *Cement and Concrete Research,* 32(8), pp. 1313-1318.

Lee, J. and Fenves, G. L. 1998. A plastic-damage concrete model for earthquake analysis of dams. *Earthquake Engineering and Structural Dynamic,* 27, pp. 937-956.

Li, S. and Roy, D. M. 1986. Investigation of relations between porosity, pore structure and chloride diffusion of fly ash blended cement pastes. *Cement and Concrete Research,* 16, pp. 749-759.

Liu, Y. and Weyers, R. E. 1998. Modeling the time-to-corrosion cracking in chloride contamined reinforced concrete structures. *ACI Material Journal*, 95 (6), pp. 675-681.

Lundgren, K. 2002. Modelling the effect of corrosion on bond in reinforced concrete. *Magazine of Concrete Research,* 54(3), pp. 165-173.

Lundgren, K. 2005a. Bond between Ribbed Bars and Concrete. Part 1: Modified Model. *Magazine of Concrete Research,* 57, pp. 371-382.

Lundgren, K. 2005b. Bond between Ribbed Bars and Concrete. Part 2: The Effect of Corrosion. *Magazine of Concrete Research,* 57, pp. 383-395.

Lundgren, K. 2007. Effect of corrosion on the bond between steel concrete: an overview. *Magazine of Concrete Research,* 59(6), pp. 447-461.

LUSAS User Manual. 2006. FEA Ltd. London, England.

Lydon, F. D. 1993. The relative permeability of concrete using nitrogen gas. *Construction and Building Materials,* 7(4), pp.213-220.

Lydon, F. D. 1995. Effect of coarse aggregate and water/cement ratio on intrinsic permeability of concrete subject to drying. *Cement and Concrete Research,* 25(8), pp. 1737-1746.

Lydon, F. D. and Mahawish, A. H. 1991. Tests of the permeability of concrete to nitrogen gas. *Construction and Building Materials,* 5(1), pp. 8-17.

Mangat, P. and Elgarf, M. S. 1999. Flexural strength of concrete beams with corroding reinforcement. *ACI Structural Journal,* 96, pp. 149-158.

Mansoor, Y. A. and Zhang, Z. Q. 2013. The Reinforcement Bond Strength Behavior under Different corrosion. *Research Journal of Applied Sciences, Engineering and Technology,* 5(7), pp. 2346-2353.

Mawson, B. Researcher BRE group at Cardiff University, unpublished data.

Martin, G. R. 1986. A method for determining the relative permeability of concrete using gas. *Magazine of Concrete Research*, 38 (135), pp.90-94.

Martín-Pérez, B .1999. Service life modelling of R.C highway structures exposed to chlorides, PhD, University of Toronto.

McCarthy, M. J. and Dhir, R. K. 2005. Development of high volume fly ash cements for use in concrete construction. *Fuel,* 84(11), pp. 1423–1432.

Megat Johari, M. A., Brooks, J. J., Kabir, S. and Rivard, S. 2011. Influence of supplementary cementitious materials on engineering properties of high strength concrete. *Construction and Building Materials,* 25(5), pp. 2639-2648.

Mehta, P. K. and Gerwick, B. C. 1982. Cracking-Corrosion Interaction in Concrete Exposed to Marine Environment. *ACI Concrete International,* 4**,** pp 45-51.

Mohamadie, T. and Wan, B. 2013. Finite Element Modeling of Debonding Failure between FRP and concrete Undergoing Mixed Mode Loading. *FRPRCS*-11, pp.1-10.

Mohammed, T., Otsuki, N., Hisada, M. and Shibata, T. 2001. Effect of Crack width and Bar Types Corrosion of Steel in Concrete. *Journal of Materials in Civil Engineering,* 13(3), pp, 194-201.

NACE. 2013. Corrosion resources for highways and bridges [Online]. Available at: http:// http://www.nace.org/Corrosion-Central/Industries/Highways-and-Bridges/ [Accessed: 12 December 2013].

Nagataki, S., Ujike, I. and Konishi, N. 1986. Influence of moisture content on air permeability of concrete, *in Review of 40th Meeting of Cement Association of Japan,* Tokyo, pp.158-161.

Naik, T. R., Singh, S. S and Hossain, M. M.1994. Permeability of concrete containing large amounts of fly ash. *Cement Concrete Research,* 24(5), pp. 913-922.

Nath, P. and Sarker, P. K. 2013. Effect of mixture proportions on the drying shrinkage and Permeation Properties of High Strength Concrete Containing Class F Fly Ash. *KSCE Journal of Civil Engineering,* 17(6), pp. 1437-1445.

Neville, A. M. 1995. *Properties of concrete*. John Wiley & Sons.

Ngo, D. and Scordelis, A. C. 1967. Finite Element Analysis of Reinforced Concrete Beams. *Journal ACI,* 64(3), pp. 152-163.

Norris, P., Wood, J. G. M. and Barr, B. I. G. 1990. A torsion test to evaluate the deterioration of concrete due to alkali-aggregate reaction. *Magazine Concrete Research,* 42(153), pp. 239-244.

Obainat, Y. T., Heyden, S. and Dahlblom, O. 2010. The effect of CFRP and CFRP/concrete interface models when modelling retrofitted RC beams with FEM. *Composite Structures,* 92, pp.1391-1398.

Oliver, J., Huespe, A. E., Pulido, M. D. G. and Chaves, E. 2002. From continuum mechanics to fracture mechanics: the strong discontinuity approach. *Engineering Fracture Mechanics,* 69, pp. 113-136.

Oner, A. and Akyuz, S. 2007. An experimental study on optimum usage of GGBS for the compressive strength of concrete. *Cement and Concrete Composites,* 29(6), pp. 505-514.

Ouglova, A., Berthaud, Y., Foct, F., François, M., Ragueneau, F. and Petre-Lazar, I . 2008. The influence of corrosion on bond properties between concrete and reinforcement in concrete structures. *Materials and Structures,* 41**,** pp. 969-980.

Owaid, H. M., Hamid, R. B. and Taha, M. R. 2012. A Review of Sustainable Supplementary Cementitious Materials as an Alternative to All-Portland Cement Mortar and Concrete. *Australian Journal of Basic and Applied Sciences,* 6(9), pp. 287-303.

Pal, S. C., Mukherjee, A. and Pathak, S. R. 2002. Corrosion behaviour of reinforcement in slag concrete. *ACI Material Journal,* 99(6), pp.521-527.

Papadakis, V. G. 2000. Effect of fly ash on Portland cement systems. Part I. Low-calcium fly ash. *Cement and Concrete Research,* 29(11), pp. 1727-1736.

Paulay, T. and Park, R . 1975. *Reinforced Concrete Structures*. *John Wiley & Sons*

Persson, B. S. M. 1998. Shrinkage of high-performance concrete. In: Proceedings of International Workshop on Autogenous Shrinkage of Concrete, Hiroshima, Japan, pp. 105–115. E & FN Spon, London.

Picandet,V., Khelidj, A. and Bastian, G. 2001. Effect of axial compressive damage on gas permeability of ordinary and high-performance concrete. *Cement and Concrete Research,* 31, pp. 1525-1532.

Rasheeduzzafar, S. E., Dakhil, F. H., Bader, M. A. and Khan, M. N. 1992. Performance of corrosion resisting steel in chloride-bearing concrete. *ACI Materials Journal,* 89, pp. 439-448.

RILEM Technical Recommendations.1983.*Bond test for reinforcement steel.2. Pull-out Test*, TC9-RC.

Roberge, P. R. 2000. *Handbook of Corrosion Engineering*. McGraw-Hill

Royles, R. and Morley, P. 1983. Response of the bond in reinforced concrete to high temperatures. *Magazine of Concrete Research,* 35(123), pp. 67-74.

Sanjuán, M. A. and Muñoz-Martialay, R. 1996. Influence of the water/cement ratio on the air permeability of concrete. *Journal of Materials Science,* 31(11), pp. 2829-2832.

Saraswathy, V., Muralidharan, S., Thangavel, K., and Srinivasan. S. 2003. Influence of activated fly ash on corrosion-resistance and strength of concrete. *Cement and Concrete Composites,* 25(7), pp. 673-680.

Sardis, M. S. 2001. *Earthquake resistance design procedure for High-strength Concrete Structures.* MSc Thesis. Cardiff University, UK.

Scott, A. and Alexander, M. G. 2007. The influence of binder type, cracking and cover on corrosion rates of steel in chloride-contaminated concrete. *Magazine of Concrete Research,* 59(7), pp. 495-505.

Shafiq, N. and Cabrera, J. G. 2004. Effects of initial curing condition on the fluid transport properties in OPC and fly ash blended cement concrete. *Cement and Concrete Composites*, 26(4), pp. 381-387.

Shi, H. S., Bi-wan, X. and Xiao-chen, Z. 2009. Influence of mineral admixtures on compressive strength, gas permeability and carbonation of high performance concrete. *Construction and Building Material,* 23(5), pp. 1980-1985.

Shi, H. S., Bi-wan, X., Shi, T. and Xiao-Chen, Z. 2008. Determination of gas permeability of high performance concrete containing fly ash. *Materials and Structures*, 44, pp. 1051-1056.

Shi, X., Xie, N., Fortune, K. and Gong, J. 2012. Durability of steel reinforced concrete in chloride environments: An overview. *Construction and Building Materials*, 30, pp.125-138.

Siddique, R. and Khan, M. I. 2011. *Supplementary cementing materials.* Springer.

Smith, K. M., Schokker, A. J. and Tikalsky, P. J. 2004. Performance of Supplementary Cementitious Materials in Concrete Resistivity and Corrosion Monitoring Evaluations. *ACI Materials Journal*, 101(5), pp.385-390.

Song, H. W. and Saraswathy, V. 2006. Studies on the corrosion resistance of reinforced steel in concrete with ground granulated blast-furnace slag-an overview. *Journal of Hazardous Materials,* 138(2), pp. 226-233.

Song, H. W., Pack, S. W., Nam, S. H., Jang, J. C. and Saraswatly, V. 2010. Estimation of the permeability of silica fume cement concrete. *Construction and Building Materials,* 24(3), pp. 315-321.

Sugiyama, T., Bremner, T. W. and Tsuji, Y. 1996. Determination of chloride diffusion coefficient and gas permeability of concrete and their relationship. *Cement and Concrete Research,* 26(5), pp. 781-790.

Sumer, M. 2012. Compressive strength and sulfate resistance properties of concretes containing Class F and Class C fly ashes. *Construction and Building Materials,* 34, pp. 531-536.

Tanyildizi, H., Coskum, A., and Somunkiran, L. 2008. An Experimental Investigation of Bond and Compressive Strength of Concrete with Mineral Admixtures at High Temperatures. *The Arabian Journal for Science and Engineering,* 33(2), pp. 443-449.

Tegguer, A. D., Bonnet, S., Khelidj, A. and Baroghel-Bouny,V. 2013. Effect of uniaxial compressive loading on gas permeability diffusion coefficient of concrete and their relationship. *Cement and Concrete Research,* 52, pp. 131-139.

Tepfers, R. 1979. Cracking of concrete cover along anchored deformed reinforcing bars. *Magazine of Concrete Research,* 31(106), pp. 3-12.

Thangavel, K. and Rengaswamy, N. S. 1998. Relationship between Chloride/hydroxide ratio and corrosion rate of steel in concrete. *Cement and Concrete Composites,* 20(04), pp. 283-292.

Thomas, M. D. A. and Matthews, J. D. 1992. The permeability of fly ash concrete. *Material and Structure,* 25(151), 388-396.

Topcu, I. B. and Boga, A. R . 2010. Effect of ground granulate blast-furnace slag on corrosion performance of steel embedded in concrete. *Materials and Design,* 31(7)**,** pp. 3358-3365.

Torii. K., Sasatani, T. and Kawamura, M. 1995. Effects of Fly Ash, blast Furnace Slag, and Silica Fume on Resistance of Mortar to Calcium Chloride Attack. *American Concrete Institute,* 153**,** pp. 931-950.

Turk, K. and Yildirim, M. S. 2003. Bond strength of reinforcement in splices in beams. *Structural Engineering and Mechanics,* 16(4), pp. 469-478.

Tuutti, K . 1982. Corrosion of Steel in concrete Research Report. Stockholm: Swedish Cement and Concrete Research Institute, pp. 469.

Uysal, M. and Akyuncu, V. 2012. Durability performance of concrete incorporating Class F and Class C fly ashes. *Construction and Building Materials* 34, pp. 170-178.

Valcuende, M. and Parra, C. 2009. Bond behaviour of reinforcement in self-compacting concretes. *Construction and Building Materials,* 23(1), pp. 162-170.

Van Den Heede, P. Gruyaert, E and De Belie, N. 2010. Transport properties of high-volume fly ash concrete: Capillary water sorption, water sorption under vacuum and gas permeability. *Cement and Concrete Composites,* 32(10), pp. 749-756.

Van der Veen C. 1992. Bond in Concrete: from Research to Practice. Cryogenic bond behaviour and tensions stiffening, *Proceedings of International Conference. CEB-RTU. Riga* Technical University, Riga, Latvia, 10.1-10.10.

Wang, K., Jansen, D. C., Shah, S. P. and Karr, A. F. 1997. Permeability study of cracked concrete. *Cement and Concrete Research,* 27 (3), pp. 381-393.

Wang, X .and Liu, X. 2003. A strain-softening model for steel-concrete bond. *Cement and Concrete Research*, 33(10), pp. 1669-1673.

Wang, X. and Liu, X. 2006. Bond strength modeling for corroded reinforcements. *Construction and Building Materials,* 20(3)**,** pp. 177-186.

Whiting, D. 1981. Rapid Determination of the Chloride Permeability of Concrete. Final Report No. FHWA-RD-81/119, Federal Highway Administration.

William, K. J. and Warnke, E. P. 1975. Constitutive models for the triaxial behavior of concrete: *Proceedings of the International Assoc. for Bridge and Structural Engineering,* 19, pp. 1- 30.

Wong, H. S., Zhao, Y. X., Karimi, A. R., Buenfeld, N. R and Jin, W. L. 2010. On the penetration of corrosion products from reinforcing steel into concrete due to chloride-induced corrosion. *Corrosion Science,* 52, pp. 2469-2480.

Yalciner, H., Eren, O. and Sensoy, S. 2012. An experimental study on bond strength between reinforcement bars and concrete as a function of concrete cover, strength and corrosion level. *Cement and Concrete Research,* 42, pp. 643-655.

Yeau. K. Y. and Kim, E. K. 2005. An experimental study on corrosion resistance of concrete with ground granulate blast-furnace slag. *Cement and Concrete Research,* 35, pp. 1391-1399.

Yi, S, T., Hyun, T. Y. and Kim, J. K. 2011. The effects of hydraulic pressure and crack width on water permeability of penetration crack-induced concrete. *Construction and Building Materials,* 25(5), pp. 2576-2583.

Yoon, S., Wang, K .,Weiss, W. J. and Shah, S. P .2000. Interaction between loading, corrosion, and serviceability of reinforced concrete. *ACI Materials Journal,* 97(6)**,** pp. 637-644.

Yuan, Y. and J i, Y. 2009. Modelling corroded section configuration of steel bar in concrete structure. *Construction and Building Materials*, 23(6), pp. 2461-2466.

APPENDIX-A

A.1: Fine aggregate data (sieve analysis)

Prepared: 28 Apr 2011 15:12 095_Cardiff_Wharf_095A289 **Hanson Aggregates**

Material Type: (3) BS EN12620(Table D1)

095A289/ 0/4mm CP Gf85 Concrete Sand from 095 Cardiff Wharf to all jobs

NDAC USE ONLY

Samples searched 17958 - 18066 (01-Apr-11 to 15-Apr-11) sorted by Date Sampled

Sample no.	Seq no.	Date sampled	14mm % pass	10mm % pass	8mm % pass	6.3mm % pass	4mm % pass	2.8mm % pass	2mm % pass	1mm % pass	0.500mm % pass	0.250mm % pass	0.125mm % pass	0.063mm % pass	Moisture content%	Chloride %	Compliance status	Category A-C inc2nd
17958	1	01 Apr 11 15:37	100	100	100	97	86	86	64	40	20	11	1	1	3.1	-	ok	A
17983	2	06 Apr 11 14:01	100	100	100	98	89	89	69	43	21	13	1	0	3.8	-	ok	A
18066	3	15 Apr 11 07:38	100	100	100	97	83	75	67	49	29	9	0	0	4.0	-	ok	A
Spec Min		low	spacer	100	spacer	95	80	spacer	spacer	30	5	spacer	spacer	0	-		0	
Spec Max		high	spacer	100	spacer	100	99	spacer	spacer	70	45	spacer	spacer	6	-		2	
Average			100.0	100.0	100.0	97.3	86.0	83.3	66.7	44.0	23.3	11.0	0.7	0.3	3.63	-		
Cat As	3	100.0%																
Cat Bs	0	0.0%																
Cat Cs	0	0.0%																
Total	3	categorised																

A.2: Course aggregate data (sieve analysis)

Material Type: (3) 10mm Single Size

110L100/ 4/10mm Single Size from all suppliers to all jobs

Samples searched 13281 - 13367 (05-Jan-11 to 31-Jan-11)

Sample no.	Seq no.	Date sampled	Supplier name	Job no.	20mm % pass	14mm % pass	10mm % pass	8mm % pass	6.3mm % pass	4mm % pass	2.8mm % pass	2mm % pass	1mm % pass	63µm % pass	Moisture content%	Flakl. Index	Compliance status	Category A-C ex 2nd
13283	1	05 Jan 11 08:29	03 Torcoed Drystone	_0010	100	100	98	74	46	5	4	4	3	3	0.4	-	ok	A in Ctrl
13308	2	12 Jan 11 08:49	03 Torcoed Drystone	_0010	100	100	95	73	41	4	3	2	2	2	1.7	-	ok	A in Ctrl
13327	3	18 Jan 11 12:00	03 Torcoed Drystone	_0010	100	100	91	30	6	2	2	2	2	1	0.6	-	ok	A in Ctrl
13349	4	25 Jan 11 07:00	03 Torcoed Drystone	_0010	100	100	95	56	9	3	2	1	1	1	1.2	18	ok	A in Ctrl
Spec Min					100	98	85	spacer	spacer	0	spacer	0	spacer	spacer	-	0		
Ctrl Min					spacer	100	91	spacer	spacer	0	spacer	1	spacer	spacer				
Ctrl Max					spacer	100	99	spacer	spacer	10	spacer	4	spacer	spacer				
Spec Max					100	100	100	spacer	spacer	20	spacer	5	spacer	spacer	-	40		
Average					100	100	95	58	26	4	3	2	2	2	1	18		
Cat As	4	100.0%																
Cat Bs	0	0.0%																
Cat Cs	0	0.0%																
Total	4	categorised																
For Control	4	qualify																
In Control	4	100.0%																

ARGICAL-M 1000

AGS MINERAUX

PRODUCT DEFINITION
Caractéristiques produit

Norme NF 18-513

ARGICAL-M 1000 is an artificial pozzolana (metakaolin). It is obtained by calcining and micronising a kaolinitic clay from the Charentes basin.
ARGICAL-M 1000 is a dehydroxylated aluminium silicate. Its general formula is $Al_2O_3.2SiO_2$. It is an amorphous non-crystallised material, constituted of lamellar particles.

ARGICAL-M 1000 est une pouzzolane artificielle (métakaolin), obtenue par calcination et broyage d'une argile kaolinique du bassin des Charentes.
ARGICAL-M 1000 est un silicate d'alumine déshydroxylé, de composition générale $Al_2O_3.2SiO_2$. C'est un matériaux amorphe, non cristallisé, dont les particules présentent une forme lamellaire.

The technical details contained in this data sheet are given in all good faith for indicative purpose only, and do not constitute a guarantee by AGS Minéraux.

Sales are in accordance with our "Conditions of Sale", copies of which will be supplied on request.

Les informations contenues dans ce document sont données à titre purement indicatif. Les valeurs indiquées n'emportent pas obligation pour le fournisseur. Elles ne constituent en aucun cas une garantie sur le produit et sur ses spécifications.

Seule la fiche de Spécification Contractuelle dans le cadre de nos Conditions Générales de Ventes engage notre société auprès des clients.

PRODUCT USE / *Domaine d'utilisation*
Additive for concretes, mortars and coatings, made from Portland cement or lime
Additif pour bétons, mortiers, revêtements à base de ciment Portland ou de chaux

CHEMICAL ANALYSIS / *Analyse chimique %*	
SiO_2	55 %
Al_2O_3	40 %
$K_2O + Na_2O$	0,8 %
Fe_2O_3	1,4 %
TiO_2	1,5 %
$CaO + MgO$	0,3 %
LOSS ON IGNITION / *Perte au feu*	1 %

TYPICAL PHYSICAL CHARACTERISTICS
Caractéristiques physiques moyennes

Pozzolanic index (Chapelle test) / Indice pouzzolanique		1100 mg $Ca(OH)_2$/g
Brightness photovolt blue filter / Blancheur photovolt filtre bleu		73
Specific area (BET) / Surface spécifique (BET)		17 m^2/g
Specific gravity / Masse spécifique		2,4 g/cm^3
Bulk density / Densité apparente	Loose / Non tassé	400 kg/m^3
	Tamped / Tassé	800 kg/m^3

PARTICLE SIZE DISTRIBUTION / *Distribution granulométrique*
Refus à 63 µm : 8% ; d_{50} = 5,3 µm

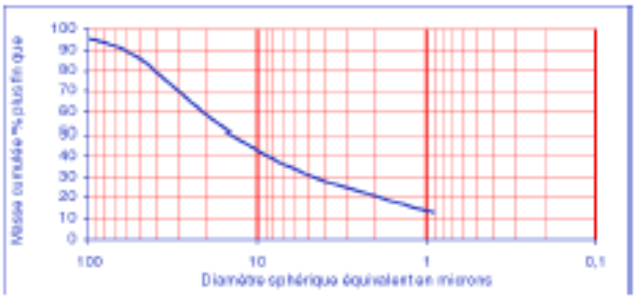

AFAQ ISO 9001

AGS
F-17270 Clérac
Tel. : +33 (0)5 46 04 17 11
Fax. : +33 (0)5 46 04 21 05
www.ags-mineraux.com
commercial@ags-mineraux.com

Revision 5 – 2009/10/15

a member of IMERYS

Elkem AS
Silicon Materials
Hoffsveien 65B
P.O. Box 5211 Majorstuen
NO-0303 OSLO
Tel: +47 22 45 01 50
Fax: +47 22 45 01 53
www.siliconmaterials.elkem.com

Product Data Sheet
Elkem Microsilica® Grade 971

1. Description

Elkem Microsilica® is a key ingredient in advanced low, ultra-low castables and gel-bonding systems. It is highly reactive during sintering, which leads to improved ceramic bonding at reduced firing temperatures. Elkem Microsilica® is also utilised in mortars, gunning mixes and other shaped and unshaped materials.

2. Chemical Analysis (weight%)

Element			Spec*	Typical**
SiO_2	%	min.	98	98.4
C	%	max.	0.7	0.50
Fe_2O_3	%	max.	0.1	0.01
Al_2O_3	%	max.	0.3	0.20
CaO	%	max.	0.3	0.20
MgO	%	max.	0.2	0.10
K_2O	%	max.	0.3	0.20
Na_2O	%	max.	0.2	0.15
P_2O_5	%	max.	0.10	0.03
SO_3	%	max.	0.3	0.10
Cl	%	max.	0.10	0.01
H_2O ***	%	max.	0.5	0.20

*Test methods are available upon request to refractories.materials@elkem.no.
**Typical values (annual moving average) are for guidance only.
*** When packed

3. Physical Data

Properties			Spec*	Typical**
Loss on Ignition	%	max.	0.8	0.50
Course Particles >45µm	%	max.	0.5	0.20
pH-value			5.5 - 7.5	6.8
Undensified 971U				
Bulk density ***	kg/m^3		250 - 350	300
Densified 971D				
Bulk density ***	kg/m^3		450 - 550	500

*Test methods are available upon request to refractories.materials@elkem.no.
**Typical values are for guidance only.
*** When packed

4. Packing

The product is available in 25 kg small bags and various sizes big bags. Please contact our sales representative for more details.

5. Customer benefits

- Improved flow
- More dense castables
- Gel in water
- Hot-strength properties

6. Local Elkem representative

For further information please contact our sales representative. Our specialists will help you to solve any individual problems.

7. Health, Safety and Environment

Please look at Microsilica Safety Data Sheet/Product Safety Information on Elkem Website: www.elkem.com/en/Silicon-materials

8. Brochure

See Elkem brochures: "Let's make a castable" No.59 and "Let's make a mullite matrix" No.61.
See technical papers on our website:
http://www.elkem.com/en/Silicon-materials/Support/Refractories/Technical-papers/

All data listed are reference values subject to production-related tolerances. Although reasonable care has been taken in the preparation of the information contained herein, it still remains the duty of the user to prove the suitability of this material for his applications.

APPENDIX-B

B.0 Pressure decay curves from experimental results

B.1: CEM II concrete- all age of testing

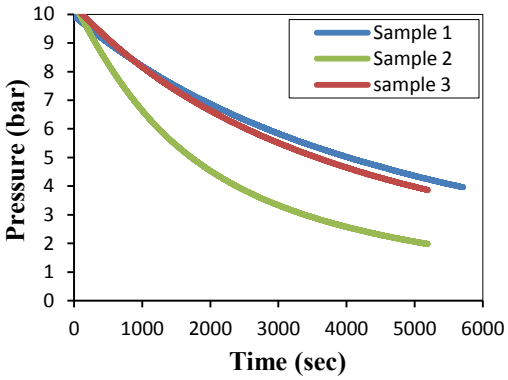

28 days of curing

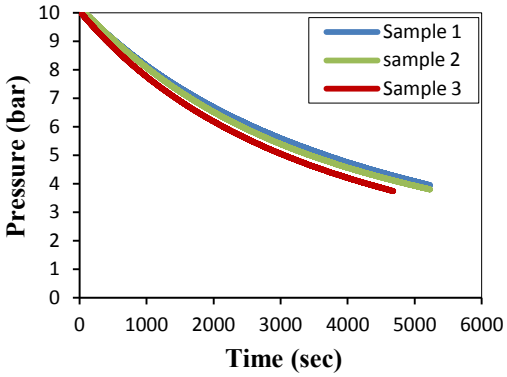

70 days of curing

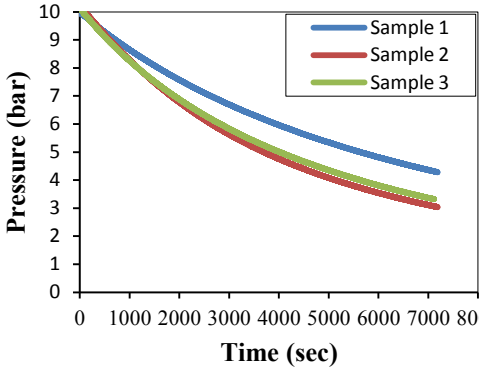

52 days of curing

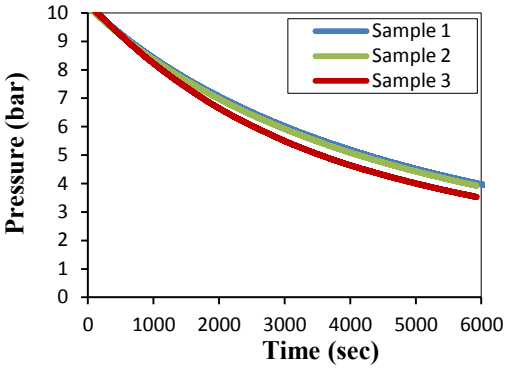

90 days of curing

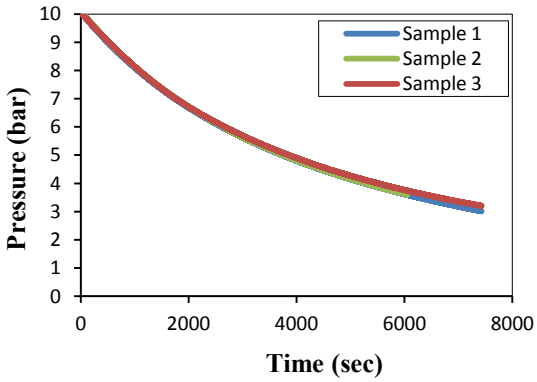

180 days of curing

B2: 50 % GGBS concrete –all age of testing

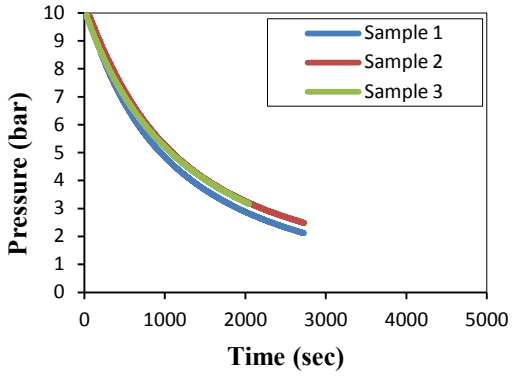

28 days of curing

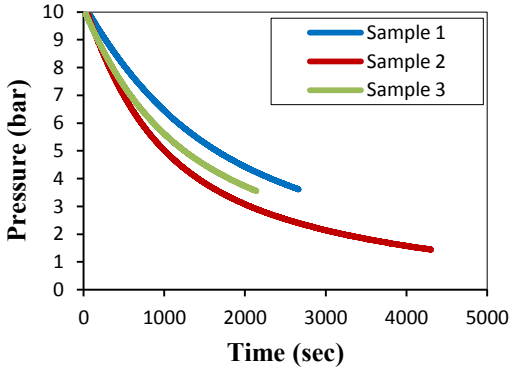

70 days of curing

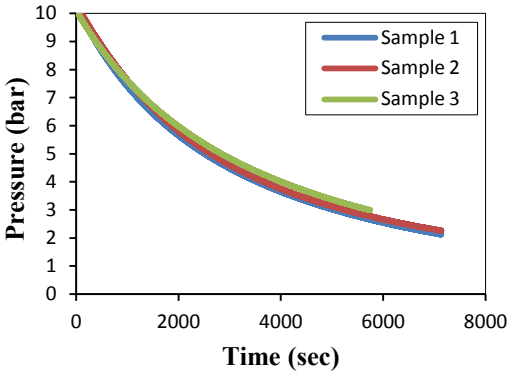

52 days of curing

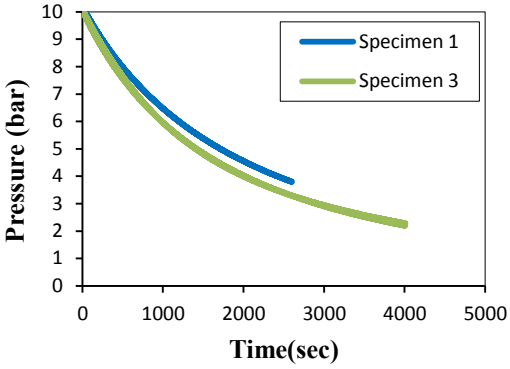

90 days of curing

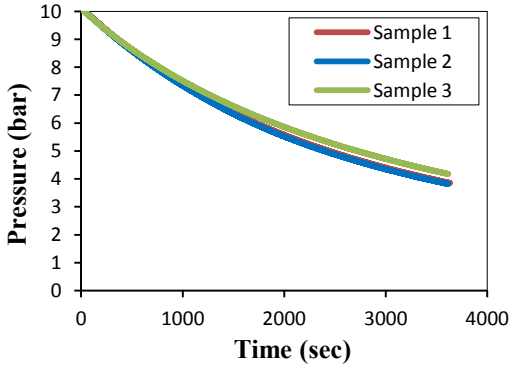

180 days of curing

B.3: 60%GGBS concrete - all testing age

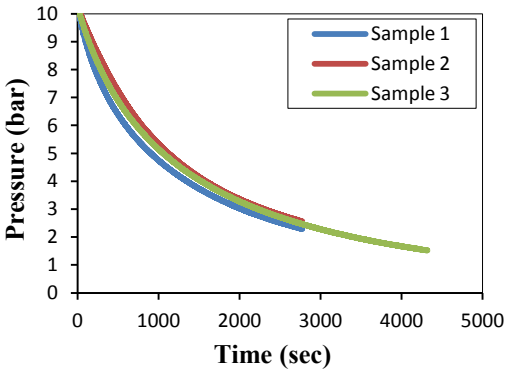

28 days of curing

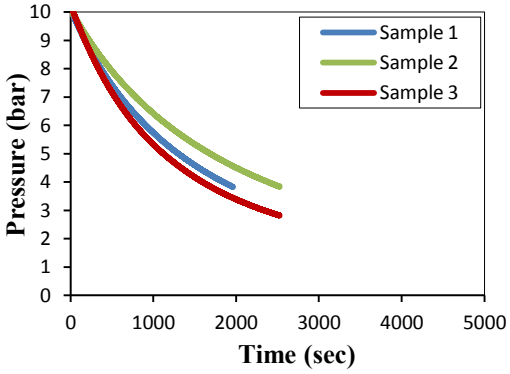

70 days of curing

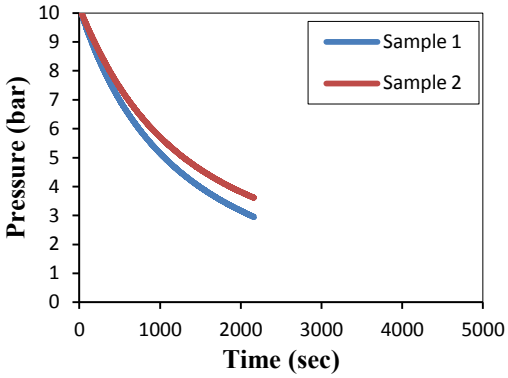

52 days of curing

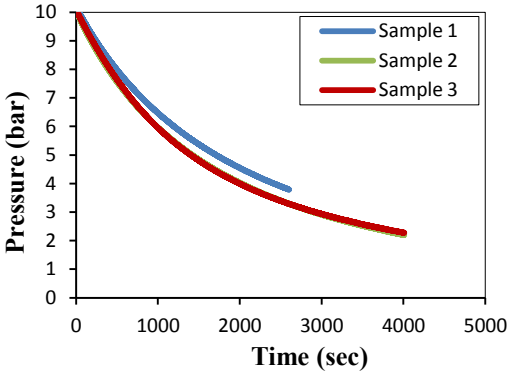

90 days of curing

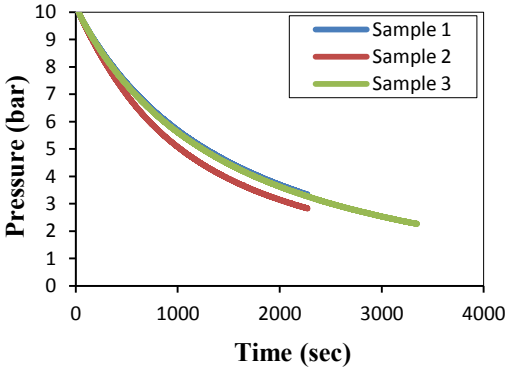

180 days of curing

B.4:30%PFA concrete- all testing

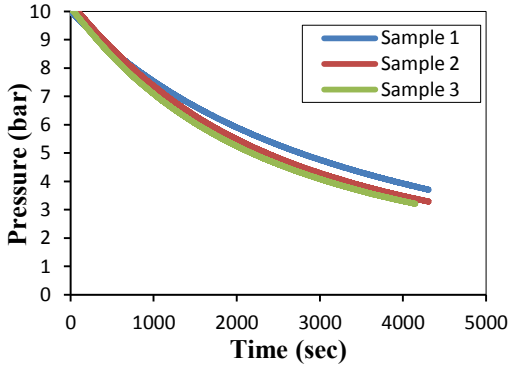

28 days of curing

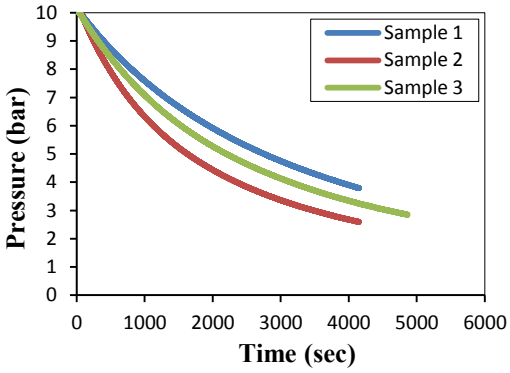

70 days of curing

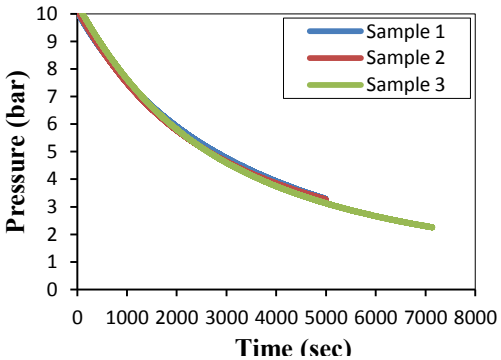

52 days of curing

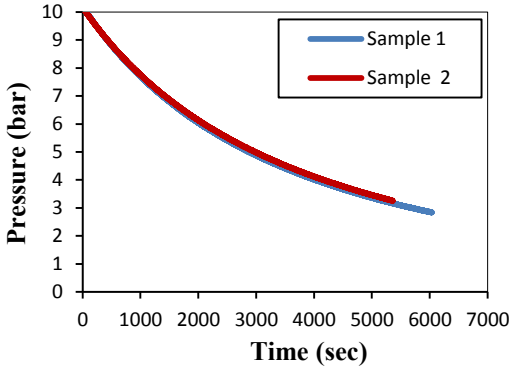

90 days of curing

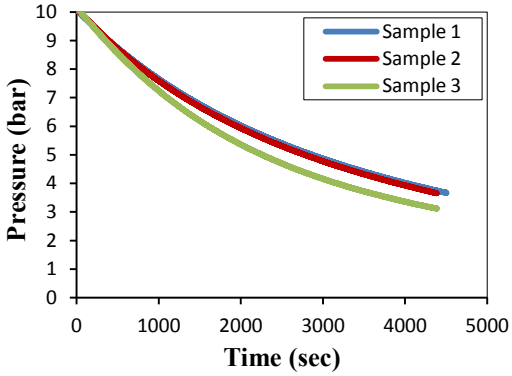

180 days of curing

B.5: 40%PFA concrete- all testing age

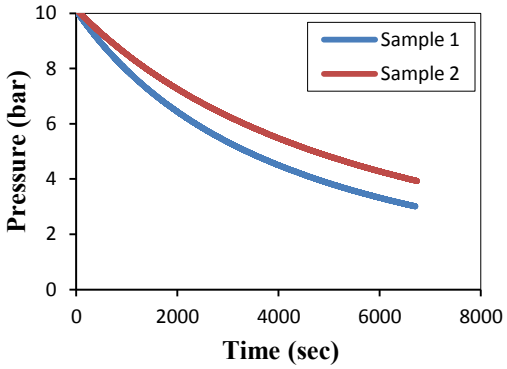

28 days of curing

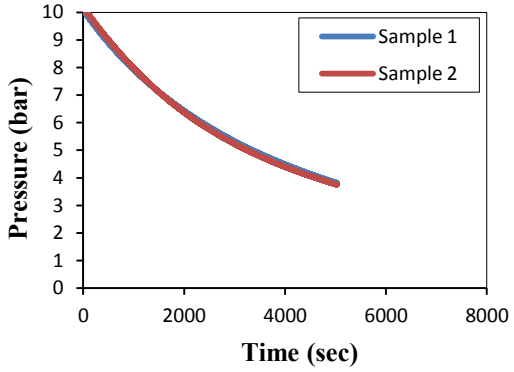

70 days of curing

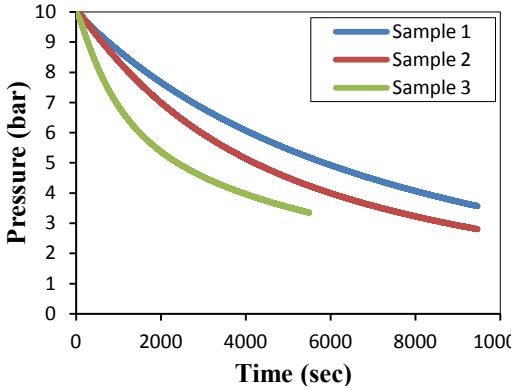

52 days of curing

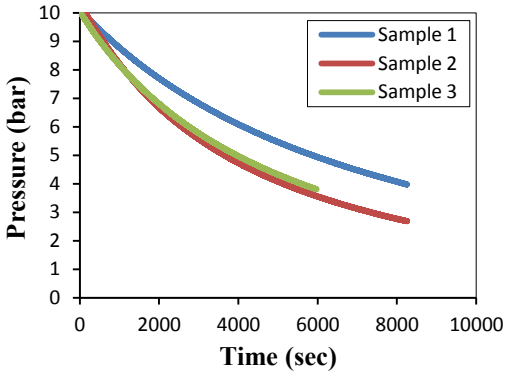

90 days of curing

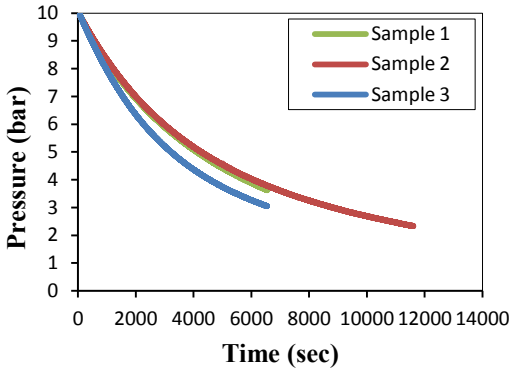

180 days of curing

B.6: 45%PFA concrete- all testing

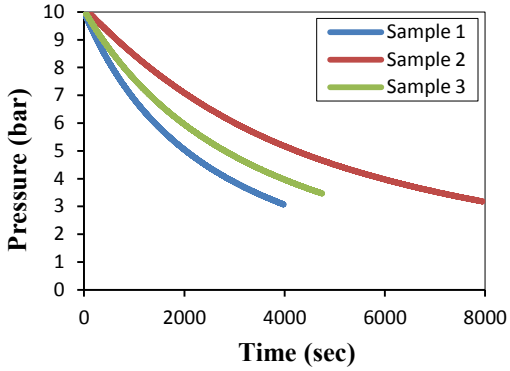

28 days of curing

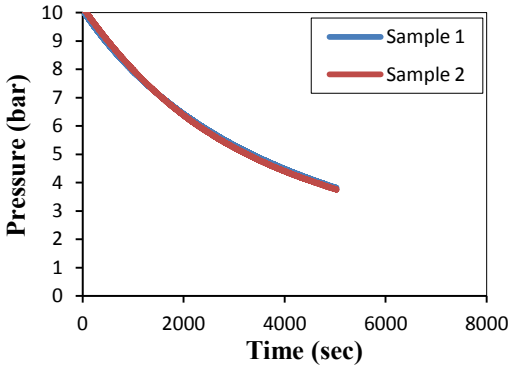

70 days of curing

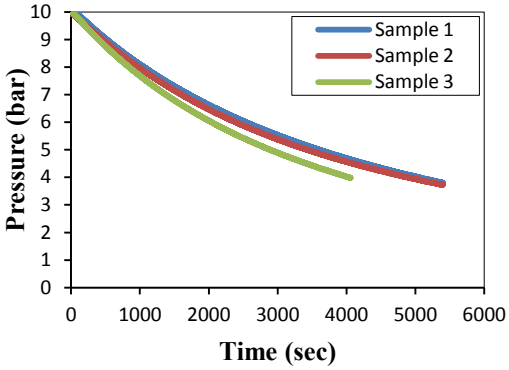

52 days of curing

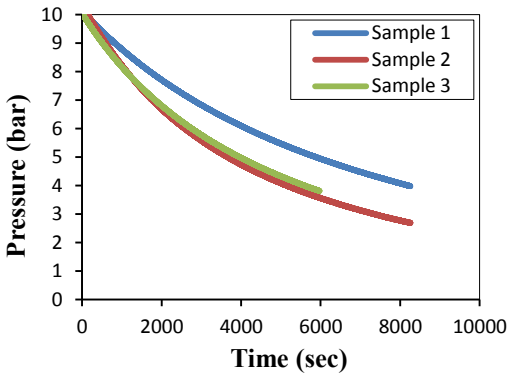

90 days of curing

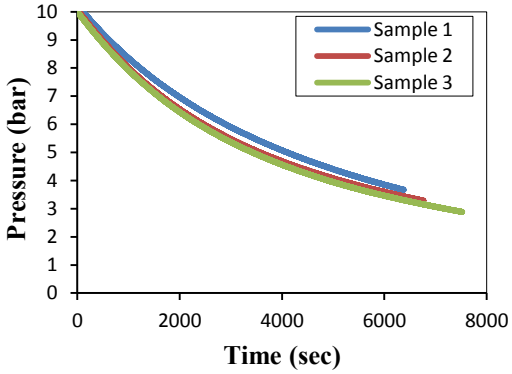

180 days of curing

APPENDIX-C

C.0 Numerical modelling data

Table C.1: The concrete properties of CEM II

Concrete properties	Values
Initial Young's modulus	E_c = 35800 N/mm^2
Poisson's ratio	ν = 0.2
Fracture energy	G_f = 78.70 N/m 0.0787 N/mm
Uniaxial strain at peak compressive strength	ε_c = 0.0022
Strain at end of softening curve	ε_{rc}= 0.00035
Uniaxial tensile strength	f_t= 4.5 N/mm^2
Uniaxial compressive strength	f_{cu} = 61.9 and fc = 49.5 N/mm^2
Steel properties	**Values**
Young's Modulus	E_c = 196000 N/mm^2
Poisson's ratio	ν = 0.3
Yield stress	f_y = 550.5 N/mm^2

Properties	Values
Initial slip	τ_0 = 9.59 N/mm^2 (F= 18076 N)
Initial bond strength	δ_0 = 0.22 mm
Maximum bond strength	τ_{max} = 18.61N/mm^2 (F =35078.91 N)
Slip at maximum bond strength	δ_{max} = 1.30 mm
Stiffness at initial bond strength	E = 82163.63 N/mm
Normal stiffness and shear stiffness	k_{nn}= 1431 and k_{ss}= k_{tt} = 14.31 N/mm^3

Table C.2: The concrete properties of CEM II + 50% GGBS

Concrete properties	Values
Initial Young's modulus	E_c = 36000 N/mm^2
Poisson's ratio	ν = 0.2
Fracture energy	G_f = 69.21 N/m 0.0692 N/mm
Uniaxial strain at peak compressive strength	ε_c = 0.0022
Strain at end of softening curve	ε_{rc}= 0.00035
Uniaxial tensile strength	f_{ct}=4.4 N/mm^2
Uniaxial compressive strength	f_{cu} = 51.6 and fc = 41.2 N/mm^2

Properties	Values
Initial slip	τ_0 = 9.81 N/mm^2 (F= 18491 N)
Initial bond strength	δ_0 = 0.23mm
Maximum bond strength	τ_{max} = 17.73N/mm^2 (F =33420.16 N)
Slip at maximum bond strength	δ_{max} = 1.26mm
Stiffness at initial bond strength	E = 80395 N/mm
Normal stiffness and shear stiffness	k_{nn}= 1407 and k_{ss}= k_{tt} = 14.07 N/mm^3

Table C.3: The concrete properties of CEM II + 30% PFA

Concrete properties	Values
Initial Young's modulus	E_c = 34870 N/mm^2
Poisson's ratio	ν= 0.2
Fracture energy	G_f= 58.11N/m 0.0581N/mm
Uniaxial strain at peak compressive strength	ε_c = 0.0022
Strain at end of softening curve	ε_{rc}= 0.00035
Uniaxial tensile strength	f_{ct}=3.2 N/mm^2
Uniaxial compressive strength	f_{cu} = 40.2 and f_c = 32.1 N/mm^2

Properties	Values
Initial slip	τ_0 = 3.90 N/mm^2 (F= 7351.30 N)
Initial bond strength	δ_0 = 0.091mm
Maximum bond strength	τ_{max} = 10.51N/mm^2 (F = 19810.82 N)
Slip at maximum bond strength	δ_{max} = 1.24mm
Stiffness at initial bond strength	E = 80783.57 N/mm
Normal stiffness and shear stiffness	k_{nn}= 847.58 and k_{ss}= k_{tt} = 8.47 N/mm^3

Table C.4: The concrete properties of CEM II +10% MK

Concrete properties	Values
Initial Young's modulus	E_c = 38360 N/mm^2
Poisson's ratio	ν = 0.2
Fracture energy	G_f= 78.4 N/m 0.0784 N/mm
Uniaxial strain at peak compressive strength	ε_c = 0.0022
Strain at end of softening curve	εrc= 0.00035
Uniaxial tensile strength	f_{ct} = 4.4 N/mm^2
Uniaxial compressive strength	f_{cu} = 61.7 and f_c = 49.3 N/mm^2

Properties	Values
Initial slip	τ_0 = 8.84 N/mm^2 (F= 16662.95 N)
Initial bond strength	δ_0 = 0.13mm
Maximum bond strength	τ_{max} = 18.19 N/mm^2 (F = 34287.24 N)
Slip at maximum bond strength	δ_{max} = 2.00mm
Stiffness at initial bond strength	E = 128176.53 N/mm
Normal stiffness and shear stiffness	k_{nn}= 909 and k_{ss}= k_{tt} = 9.09 N/mm^3

Table C.5: The concrete properties of CEM II+10%SF

Concrete properties	Values
Initial Young's modulus	E_c = 36760 N/mm^2
Poisson's ratio	ν = 0.2
Fracture energy	G_f = 76.68 N/m 0.0766N/mm
Uniaxial strain at peak compressive strength	ε_c = 0.0022
Strain at end of softening curve	ε_{rc} = 0.00035
Uniaxial tensile strength	f_{ct} = 4.4 N/mm^2
Uniaxial compressive strength	f_{cu} = 59.7 and f_c = 47.7 N/mm^2

Properties	Values
Initial slip	τ_0 = 11.91 N/mm^2 (F= 22449.75 N)
Initial bond strength	δ_0 = 0.13mm
Maximum bond strength	τ_{max} = 21.45 N/mm^2 (F = 40432.17 N)
Slip at maximum bond strength	δ_{max} = 1.44mm
Stiffness at initial bond strength	E = 172690.38 N/mm
Normal stiffness and shear stiffness	k_{nn}= 1489 and k_{ss}= k_{tt} = 14.89 N/mm^3

C.1 The description of corrosion model data

The radius increases of the original reinforcing bar due to corrosion products are obtained from the following equation:

$$\Delta r = -r + \sqrt{r^2 + (v-1).(2rx - x^2)}$$

Where:

Δr = the radius increase (mm)

r = the original of steel reinforcement radius (mm)

v = volume factor of corrosion product on iron (-), the volume factor is set to v=2.

x = is the corrosion penetration (corrosion rate) (mm)

This equation is the free radius increase because of the embedding of the steel bar in the concrete is opposite this free radius increase the resistance of the corrosion, so build up a voltage as a function of the stiffness of steel , corrosion coating and concrete may , in turn, determines the actual radius increase of the contact layer .

The corrosion penetration is determined from the following equation:

$$x = 11.6.(t.I)$$

Where:

x is the corrosion penetration depth into the steel bar in (mm);

t is the corrosion time in year; and

I is the impressed current density in μA/cm^2

This results in a total strain in the corrosion products, ε_{cor},

$$\varepsilon_{Cor} = \frac{u_{ucor} - \Delta r}{x + \Delta r}$$

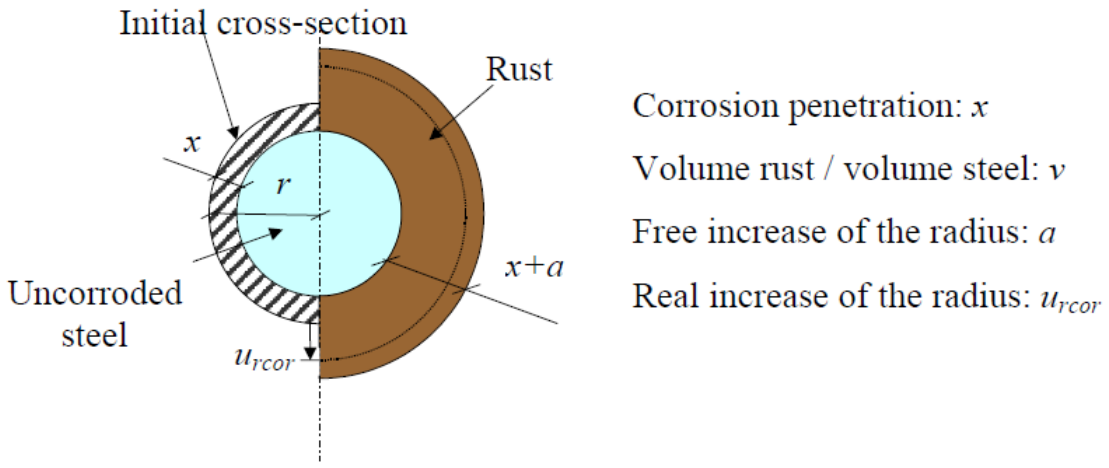

Figure C.1: Physical interpretations of the variables in the corrosion model, modified from (Lundgren 2005b)

Table C.6: The example of parameters input data

Diameter	Corrosion data	x_{corr}	u_{ncor}	Δr
12	0	0	0	0
12	3	0.047698	-0.00038	0.047321
12	7	0.111294	-0.00203	0.109267
12	10	0.158992	-0.00411	0.154886
12	14	0.222588	-0.00797	0.214621
12	20	0.317984	-0.01603	0.301959